Appendix A Description of the experiments

A.1 The experiments

Until recently the knowledge of flow through sharp open-channel bends was poor. Therefore a research was started to gain more insight into the phenomena occurring in sharp bend flows and to develop a better model for flows through sharp bends.

The research consists of an experimental part conducted at the École Polytechnique Fédérale de Lausanne (EPFL), a theoretical research, performed by Blanckaert, (Blanckaert, 2002) and a simulation part done at the TU Delft.

In this appendix a description of the experimental part is given as far as it is relevant for this thesis.

A.2 Setup of the performed experiment

The experiment consists of several measurements on different configurations of a flume. The flume configuration is shown in Figure A-2.

The flume consists of a 2 m long inlet basin (II), followed by a 9 m long straight inflow reach (III), a 193º bend with constant centre line radius of curvature, R= 1.7 m (IV), a 3 m long straight outflow reach (V, VI), a 2 m long sediment deposition basin (VII) and a 2 m long outflow basin (VIII). The overall length of the flume is 22.7 m along the centre line. By covering the sediment deposition basin with a flat Plexiglas plate, the length of the straight outflow reach can be extended to 5 m. The depth of the sections in the straight inflow (III) and outflow (VI, VII) reaches is 0.6 m. To allow the study of local bend scour, sections with a depth of 0.85 m are foreseen in the bend (IV) and in the straight outflow reach just downstream of it (V). The entire flume is posed on adjustable feet (e) with a maximum height of about 0.1 m (Blanckaert, 2009).

Two different types of experiments were carried out in this flume. Experiments with a flat bed configuration (indicated by a capital *Q*) and with an equilibrium-bed configuration (indicated by a capital *M*). For the flat bed experiments the sand was fixed by spraying paint on it. For the equilibrium-bed experiment, at the inflow boundary a constant sediment inflow was generated. The diameter of the sand grains was between 1.6 mm and 2.2 mm. After reaching equilibrium, the bed was fixed by spraying paint on it and the measurements were performed. Some results of the experiments are shown in Table A-1.

Name	Q[l/s]	H[m]	U[m/s]	$1/\sqrt{C_{f0}}$ [/]	Re = UH/ν [/]	$Fr = U/(gH)^{1/2}$ [/]
Q89	89	0.159	0.43	14.4	69	0.35
Q104	104	0.212	0.38	15.2	81	0.26
M89	89	0.141	0.49	9.99	68	0.41

Table A-1 Measured quantities of relevant experiments

The measurements of the velocity components were performed with an ADVP (Acoustic Dopler Velocity Profiler) at a high spatial and temporal resolution. An ADVP consists of a central emitter, surrounded by four receivers, placed in a water filled box that touches the water surface by means of an acoustically transparent mylar film (Figure A-1). The working principle of the ADVP has been reported by Lemmin and Rolland (1997), Hurther and Lemmin (1998), Blanckaert and Graf (2001) and Blanckaert and Lemmin, (2006). The measured cross-sections (for the flat bed experiment) are shown in Figure A-3. For the

equilibrium-bed, the cross-sections in the straight reaches were performed at slightly different locations. For this case the cross-section at 2.2 m upstream of the bend and the cross-sections 0.5 m, 1.3 m, 2.2 m and 2.9 m downstream of the bend were measured. In these cross-sections, vertical profiles were measured on a grid that refines toward the banks including the verticals at, n = ±[0, 0.05, 0.1, 0.15, 0.2, 0.25, 0.3, 0.325, 0.35, 0.375, 0.4, 0.425, 0.45, 0.475, 0.5, 0.515, 0.53, 0.545, 0.56, 0.575, 0.59, 0.60, 0.61, 0.62]m.

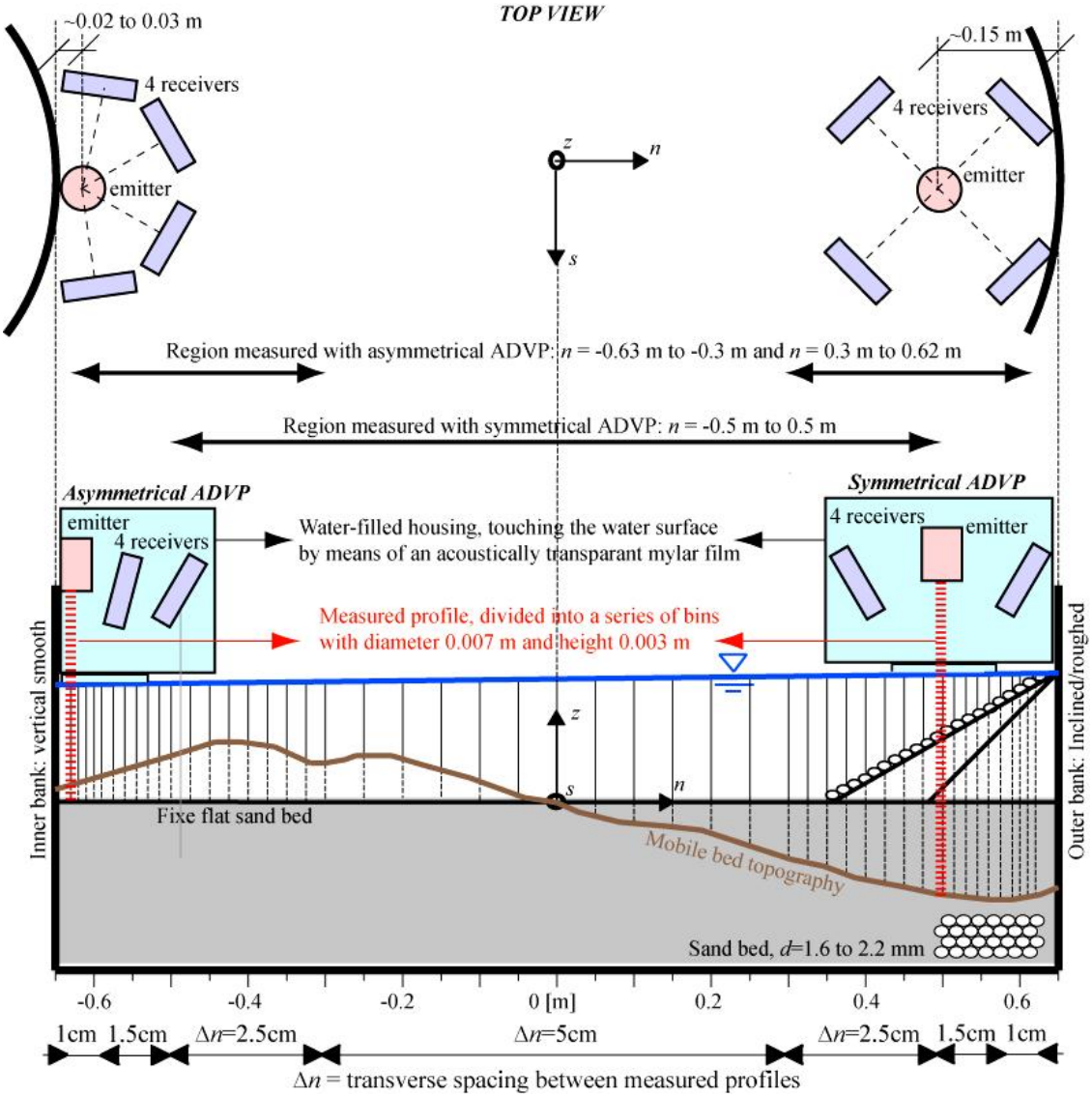

Figure A-1 The configuration of the Acoustic Dopler Velocity Profiler (Blanckaert, 2009)

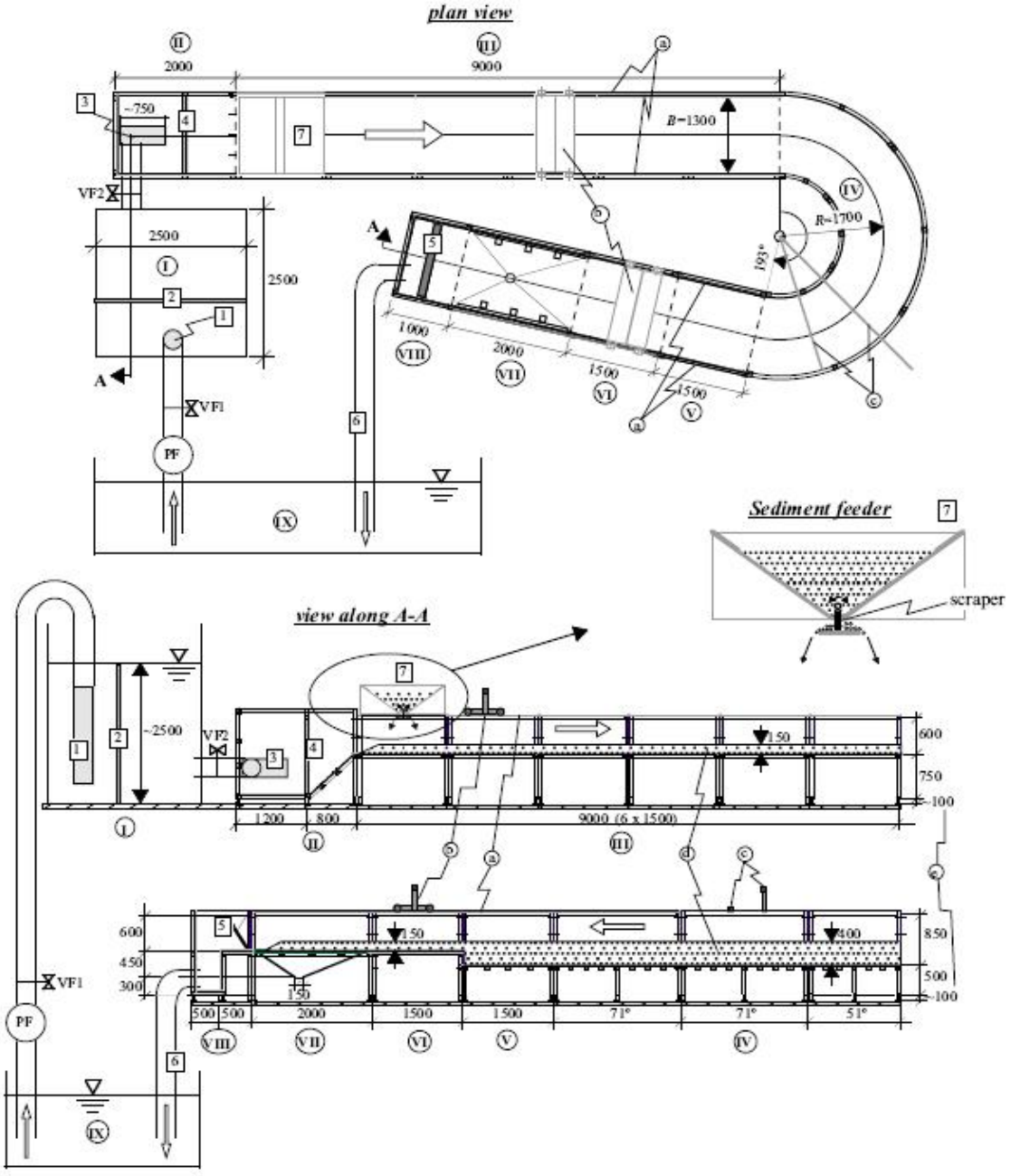

Legend: (all scales in mm)

I: Constant discharge basin
II: Inlet basin
III: Straight inflow reach (depth 600 mm)
IV: Constant curvature bend (depth 850 mm)
V: Straight outflow reach (depth 850 mm)
VI: Straight outflow reach (depth 600 mm)
VII: Sediment deposition basin / straight outflow reach (depth 600 mm)
VIII: Outlet basin
IX: Laboratory sump

PF: Pump for flow recirculation
VF1: Electrical valve on flow supply pipe, ϕ=315 mm
VF2: Manual valve on pipe, ϕ=315 mm, to regulate water level in I

1: Perforated pipe, ϕ=315 mm
2: Porous plate filter
3: Perforated pipe, ϕ=315 mm
4: Porous polyether filter 10 ppi, 10 mm thick
5: Adjustable water level control weir
6: Restitution pipe, ϕ=315 mm
7: Sediment feeder

a: Inclinable guiding rail for carriage
b: Carriage for straight inflow and outflow reaches
c: Two pivoting-arm carriages for bendway
d: sediment bed
e: adjustable feet

Figure A-2 Experiment preparation (Blanckaert, 2009)

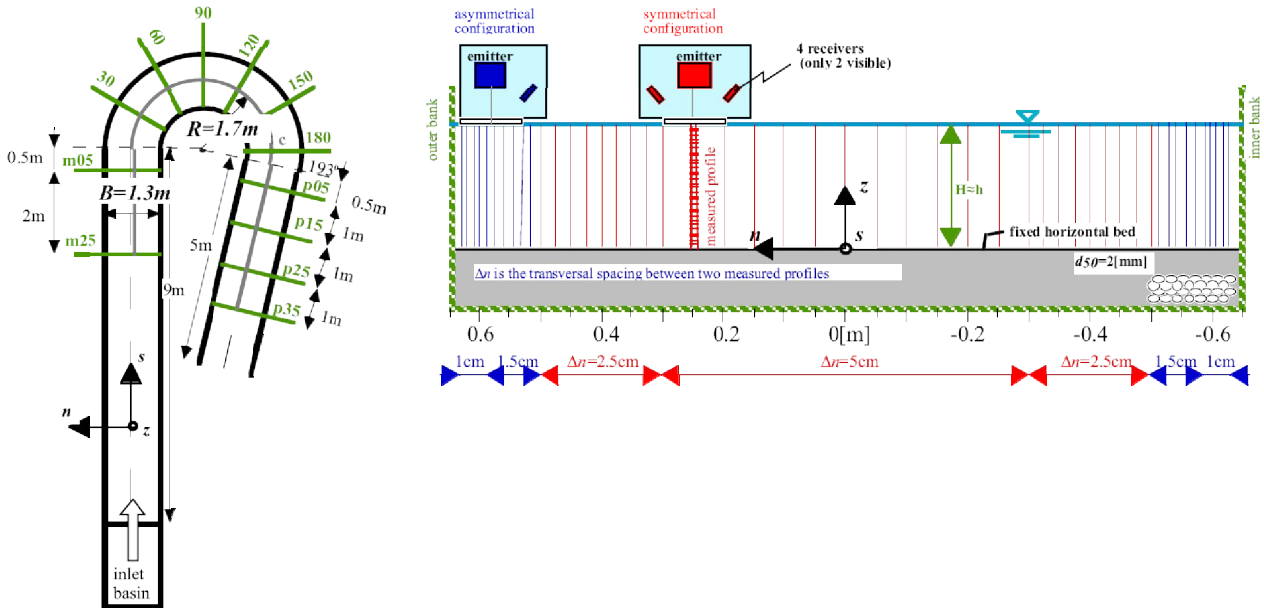

Figure A-3 Measured cross-sections and profiles (Blanckaert, 2002)

A.3 Measuring data

The measured quantities that are used during this research are the water level, the bottom profile (of the M89 experiment), the three velocity components and the Reynolds stresses. The water level and bottom profile are displayed with respect to the mean bottom level (for both experiments, the lowest bottom level for the M89 experiment is 0.2885 m below this reference level).

Some cross-sections show gaps in the data. These gaps can be caused by the fact that the water depth was to low to be able to measure. This occurs especially along the inner bend of the flume. There is also a gap in the velocity data in cross-section 150 at the bottom, at 0.450 m, 0.475 m and 0.500 m from the centreline. To be able to calculate several quantities, the velocities at these points are linear interpolated over the width to fill the gap.

The M89 experiment is the experiment with the equilibrium-bed and a flow of 0.089 m^3/s. The equilibrium-bed level was obtained by adding sediment at the upstream boundary during the flow. Afterwards the bed was fixed by spraying paint on it. With this fixed bed the measurements were performed. The bottom profile in the M89 experiment was measured by both the limni meter and the ADVP. The ADVP measured the bottom only along the cross-sections where the other quantities (like the velocities) were measured too. The limni meter measured the bottom along a whole grid with a grid spacing in the downstream direction of 5 cm and a grid spacing in the transverse direction of 1 cm. This resulted in a more smooth bathymetry than the one that was measured by the ADVP. The measured bathymetry starts 6.5 m upstream of the bend entrance and stops 3.5 m downstream of the bend exit.

The bed level that was measured by the ADVP is only used to calculate the right level for the quantities that are also measured with the ADVP. Because they are all measured by the ADVP, the levels of the measurements are strongly related.

Appendix B Description of simulations

B.1 Introduction

This appendix describes how the Delft3D-FLOW model is calibrated. For the calibration the results of the Q89 experiments are used. Also is analyzed how the outcome of the simulations changes with changing input parameters. Among others will be looked at the effect of different grid sizes, changes in the roughness and changes in the viscosity. To compare the different simulations, the water level is taken as an important indicator. Figure B-1 gives a plan view of the measured water level along the flume. This figure is used to decide which of the simulations performs best.

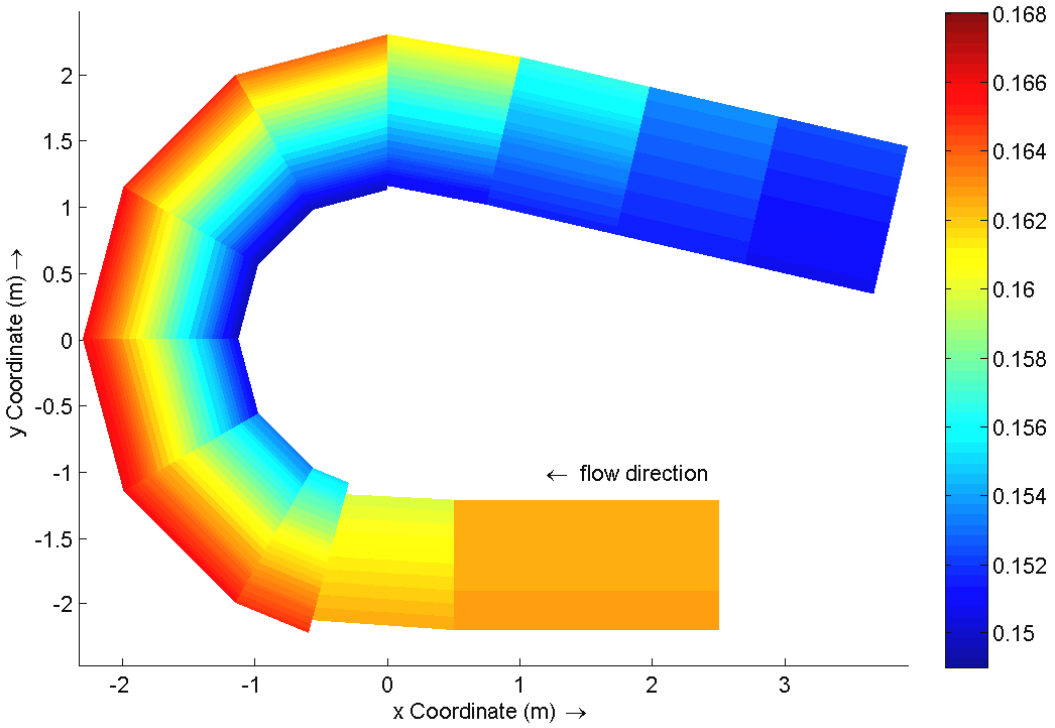

Figure B-1 Measured water level

In Table B-1 and Table B-2 the simulations are listed which are used to model the Q89 experiment. They all start with the capital '*Q*'. In Table B-1 the properties of the used grid and the used closure models per simulation are shown. In Table B-2 the used roughness formula and parameters are shown.

Name	Modelled area	Grid size [m * m]	Nr. of layers	horizontal viscosity [m^2/s]	vertical viscosity [m^2/s]	Turbulence model
Q89_1_D3Da	Part of flume	0.086*0.057	20	$1*10^{-4}$	$1*10^{-5}$	k-ε
Q89_1_D3Db	Part of flume	0.086*0.057	20	$1*10^{-6}$	$1*10^{-6}$	k-ε
Q89_1_D3Dc	Part of flume	0.086*0.057	20	$1*10^{-2}$	$1*10^{-2}$	k-ε
Q89_1_D3Dd	Part of flume	0.086*0.057	20	$1*10^{-6}$	$1*10^{-6}$	k-ε
Q89_1_D3De	Part of flume	0.050*0.050	20	$1*10^{-6}$	$1*10^{-6}$	k-ε
Q89_1_D3Df	Part of flume	0.050*0.050	20	$1*10^{-6}$	$1*10^{-6}$	k-ε
Q89_1_D3Dg	Part of flume	0.050*0.050	20	$1*10^{-6}$	$1*10^{-6}$	algebraic
Q89_1_D3Dh	Part of flume	0.050*0.050	20	$1*10^{-6}$	$1*10^{-6}$	k-L
Q89_1_D3Di	Part of flume	0.100*0.100	40	$1*10^{-6}$	$1*10^{-6}$	k-ε
Q89_1_D3Dj	Complete flume	0.050*0.050	20	$1*10^{-6}$	$1*10^{-6}$	k-ε
Q89_1_D3Dk	Complete flume	0.100*0.100	20	$1*10^{-6}$	$1*10^{-6}$	k-ε
Q89_1_D3Dl	Part of flume	0.100*0.100	20	$1*10^{-6}$	$1*10^{-6}$	k-ε
Q89_1_D3Dm	Complete flume	0.100*0.100	20	$1*10^{-6}$	$1*10^{-6}$	k-ε
Q89_1_D3Dn	Complete flume	0.100*0.100	20	$1*10^{-6}$	$1*10^{-6}$	k-ε
Q89_1_D3D	Complete flume	0.050*0.050	20	$1*10^{-6}$	$1*10^{-6}$	k-ε
Q89_2_D3D	Complete flume	0.050*0.050	20	$1*10^{-2}$	$1*10^{-6}$	k-ε

Table B-1 Relevant simulations to model the Q89 experiment

Name	Wall condition	Roughness formula	z_0 [m], C [$m^{1/2}/s$], k_s [m]
Q89_1_D3Da	No slip	Chezy [C]	45
Q89_1_D3Db	Free	White-Colebrook [k_s]	0.006
Q89_1_D3Dc	No slip	Chezy [C]	45
Q89_1_D3Dd	No slip	White-Colebrook [k_s]	0.006
Q89_1_D3De	Free	White-Colebrook [k_s]	0.006
Q89_1_D3Df	Free	White-Colebrook [k_s]	0.003
Q89_1_D3Dg	Free	White-Colebrook [k_s]	0.003
Q89_1_D3Dh	Free	White-Colebrook [k_s]	0.003
Q89_1_D3Di	Free	z_0	0.0001
Q89_1_D3Dj	Partial (with z_0;wall = $5*10^{-6}$m)	z_0	0.0001
Q89_1_D3Dk	Partial (with z_0;wall = $5*10^{-6}$m)	z_0	0.0001
Q89_1_D3Dl	Free	z_0	0.0001
Q89_1_D3Dm	Free	z_0	0.0001
Q89_1_D3Dn	Free	z_0	0.0001 ($z_{0;transverse}$= $1*^{10-5}$m)
Q89_1_D3D	Partial (with z_0; wall = $5*10^{-6}$m)	z_0	0.0001
Q89_2_D3D	Partial (with z_0; wall = $5*10^{-6}$m)	z_0	0.0001

Table B-2 Relevant simulations to model the Q89 experiment with some of the variables

B.2 Used grid

B.2.1 Grid size

To reduce the simulation time, especially for the morphologic simulations, as less as possible grid points are preferred. The simulations Q89_1_D3Dj (fine grid) and Q89_1_D3Dk (rough grid) are compared to see the effect of the grid size on the simulation results. The size of the grid cells in the straight reaches are 0.050 m * 0.050 m for the Q89_1_D3Dj simulation and 0.100 m * 0.100 m for the Q89_1_D3Dk simulation. In the bend, the length of the grid varies over the width of the flume because of the curvature. When we compare the results of simulation Q89_1_D3Dj and Q89_1_D3Dk (see Figure B-2), we can conclude that there is little effect of the grid size on the flow (when keeping the grid size reasonable). The only difference between Q89_1_D3Dj and Q89_1_D3Dk is the smoothness of the water surface. Both compare quite well with the results of the Q89 experiment.

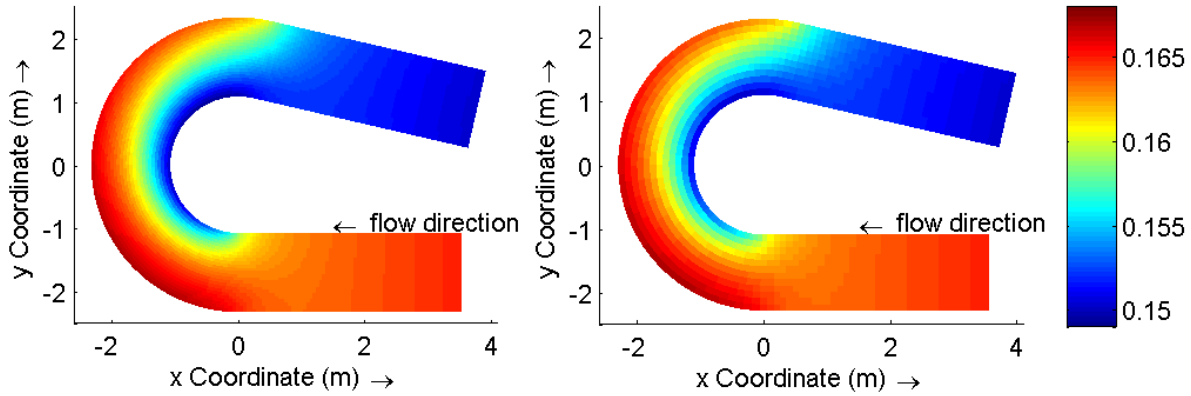

Figure B-2 Water level, simulation Q89_1_D3Dj (left, fine grid) and Q89_1_D3Dk (right, rough grid)

B.2.2 Number of layers and distribution type

Several simulations are performed with different number of layers and different layer distributions in the vertical direction to gain insight in the effects of the number of layers. Firstly the number of layers is changed. Simulation Q89_1_D3Di is set up with 40 layers and simulation Q89_1_D3Dm is set up with 20 layers, both with logarithmic distributions. The layer distribution is shown in Figure B-4, Table B-3 and Table B-4.

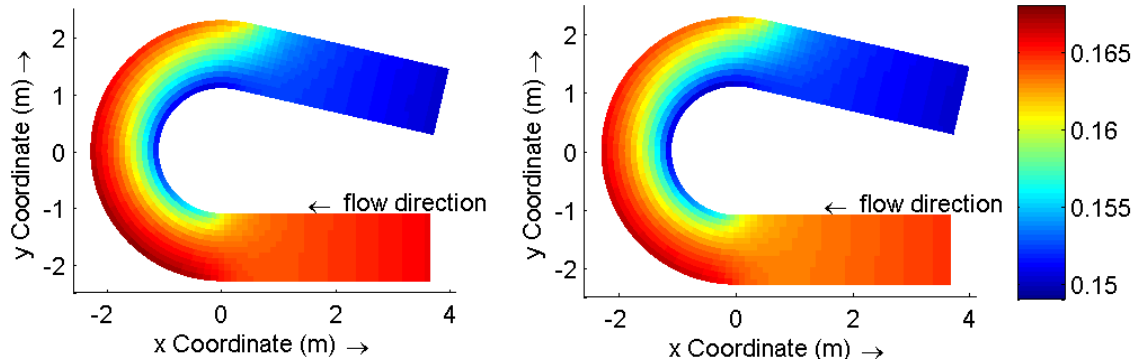

Figure B-3 Water level, simulation Q89_1_D3Di (left, 40 layers) and simulation Q89_1_D3Dl (right, 20 layers), both logarithmic distributed

There is a small difference visible in the water levels for simulation Q89_1_D3Di and Q89_1_D3Dl (see Figure B-3). The water level of simulation Q89_1_D3Dl is somewhat lower than the water level of simulation Q89_1_D3Di. We continue with the 20 layer distribution because this is less time consuming to compute.

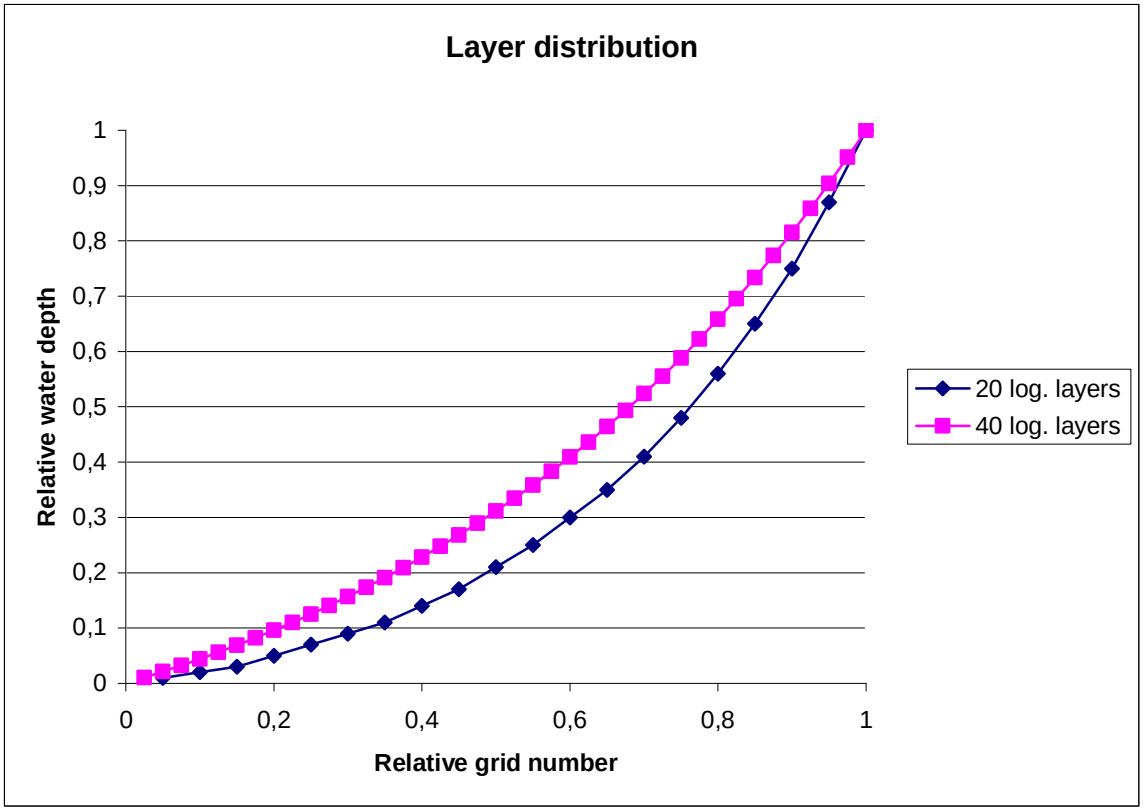

Figure B-4 Graph of relative layer distribution

Layer nr	% of depth [20 layers]	cum % [20 layers]	% of depth [40 layers]	cum % [40 layers]
1	1	1	1.04	1.04
2	1	2	1.08	2.12
3	1	3	1.13	3.25
4	2	5	1.17	4.42
5	2	7	1.22	5.64
6	2	9	1.27	6.91
7	2	11	1.32	8.23
8	3	14	1.37	9.60
9	3	17	1.43	11.03
10	4	21	1.49	12.52
11	4	25	1.55	14.07
12	5	30	1.61	15.68
13	5	35	1.68	17.36
14	6	41	1.74	19.10
15	7	48	1.81	20.91

Table B-3 Distribution of layer thickness (layers are numbered from water surface to bottom)

Layer nr	% of depth [20 layers]	cum % [20 layers]	% of depth [40 layers]	cum % [40 layers]
16	8	56	1.89	22.80
17	9	65	1.96	24.76
18	10	75	2.04	26.80
19	12	87	2.13	28.93
20	13	100	2.21	31.14
21			2.30	33.44
22			2.39	35.83
23			2.49	38.32
24			2.59	40.91
25			2.70	43.61
26			2.81	46.42
27			2.92	49.34
28			3.04	52.38
29			3.16	55.54
30			3.29	58.83
31			3.42	62.25
32			3.56	65.81
33			3.71	69.52
34			3.85	73.37
35			4.01	77.38
36			4.17	81.55
37			4.34	85.89
38			4.52	90.41
39			4.70	95.11
40			4.89	100.00

Table B-4 Distribution of layer thickness (layers are numbered from water surface to bottom)

Figure B-5 shows the difference between a logarithmic layer distribution (simulation Q89_1_D3Dj) and an equidistant layer distribution (simulation Q89_1_D3D). The equidistant distribution gives a lower water level at the entrance which is more according to the measurements.

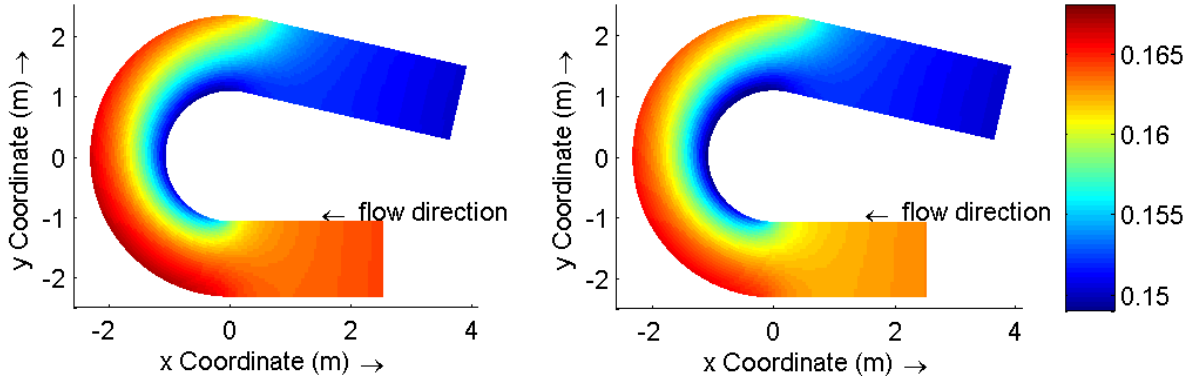

Figure B-5 Water level, simulation Q89_1_D3Dj (left, 20 logarithmic) and simulation Q89_1_D3D (right, 20 layers equidistant)

B.2.3 Simulated area

A simulation is done for the complete flume and one for a part of the flume (see Figure B-6). This part starts 3.8 m before the bend entrance and ends 3.8 meters after the bend. The results are shown in Figure B-7. The results for the area of interest are not different. To reduce the simulation time, it is possible to use the grid which represents only a part of the flume.

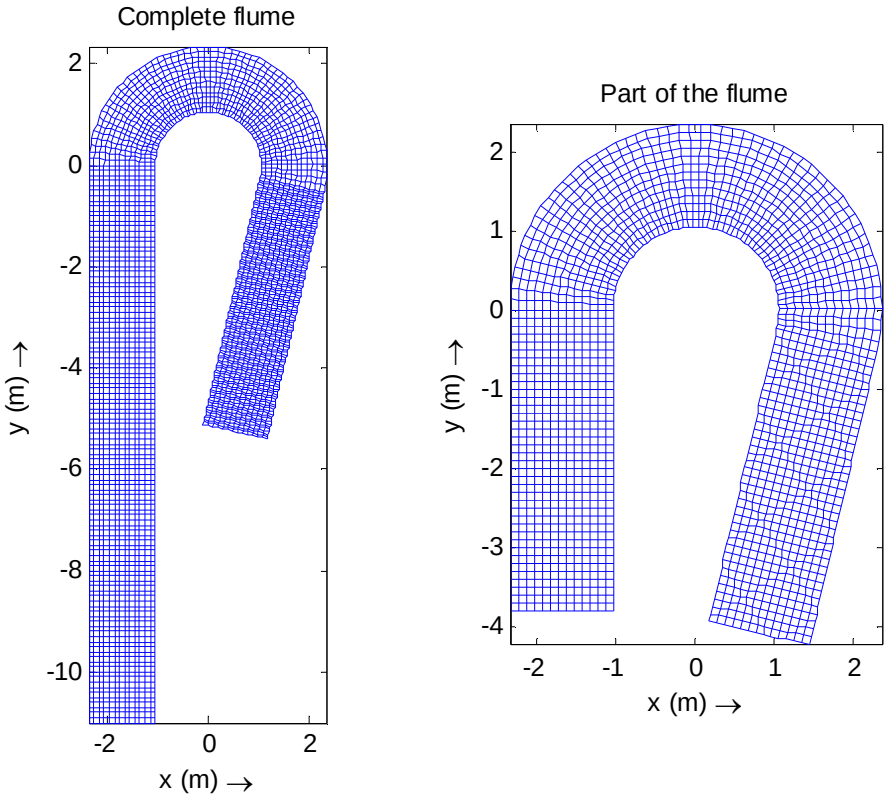

Figure B-6 Grids used (left: complete flume; right: part of the flume)

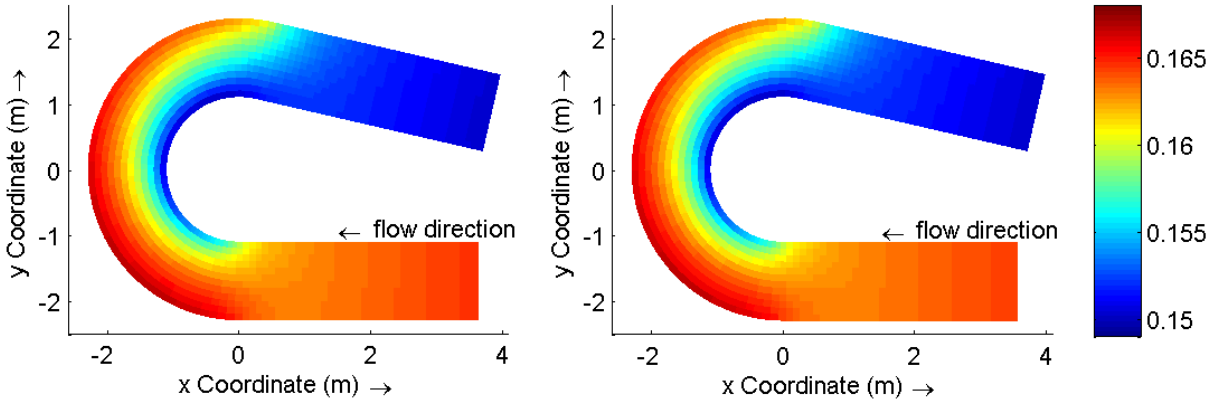

Figure B-7 Water level, simulation Q89_1_D3Dl (left, part of flume) and Q89_1_D3Dm (right, complete flume)

B.3 Bathymetry

The bottom profile of the Q89 experiment is described in paragraph A.2. The bottom profile in the complete flume is taken equal to that of the real experiment (first 1.2 m at a level of 0.8 m below reference level, a slope of 45 degrees over a length of 0.8 m and further the whole bottom at reference level). For the part of the flume is the depth taken at reference level.

The M89 experiment is the experiment with the equilibrium-bed and a flow of 0.089 m^3/s. The bed level that was obtained during this experiment by the limni meter is used as bathymetry to simulate the M89 experiment (See also paragraph A.3). The bed that was measured by the limni meter is more smooth and this bathymetry (see Figure B-8) is used for the equilibrium-bed simulation.

The measured bathymetry starts 6.5 m upstream of the bend entrance and stops 3.5 m downstream of the bend exit. Because the grid used for some of the simulation covered a larger range, the bathymetry is extrapolated. At the downstream end this extension was only 0.3 m. At the upstream end the extension is about 2.5 m. Because the bathymetry shows less variation at this side, it is expected that it has minor influence on the results.

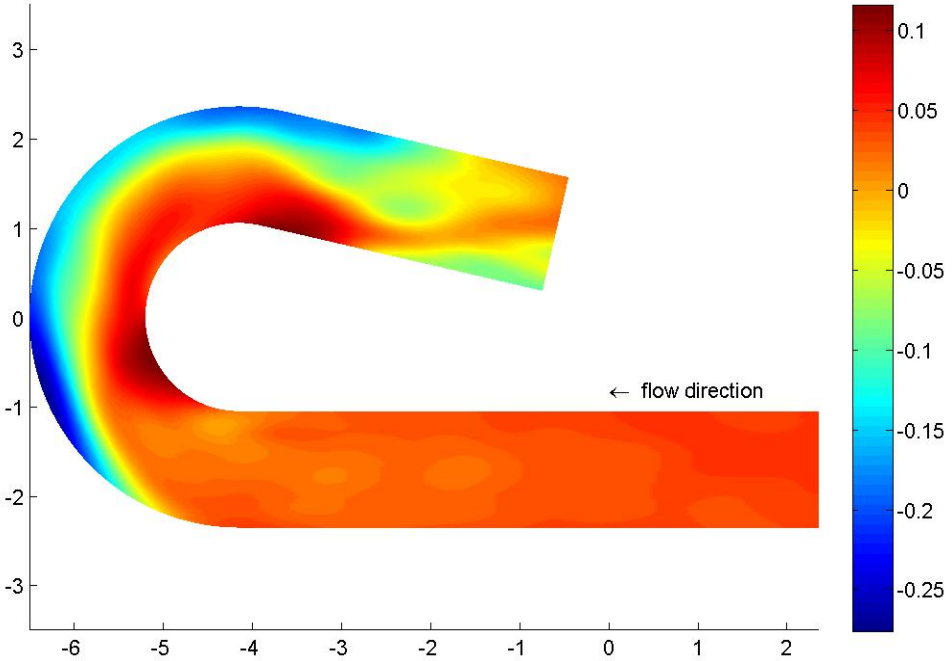

Figure B-8 Bottom topography, equilibrium-bed, measured with limni meter

B.4 Viscosity and turbulence

B.4.1 Viscosity (background eddy viscosity)

Turbulence and the eddy viscosity are strongly related. In Delft3D-FLOW you have to specify a closure model for the turbulent stresses. Besides that, you have to specify a background eddy viscosity whereas the horizontal background eddy viscosity should be an order of magnitude larger than the vertical eddy viscosity calculated by the closure model. The total vertical eddy viscosity is determined by adding up the vertical background viscosity and the by the turbulence model calculated viscosity. The horizontal eddy viscosity coefficients are determined by adding up a 2D-turbulence part, a 3D-turbulence part (determined by the closure model) and the background molecular viscosity. The 2D-turbulence part is in this case included in the background viscosity.

To see how the background eddy viscosity affects the solution, the simulations Q89_1_D3Da and Q89_1_D3Dc are compared. Simulation Q89_1_D3Da has a horizontal background eddy viscosity of 10^{-4} m^2/s and a vertical eddy viscosity of 10^{-5} m^2/s while for simulation Q89_1_D3Dc both the horizontal and vertical background eddy viscosity are 10^{-2} m^2/s. Both simulations made use of the k-ε closure model. The results are shown in Figure B-9. The higher background viscosity of simulation Q89_1_D3Dc results in a much steeper water level gradient. The flow seems to be very viscous. All gradients are smoothed. The results according to simulation Q89_1_D3Da are more equal to the measurements than the results of simulation Q89_1_D3Dc.

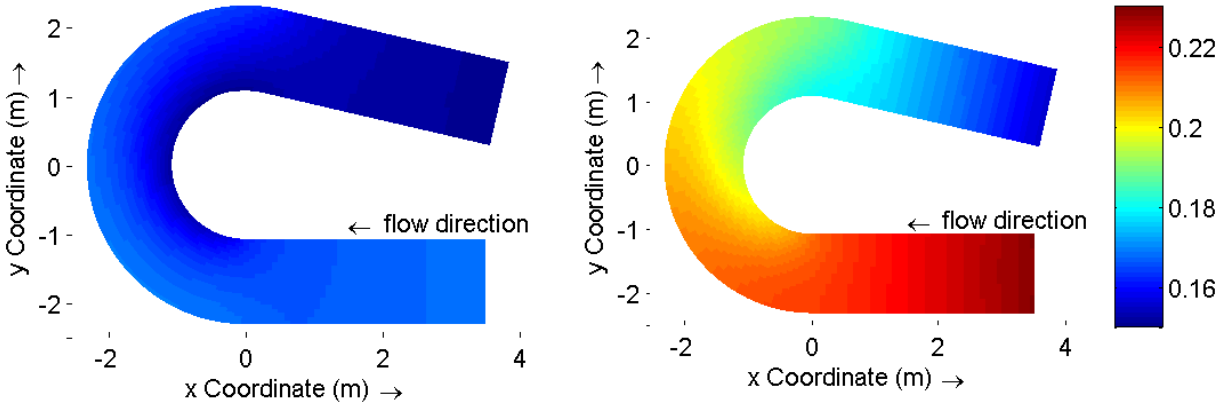

Figure B-9 Water level of simulation Q89_1_D3Da (left, low viscosity) and Q89_1_D3Dc (right, high viscosity)

B.4.2 Turbulence models

Three different turbulence closure models are compared namely the algebraic model (Q89_1_D3Dg), the k-L model (Q89_1_D3Dh) and the k-ε model (Q89_1_D3Df). The k-ε model is the most advanced model available in Delft3D-FLOW at the moment. The results are shown in

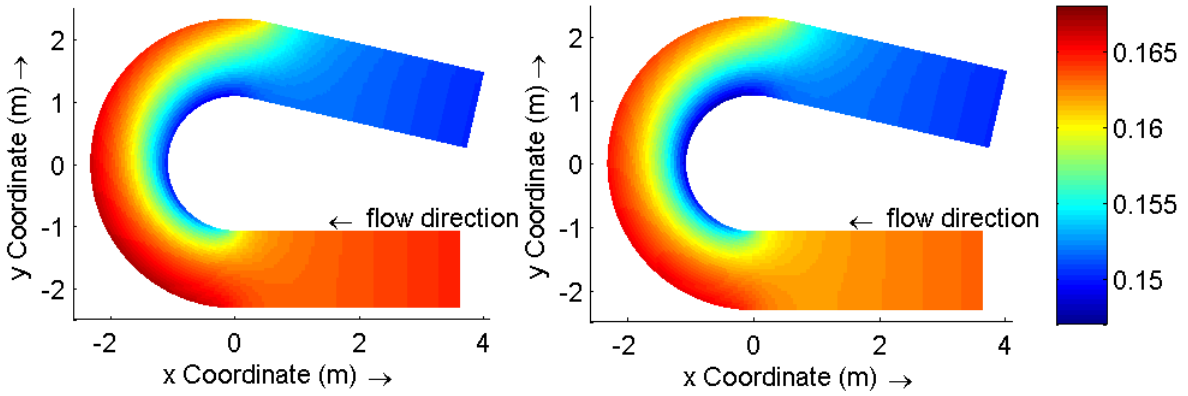

Figure B-10 Water level of simulation Q89_1_D3Df (left, k-ε model) and Q89_1_D3Dg (algebraic)

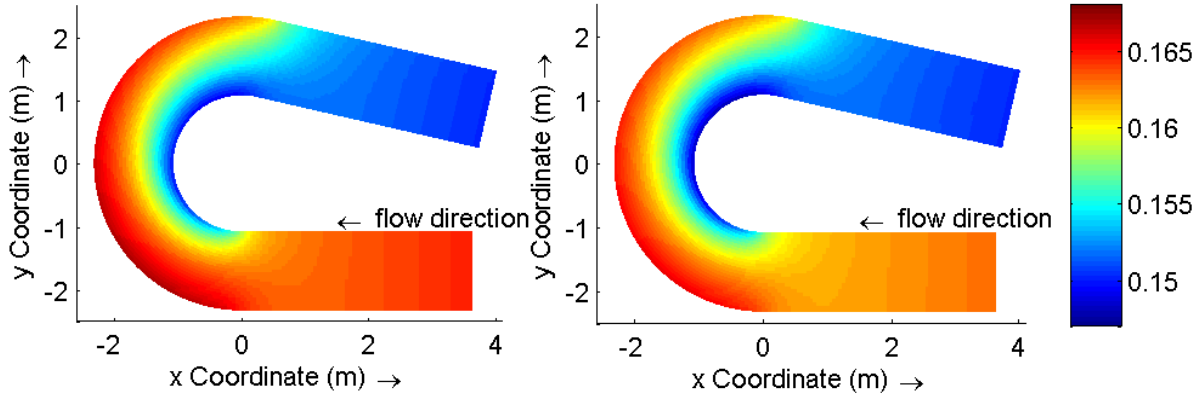

Figure B-11 Water level of simulation Q89_1_D3Df (left, k-ε model) and Q89_1_D3Dh (k-L model)

From the comparison of the water levels (Figure B-10 and Figure B-11) it is visible that both the algebraic and k-L closure model give somewhat lower water levels at the entrance of the flume than the k-ε model does. The difference in water level is only 1 mm and the k-ε model is the most advanced model, so the k-ε model is used in the simulations.

B.5 Roughness

The roughness is a very important parameter because the flow is mainly determined by the gravitational force and this force is opposed by the resistance of the walls. The resistance is mainly determined by the roughness of the wall.

According to Jansen *et al*. (1979), a wall is called hydraulically smooth if δ is smaller than the roughness (k). δ is estimated as follows:

$$\delta = 11.6 * \frac{\nu}{u_*}$$

For the Q89 case this results in $\delta = 2.9 * 10^{-4}$ m and k_s is about $6 * 10^{-3}$ m ($u_* = 0.040$ m/s) (Blanckaert, 2002, section IV.8). This means that the flow at the wall is classified as hydraulically rough.

For the case with the equilibrium-bed, this results in $\delta = 2.37 * 10^{-4}$ m and k_s is $6.4 * 10^{-3}$ m ($u_* = 0.049$ m/s (Blanckaert, 2009) and $\nu = 1 * 10^{-6}$ m^2/s). This means that the flow at the wall can be classified as hydraulically rough.

For hydraulically rough conditions, z_0 is determined by:

$$z_0 \simeq k/33 \text{ if } k > 70\frac{\nu}{u_*}$$

B.5.1 Bottom roughness

The bottom roughness is varied in the simulations Q89_1_D3De (k_s = 0.006 m) and simulation Q89_1_D3Df (k_s = 0.003 m). As can be seen from Figure B-12, the flow with the higher roughness shows an increased water level gradient. The increase of the roughness causes an increase of the resistance and because the same amount of water has to be discharged, the driving force (the water level gradient) increases.

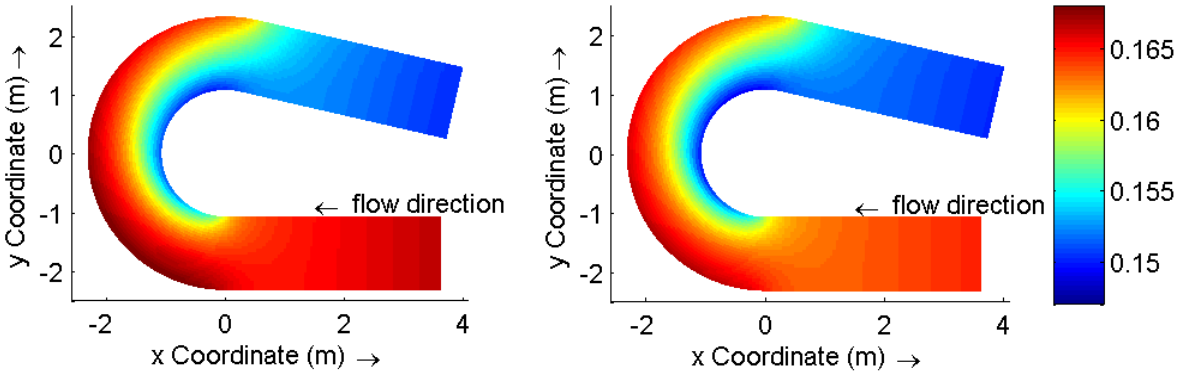

Figure B-12 Water level, simulation Q89_1_D3De (left, k_s = 0.006 m) and Q89_1_D3Df (right, k_s = 0.003 m)

Reduction of the transverse bottom roughness (simulation Q89_1_D3Dm and Q89_1_D3Dn) results in an increase of the water level gradient. This increase of the downstream water level gradient can be explained by the fact that the downstream velocity profile will be more flattened. Because the bottom resistance in the transverse direction decreases, the secondary flow increases. This increase of the secondary flow and the concomitant increase of the advective transport of momentum will cause a flattening of the downstream velocity profile (Blanckaert, 2002, section IV.4). This in its case will result in more downstream resistance and thus an increase of the downstream water level gradient.

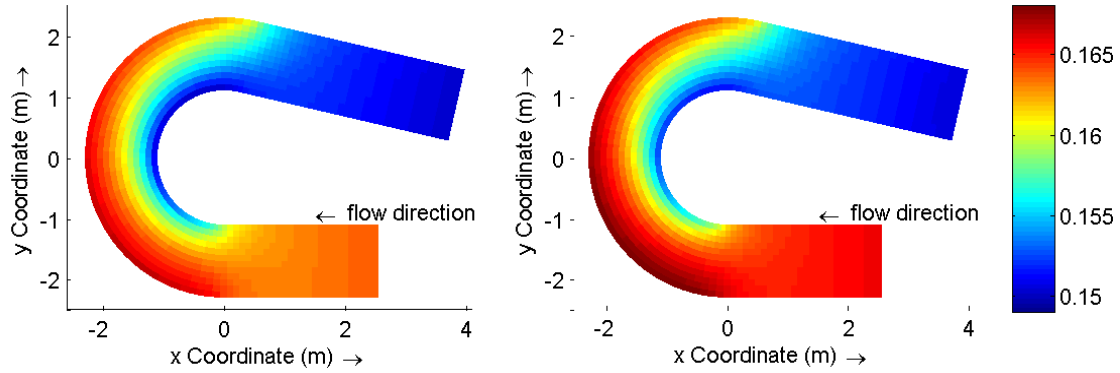

Figure B-13 Water level, simulation Q89_1_D3Dm (left, transverse z_0 = 0.0001), Q89_1_D3Dn (right, transverse z_0 = 0.00001)

B.5.2 Wall roughness

In Delft3D-FLOW, the following options can be selected to model the effect of the wall on the flow:

Free slip : No tangential shear stress at the wall

No slip : Zero velocity at the wall

Partial slip : This is the way in between *Free slip* and *No slip*. You have to define a z_0 value which represent the distance from the wall where the velocity is reduced to zero.

Simulation Q89_1_D3Db is a *Free slip* case and simulation Q89_1_D3Dd is a *No slip* case. It is visible that the flow in simulation Q89_1_D3Dd experiences more resistance than according to simulation Q89_1_D3Db (Figure B-14). Especially the water level along the outer wall increases but also at the entrance of the flume. It is difficult to compare the wall region with the measurements but it is more likely that the flow behaviour is like predicted in simulation Q89_1_D3Db (*Free slip*) because the walls are made of Plexiglas.

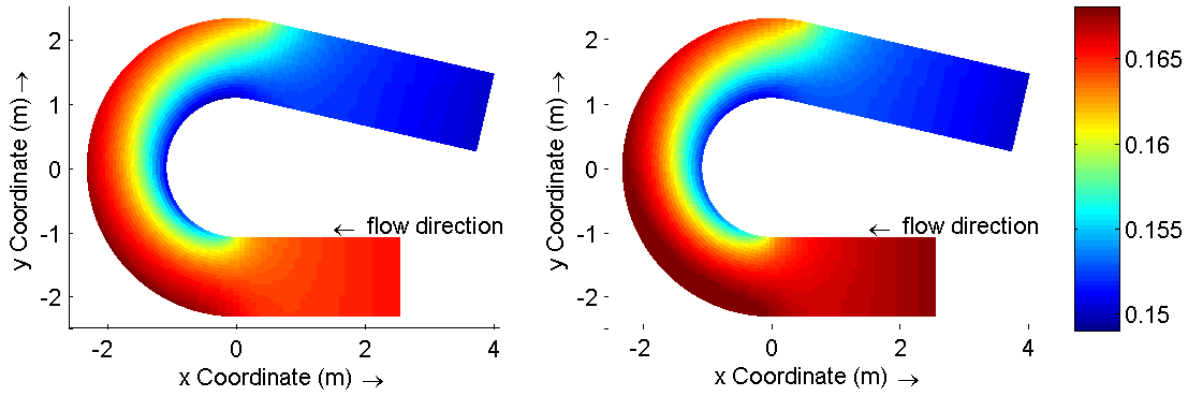

Figure B-14 Water level, simulation Q89_1_D3Db (left, free slip) and Q89_1_D3Dd (right, no slip)

Appendix C Figures Q89 results

In this appendix are many figures given of several quantities. Where needed, the data is interpolated. These interpolations are all linear interpolations. Most quantities are normalized. Important information of the figures is written in the captions and at the start of each paragraph.

C.1 Downstream profiles

The profiles shown in this paragraph represent the downstream velocity profiles per cross-section, starting at the m25 cross-section till the last measured cross-section (p35) in the straight outflow. The '*-0.5*' above the first subplot means the location at 0.5 m from the centre line towards the inner bend and the positive numbers give the distances from the centre line to the outer bend. The profiles are plotted for the measurements, the Q89_LES and the Delft3D-FLOW simulation Q89_1_D3D. The green lines represent the 10 % band width of the measuring error. It has to be said that the measurements near the bottom are more affected by noise and uncertainty than the velocity in the upper part of the flow, as said in paragraph 5.4, but this is not visible in the green lines.

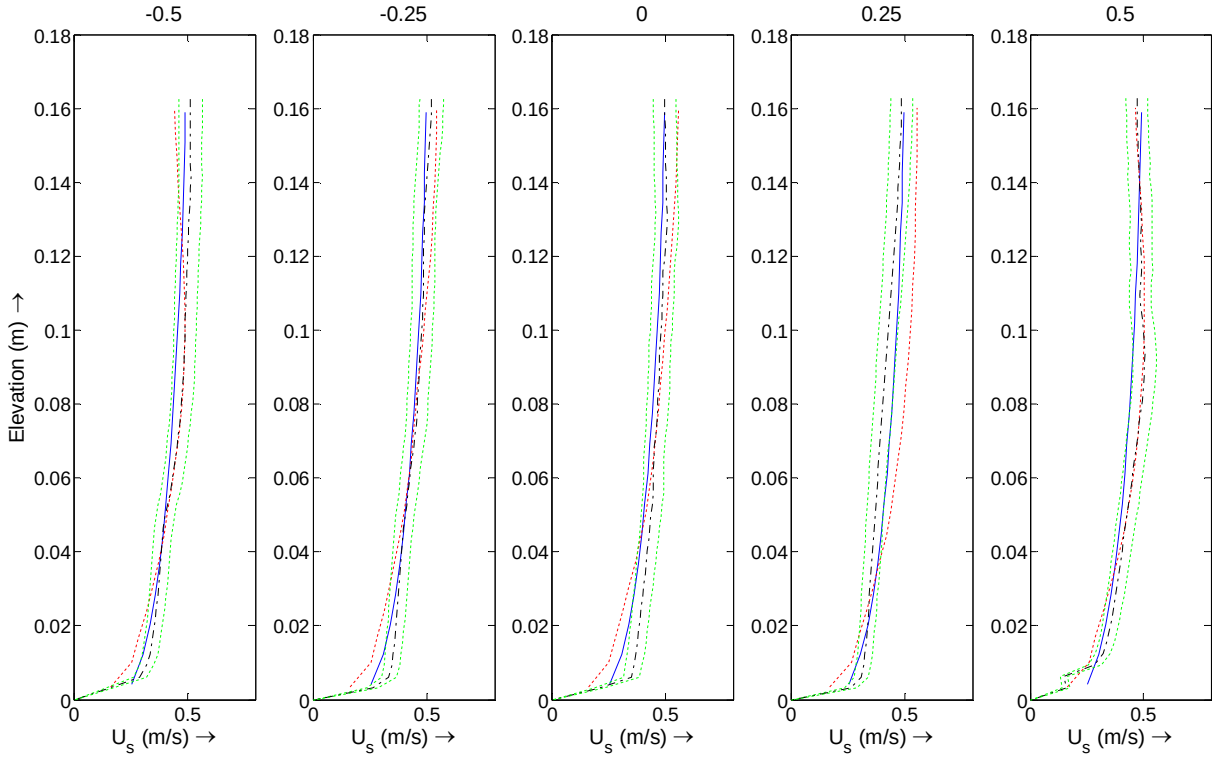

Figure C-1 Downstream velocity profiles over the depth at m25 [black -. = measurement; red := Q89_LES; blue -= simulation Q89_1_D3D; green := 10% margin of measurements]

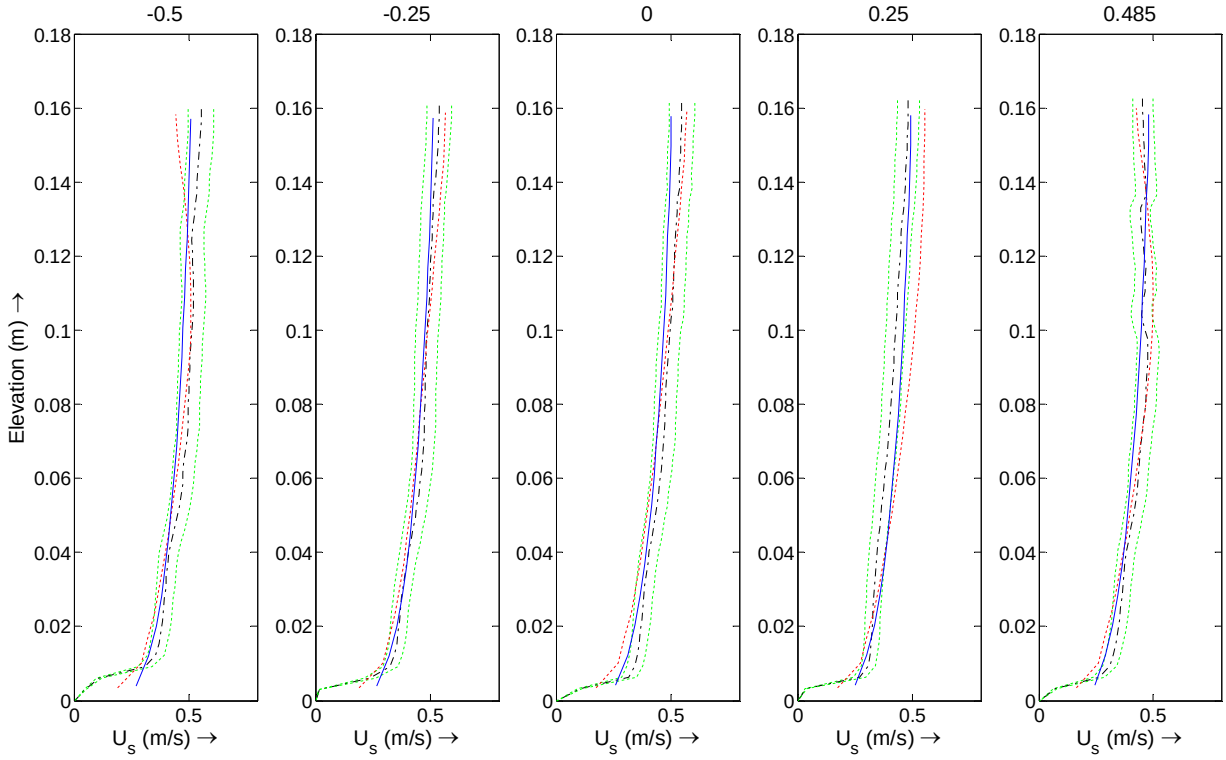

Figure C-2 Downstream velocity profiles over the depth at m05 [black -. = measurement; red := Q89_LES; blue -= simulation Q89_1_D3D; green := 10% margin of measurements]

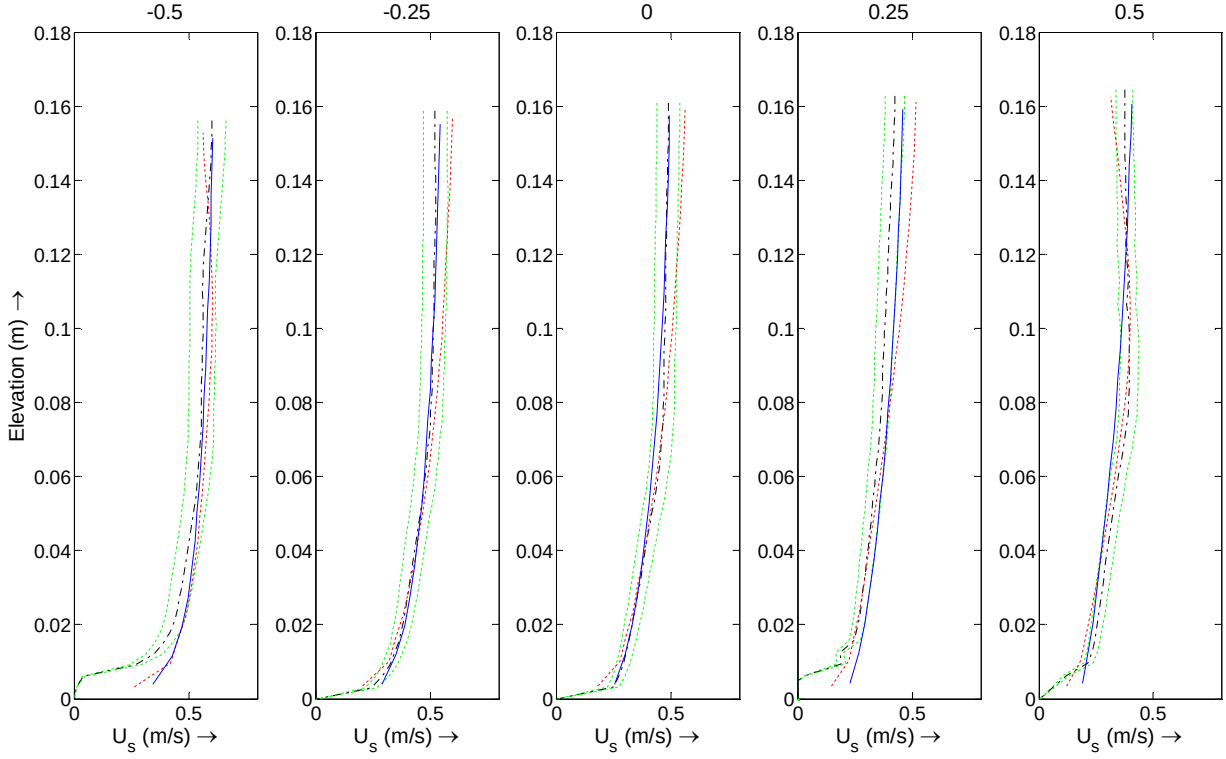

Figure C-3 Downstream velocity profiles over the depth at 15 [black -. = measurement; red := Q89_LES; blue -= simulation Q89_1_D3D; green := 10% margin of measurements]

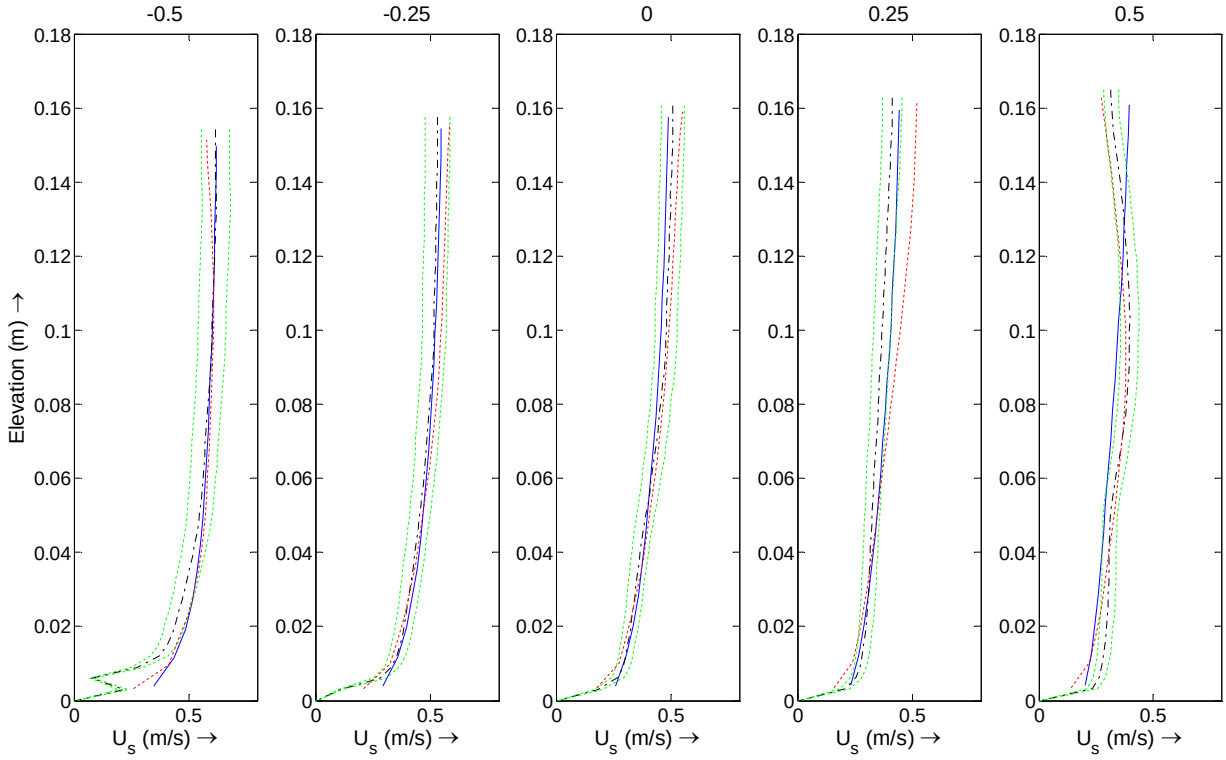

Figure C-4 Downstream velocity profiles over the depth at 30 [black -. = measurement; red := Q89_LES; blue -= simulation Q89_1_D3D; green := 10% margin of measurements]

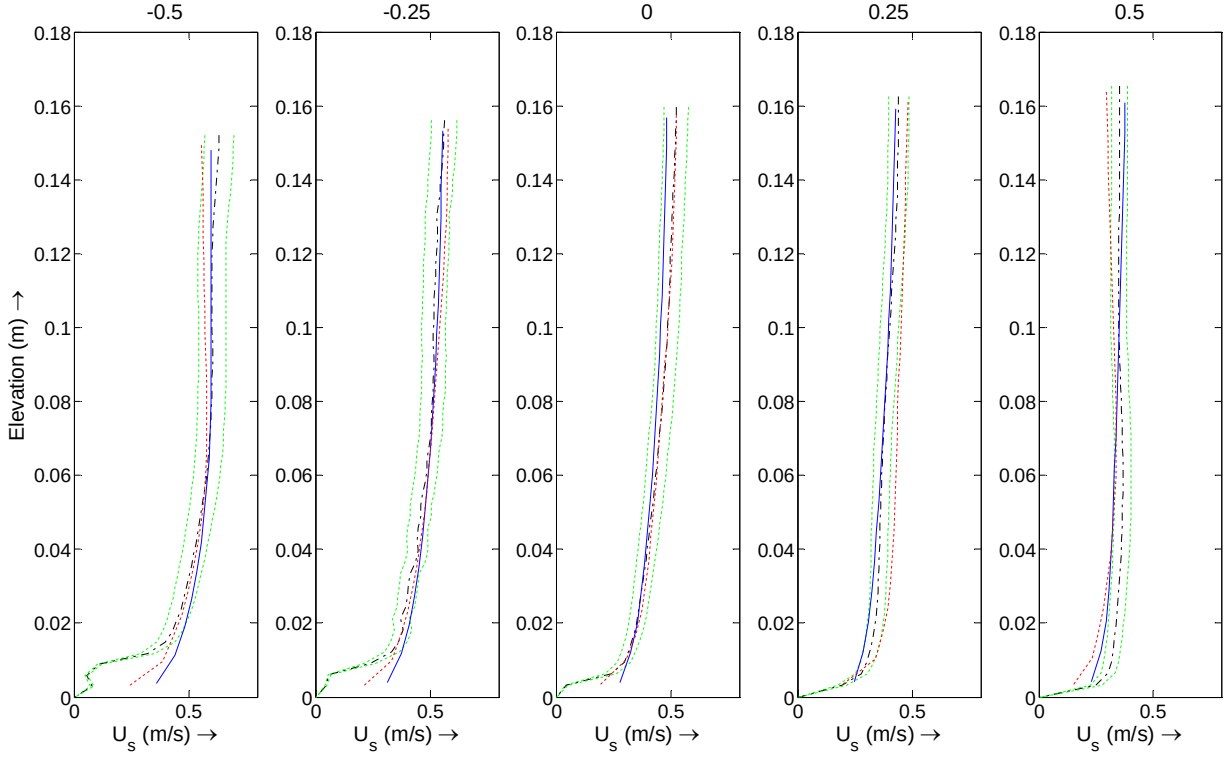

Figure C-5 Downstream velocity profiles over the depth at 60 [black -. = measurement; red := Q89_LES; blue -= simulation Q89_1_D3D; green := 10% margin of measurements]

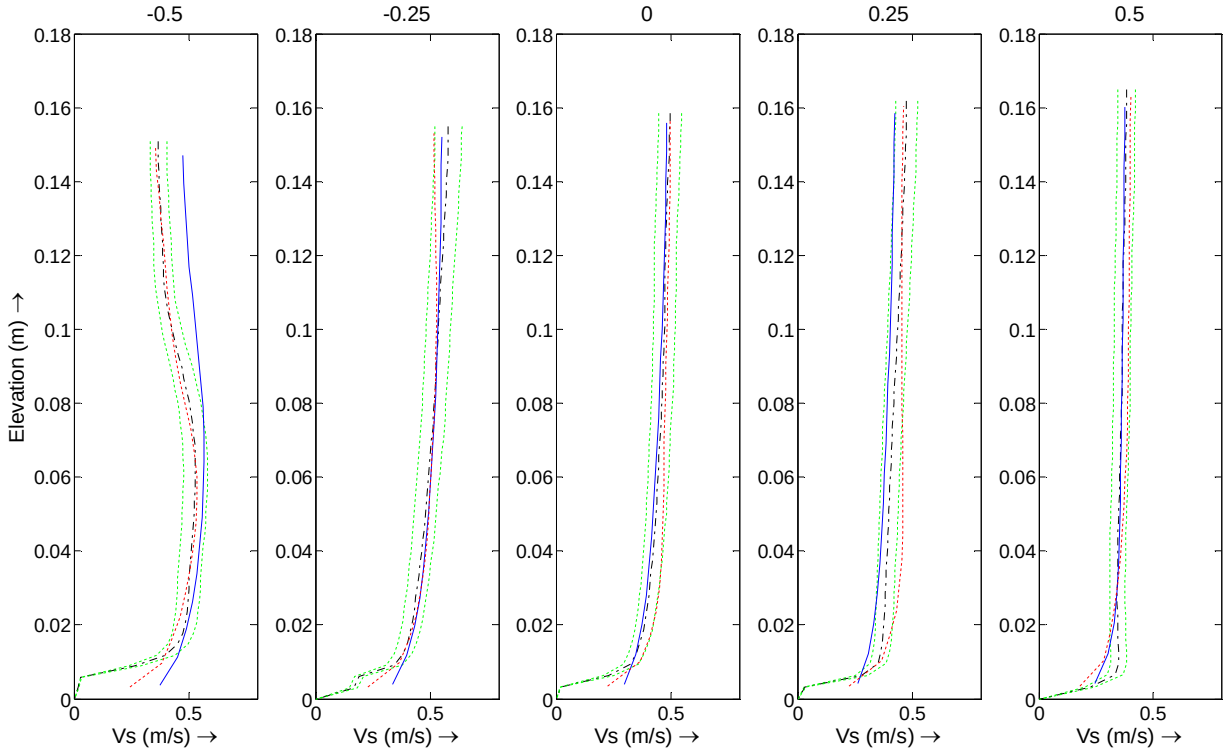

Figure C-6 Downstream velocity profiles over the depth at 90 [black -. = measurement; red := Q89_LES; blue -= simulation Q89_1_D3D; green := 10% margin of measurements]

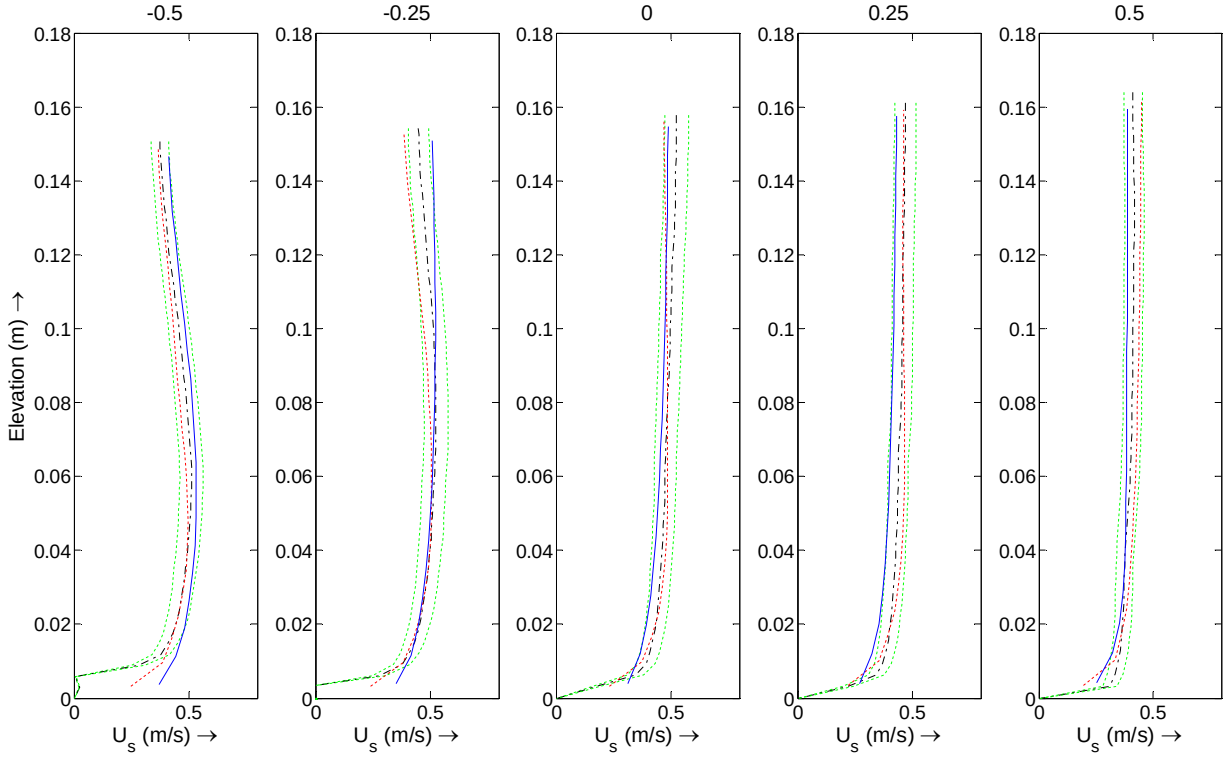

Figure C-7 Downstream velocity profiles over the depth at 120 [black -. = measurement; red := Q89_LES; blue -= simulation Q89_1_D3D; green := 10% margin of measurements]

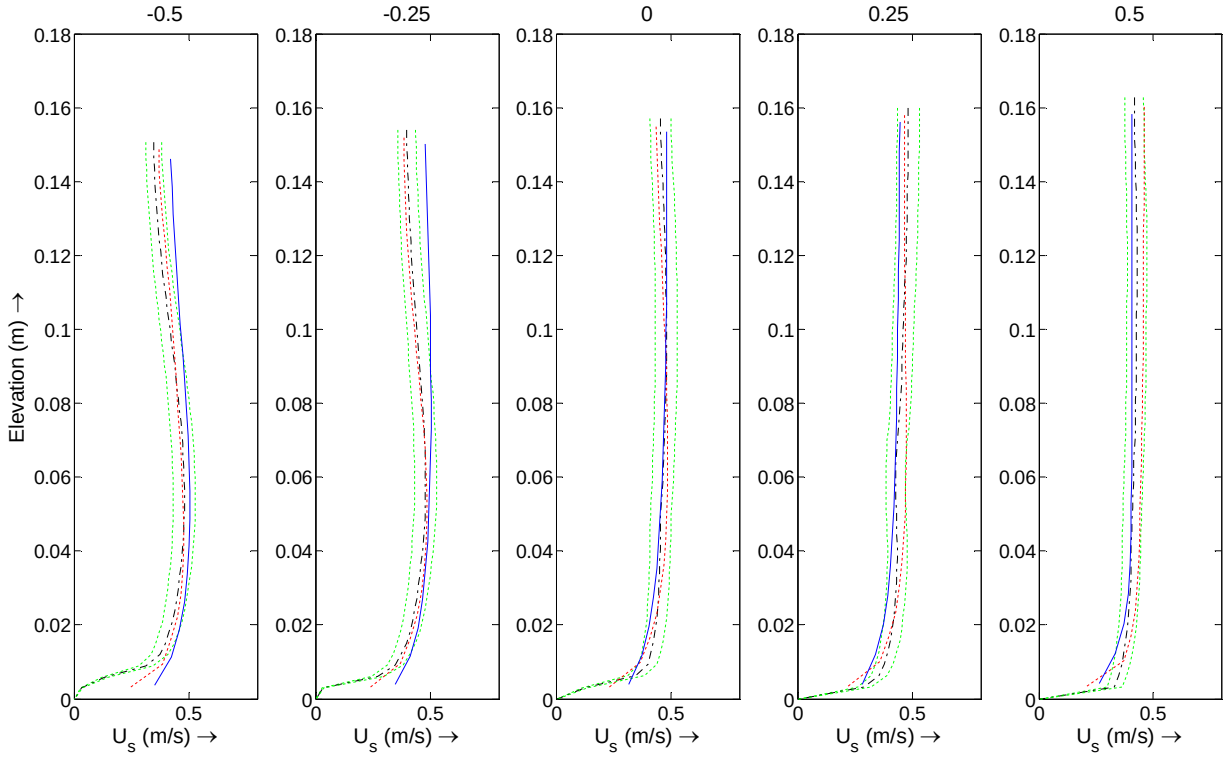

Figure C-8 Downstream velocity profiles over the depth at 150 [black -. = measurement; red := Q89_LES; blue -= simulation Q89_1_D3D; green := 10% margin of measurements]

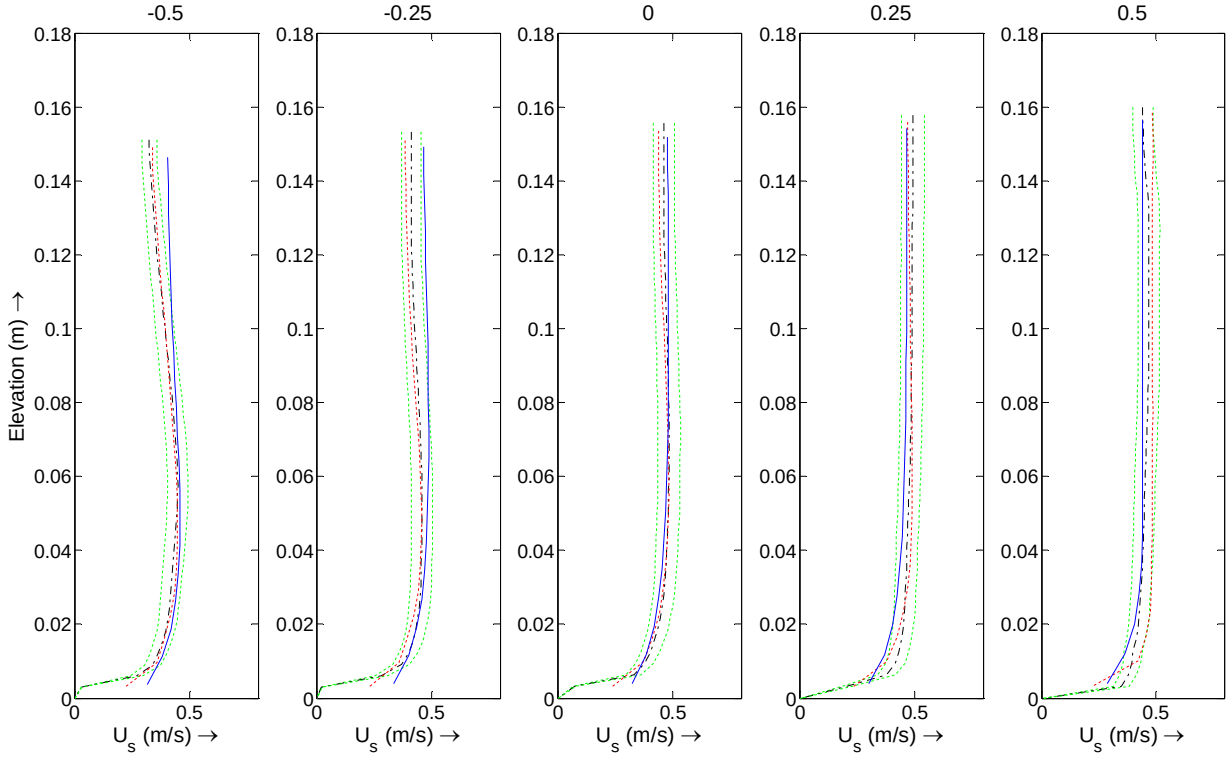

Figure C-9 Downstream velocity profiles over the depth at 180 [black -. = measurement; red := Q89_LES; blue -= simulation Q89_1_D3D; green := 10% margin of measurements]

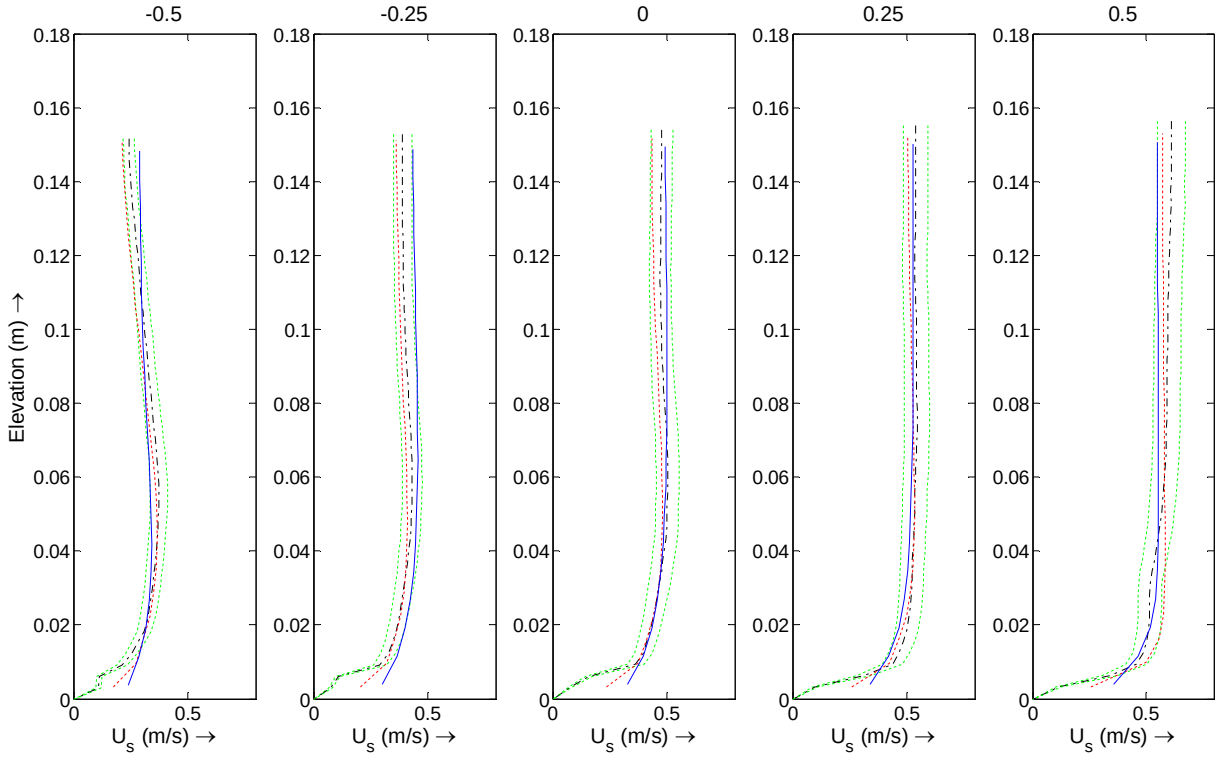

Figure C-10 Downstream velocity profiles over the depth at p05 [black -. = measurement; red := Q89_LES; blue -= simulation Q89_1_D3D; green := 10% margin of measurements]

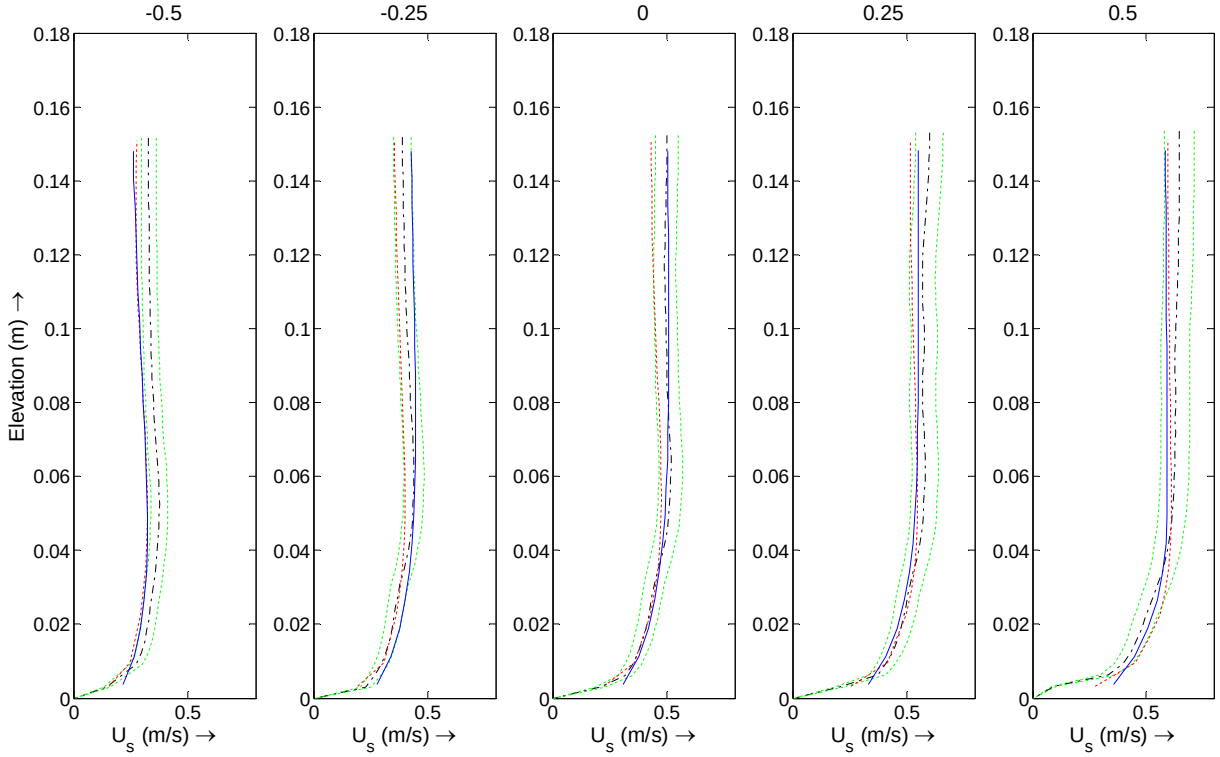

Figure C-11 Downstream velocity profiles over the depth at p15 [black -. = measurement; red := Q89_LES; blue -= simulation Q89_1_D3D; green := 10% margin of measurements]

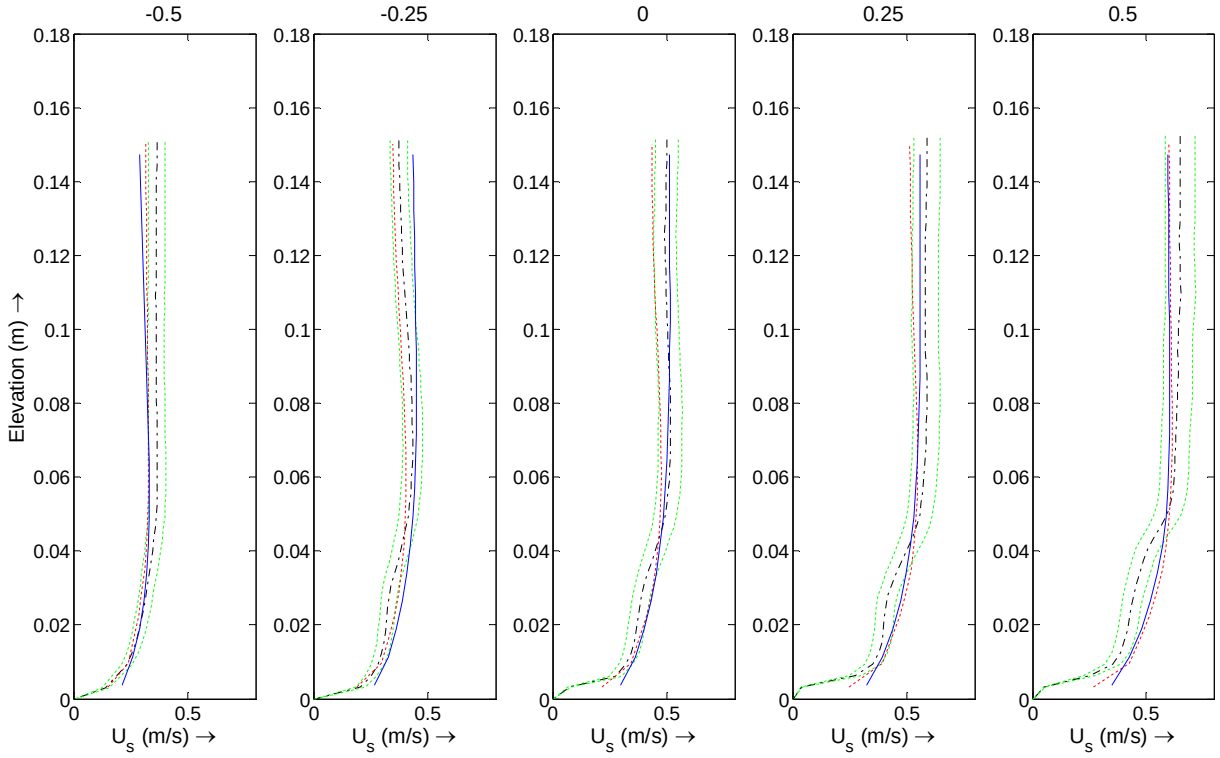

Figure C-12 Downstream velocity profiles over the depth at p25 [black -. = measurement; red := Q89_LES; blue -= simulation Q89_1_D3D; green := 10% margin of measurements]

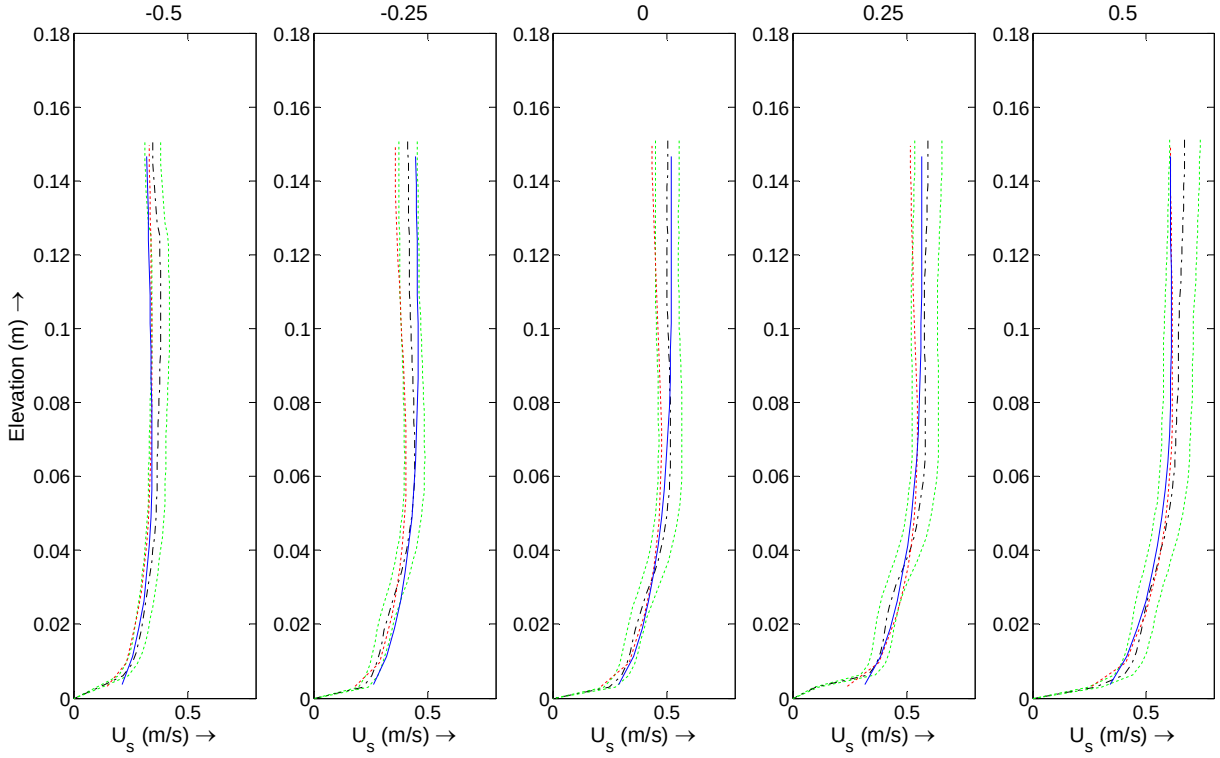

Figure C-13 Downstream velocity profiles over the depth at p35 [black -. = measurement; red := Q89_LES; blue -= simulation Q89_1_D3D; green := 10% margin of measurements]

C.2 Transverse profiles

The profiles shown in this paragraph represent the transverse velocity profiles per cross-section, starting at the m25 cross-section till the last measured cross-section (p35) in the

straight outflow. The '*-0.5*' above the first subplot means the location at 0.5 m from the centre line towards the inner bend and the positive numbers give the distances from the centre line to the outer bend. The profiles are plotted for the measurements, the Q89_LES and the Delft3D-FLOW simulation Q89_1_D3D. The cyan line represents the line where the transverse velocity is zeros (the elevation axis).

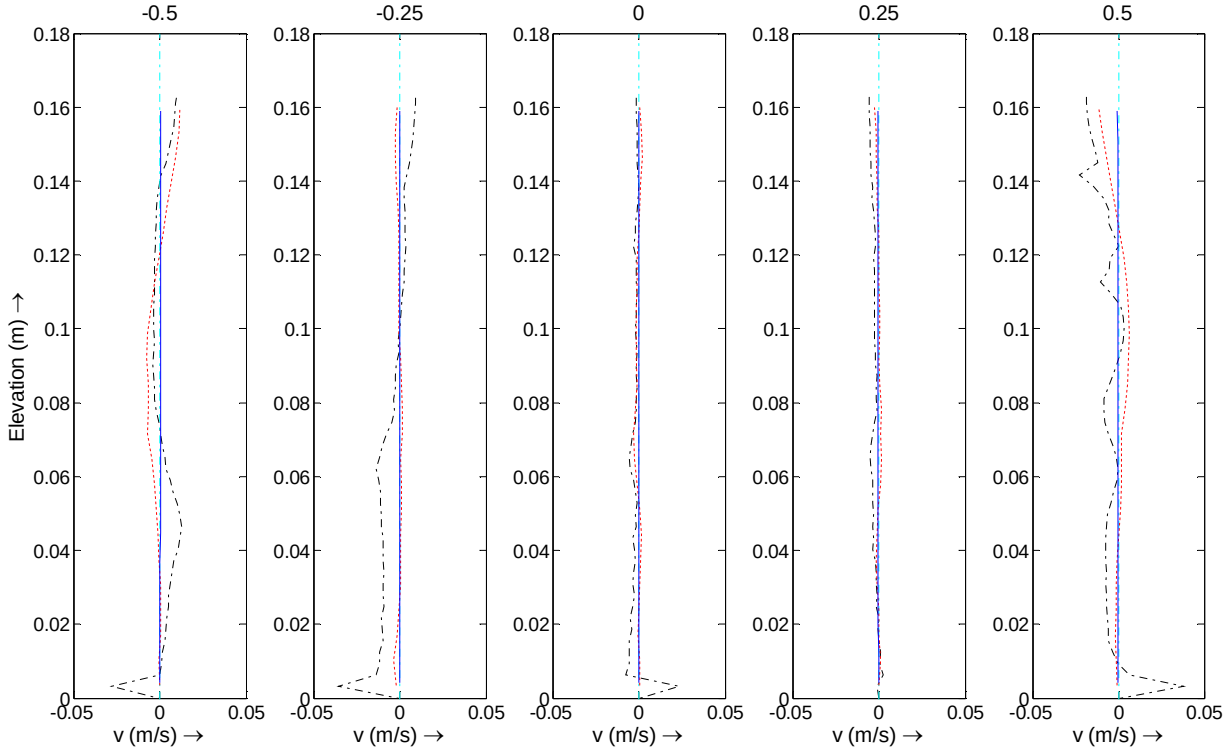

Figure C-14 Transverse velocity profiles over the depth at m25 [black -. = measurement; red := Q89_LES; blue -= simulation Q89_1_D3D]

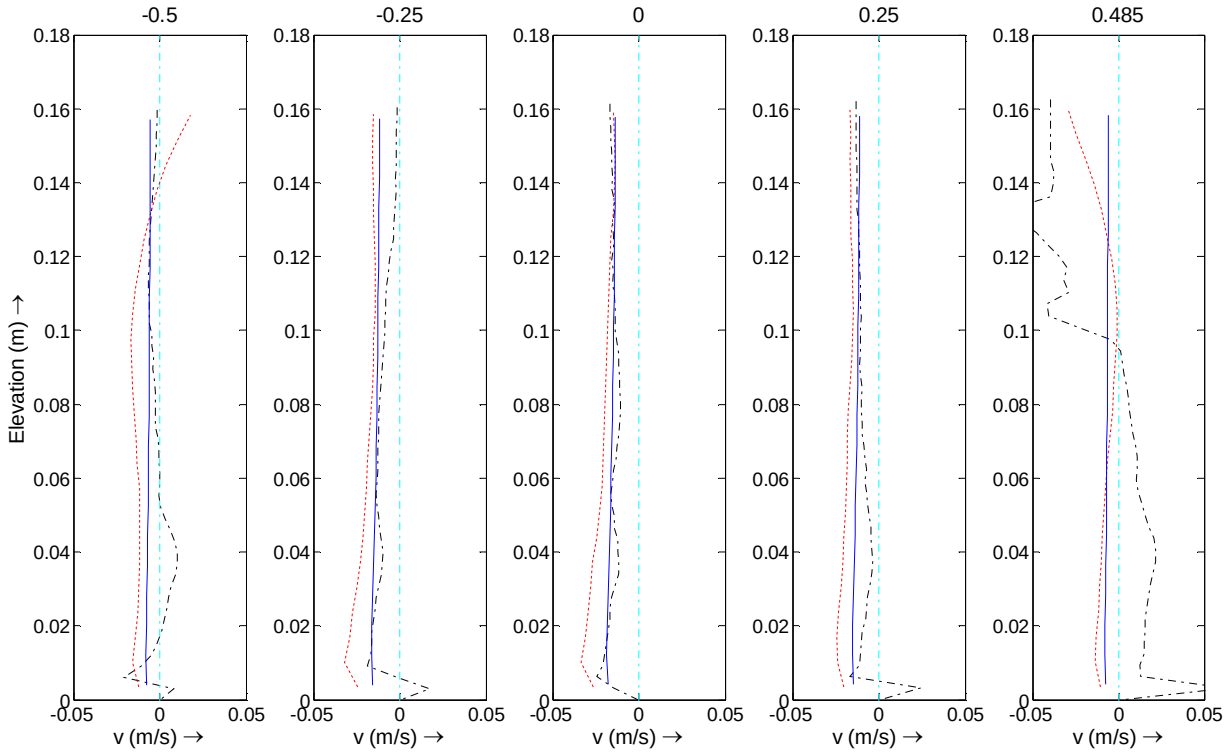

Figure C-15 Transverse velocity profiles over the depth at m05 [black -. = measurement; red := Q89_LES; blue -= simulation Q89_1_D3D]

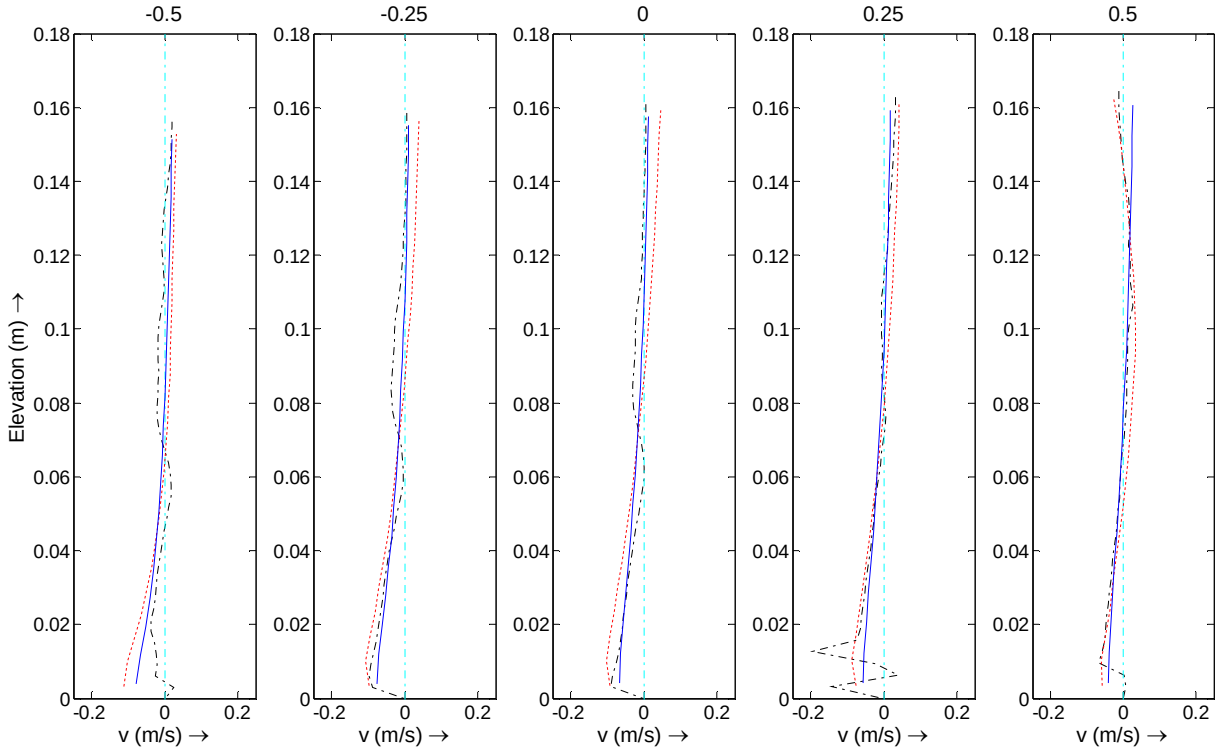

Figure C-16 Transverse velocity profiles over the depth at 015 [black -. = measurement; red := Q89_LES; blue -= simulation Q89_1_D3D]

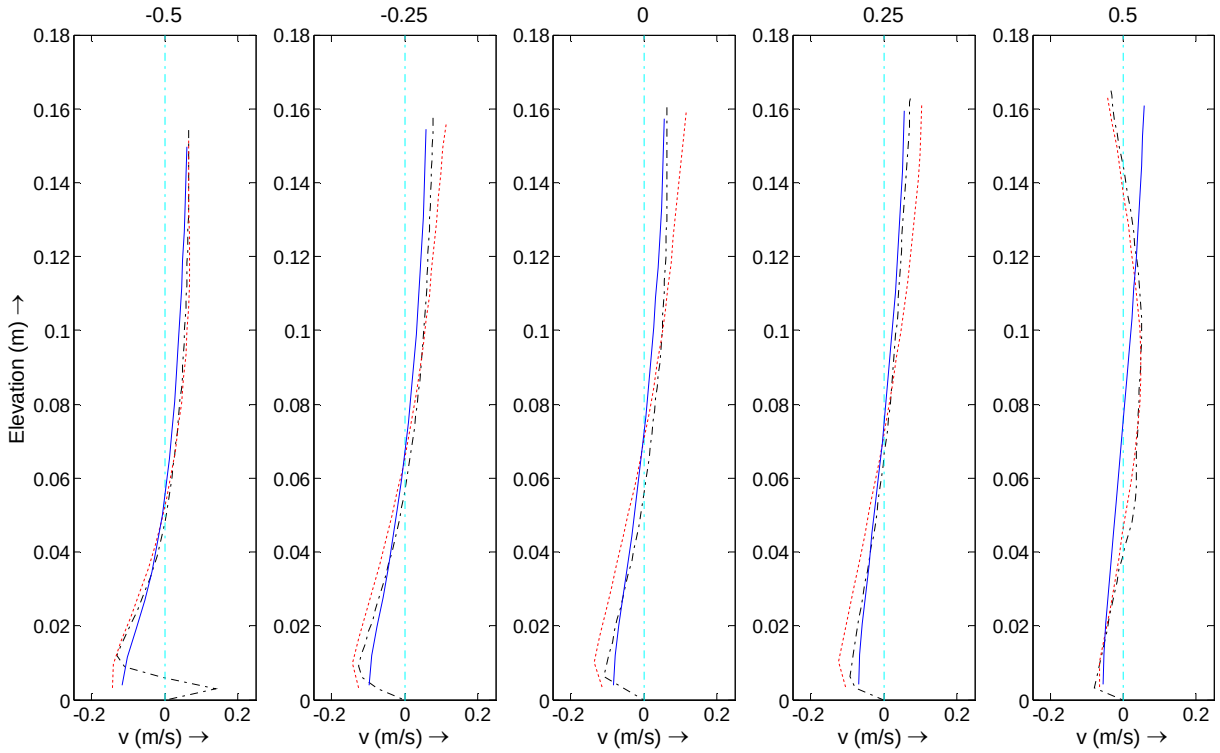

Figure C-17 Transverse velocity profiles over the depth at 030 [black -. = measurement; red := Q89_LES; blue -= simulation Q89_1_D3D]

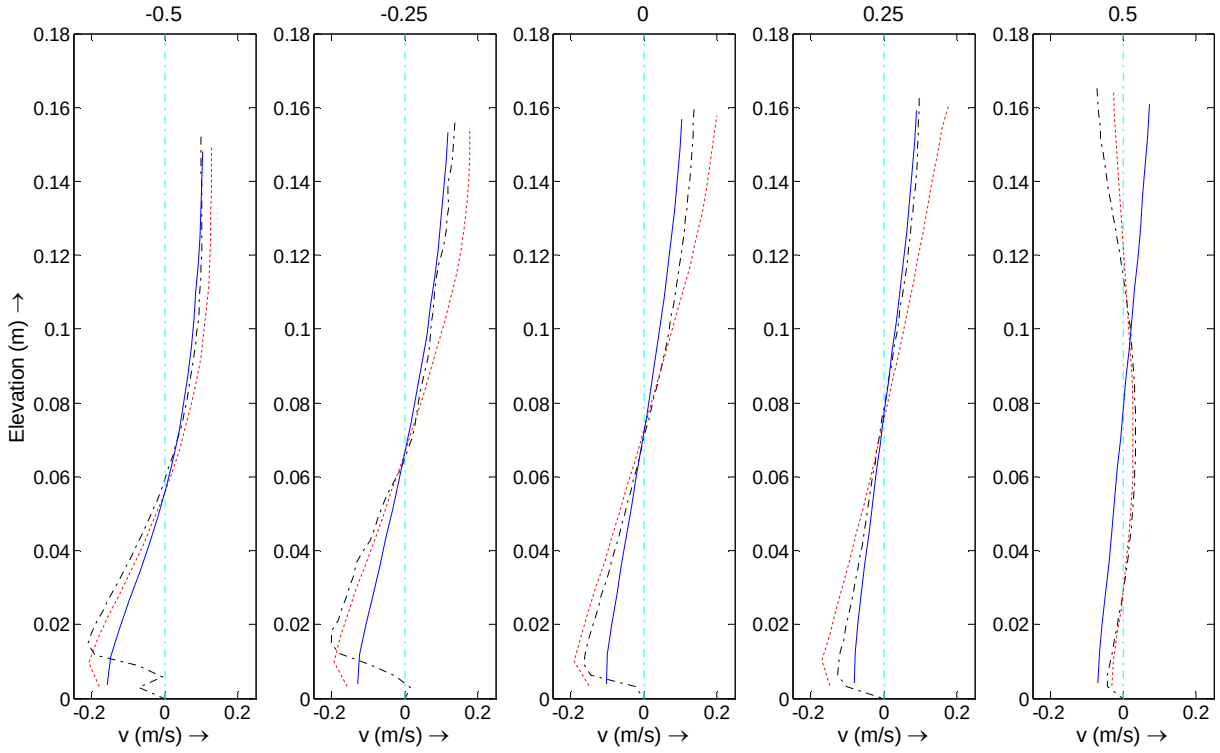

Figure C-18 Transverse velocity profiles over the depth at 060 [black -. = measurement; red := Q89_LES; blue -= simulation Q89_1_D3D]

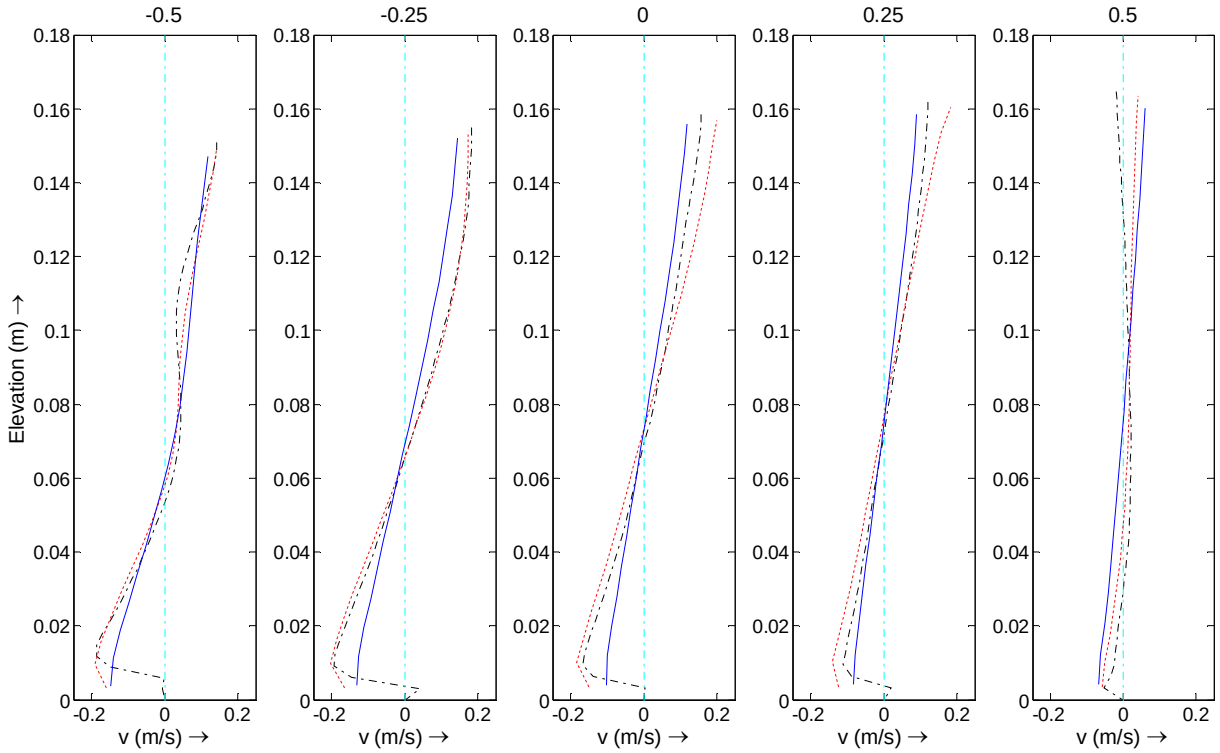

Figure C-19 Transverse velocity profiles over the depth at 090 [black -. = measurement; red := Q89_LES; blue -= simulation Q89_1_D3D]

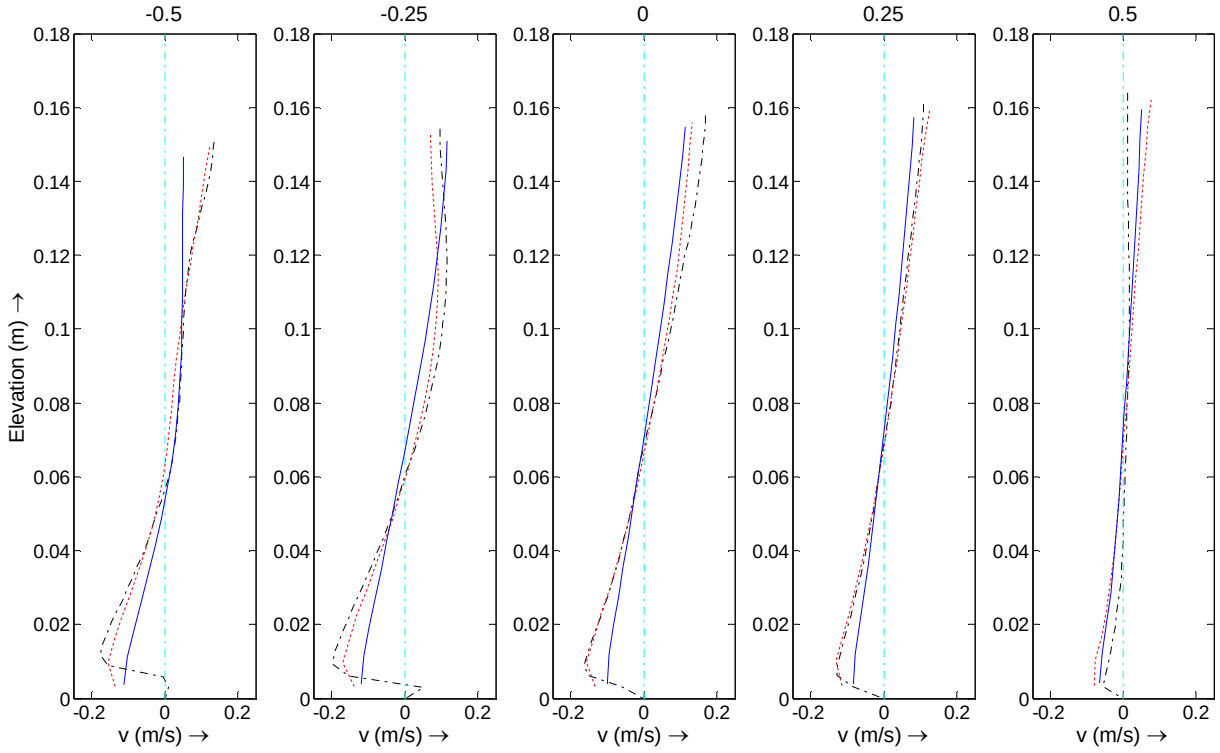

Figure C-20 Transverse velocity profiles over the depth at 120 [black -. = measurement; red := Q89_LES; blue -= simulation Q89_1_D3D]

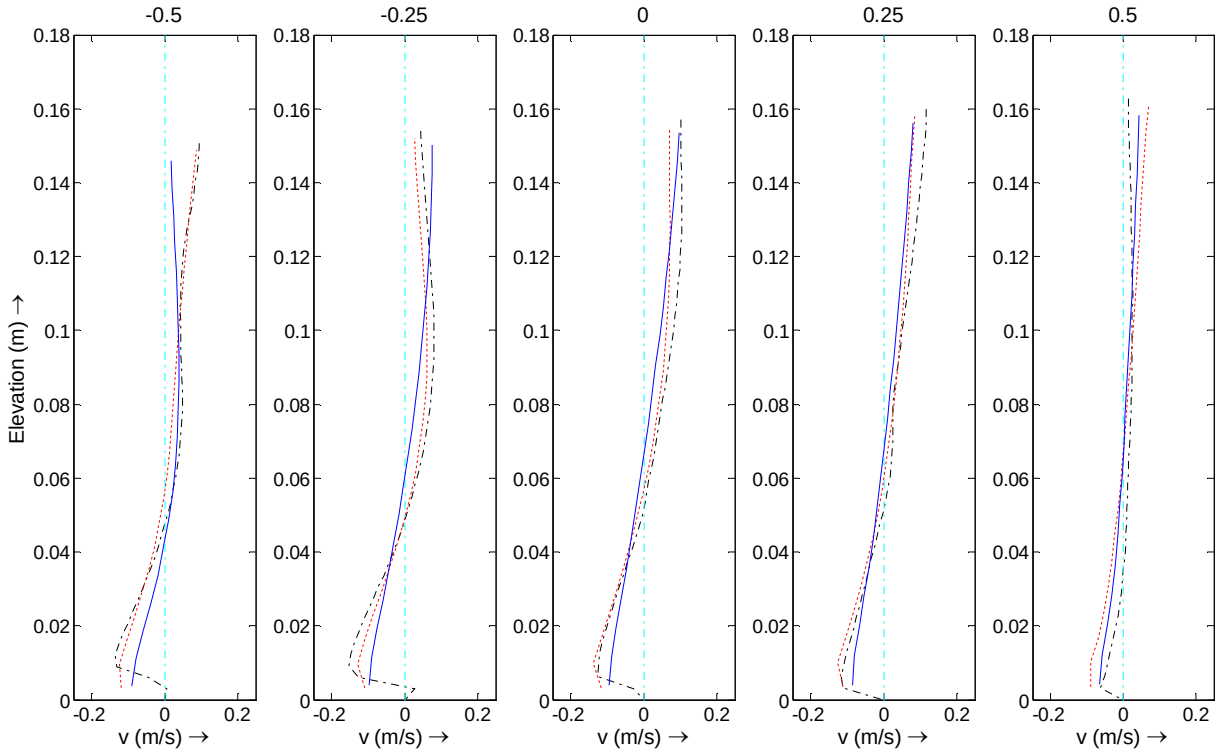

Figure C-21 Transverse velocity profiles over the depth at 150 [black -. = measurement; red := Q89_LES; blue -= simulation Q89_1_D3D]

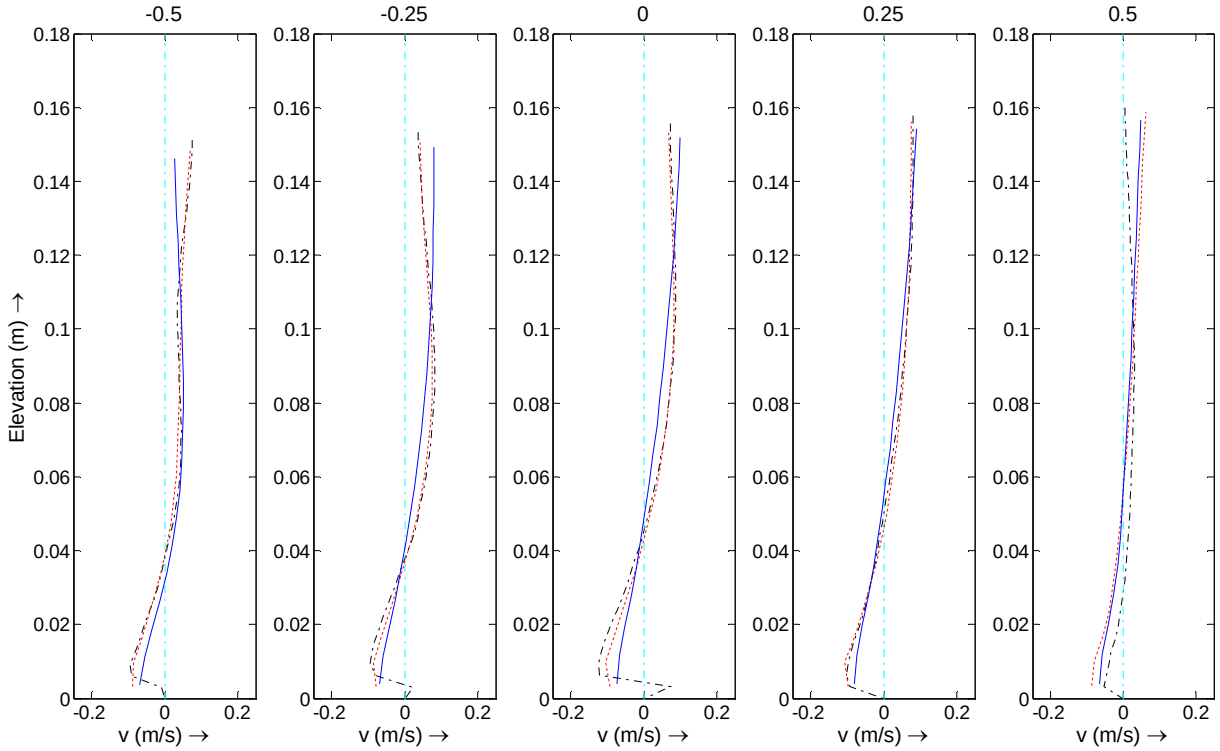

Figure C-22 Transverse velocity profiles over the depth at 180 [black -. = measurement; red := Q89_LES; blue -= simulation Q89_1_D3D]

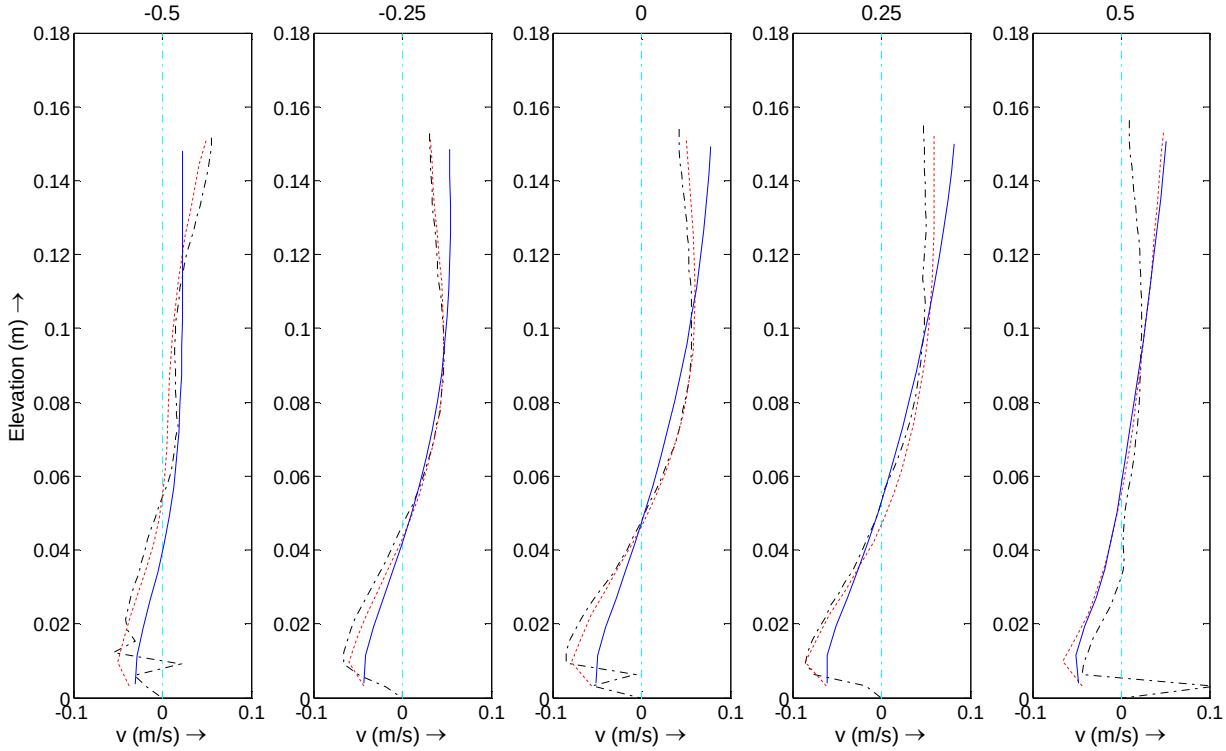

Figure C-23 Transverse velocity profiles over the depth at p05 [black -. = measurement; red := Q89_LES; blue -= simulation Q89_1_D3D]

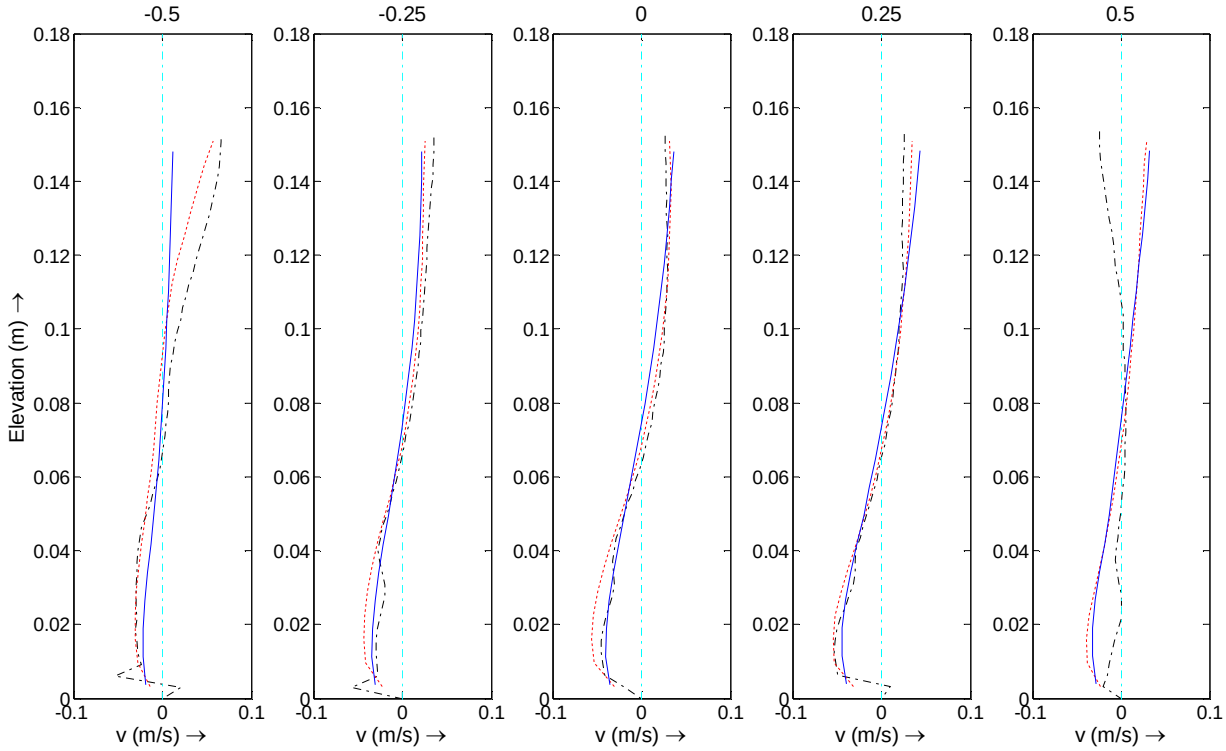

Figure C-24 Transverse velocity profiles over the depth at p15 [black -. = measurement; red := Q89_LES; blue -= simulation Q89_1_D3D]

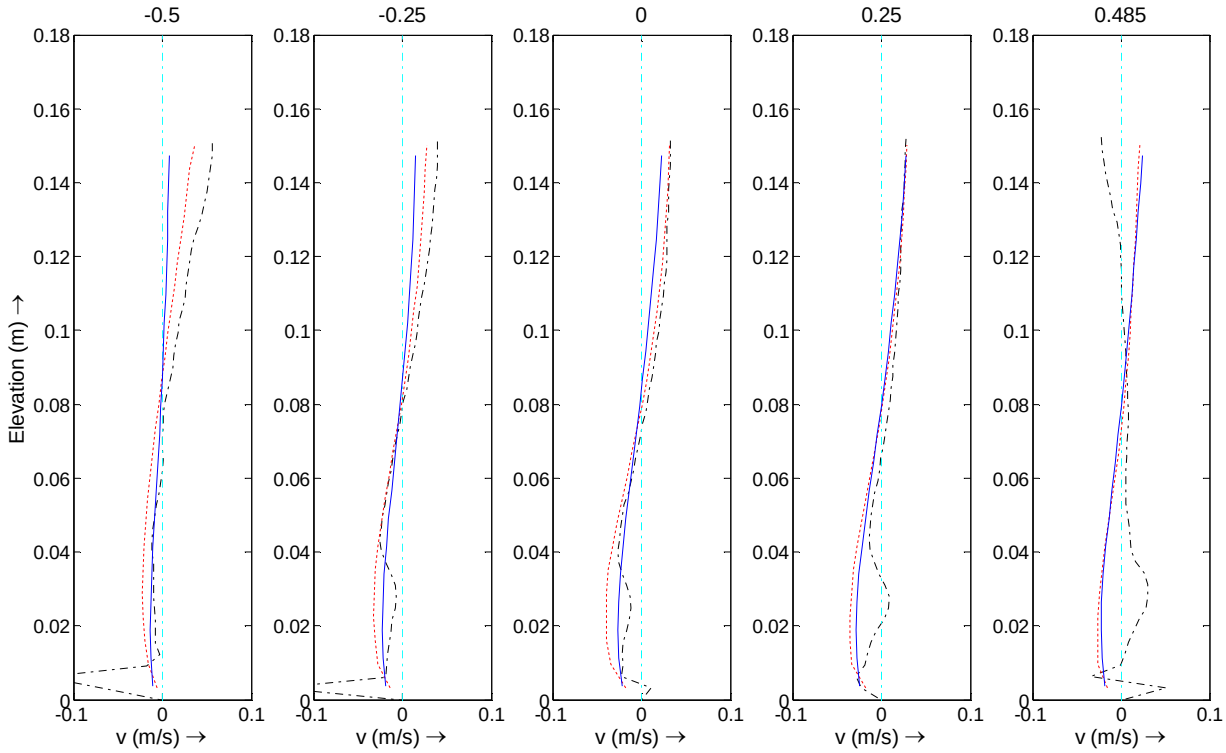

Figure C-25 Transverse velocity profiles over the depth at p25 [black -. = measurement; red := Q89_LES; blue -= simulation Q89_1_D3D]

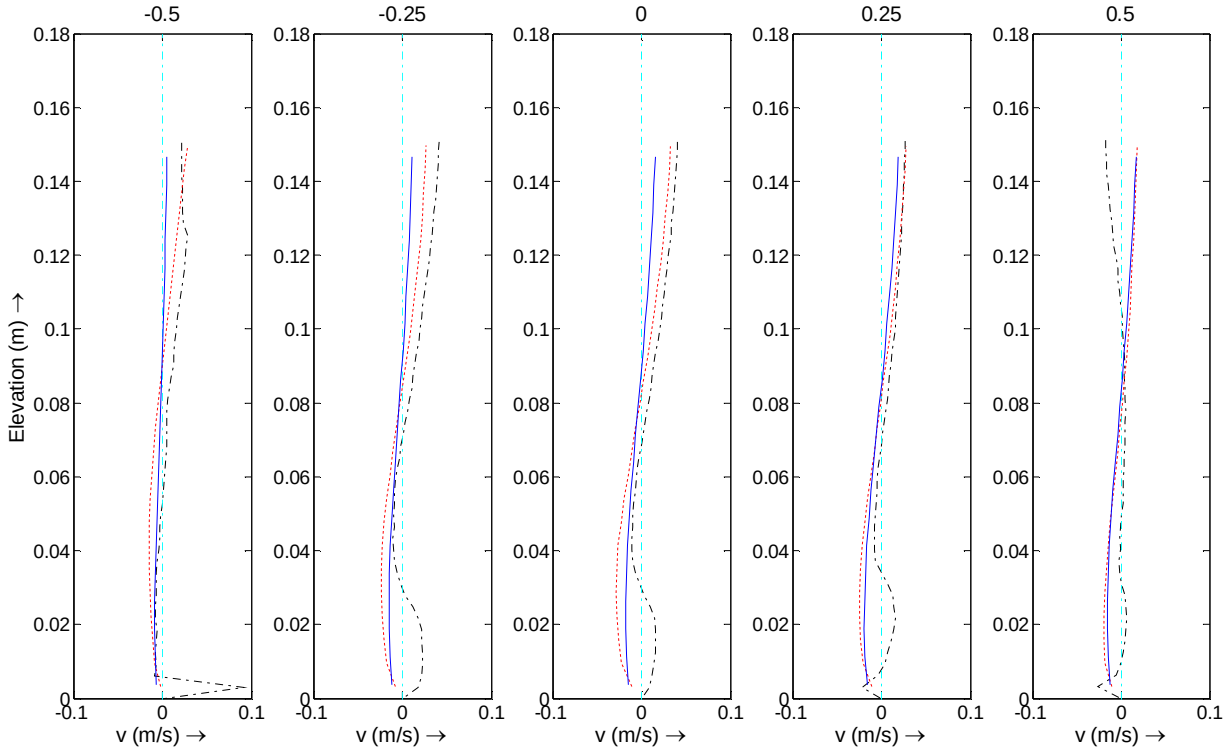

Figure C-26 Transverse velocity profiles over the depth at p35 [black -. = measurement; red := Q89_LES; blue -= simulation Q89_1_D3D]

C.3 Vertical velocities

The figures in this paragraph represent the vertical velocities in the cross-sections m25, 060 and 150 according to the measurements, the Q89_LES and Delft3D-FLOW simulation Q89_1_D3D.

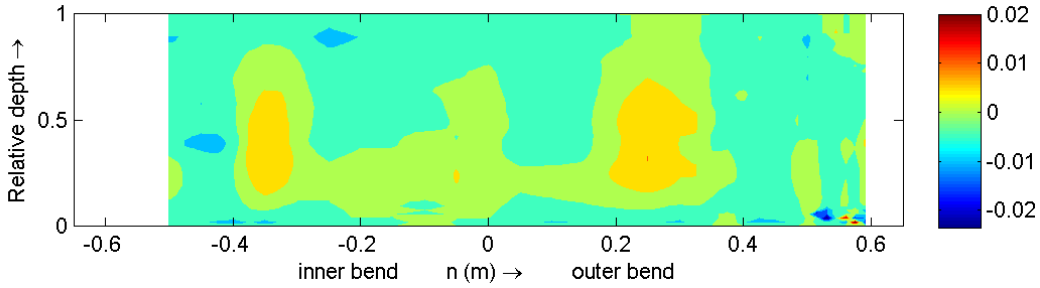

Figure C-27 Vertical velocities at cross-section m25, according to the measurements

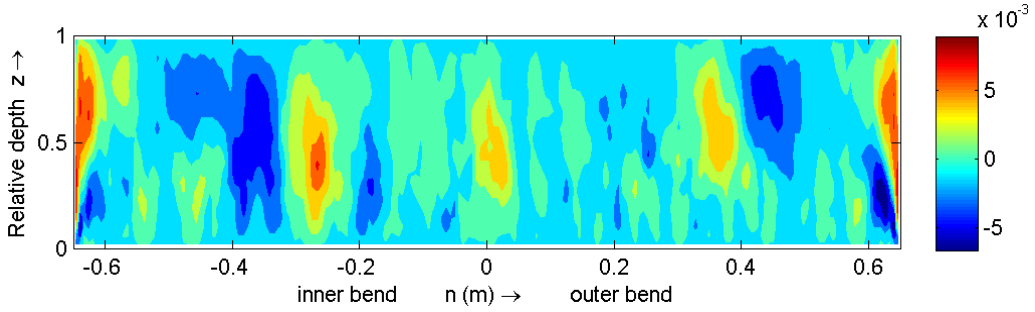

Figure C-28 Vertical velocities at cross-section m25, according to the Q89_LES

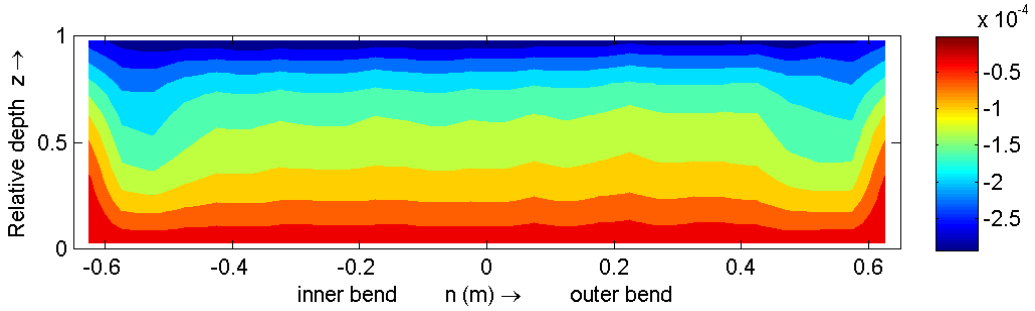

Figure C-29 Vertical velocities at cross-section m25, according to simulation Q89_1_D3D

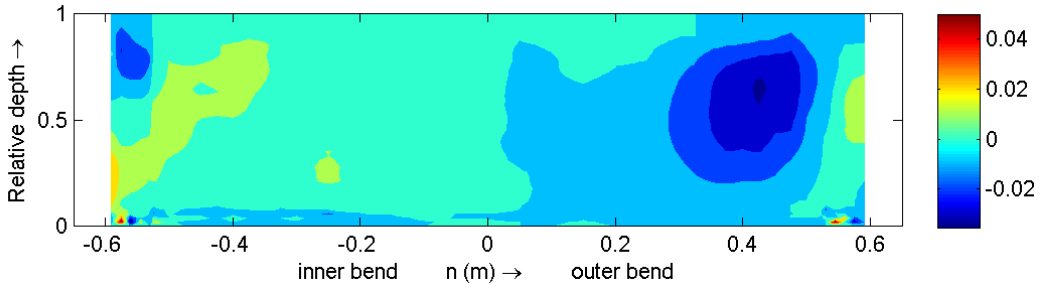

Figure C-30 Vertical velocities at cross-section 060, according to the measurements

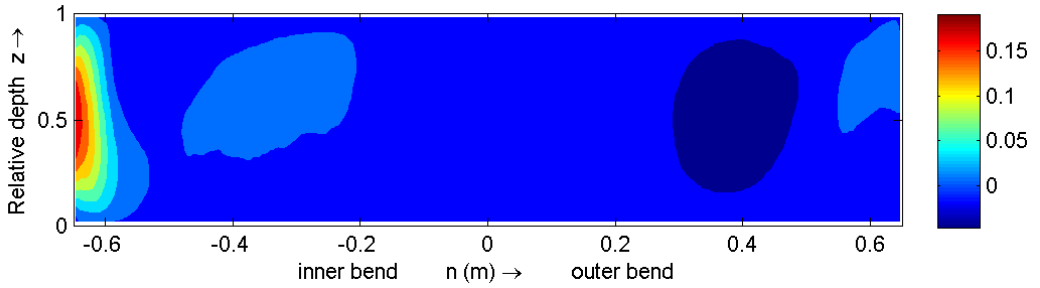

Figure C-31 Vertical velocities, w, Q89_LES, cross-section 060

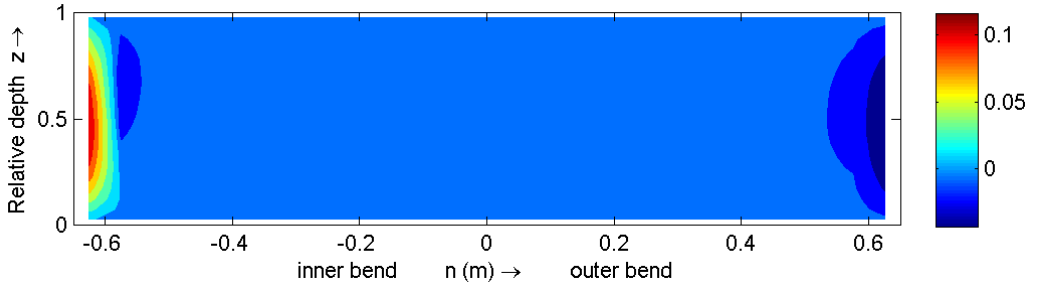

Figure C-32 Vertical velocities, w, simulation Q89_1_D3D, cross-section 060

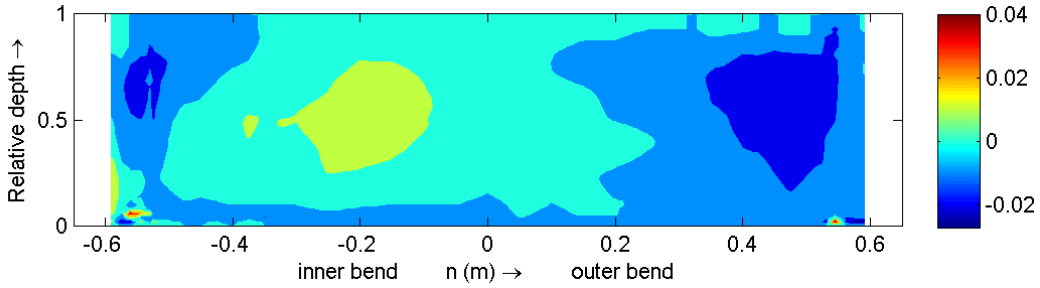

Figure C-33 Vertical velocities, w, measurements, cross-section 060

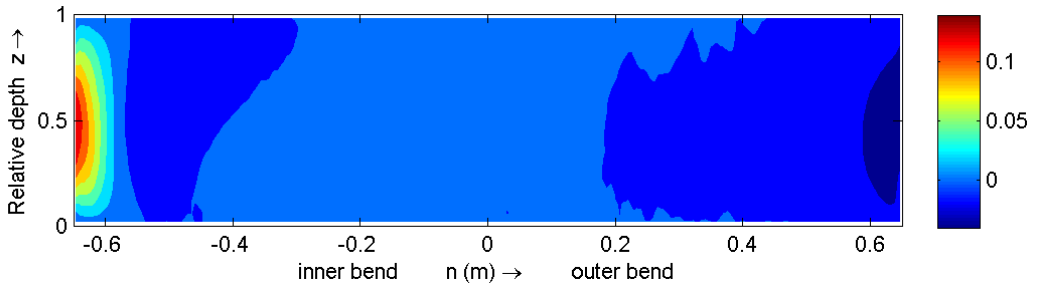

Figure C-34 Vertical velocities, w, Q89_LES, cross-section 150

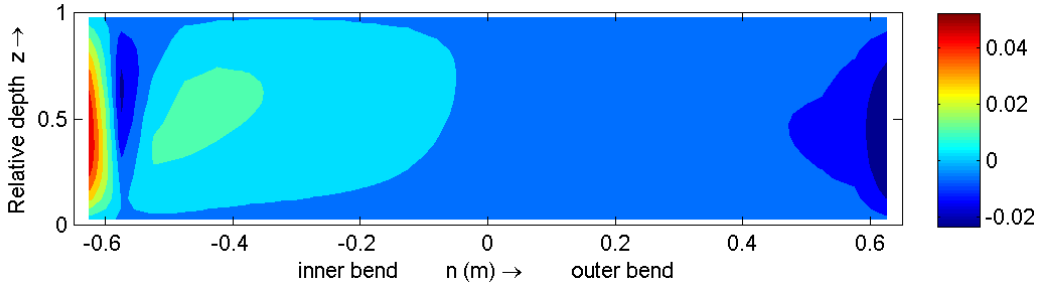

Figure C-35 Vertical velocities at cross-section 150, according to simulation Q89_1_D3D

C.4 Psi, cross-sections

In this paragraph are the figures shown of the quantity ψ, normalized by $100/(U_{bulk}\ H)$, with U_{bulk} = 0.43 m/s and H = 0.159 m. The figures are shown per cross-section for all three data sets.

The following remarks have to be placed:

- all interpolations are linear
- all quantities of the Delft3D-FLOW simulation are calculated at zeta point locations and the results of differentiations are interpolated to zeta points
- downstream derivatives for the measurements are calculated between two successive cross-sections

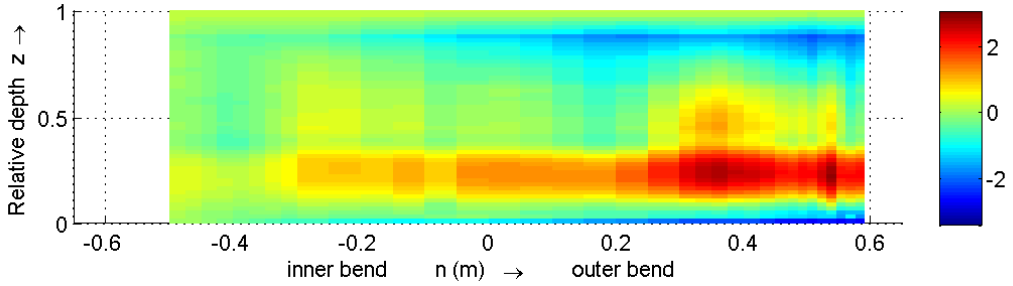

Figure C-36 Normalized quantity ψ, in cross-section m25 according to the measurements

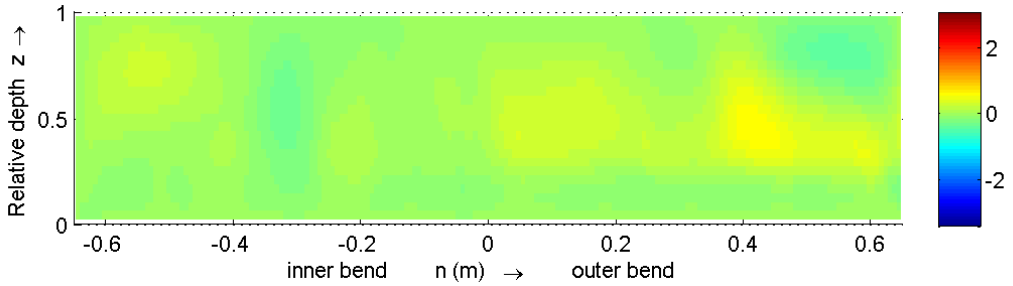

Figure C-37 Normalized quantity ψ, in cross-section m25 according to the Q89_LES

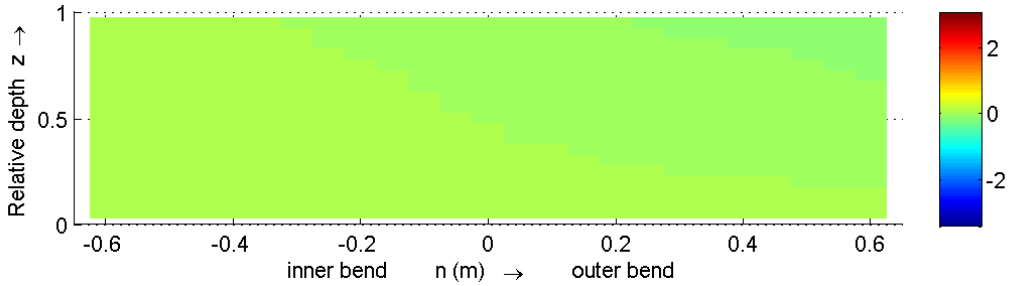

Figure C-38 Normalized quantity ψ, in cross-section m25 according to simulation Q89_1_D3D

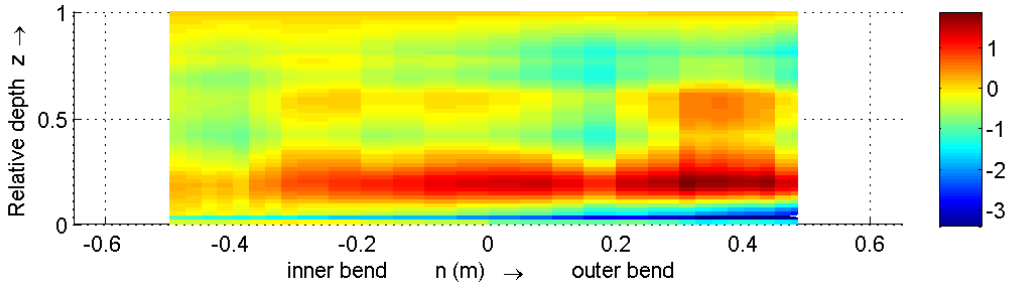

Figure C-39 Normalized quantity ψ, in cross-section m05 according to the measurements

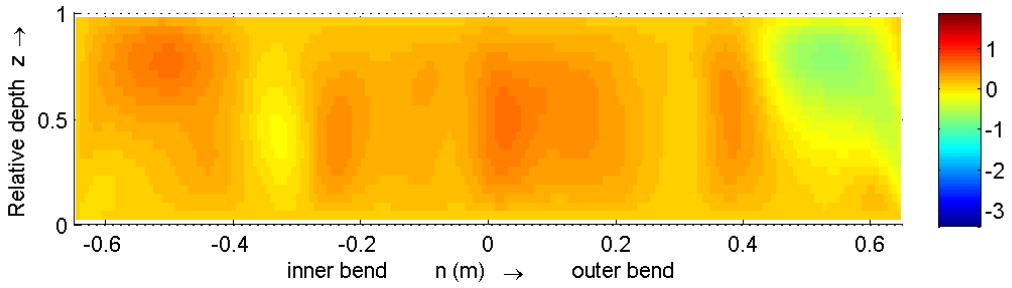

Figure C-40 Normalized quantity ψ, in cross-section m05 according to the Q89_LES

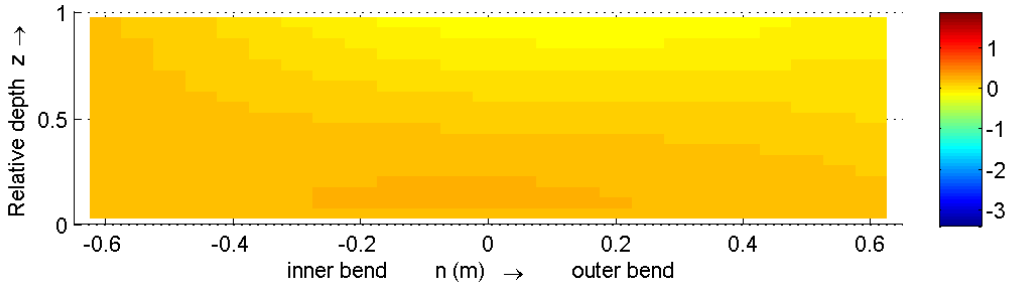

Figure C-41 Normalized quantity ψ, in cross-section m05 according to simulation Q89_1_D3D

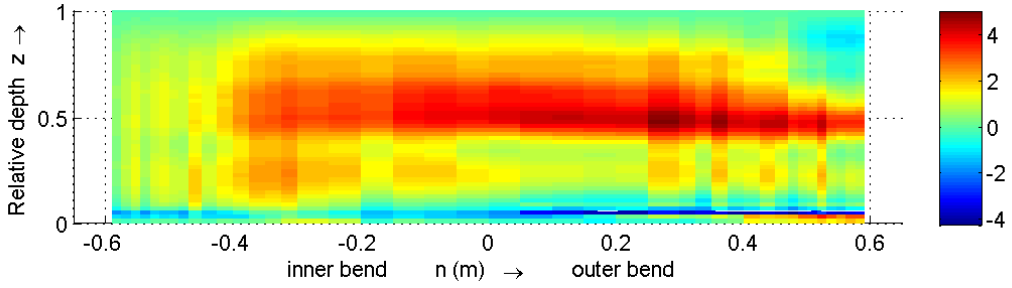

Figure C-42 Normalized quantity ψ, in cross-section 015 according to the measurements

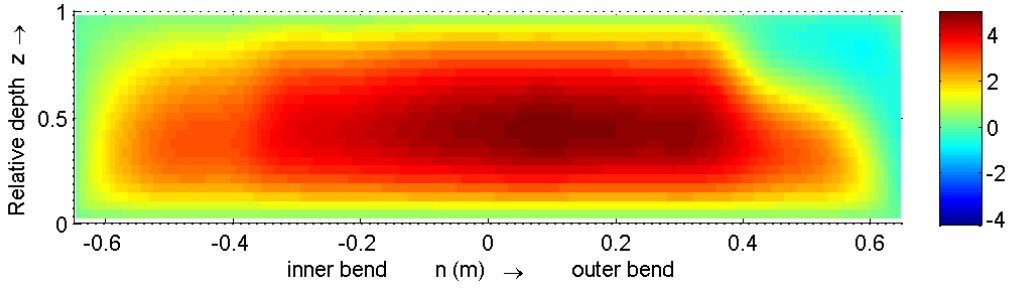

Figure C-43 Normalized quantity ψ, in cross-section 015 according to the Q89_LES

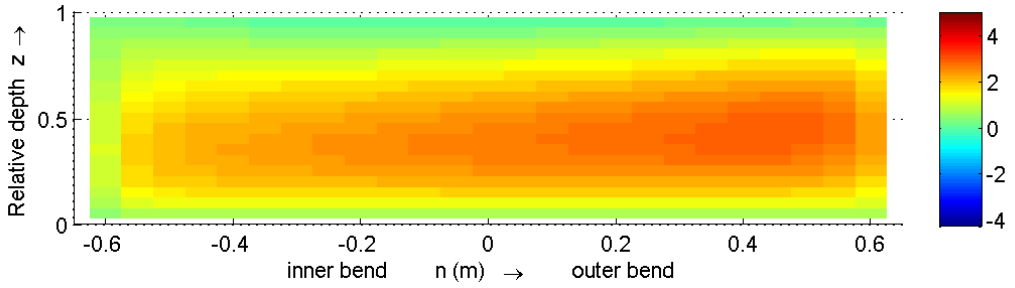

Figure C-44 Normalized quantity ψ, in cross-section 015 according to simulation Q89_1_D3D

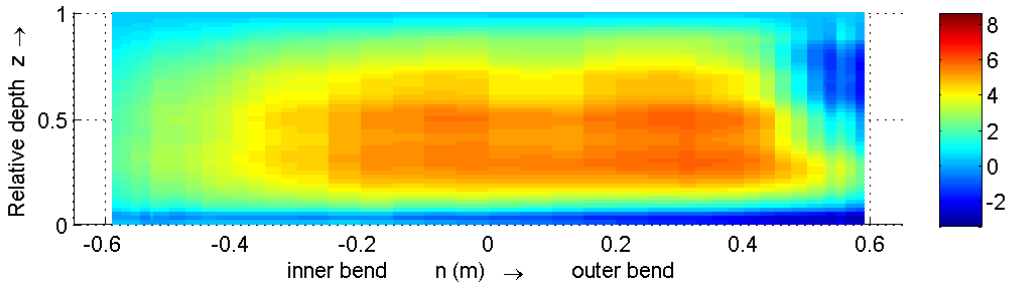

Figure C-45 Normalized quantity ψ, in cross-section 030 according to the measurements

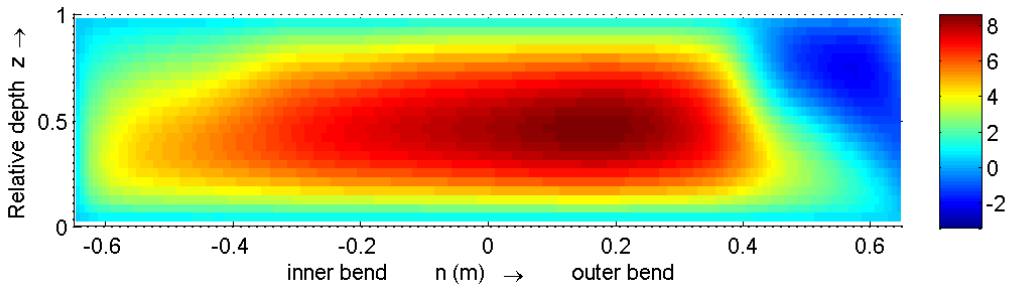

Figure C-46 Normalized quantity ψ, in cross-section 030 according to the Q89_LES

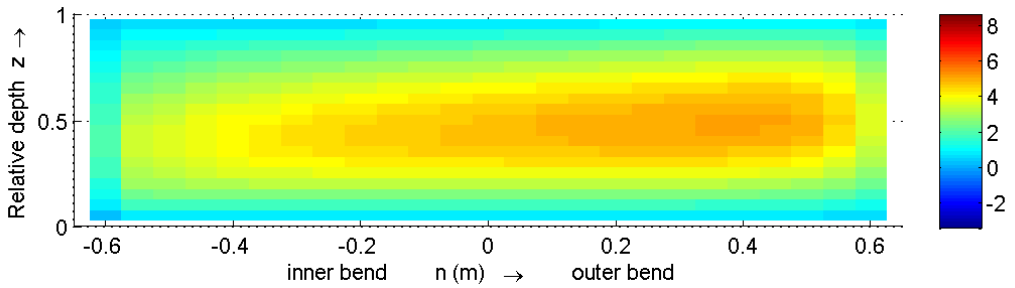

Figure C-47 Normalized quantity ψ, in cross-section 030 according to simulation Q89_1_D3D

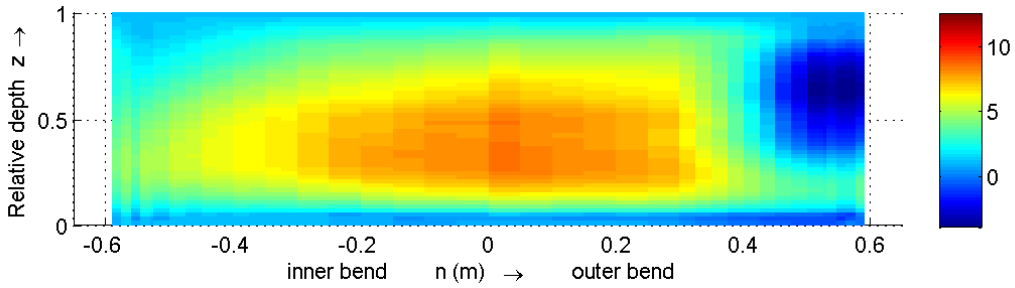

Figure C-48 Normalized quantity ψ, in cross-section 060 according to the measurements

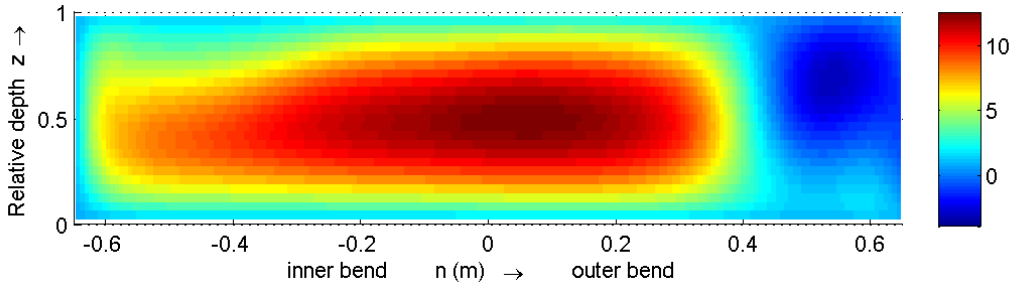

Figure C-49 Normalized quantity ψ, in cross-section 060 according to the Q89_LES

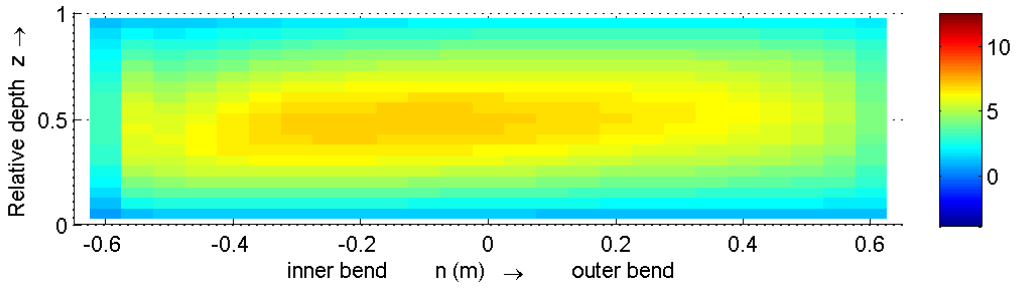

Figure C-50 Normalized quantity ψ, in cross-section 060 according to simulation Q89_1_D3D

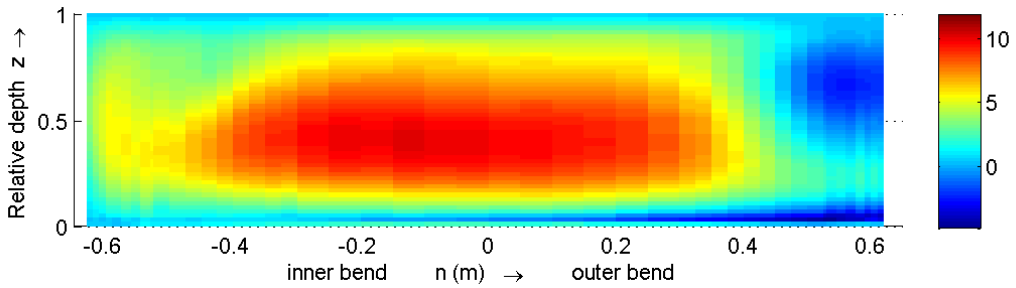

Figure C-51 Normalized quantity ψ, in cross-section 090 according to the measurements

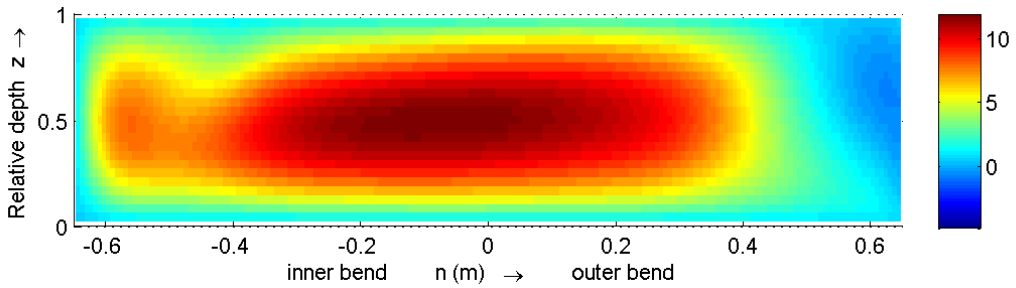

Figure C-52 Normalized quantity ψ, in cross-section 090 according to the Q89_LES

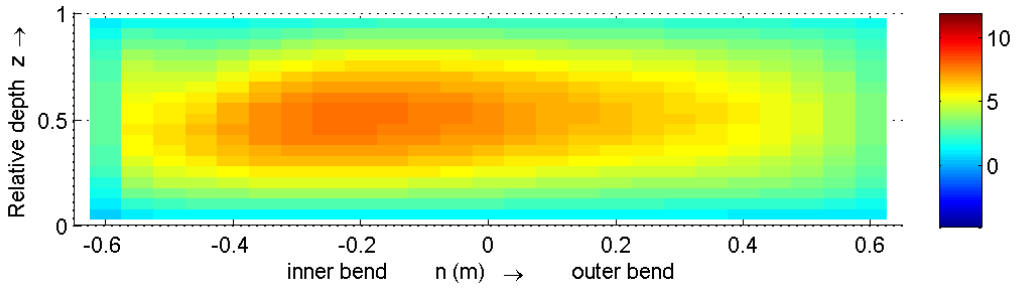

Figure C-53 Normalized quantity ψ, in cross-section 090 according to simulation Q89_1_D3D

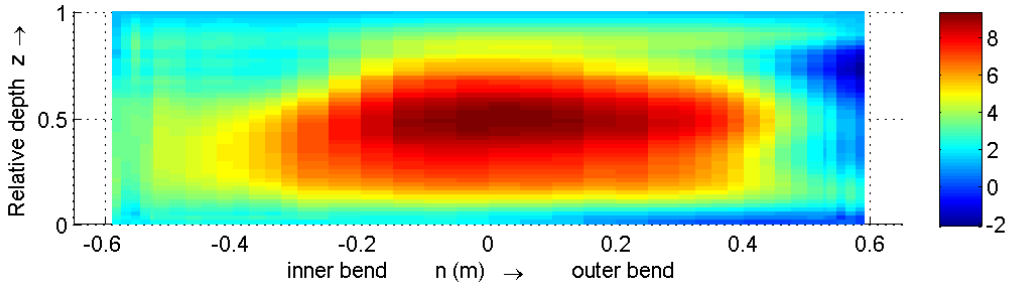

Figure C-54 Normalized quantity ψ, in cross-section 120 according to the measurements

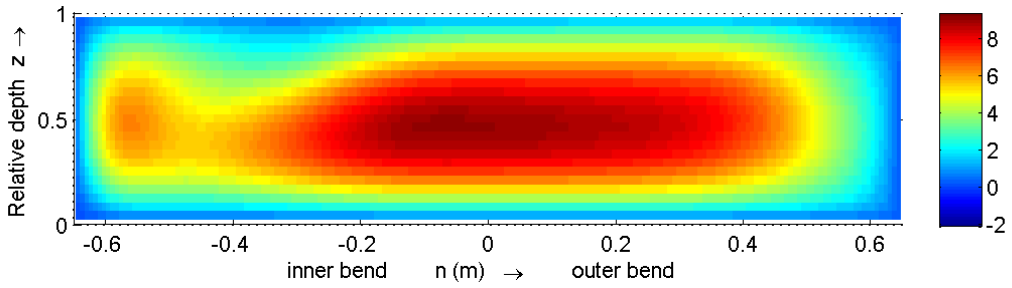

Figure C-55 Normalized quantity ψ, in cross-section 120 according to the Q89_LES

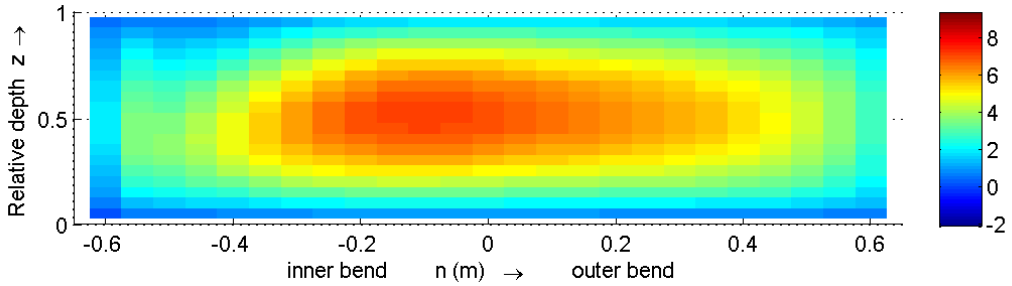

Figure C-56 Normalized quantity ψ, in cross-section 120 according to simulation Q89_1_D3D

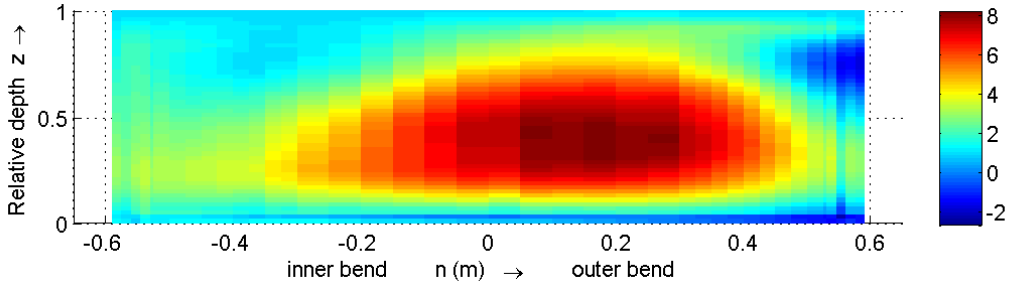

Figure C-57 Normalized quantity ψ, in cross-section 150 according to the measurements

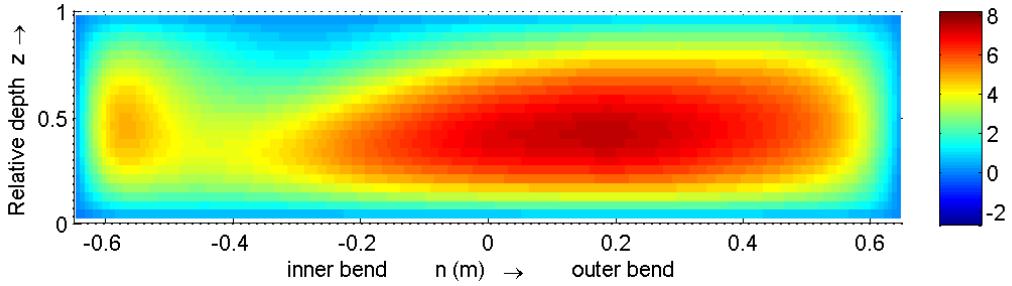

Figure C-58 Normalized quantity ψ, in cross-section 150 according to the Q89_LES

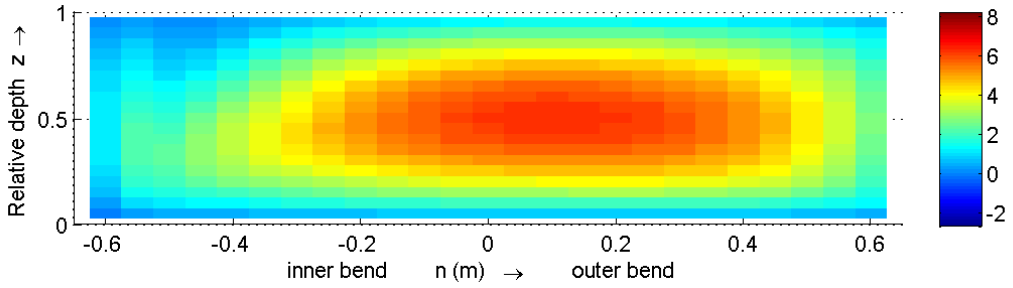

Figure C-59 Normalized quantity ψ, in cross-section 150 according to simulation Q89_1_D3D

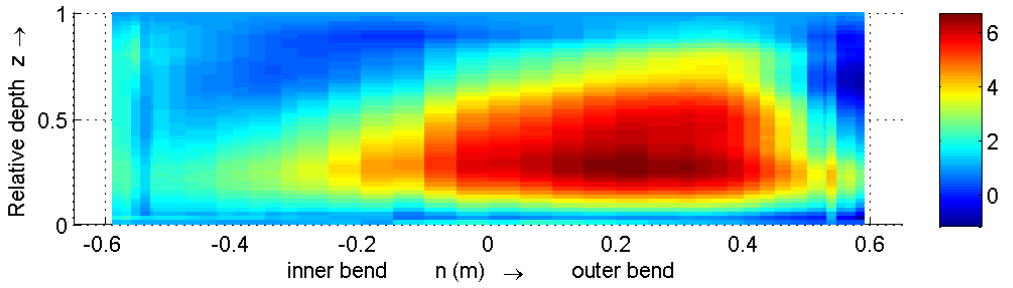

Figure C-60 Normalized quantity ψ, in cross-section 180 according to the measurements

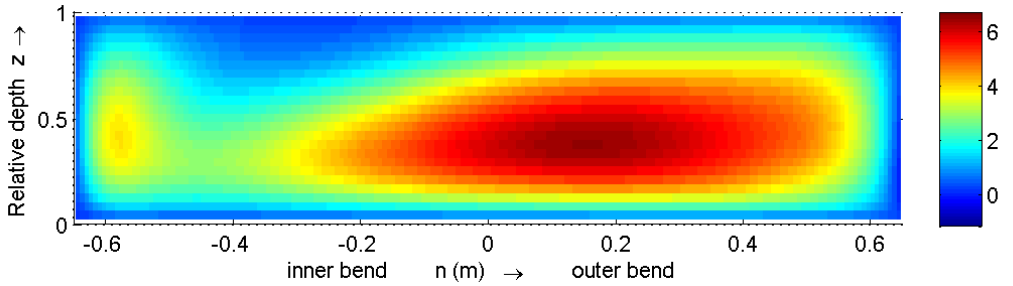

Figure C-61 Normalized quantity ψ, in cross-section 180 according to the Q89_LES

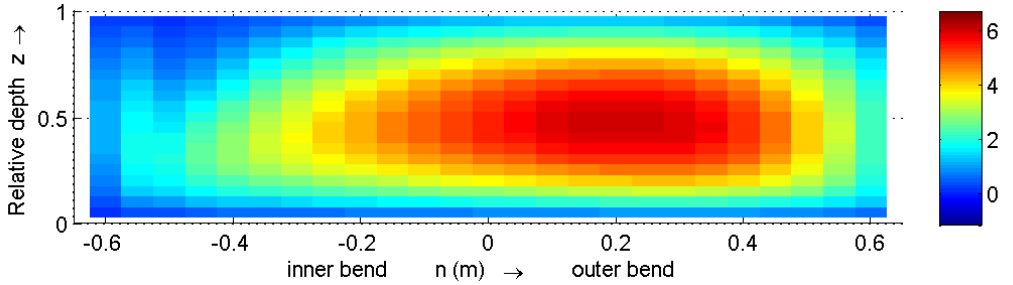

Figure C-62 Normalized quantity ψ, in cross-section 180 according to simulation Q89_1_D3D

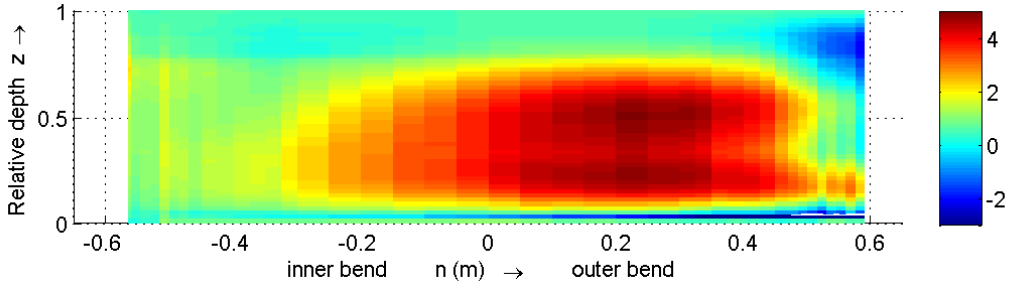

Figure C-63 Normalized quantity ψ, in cross-section p05 according to the measurements

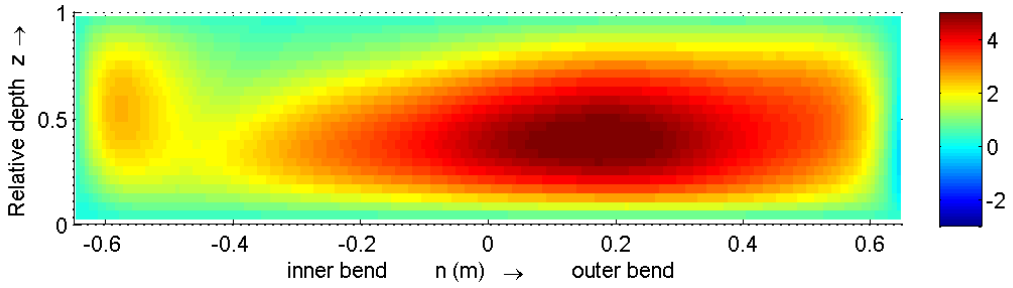

Figure C-64 Normalized quantity ψ, in cross-section p05 according to the Q89_LES

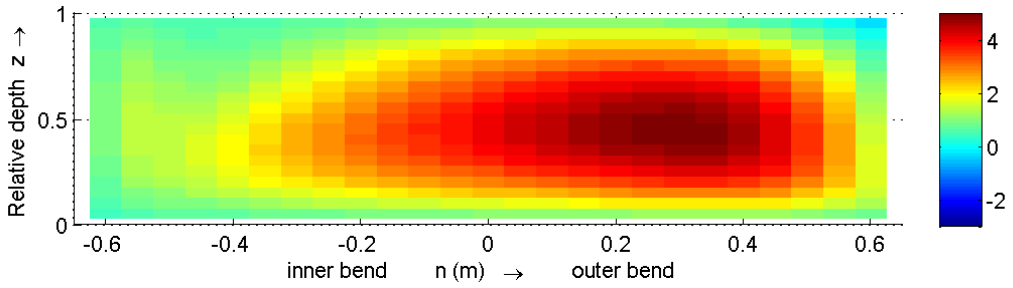

Figure C-65 Normalized quantity ψ, in cross-section p05 according to simulation Q89_1_D3D

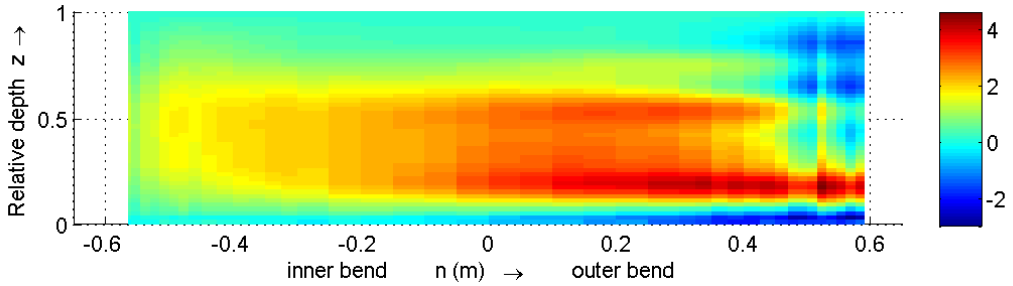

Figure C-66 Normalized quantity ψ, in cross-section p15 according to the measurements

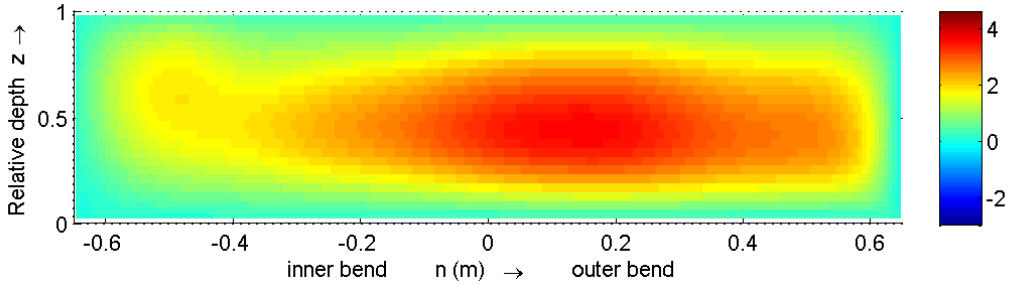

Figure C-67 Normalized quantity ψ, in cross-section p15 according to the Q89_LES

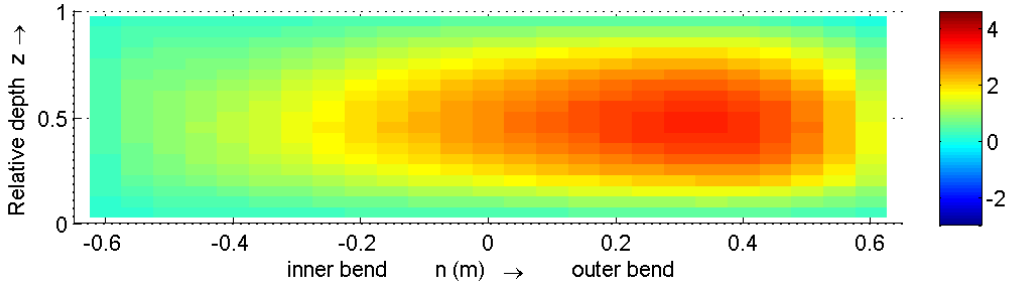

Figure C-68 Normalized quantity ψ, in cross-section p15 according to simulation Q89_1_D3D

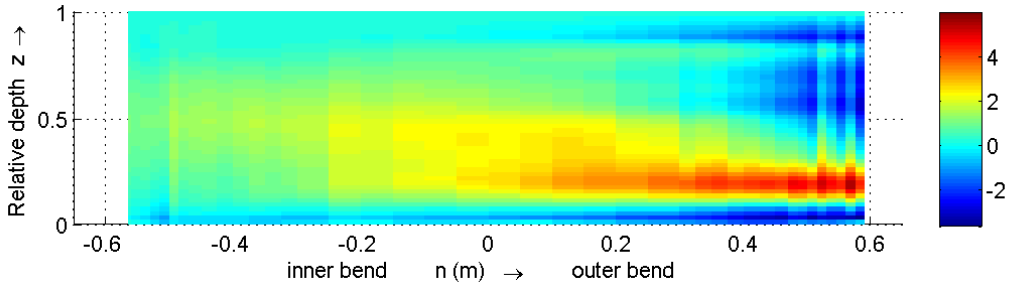

Figure C-69 Normalized quantity ψ, in cross-section p25 according to the measurements

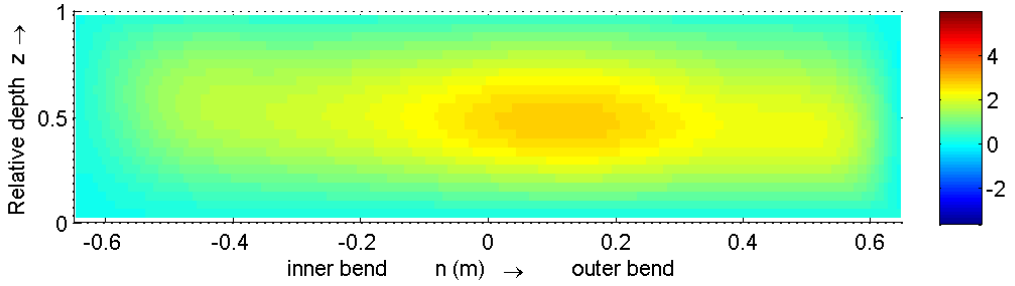

Figure C-70 Normalized quantity ψ, in cross-section p25 according to the Q89_LES

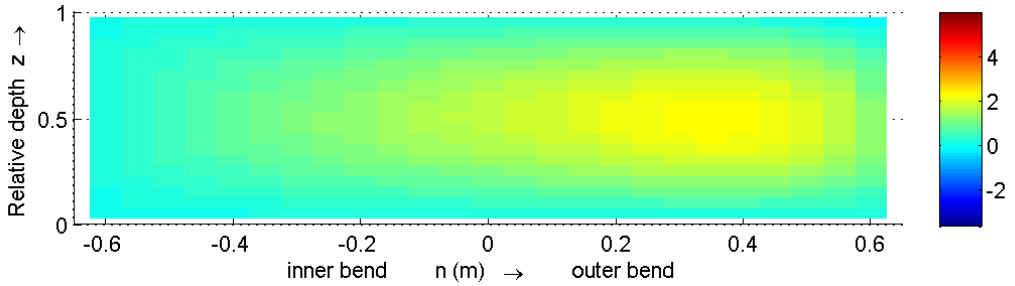

Figure C-71 Normalized quantity ψ, in cross-section p25 according to simulation Q89_1_D3D

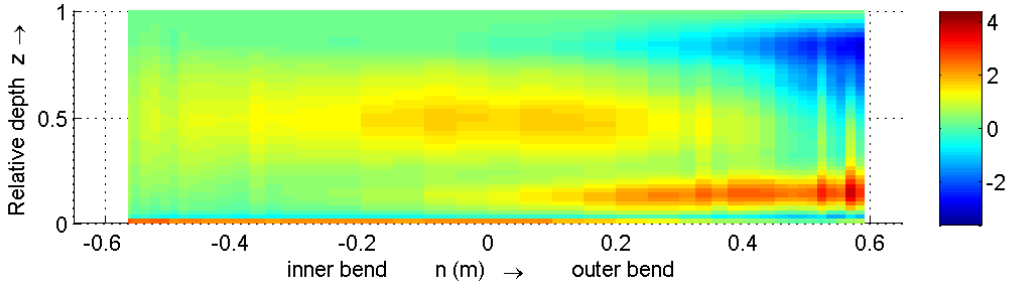

Figure C-72 Normalized quantity ψ, in cross-section p35 according to the measurements

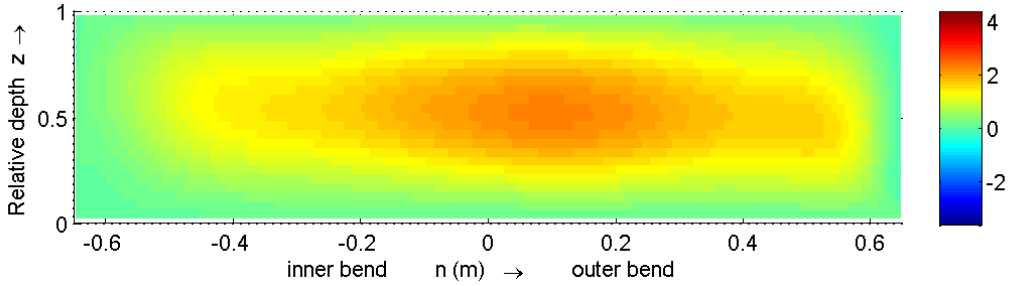

Figure C-73 Normalized quantity ψ, in cross-section p35 according to the Q89_LES

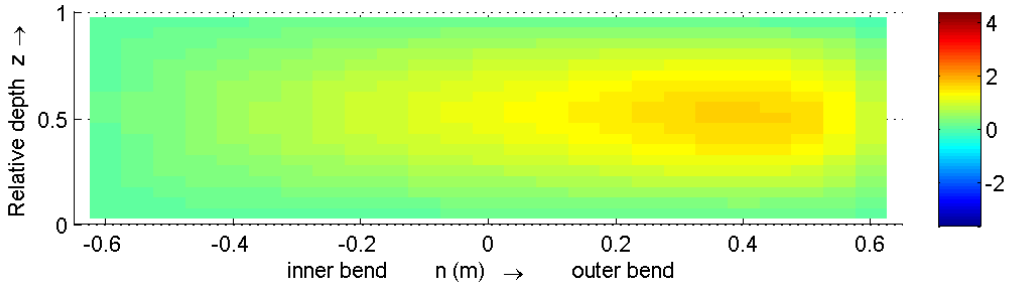

Figure C-74 Normalized quantity ψ, in cross-section p35 according to simulation Q89_1_D3D

C.5 Vorticity

In this paragraph are figures presented which show the downstream vorticity for the three data sets (measurements, Q89_LES and Delft3D-FLOW simulation Q89_1_D3D) in the m25, 060 and 150 cross-sections. The downstream vorticity is defined as:

$$\omega_s = \frac{\partial w}{\partial r} - \frac{\partial v}{\partial z}$$

The terms $\frac{\partial w}{\partial r}$ and $-\frac{\partial v}{\partial z}$ are shown too. Notice that the range of the colour bar is not for every picture the same. All pictures are normalized by H/U. The results for the different cross-sections are discussed in this section.

M25 cross-section

Starting from cross-section m25 it can be seen that ω_s is nearly zero for simulation Q89_1_D3D with respect to the measurements and the Q89_LES. It is hard to say something useful about the vorticity in the m25 cross-section. There are some kinds of bars visible in Figure C-75. They have negative and positive signs in turn. The bars can be seen as a result of the circulatory cells in the straight channel. The Q89_LES shows a more clear pattern. In the upper part of the inner bend, the vorticity has negative values and in the upper part of the outer bend the vorticity has positive values. This pattern is mainly caused by the $-\frac{\partial v}{\partial z}$ term. The $\frac{\partial w}{\partial r}$ term shows a random fluctuation over the width of the flow. At the wall boundaries there are vertical bars with higher vortices. Looking at the $-\frac{\partial v}{\partial z}$ and $\frac{\partial w}{\partial r}$ terms for simulation Q89_1_D3D, (Figure C-96and Figure C-97) it can be seen that the $\frac{\partial w}{\partial r}$ term has only some influence at the wall boundaries.

060 cross-section

As we can see in Figure C-78 to Figure C-80, the comparison of ω_s for the Q89_LES and the measurements is quiet good. As was remarked before, the outer bank cell is not visible in the results of simulation Q89_1_D3D. Both the Q89_LES and the measurements show the outer bank cell and some kind of a cell in the upper part of the cross-section from -0.55 m to -0.3 m from the centre (the red circle in Figure C-79). In both cells the vorticity has positive values while in the most of the cross-section the vorticity has negative values. The positive valued vorticity is mainly caused by the flow separation and the reduction of the transverse velocity due to this. Especially in the lower part, inner bend (the blue circle in Figure C-79), the

vorticity becomes strongly negative. The values of the vorticity according to simulation Q89_1_D3D are, in general, lower than the Q89_LES and the measurements.

From the figures with the $-\frac{\partial v}{\partial z}$ and $\frac{\partial w}{\partial r}$ terms (Figure C-86and Figure C-87, Figure C-92 and Figure C-93, Figure C-98 and Figure C-99) it follows that the term $\frac{\partial w}{\partial r}$ has only at the wall in the inner bend a contribution to the downstream vorticity. In the most parts of the cross-section the downstream vorticity is mainly determined by the $-\frac{\partial v}{\partial z}$ term. This holds for all three data sets.

About the bar at the bottom of the flume with high positive vorticity can be said that this is caused by the high gradient in the vertical direction of the transverse velocity. This gradient is caused by the wall friction (the velocity at the wall is zero).

Cross-section 150

Figure C-81 to Figure C-83 show the vorticity in cross-section 150. The strength of the outer bank cell is decreased (for the Q89_LES and measurements). The strength of the cell with negative valued vorticity at the inner bank (the blue circle) decreases also and becomes wider (for all three data sets). The cell in the upper part of the inner bend (the one in the red circle) becomes also wider, the strength remains the same for the Q89_LES and the measurement but the strength increases for simulation Q89_1_D3D. For the Q89_LES, this cell grows towards the outer bank cell and merges with the outer bank cell. The measurements still show some kind of separation between those two cells.

For this cross-section it still holds that the vorticity mainly is determined by the $-\frac{\partial v}{\partial z}$ term and that the $\frac{\partial w}{\partial r}$ term contributes to the vorticity at the side walls only.

It can be concluded that the vertical velocities and the gradient of the vertical velocities in transverse direction, are only important at the side walls. This is the place where the ‘up welling’ and ‘down welling’ of the secondary flow takes place.

Vorticity is mainly generated along the walls and at the borders of the outer bank cell where the velocity gradients are high. Simulation Q89_1_D3D generally under predicts the ADV-term.

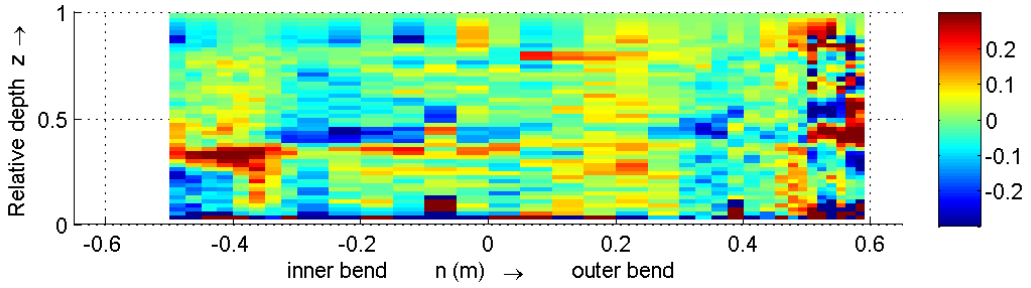

Figure C-75ω_s, normalized (with H/U), for cross-section m25, according to the measurements. The range of the colour bar is shortened with respect to the range of the data.

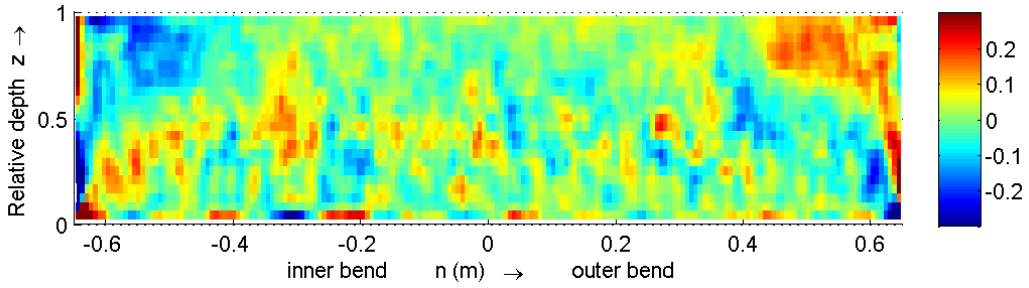

Figure C-76 ω_s, normalized (with H/U), for cross-section m25, according to the Q89_LES. The range of the colour bar is shortened with respect to the range of the data

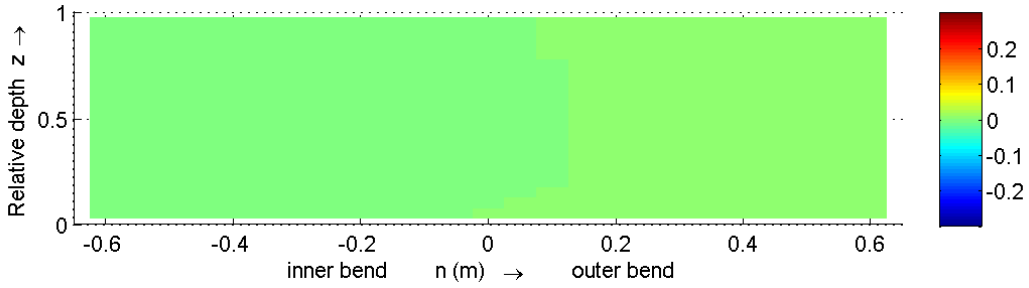

Figure C-77 ω_s, normalized (with H/U), for cross-section m25, according to simulation Q89_1_D3D

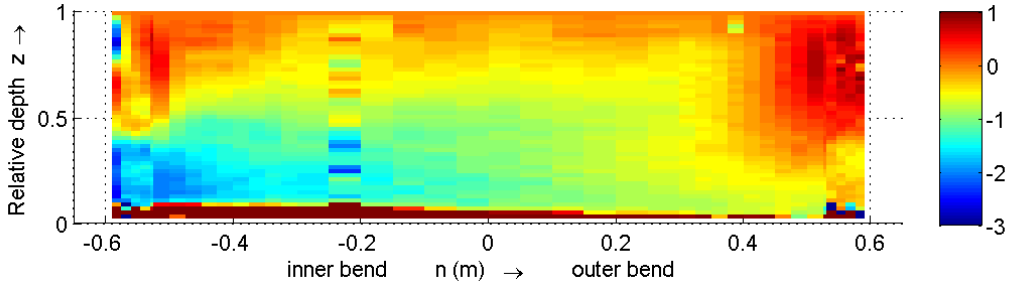

Figure C-78ω_s, normalized (with H/U), for cross-section 060, according to the measurements. The range of the colour bar is shortened with respect to the range of the data

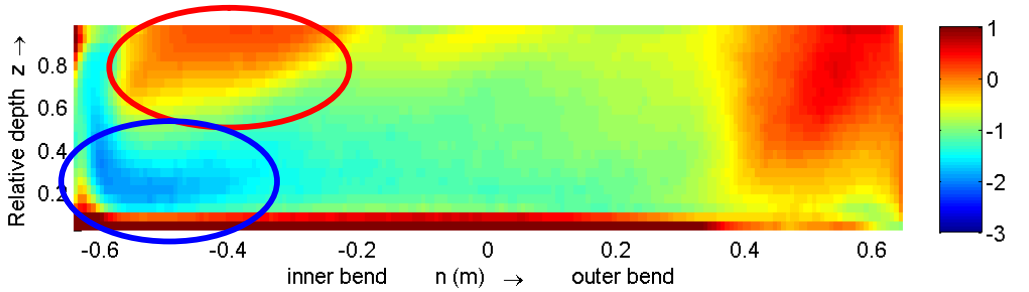

Figure C-79 ω_s, normalized (with H/U), for cross-section 060, according to the Q89_LES. The range of the colour bar is shortened with respect to the range of the data

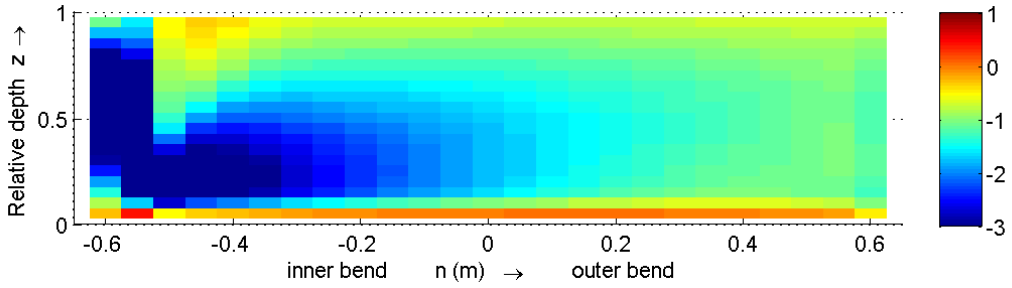

Figure C-80ω_s, normalized (with H/U), for cross-section 060, according to simulation Q89_1_D3D. Shortened colour bar

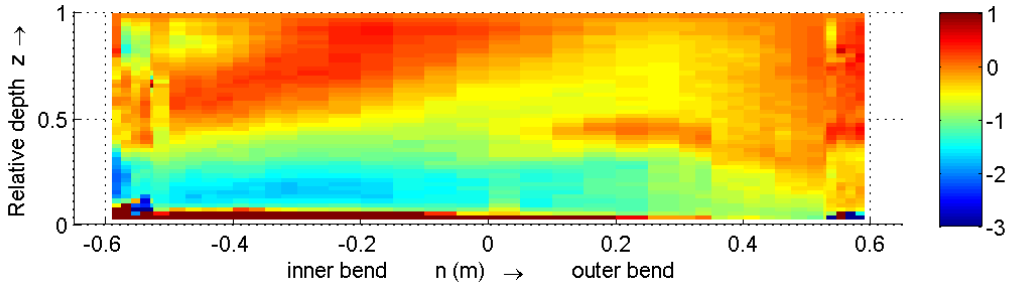

Figure C-81 ω_s, normalized (with H/U), for cross-section 150, according to the measurements. The range of the colour bar is shortened with respect to the range of the data

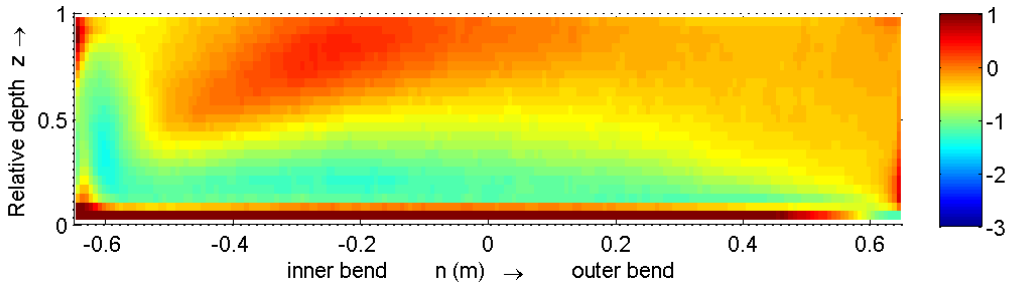

Figure C-82 ω_s, normalized (with H/U), for cross-section 150, according to the Q89_LES. The range of the colour bar is shortened with respect to the range of the data

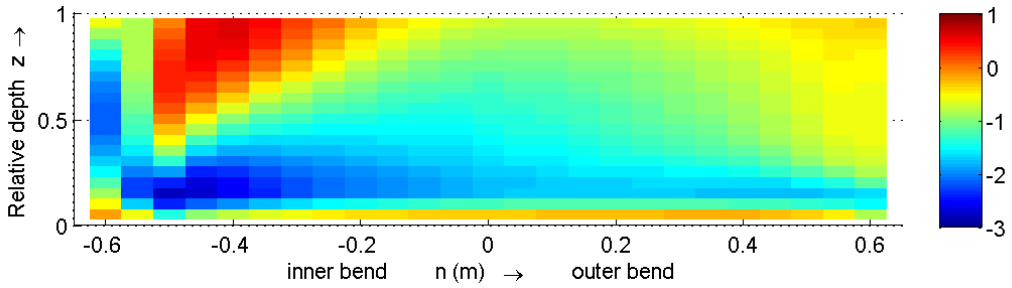

Figure C-83 ω_s, normalized (with H/U), for cross-section 150, according to simulation Q89_1_D3D. The range of the colour bar is shortened with respect to the range of the data

C.5.1 The sub terms of the vorticity

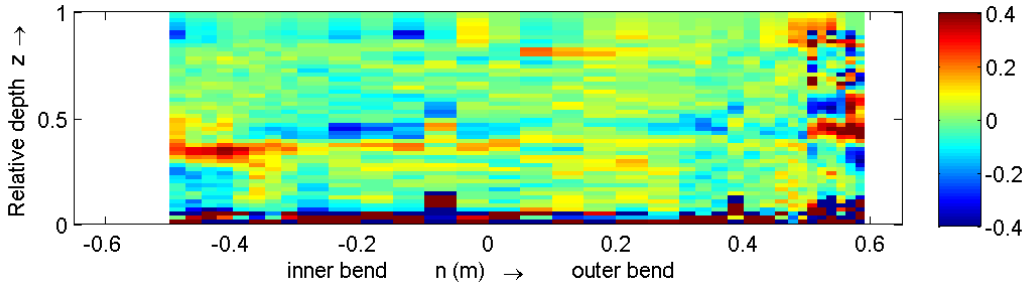

Figure C-84 -dV/dz for cross-section m25, according to the measurements, normalized. Shortened colour bar

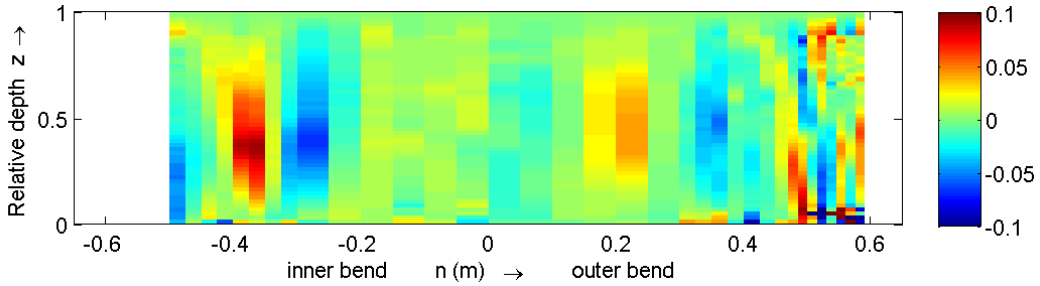

Figure C-85 dW/dn for cross-section m25, according to the measurements, normalized. Shortened colour bar

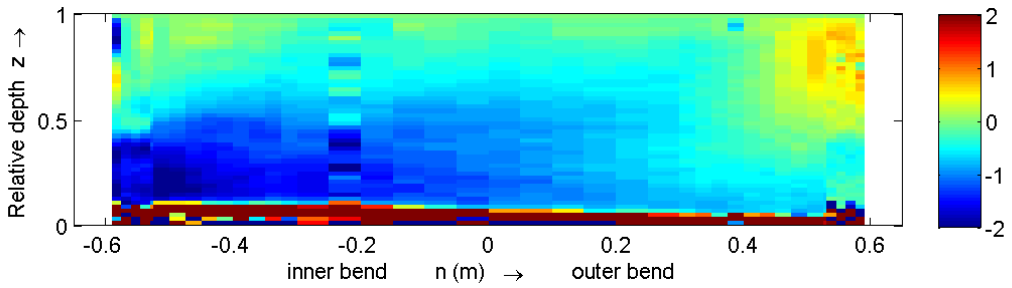

Figure C-86 -dV/dz, normalized, cross-section 060, measurement. The range of the colour bar is shortened with respect to the range of the data.

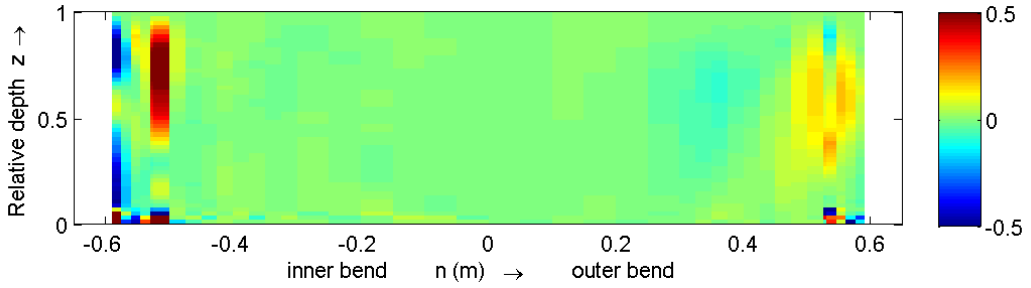

Figure C-87 dW/dn, normalized, cross-section 060, measurements. The range of the colour bar is shortened with respect to the range of the data

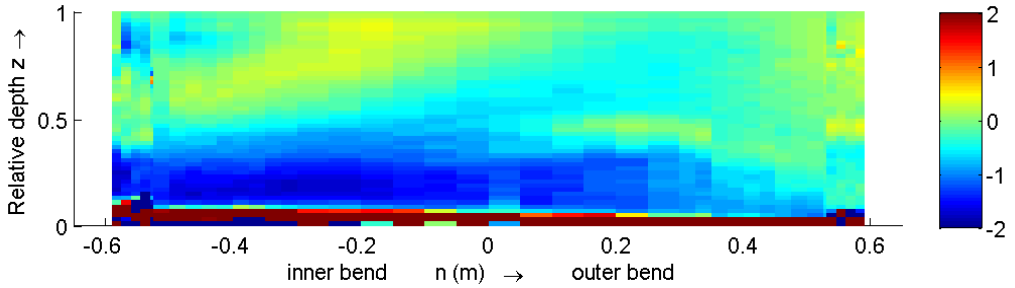

Figure C-88 -dV/dz, normalized, cross-section 150, measurements. The range of the colour bar is shortened with respect to the range of the data

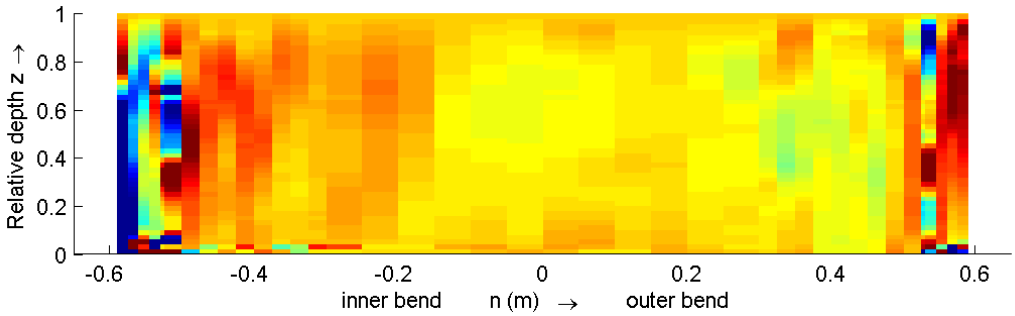

Figure C-89 dW/dn, normalized, cross-section 150, measurements. The range of the colour bar is shortened with respect to the range of the data

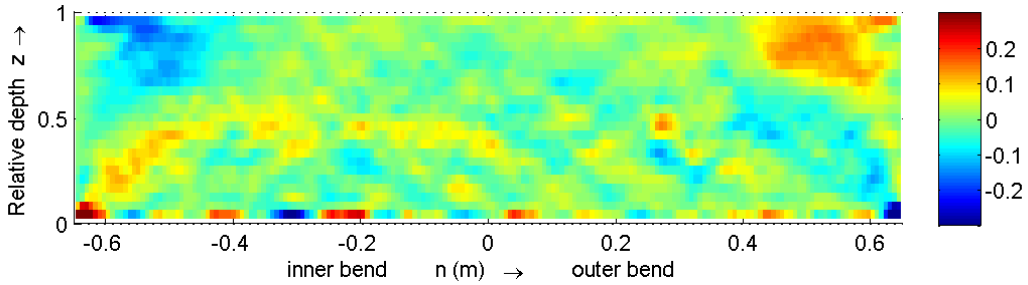

Figure C-90 -dV/dz, for cross-section m25, according to the Q89_LES, normalized. Shortened colour bar

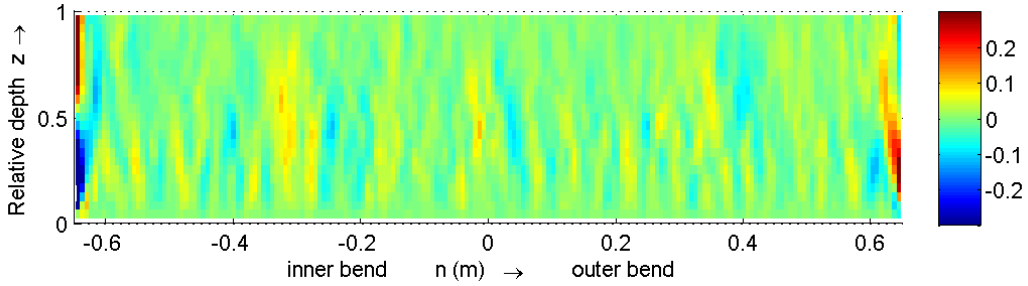

Figure C-91 dW/dr for cross-section m25, according to the Q89_LES, normalized. Shortened colour bar

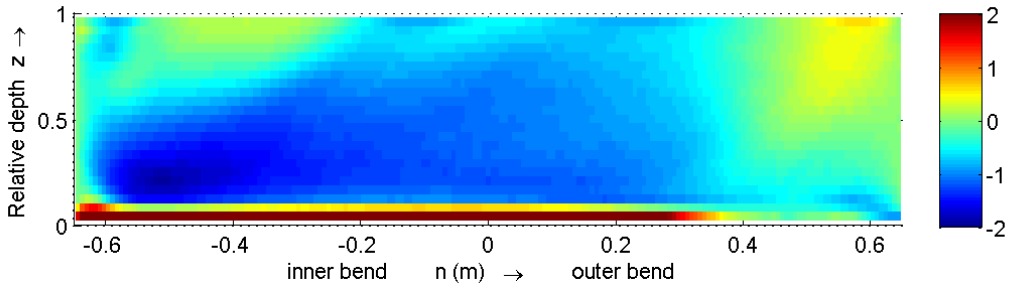

Figure C-92 -dV/dz, normalized, cross-section 060, Q89_LES. The range of the colour bar is shortened with respect to the range of the data

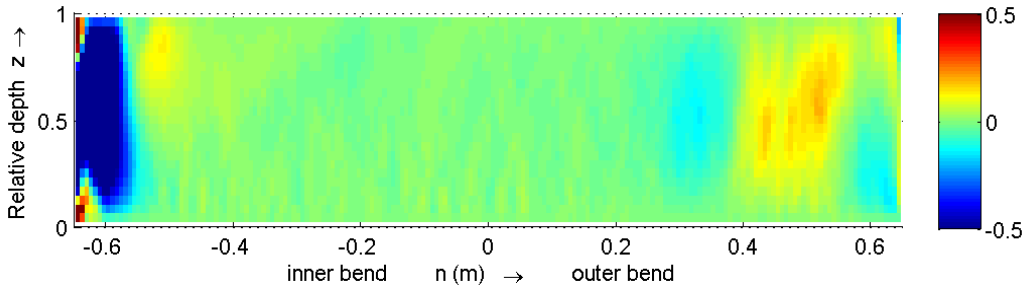

Figure C-93 dW/dn, normalized, cross-section 060, Q89_LES. The range of the colour bar is shortened with respect to the range of the data

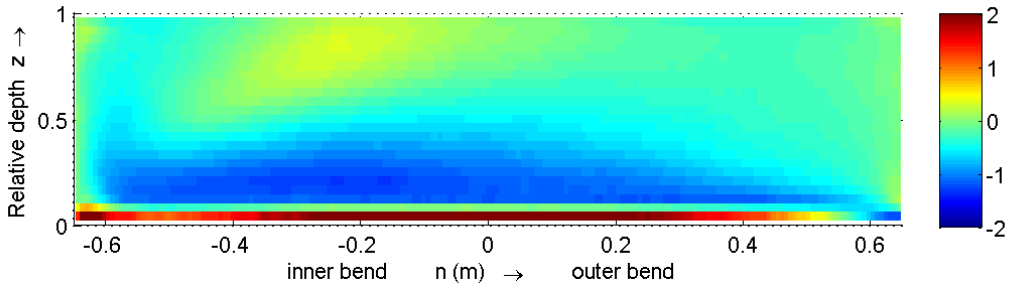

Figure C-94 -dV/dz, normalized, cross-section 150, Q89_LES. The range of the colour bar is shortened with respect to the range of the data

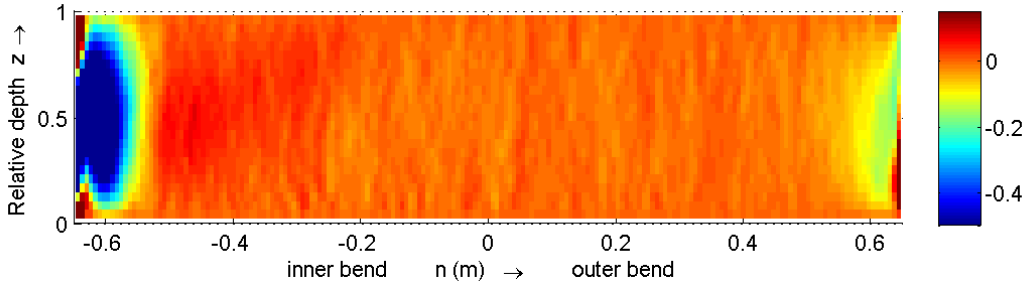

Figure C-95 dW/dn, normalized, cross-section 150, Q89_LES. The range of the colour bar is shortened with respect to the range of the data

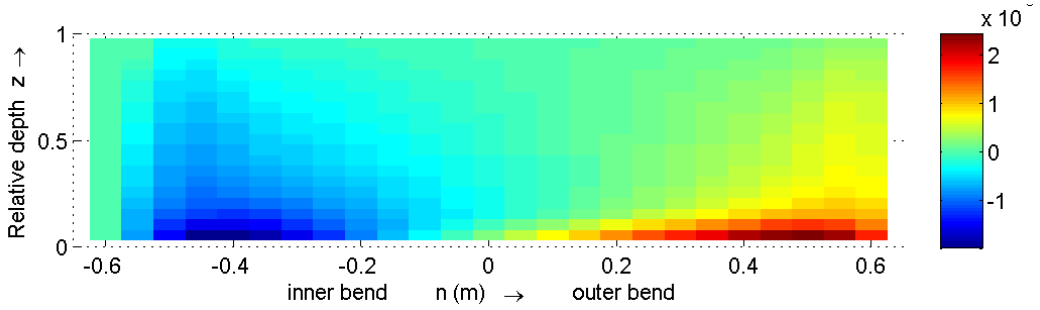

Figure C-96 - dV/dz for cross-section m25, according to simulation Q89_1_D3D, normalized

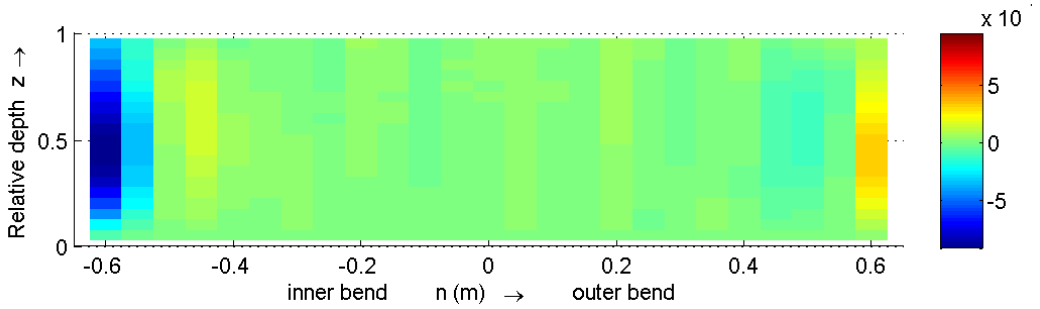

Figure C-97 dW/dr for cross-section m25, according to simulation Q89_1_D3D, normalized

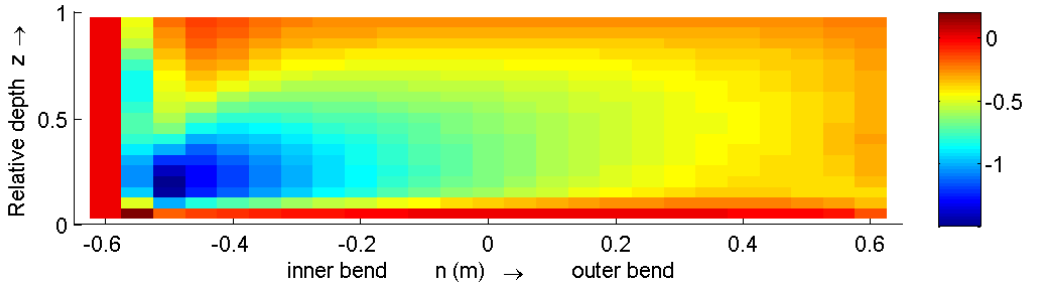

Figure C-98 -dV/dz, normalized, cross-section 060, simulation Q89_1_D3D

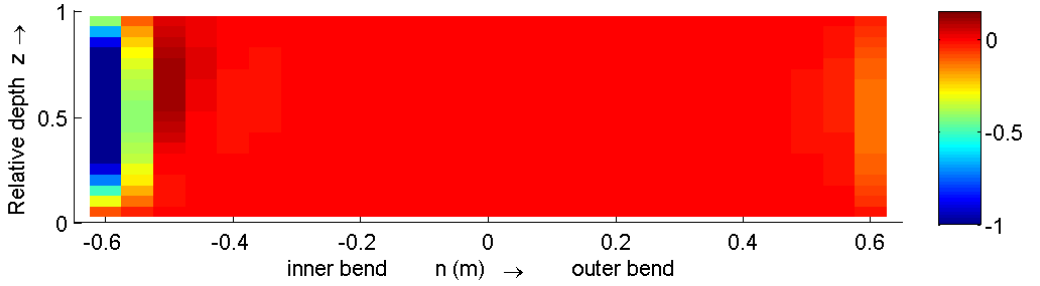

Figure C-99 dW/dn, normalized, cross-section 060, simulation Q89_1_D3D

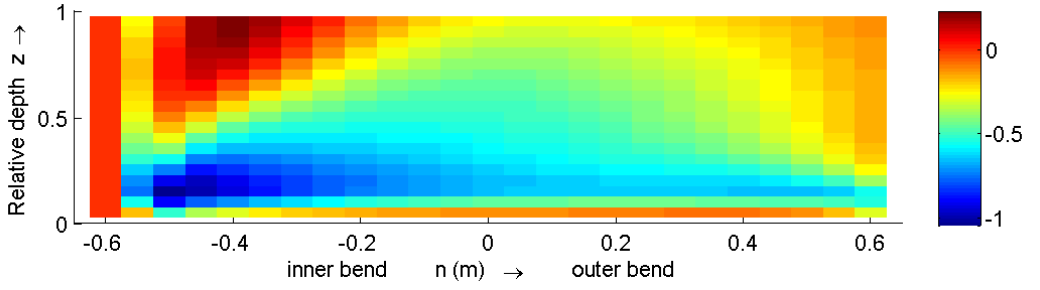

Figure C-100 -dV/dz, normalized, cross-section 150, simulation Q89_1_D3D

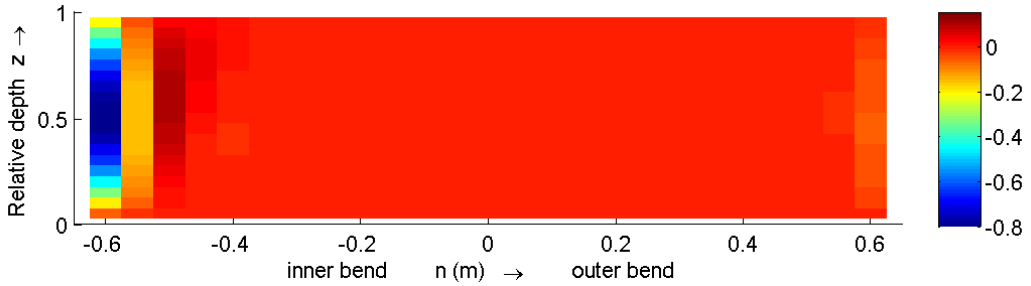

Figure C-101 dW/dn, normalized, cross-section 150, simulation Q89_1_D3D

C.6 Advection term

In this paragraph the advection term (ADV) of the downstream vorticity balance equation will be shown. All figures are normalized by H^2/U^2 * 1000 and for some figures is the range of the colour bar shortened with respect to the range of the data which is represented.

The advection term is defined as (van Balen *et al.*, 2009b)

$$-\left(\frac{u}{r}\frac{\partial \omega_s}{\partial \theta}+v\frac{\partial \omega_s}{\partial r}+w\frac{\partial \omega_s}{\partial z}\right)$$

Each of the sub terms is also plotted to figure out which ones are important.

$$\text{Term 1} \quad = -\frac{u}{r}\frac{\partial \omega_s}{\partial \theta}$$

$$\text{Term 2} \quad = -v\frac{\partial \omega_s}{\partial r}$$

$$\text{Term 3} \quad = -w\frac{\partial \omega_s}{\partial z}$$

For all three data sets (measurement, Q89_LES and simulation Q89_1_D3D) the advection term can be calculated. Some remarks have to be made on the calculations of the *downstream* derivatives of the measured data. The downstream derivatives according to the measurements are calculated between two consecutive measured cross-sections which means that the distance '*1/r*dθ*' is a large distance.

The results for the m25, 060 and 150 cross sections are shown in Figure C-102 to Figure C-110.

Cross-section m25

The advection term according to the measured data shows big fluctuations. At the boundaries are the absolute values of the advection term much higher than in the middle of the flow. The advection term according to the Q89_LES has a somewhat different structure than the measurements. For the Q89_LES, the advection term fluctuates too. The lower half of the cross-section shows more and higher negative values than the upper half of the flow. When comparing these results with the results of simulation Q89_1_D3D, we see a big difference. There is nearly no advection of vorticity in the straight inflow of the flume. There are some fluctuations purely caused by transport in downstream direction of vorticity (the $-u\frac{1}{r}\frac{\partial \omega_s}{\partial \theta}$ term, see Figure C-129) but these are more than two orders of magnitude smaller than the fluctuations of the advection term in the measurements and the Q89_LES. For the Q89_LES

the downstream advection term ($-u\frac{1}{r}\frac{\partial \omega_s}{\partial \theta}$) largely determines the advection term. The two other terms have only some influence in the lower corners of the cross-section. The fluctuations in the measured data are mainly caused by the downstream ($-u\frac{1}{r}\frac{\partial \omega_s}{\partial \theta}$) and vertical ($-w\frac{\partial \omega_s}{\partial z}$) advection terms. The term for advection in transverse direction ($-v\frac{\partial \omega_s}{\partial r}$) influences the advection term only along the boundaries. That the downstream advection term has such a large influence seems to be right compared with the Q89_LES and can be explained by the fact that the downstream velocity is much higher than the transverse and vertical velocity. Despite the derivative in downstream direction is taken between two cross-sections (for the measured data), it seems that the downstream advection term gives a quite good approximation. This is not really strange because the cross-sections that are used are both situated in the straight inflow channel.

Cross-section 060

Starting in the inner bend, we see that the advection term attains high positive and negative values. In the lower corner all three data sets show a positive value. When going in the upward direction along the inner wall, the measurements show a concatenation of strong negative and positive valued areas while the Q89_LES shows mainly negative values in the upper part, inner bend. Simulation Q89_1_D3D shows a pattern of positive and negative values which correspond with the measurements but the values of the advection term are lower. In the direction of the centre of the channel, all three data sets show a region with positive values, whereas the values are lowest for simulation Q89_1_D3D and highest for the measurements. Towards the outer bend, the Q89_LES shows a fleck with negative values at the water surface (see Figure C-106, the blue circle), this fleck is much less clear for the measurements (there is something that looks alike the fleck) and it is completely absent in the results of simulation Q89_1_D3D. The fleck is located at the boundary of the outer bank cell. It can be explained by the presence of the big velocity gradients which will cause vorticity. As we will see in cross-section 150, this fleck is absent in the Q89_LES data (where the outer bank cell also disappeared, compare Figure C-109 and Figure C-58 where the outer bank cell is absent). The negative valued bar at the bottom is also absent in simulation Q89_1_D3D.

Looking at the different contributions of the advection term (section C.6.1), it can be concluded that all three partial advection terms are important. It is difficult to determine which of the partial advection terms contributes most to the total advection of vorticity. Especially because of the big fluctuations, which are also present in the partial advection terms. Sometimes the partial advection terms have opposite signs, and the patterns of these terms of the Q89_LES and measurements often do not correspond with each other. The term for vertical advection is for all three data sets less important in most part of the centre of the flow. Most of the vorticity is generated near the bottom and the walls and in internal shear layers because of the relative high velocity gradients. This can be seen as the reason why the advection in these regions is high. The vorticity will be spread through the flow by advection.

Cross-section 150

Figure C-109 shows the advection term according to the Q89_LES for cross-section 150. The fluctuations in the inner bend show the same pattern for the 060 and 150 cross-sections. In most of the cross-section it holds that the pattern is the same however, the strength of the advection is lower (about half of the strength in the 060 cross-section). The size of the positive region in the direction of the centre is strongly reduced and a strong negative valued

region appears beside it. At the bottom in the inner bend a positive valued bar appears. The changes hold for all three data sets.

The negative valued fleck at the place where in the 060 cross-section the boundary of the outer bank cell is found, is disappeared. This confirms the idea that this fleck is caused by the strong velocity gradients at the boundaries of the outer bank cell.

Especially the downstream and vertical advection terms attain negative values. The transverse advection term does not change much, the advection in the centre of the flow is more plain except for the walls and bottom.

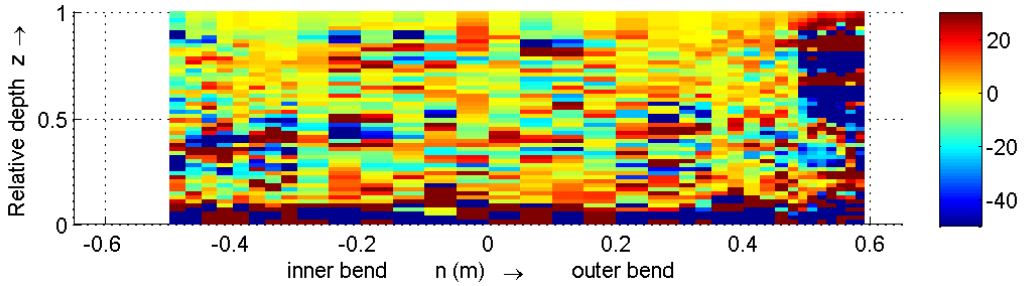

Figure C-102 Normalized ADV for cross-section m25, according to measurements. The range of the colour bar is shortened with respect to the range of the data

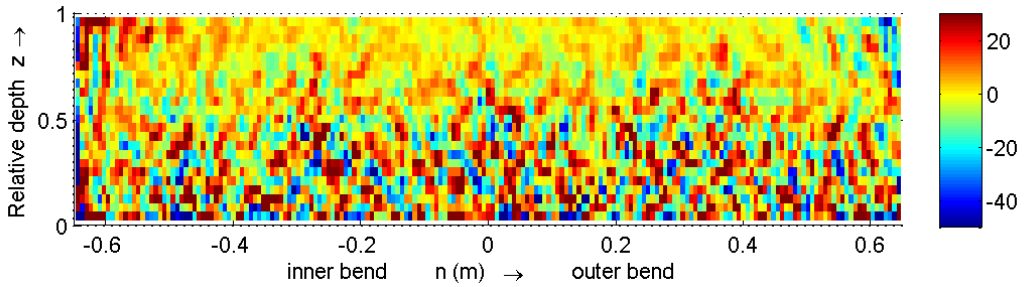

Figure C-103 Normalized ADV for cross-section m25, according to the Q89_LES. The range of the colour bar is shortened with respect to the range of the data

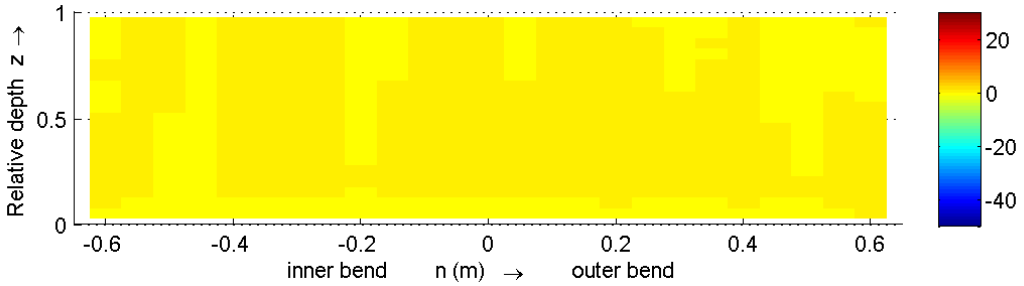

Figure C-104 Normalized ADV for cross-section m25, according to simulation Q89_1_D3D

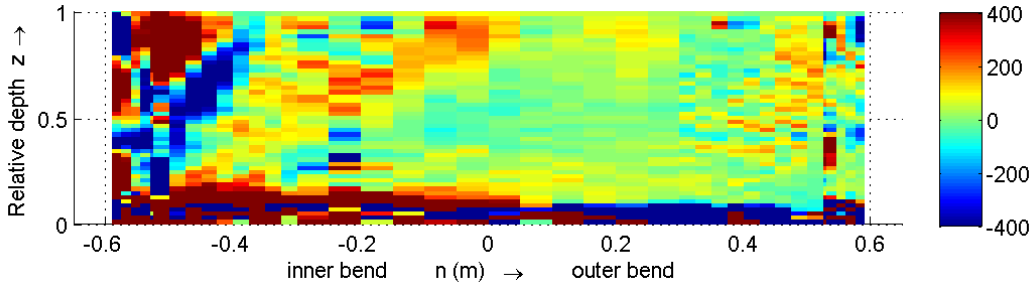

Figure C-105 Normalized ADV for cross-section 060, according to the measurements. The range of the colour bar is shortened with respect to the range of the data

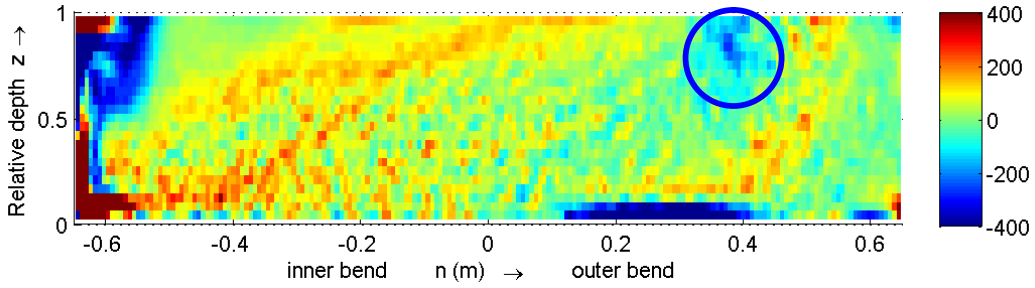

Figure C-106 Normalized ADV for cross-section 060, according to the Q89_LES. The range of the colour bar is shortened with respect to the range of the data

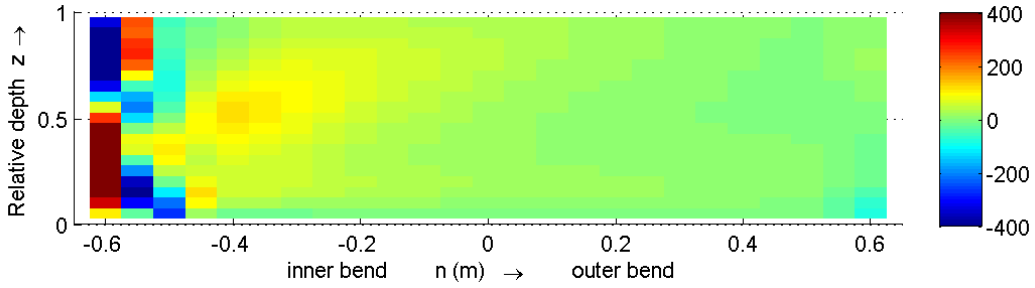

Figure C-107 Normalized ADV for cross-section 060, according to simulation Q89_1_D3D. The range of the colour bar is shortened with respect to the range of the data

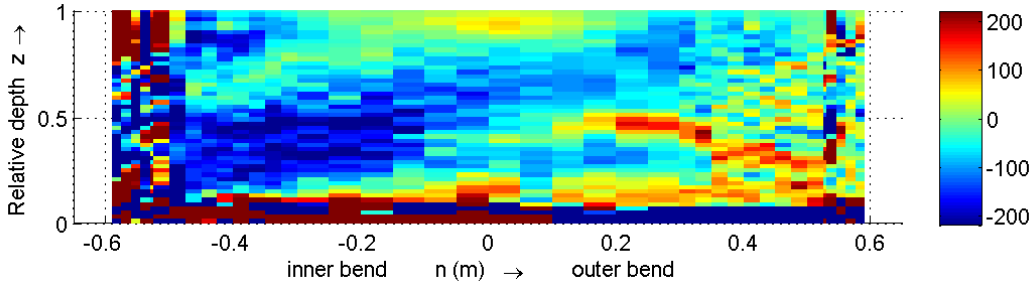

Figure C-108 ADV for cross-section 150, according to the measurements. The range of the colour bar is shortened with respect to the range of the data

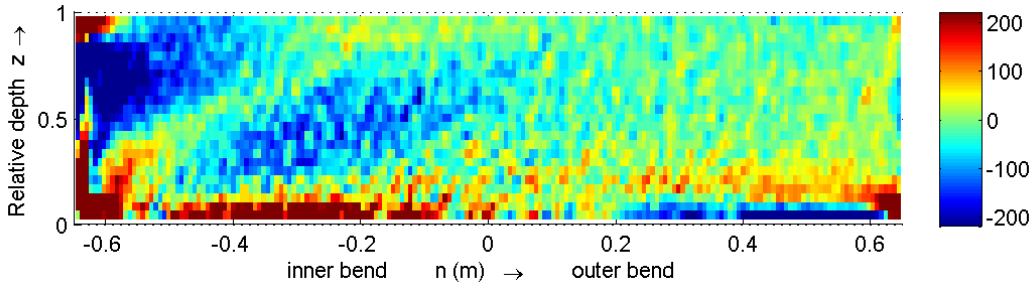

Figure C-109 Normalized ADV for cross-section 150, according to the Q89_LES. The range of the colour bar is shortened with respect to the range of the data

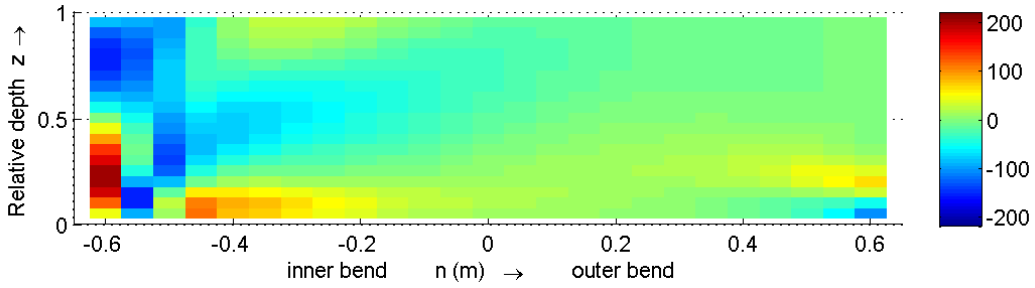

Figure C-110 Normalized ADV for cross-section 150, according to simulation Q89_1_D3D

C.6.1 Sub terms of the advection term

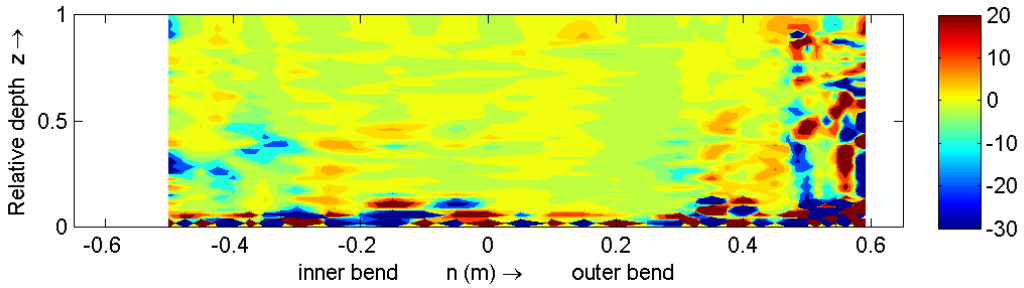

Figure C-111 Term 1, normalized, cross-section m25, measured. The range of the colour bar is shortened with respect to the range of the data

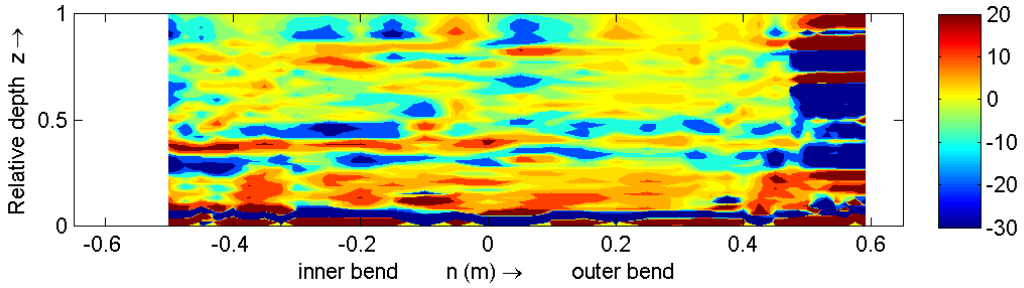

Figure C-112 Term 2, normalized, cross-section m25, measured. The range of the colour bar is shortened with respect to the range of the data

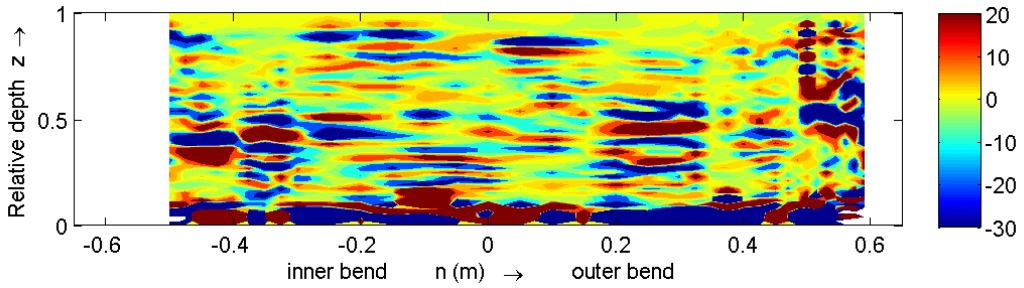

Figure C-113 Term 3, normalized, cross-section m25, measured. The range of the colour bar is shortened with respect to the range of the data

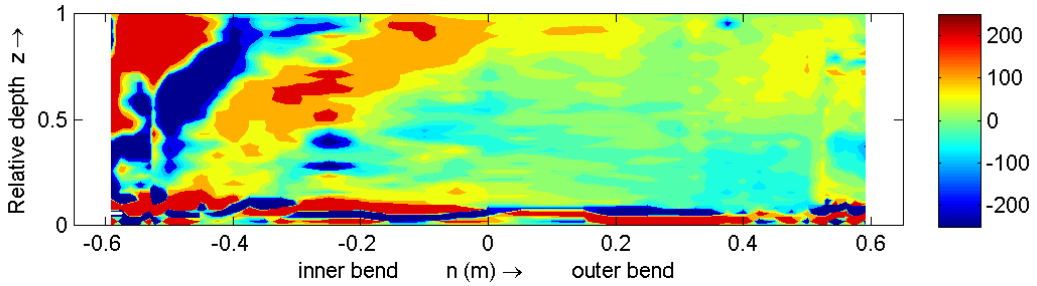

Figure C-114 Term 1, normalized, cross-section 060, measured. The range of the colour bar is shortened with respect to the range of the data

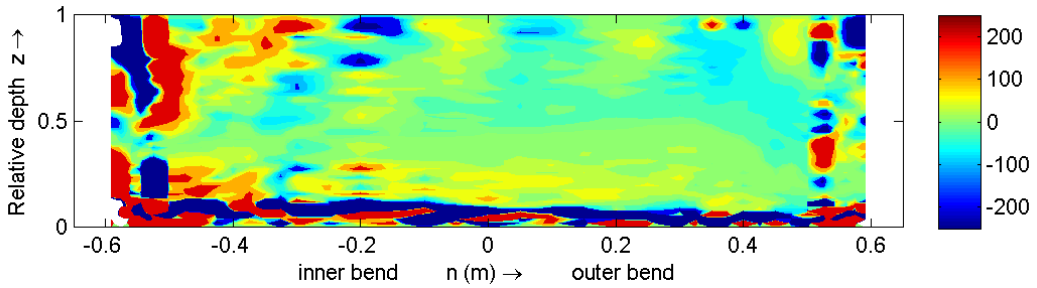

Figure C-115 Term 2, normalized, cross-section 060, measured. The range of the colour bar is shortened with respect to the range of the data

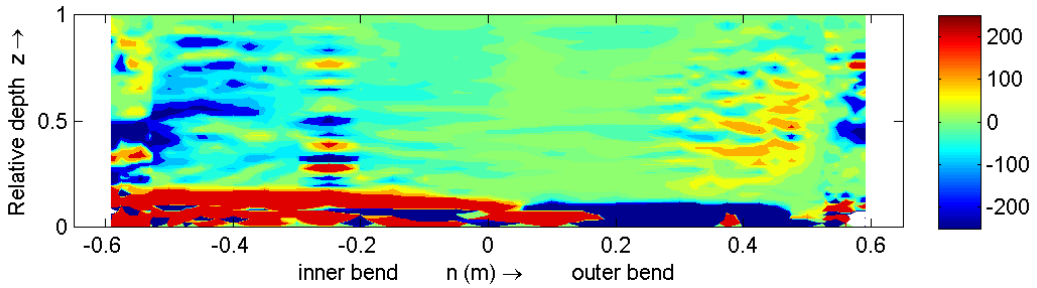

Figure C-116 Term 3, normalized, cross-section 060, measured. The range of the colour bar is shortened with respect to the range of the data

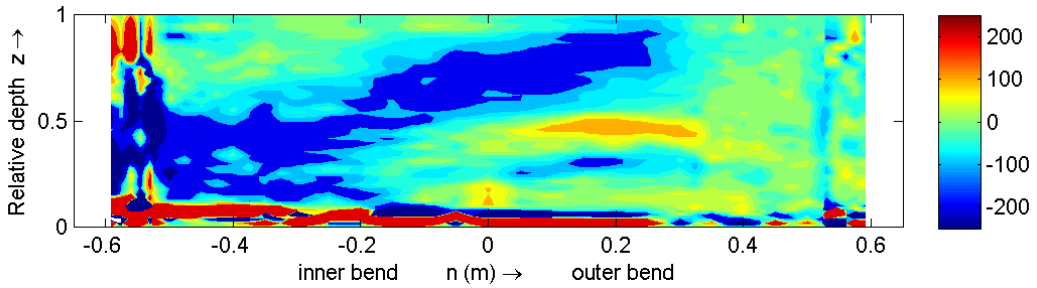

Figure C-117 Term 1, normalized, cross-section 150, measured. The range of the colour bar is shortened with respect to the range of the data

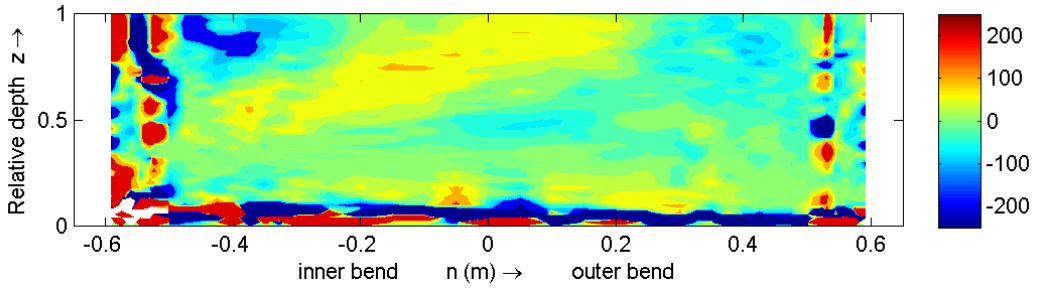

Figure C-118 Term 2, normalized, cross-section 150, measured. The range of the colour bar is shortened with respect to the range of the data

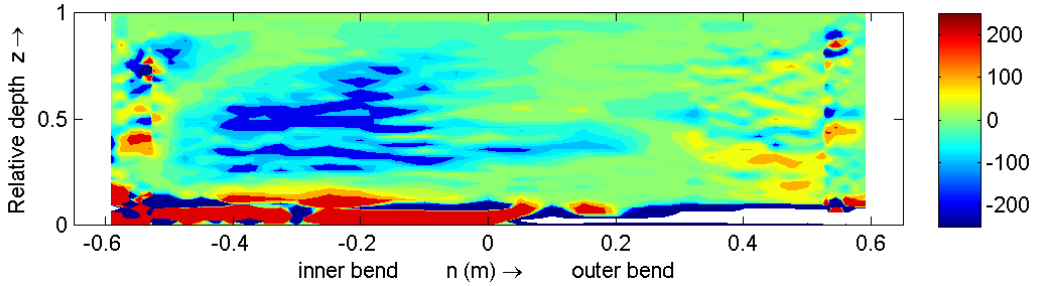

Figure C-119 Term 3, normalized, cross-section 150, measured. The range of the colour bar is shortened with respect to the range of the data

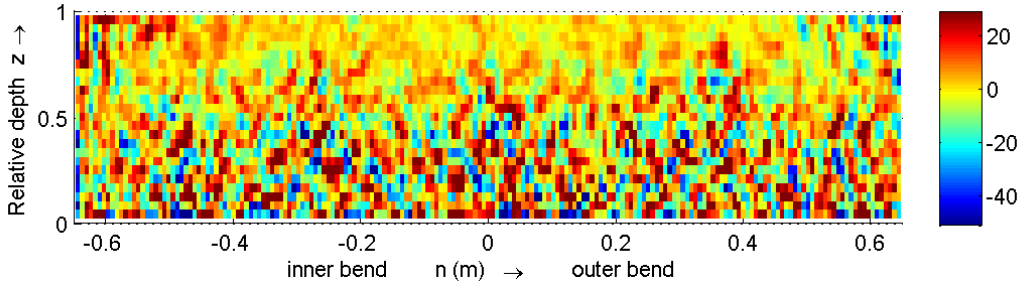

Figure C-120 Term 1, normalized, cross-section m25, Q89_LES. The range of the colour bar is shortened with respect to the range of the data

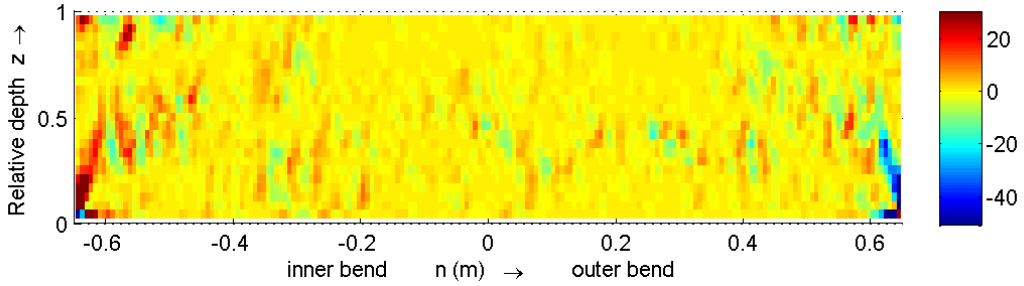

Figure C-121 Term 2, normalized, cross-section m25, Q89_LES. The range of the colour bar is shortened with respect to the range of the data

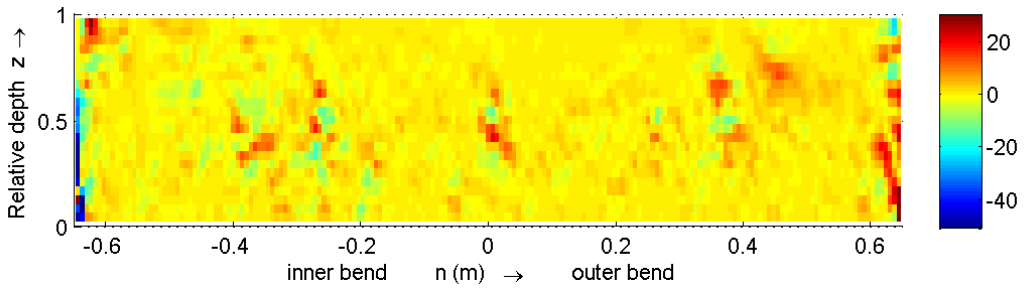

Figure C-122 Term 3, normalized, cross-section m25, Q89_LES. The range of the colour bar is shortened with respect to the range of the data

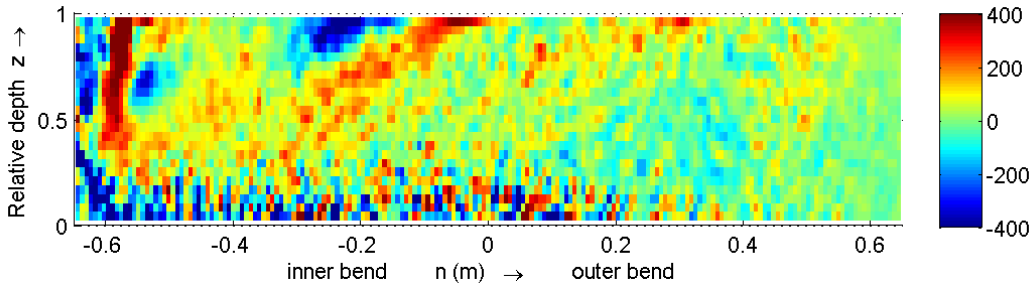

Figure C-123 Term 1, normalized, cross-section 060, Q89_LES. The range of the colour bar is shortened with respect to the range of the data

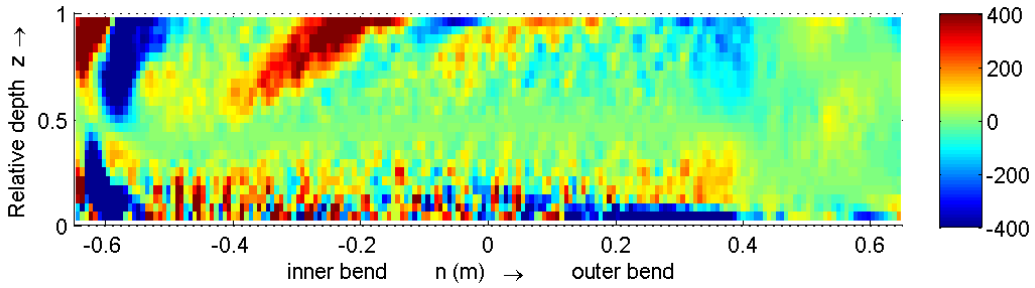

Figure C-124 Term 2, normalized, cross-section 060, Q89_LES. The range of the colour bar is shortened with respect to the range of the data

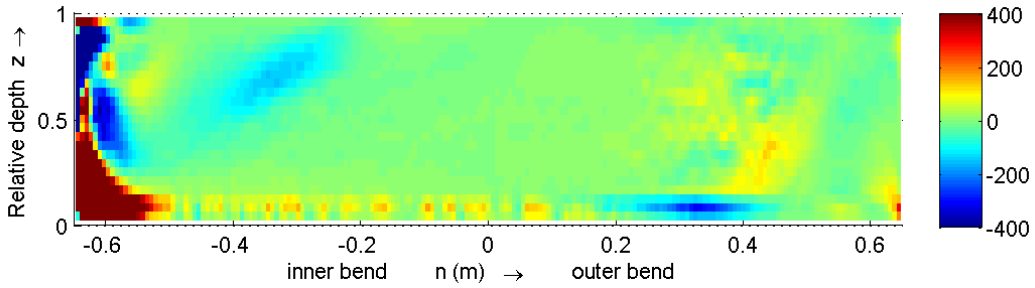

Figure C-125 Term 3, normalized, cross-section 060, Q89_LES. The range of the colour bar is shortened with respect to the range of the data

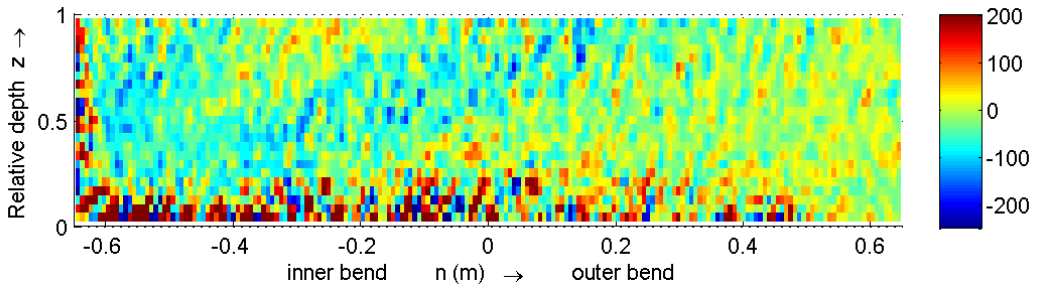

Figure C-126 Term 1, normalized, cross-section 150, Q89_LES. The range of the colour bar is shortened with respect to the range of the data

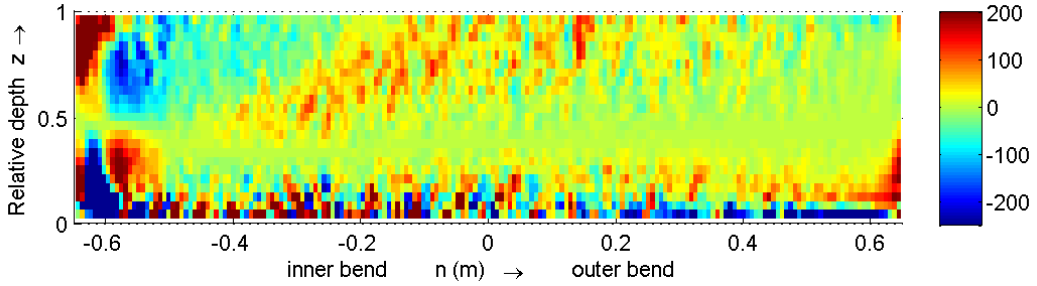

Figure C-127 Term 2, normalized, cross-section 150, Q89_LES. The range of the colour bar is shortened with respect to the range of the data

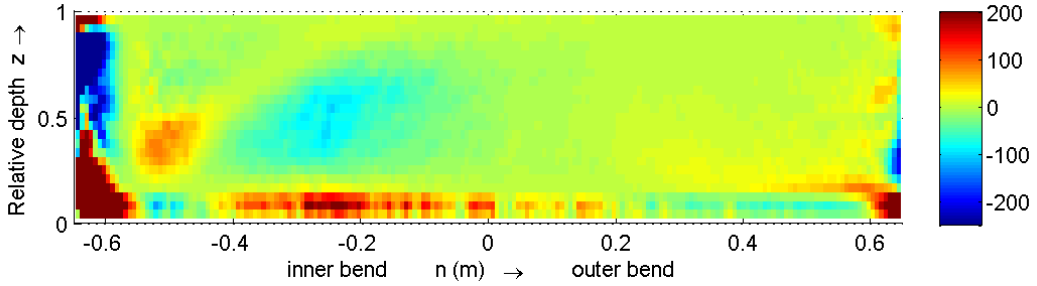

Figure C-128 Term 3, normalized, cross-section 150, Q89_LES. The range of the colour bar is shortened with respect to the range of the data

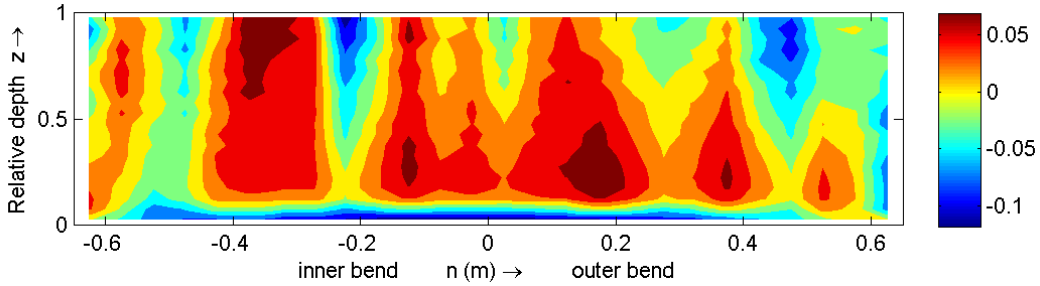

Figure C-129 Term 1, normalized, cross-section m25, simulation Q89_1_D3D

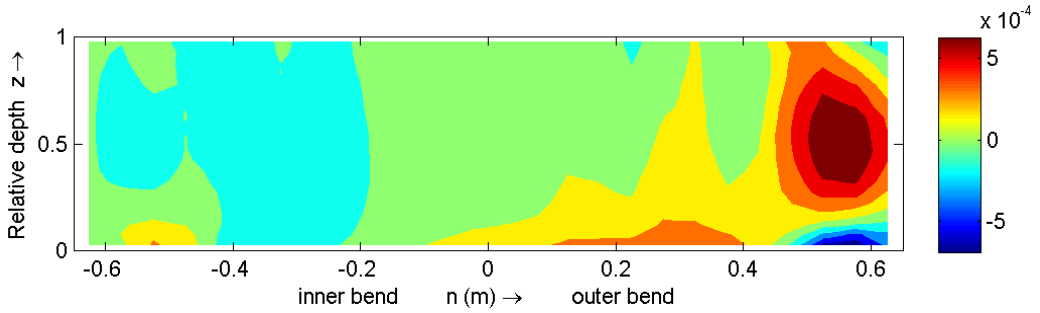

Figure C-130 Term 2, normalized, cross-section m25, simulation Q89_1_D3D

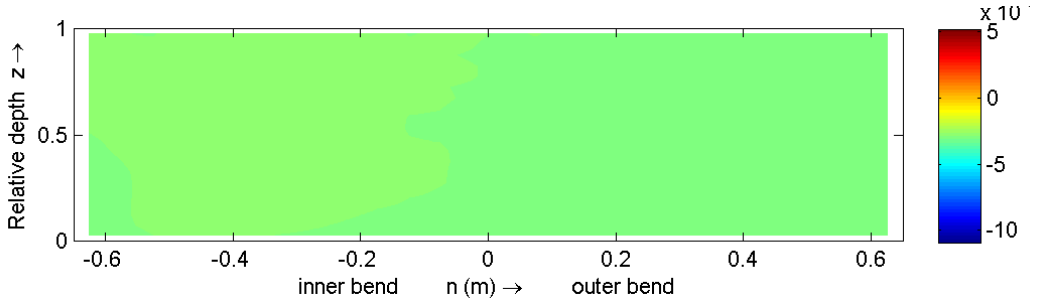

Figure C-131 Term 3, normalized, cross-section m25, simulation Q89_1_D3D

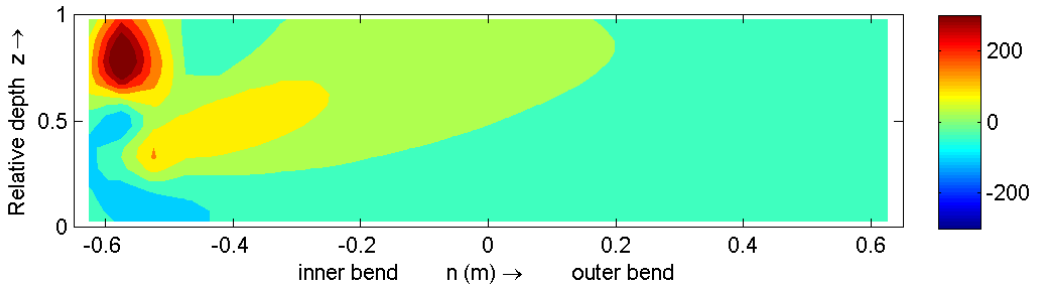

Figure C-132 Term 1, normalized, cross-section 060, simulation Q89_1_D3D. The range of the colour bar is shortened with respect to the range of the data

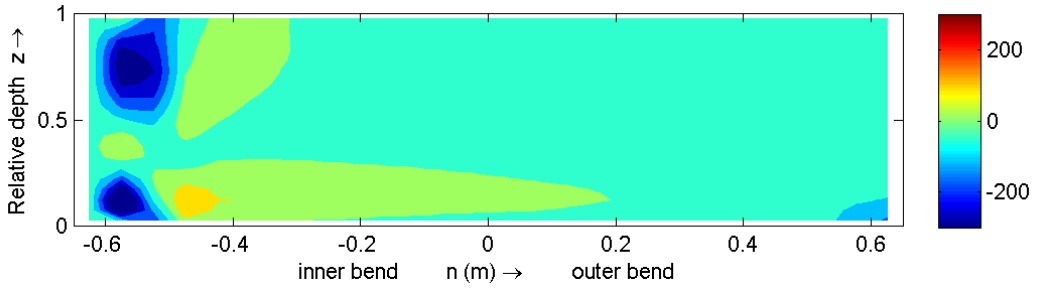

Figure C-133 Term 2, normalized, cross-section 060, simulation Q89_1_D3D. The range of the colour bar is shortened with respect to the range of the data

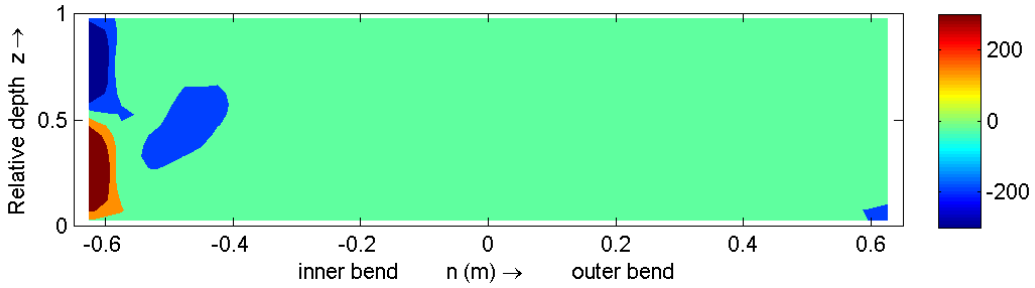

Figure C-134 Term 3, normalized, cross-section 060, simulation Q89_1_D3D. The range of the colour bar is shortened with respect to the range of the data

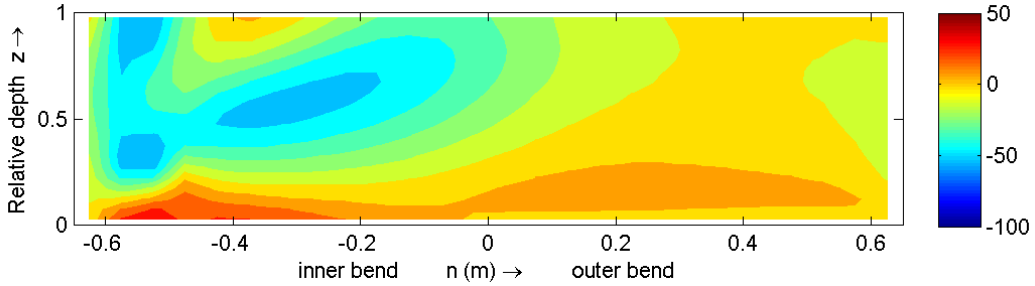

Figure C-135 Term 1, normalized, cross-section 150, simulation Q89_1_D3D

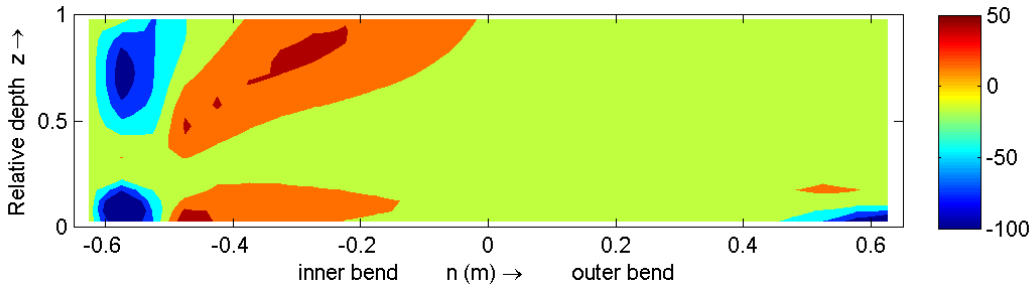

Figure C-136 Term 2, normalized, cross-section 150, simulation Q89_1_D3D. The range of the colour bar is shortened with respect to the range of the data

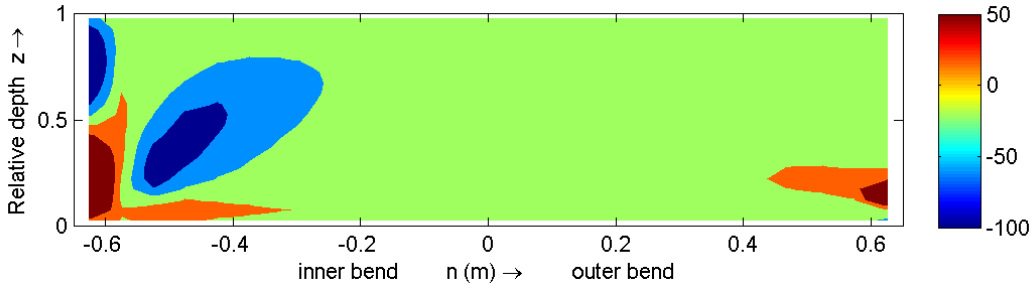

Figure C-137 Term 3, normalized, cross-section 150, simulation Q89_1_D3D. The range of the colour bar is shortened with respect to the range of the data

C.7 Centrifugal term

In this paragraph some plots of the centrifugal term (CFG) of the downstream vorticity balance equation will be shown. All figures are normalized by H^2/U^2 * 1000.

The centrifugal term is defined as (Balen *et al.*, 2009b)

$$\frac{1}{r}\frac{\partial}{\partial z}\left(u^2+\overline{u'^2}\right)$$

whit u the velocity in downstream direction, v' is the turbulent fluctuation of the downstream velocity, the over bar means averaging in time and r is the radius. For the Delft3D-FLOW simulation are the turbulent fluctuating velocities calculated based on the Bousinesq hypothesis (see section 2.1). The turbulent viscosity used in formula (2.8) is calculated as the average of the horizontal and vertical eddy viscosity.

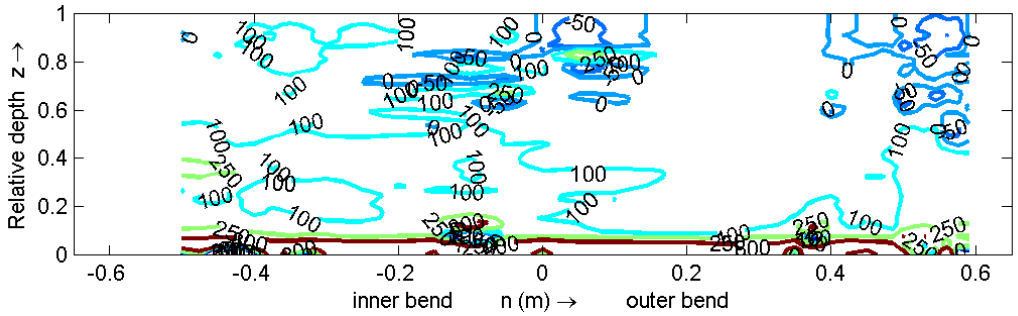

Figure C-138 Contour plot of CFG-term, according to measurements, cross-section m25, normalized

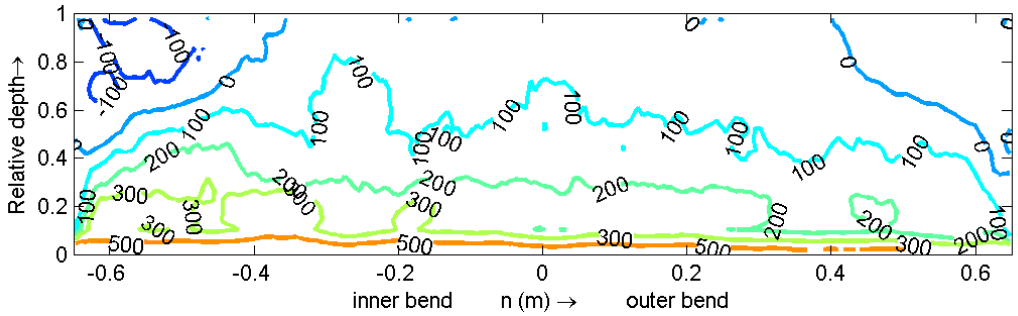

Figure C-139 Contour plot of CFG-term, according to the Q89_LES, cross-section m25, normalized

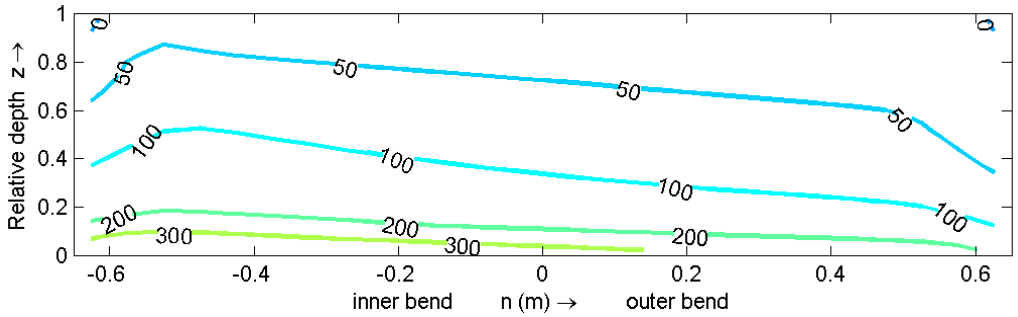

Figure C-140 Contour plot of CFG-term, according to simulation Q89_1_D3D, cross-section m25, normalized

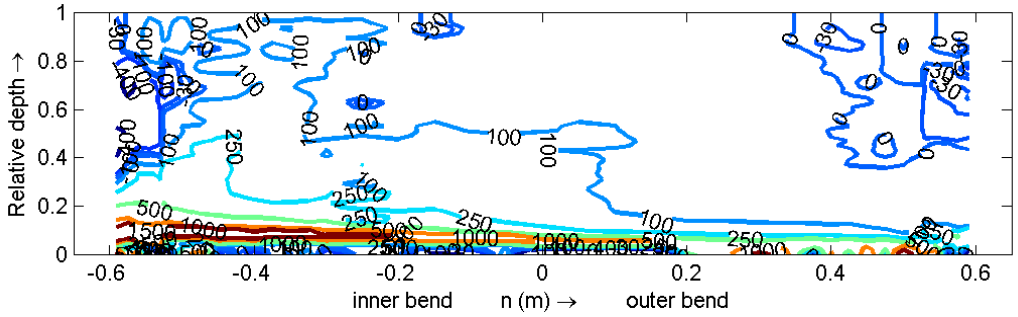

Figure C-141 Contour plot of CFG-term, according to measurements, cross-section 060, normalized

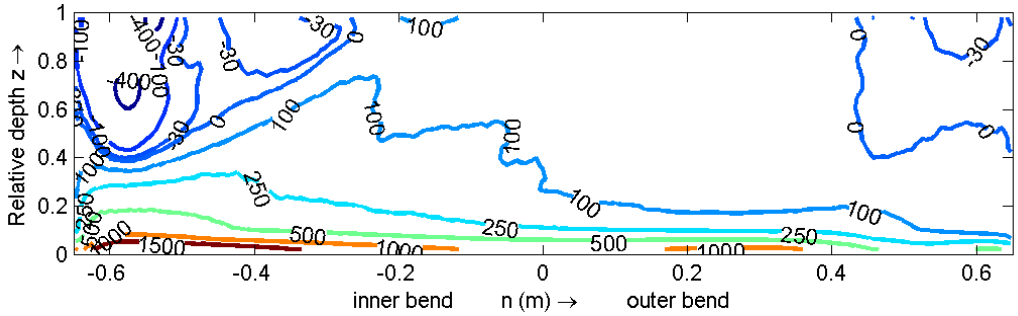

Figure C-142 Contour plot of CFG-term, according to the Q89_LES, cross-section 060, normalized

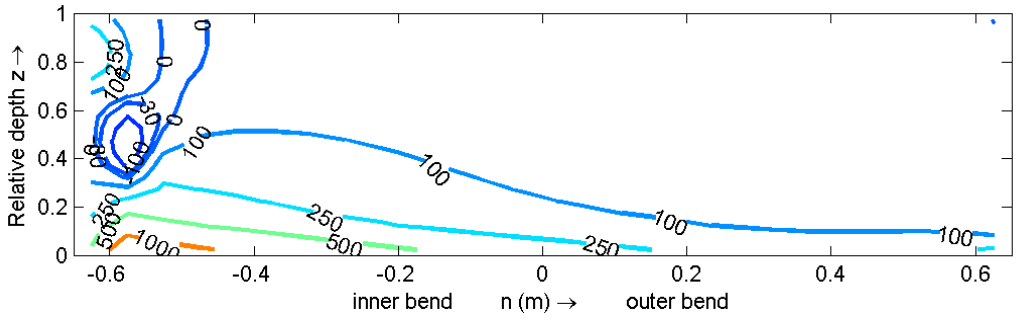

Figure C-143 Contour plot of CFG-term, according to simulation Q89_1_D3D, cross-section 060, normalized

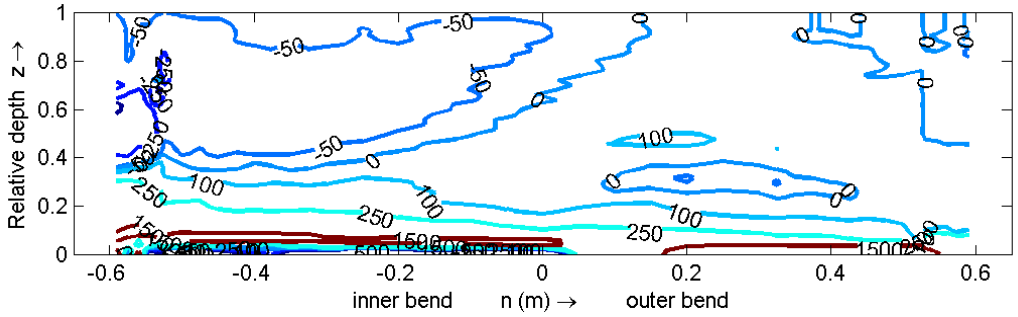

Figure C-144 Contour plot of CFG-term, according to measurements, cross-section 150, normalized

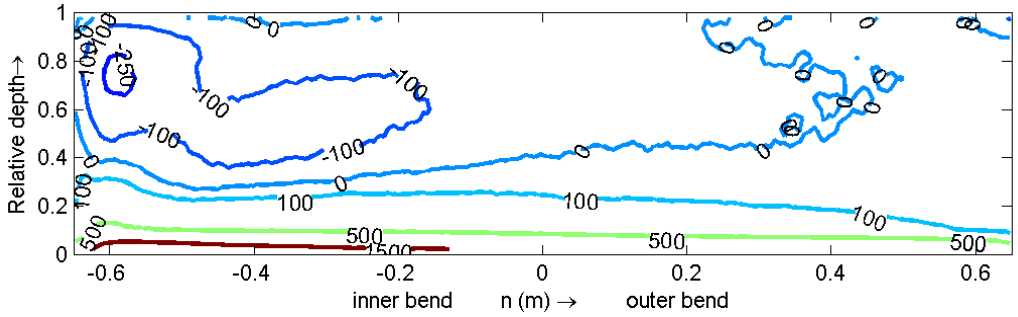

Figure C-145 Contour plot of CFG-term, according to the Q89_LES, cross-section 150, normalized

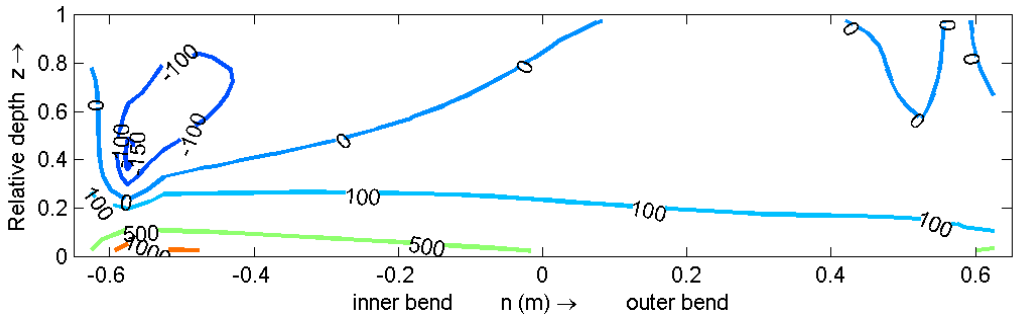

Figure C-146 Contour plot of CFG-term, according to simulation Q89_1_D3D, cross-section 150, normalized

C.8 Anisotropy term

In this paragraph are figures of the anisotropy term (ISO) for the cross-sections m25, 060 and 150. All figures are normalized by 1000 * H^2/U^2.

The anisotropy term is defined as (van Balen *et al.*, 2009b)

$$\text{ISO} = \frac{\partial^2}{\partial r \partial z}\left(\overline{v'^2} - \overline{w'^2}\right) + \frac{1}{r}\frac{\partial \overline{v'^2}}{\partial z}$$

Where v' and w' are the turbulent fluctuation of the transverse respectively the vertical velocity.

Each of the sub terms is also plotted to figure out which ones are important.

$$\text{Term 1} = \frac{\partial^2}{\partial r \partial z}\left(\overline{v'} - \overline{w'}\right)$$

$$\text{Term 2} = \frac{1}{r}\frac{\partial \overline{v'^2}}{\partial z}$$

Starting from the m25 cross-section, we see that the results of simulation Q89_1_D3D are one order of magnitude smaller than the ones according to the Q89_LES and the measurements and the values of simulation Q89_1_D3D are only negative (compare Figure C-149 with Figure C-147 and Figure C-148). At the inner bend wall the pattern of all data sets looks a bit the same, a fluctuating bar is visible. For the centre region holds that the measurements show a nearly constant value for the ISO-term and only in the upper half of the flow are fluctuations visible while for the Q89_LES are the fluctuations visible in the lower part of the flume.

In the 060 cross-section the figures show high valued bars (in absolute sense) along the side walls (Figure C-150 to Figure C-152). There are some regions with higher positive valued anisotropy but they show no clear patterns. Simulation Q89_1_D3D and the Q89_LES show only the bar along the inner bend and the negative and positive values in that specific bar are in reversed order compared to the measurements. For both the measurements and the Q89_LES an increase of anisotropy is visible in the region of the outer bank cell. This underpins the idea that the outer bank cell is initiated by anisotropic turbulent stresses (see the blue circle in Figure C-151).

In the 150 cross-section, the strength of the ISO-term is decreased but furthermore most of the patterns are the same as in the 060 cross-section. The clear increase of the anisotropy at outer bank cell region is disappeared. The increase along the walls can be explained by the presence of the walls. The turbulent velocities are bounded by the presence of the wall which causes the anisotropy.

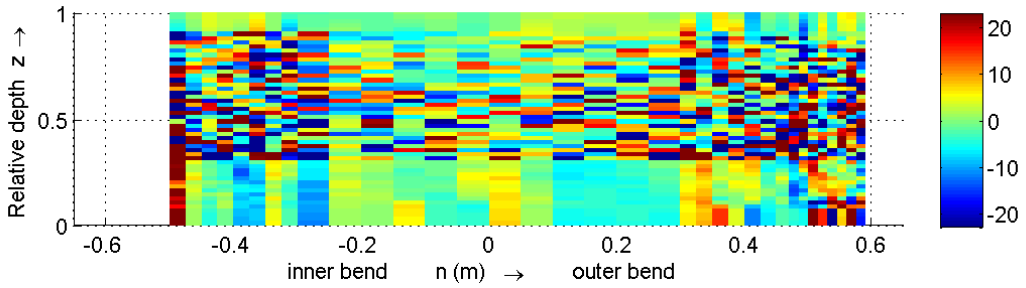

Figure C-147 ISO-term, according to measurements, cross-section m25, normalized, shortened colour bar

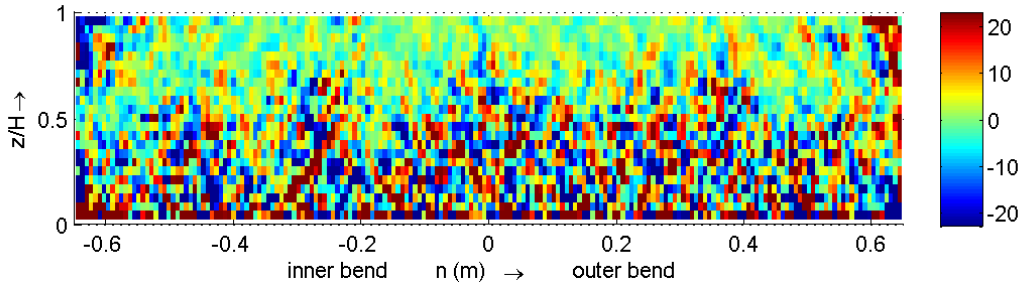

Figure C-148 ISO-term, according to the Q89_LES, cross-section m25, normalized, shortened colour bar

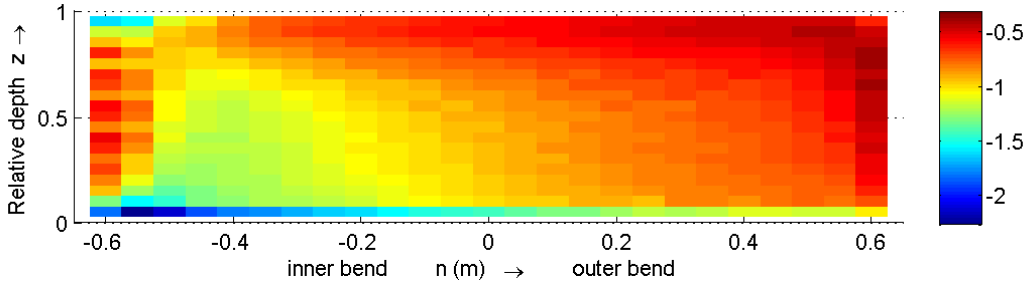

Figure C-149 ISO-term, according to simulation Q89_1_D3D, cross-section m25, normalized

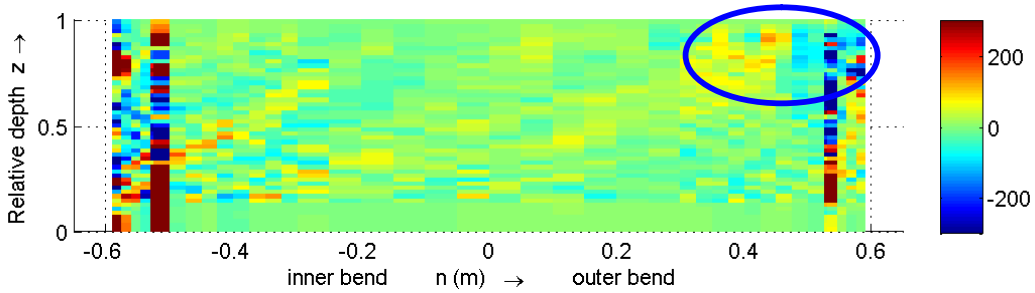

Figure C-150 ISO-term, according to measurement, cross-section 060, normalized, shortened colour bar

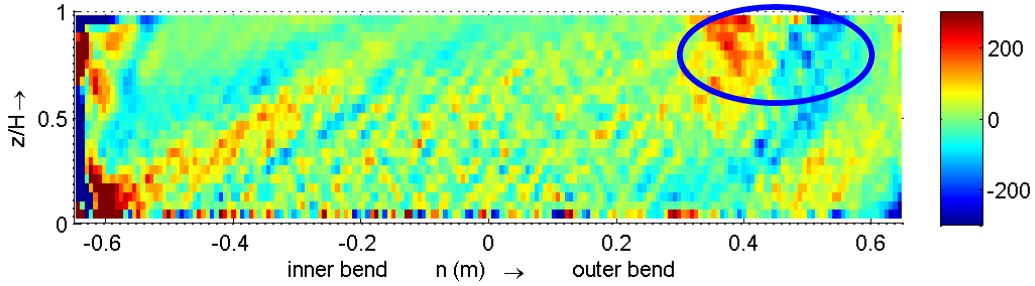

Figure C-151 ISO-term, according to the Q89_LES, cross-section 060, normalized, shortened colour bar

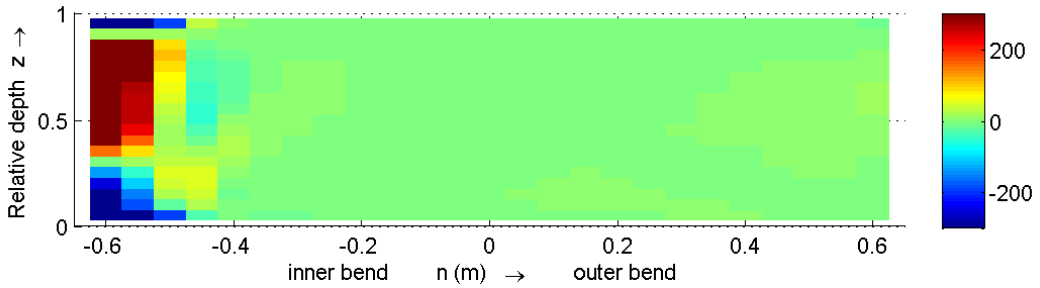

Figure C-152 ISO-term, according to simulation Q89_1_D3D, cross-section 060, normalized, shortened colour bar

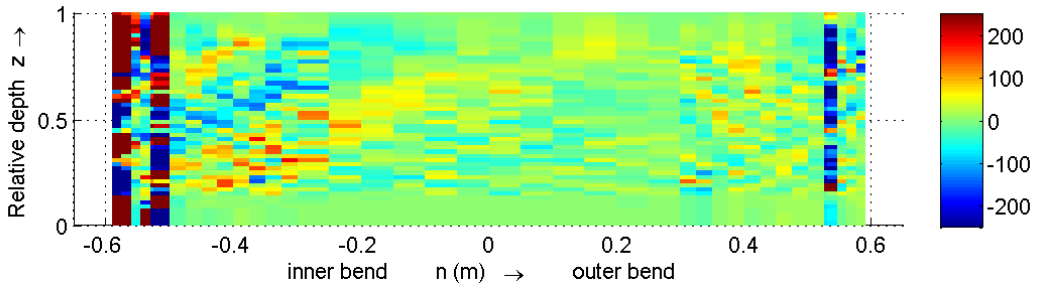

Figure C-153 ISO-term, according to measurement, cross-section 150, normalized, shortened colour bar

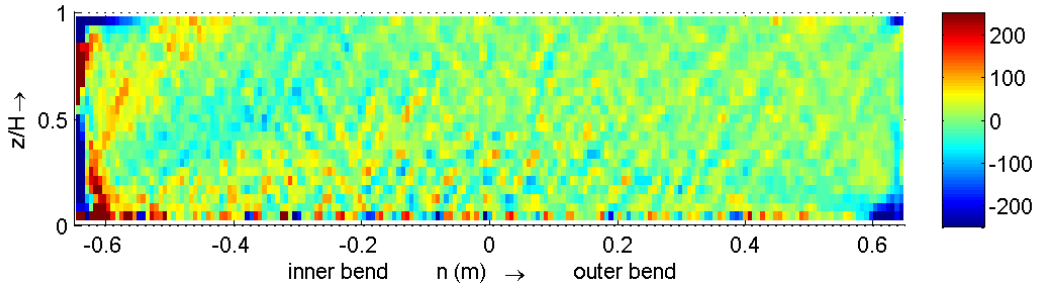

Figure C-154 ISO-term, according to the Q89_LES, cross-section 150, normalized, shortened colour bar

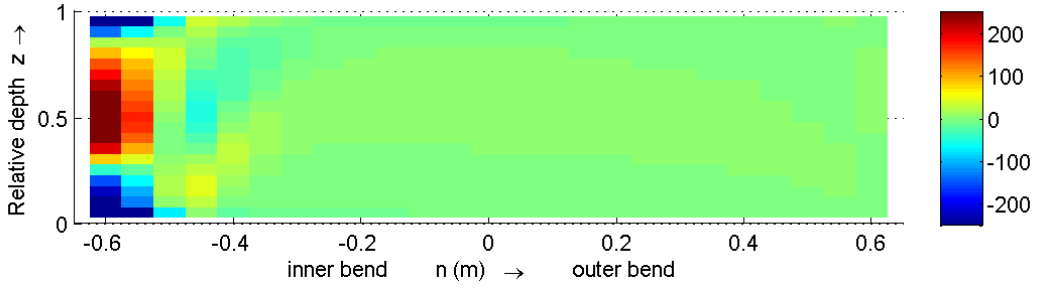

Figure C-155 ISO-term, according to simulation Q89_1_D3D, cross-section 150, normalized, shortened colour bar.

C.8.1 Sub terms of the anisotropy term

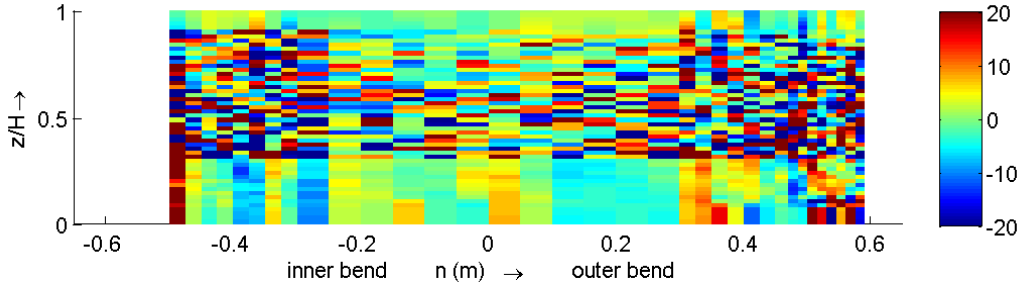

Figure C-156 Normalized term 1, according to measurements, m25, shortened colour bar.

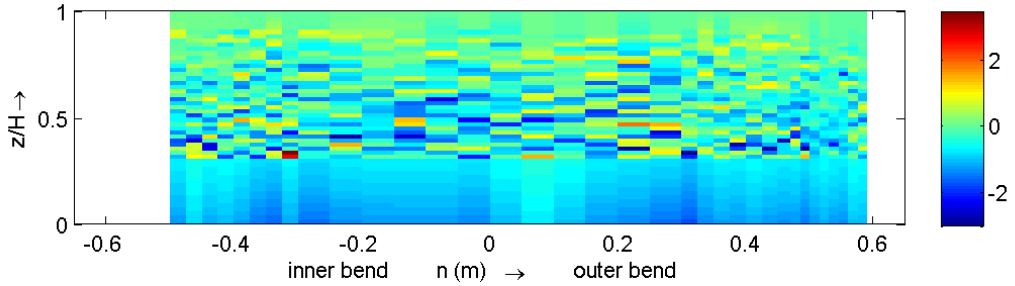

Figure C-157 Normalized term 2, according to measurements, m25

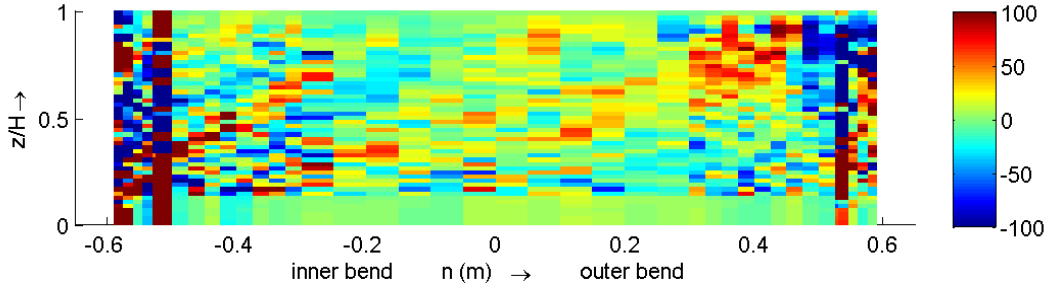

Figure C-158 Normalized term 1, according to measurements, 060, shortened colour bar.

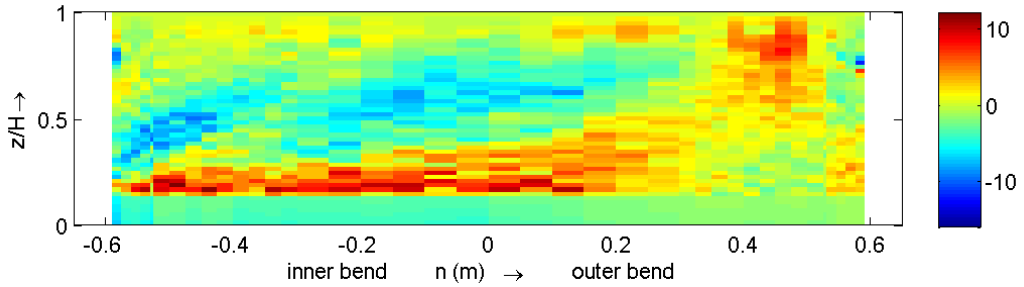

Figure C-159 Normalized term 2, according to measurements, 060

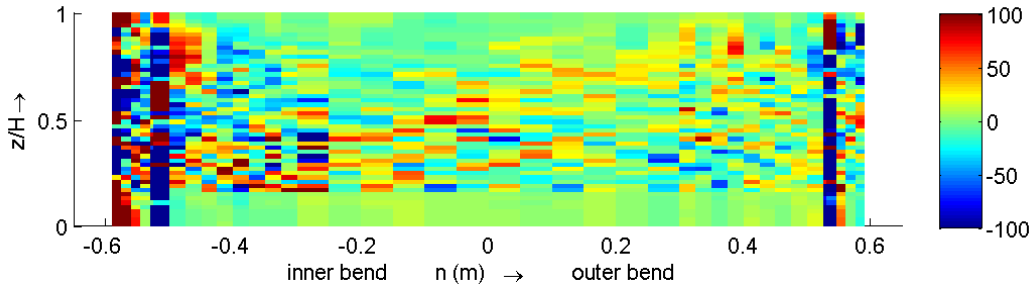

Figure C-160 Normalized term 1, according to measurements, 150, shortened colour bar.

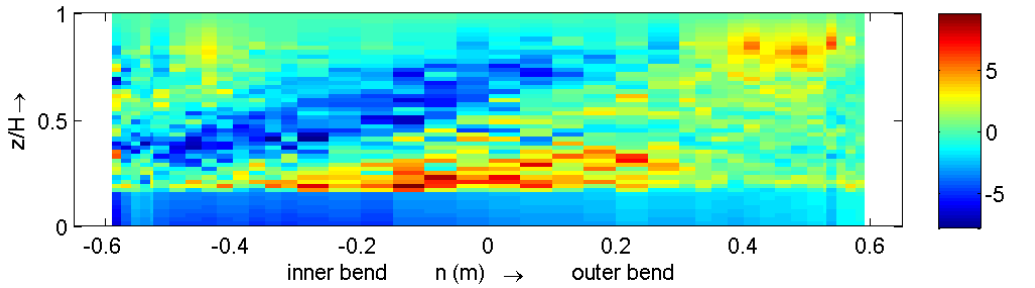

Figure C-161 Normalized term 2, according to measurements, 150

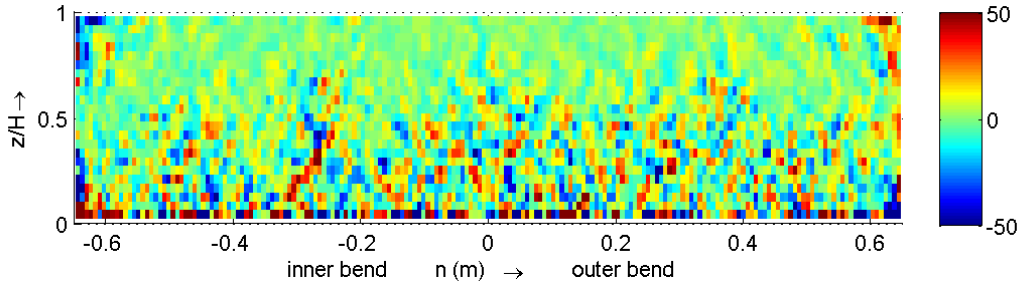

Figure C-162 Normalized term 1, according to the Q89_LES, m25, shortened colour bar

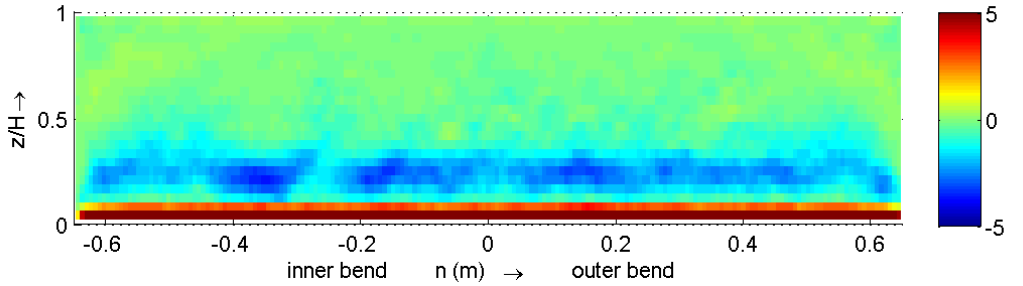

Figure C-163 Normalized term 2, according to the Q89_LES, m25, shortened colour bar

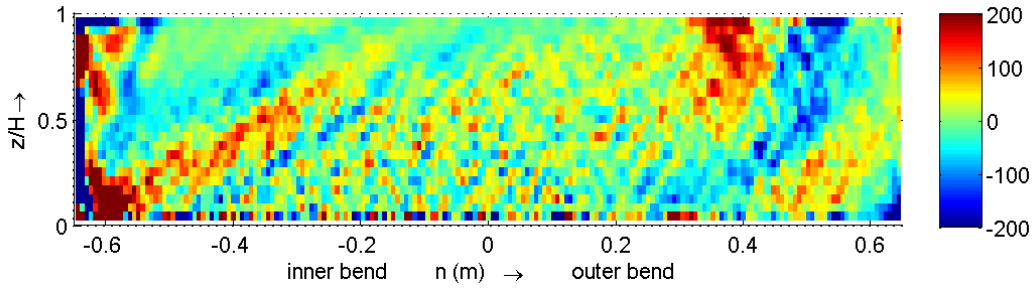

Figure C-164 Normalized term 1, according to the Q89_LES, 060, shortened colour bar

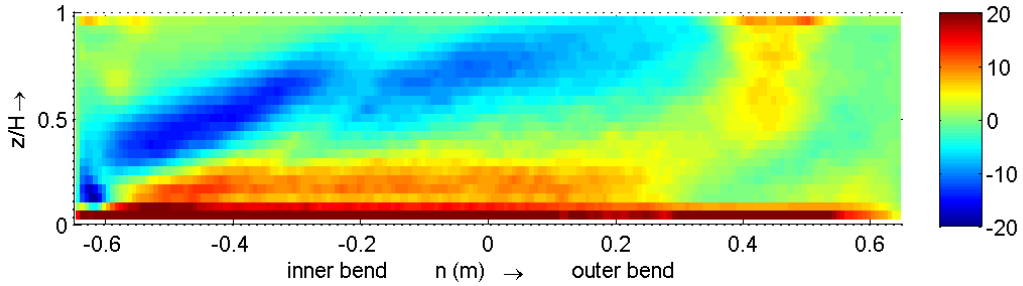

Figure C-165 Normalized term 2, according to the Q89_LES, 060, shortened colour bar

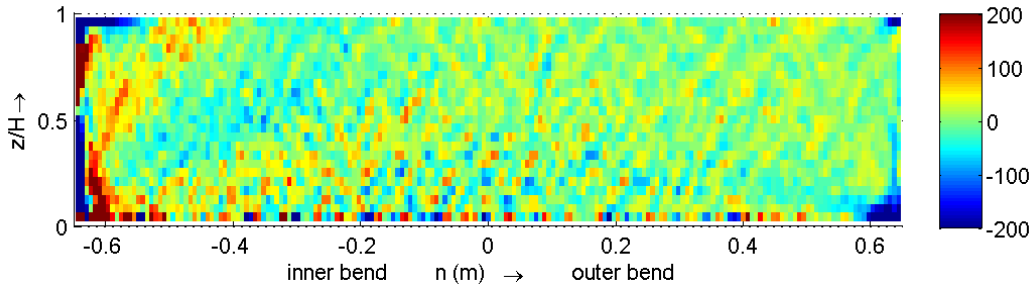

Figure C-166 Normalized term 1, according to the Q89_LES, 150, shortened colour bar

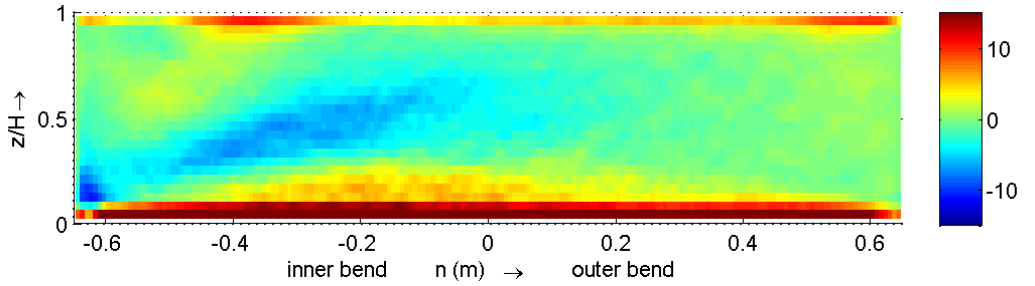

Figure C-167 Normalized term 2, according to the Q89_LES, 150, shortened colour bar

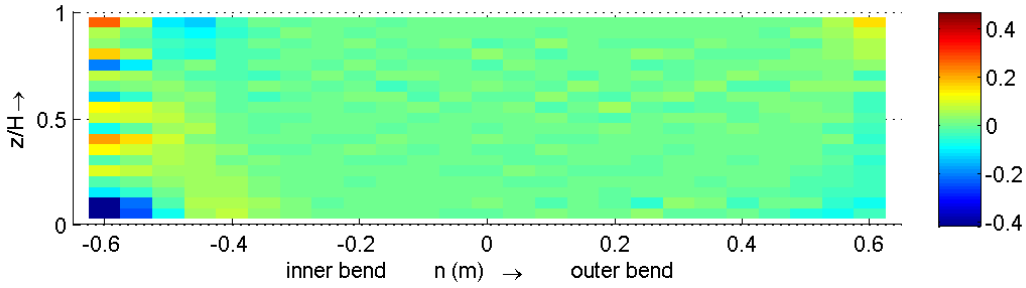

Figure C-168 Normalized term 1, according to simulation Q89_1_D3D, m25, shortened colour bar

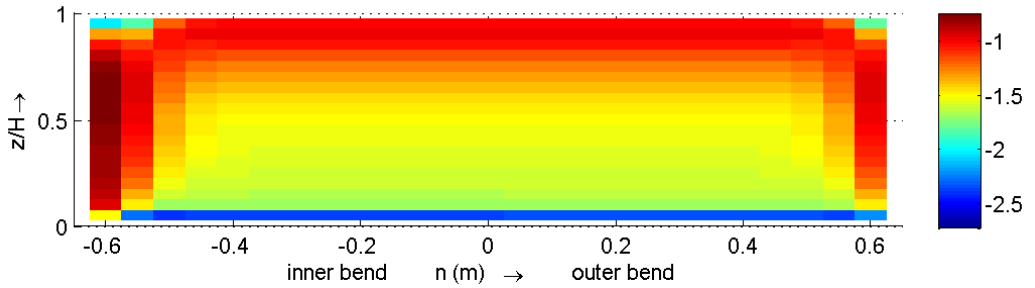

Figure C-169 Normalized term 2, according to simulation Q89_1_D3D, m25

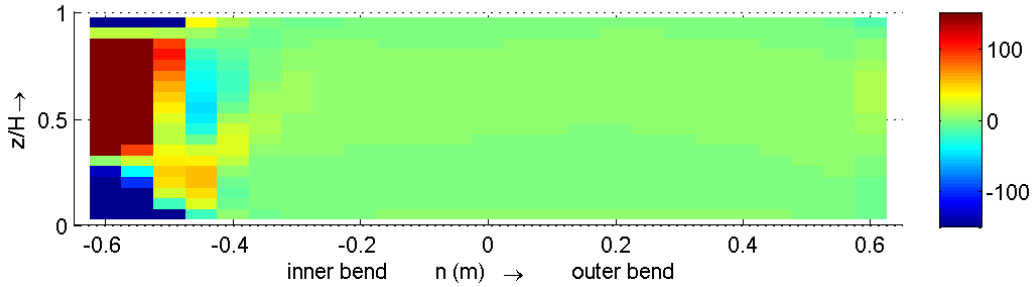

Figure C-170 Normalized term 1, according to simulation Q89_1_D3D, 060, shortened colour bar.

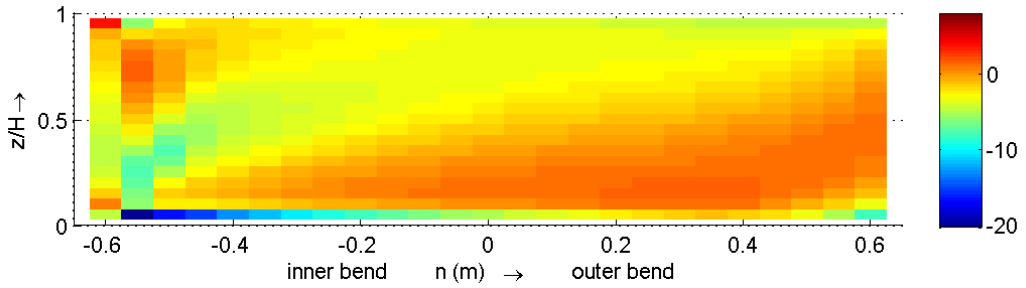

Figure C-171 Normalized term 2, according to simulation Q89_1_D3D, 060

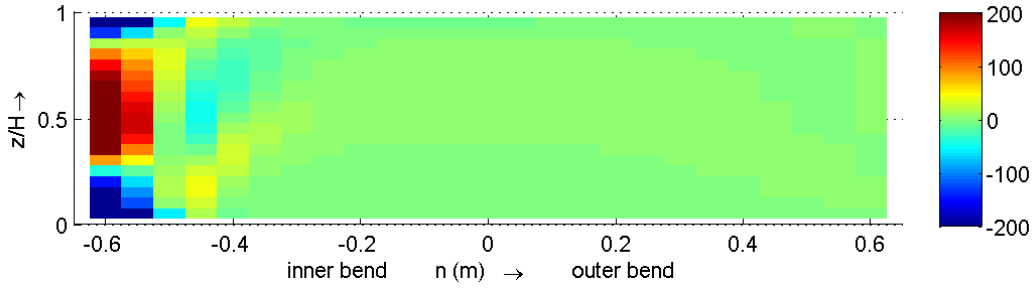

Figure C-172 Normalized term 1, according to simulation Q89_1_D3D, 150, shortened colour bar.

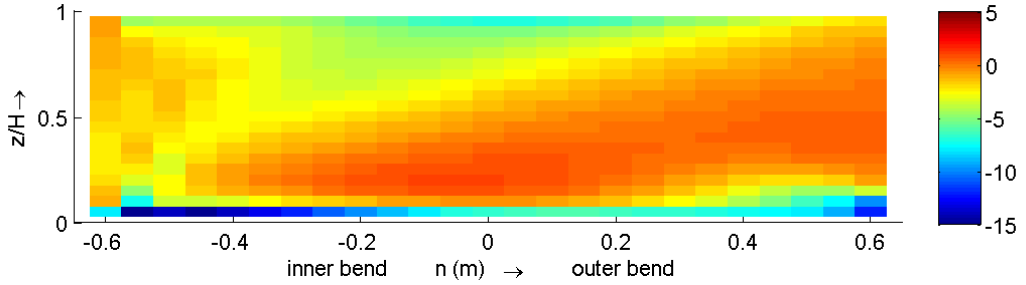

Figure C-173 Normalized term 2, according to simulation Q89_1_D3D, 150, shortened colour bar.

C.9 Homogeneity term

In this paragraph some plots of the inhomogeneity term (HOM) of the downstream vorticity balance equation will be shown. All figures are normalized by 1000 * H^2/U^2. This term represents the inhomogeneity of the turbulence stresses.

The homogeneity term is defined as (van Balen *et al.*, 2009b)

$$\left(\frac{\partial^2}{\partial z^2}-\frac{\partial^2}{\partial n^2}-\frac{1}{r}\frac{\partial}{\partial n}+\frac{1}{r^2}\right)\overline{v'w'}$$

This term is divided in four sub terms.

$$\text{Term 1} \quad = \frac{\partial^2 \overline{v'w'}}{\partial z^2}$$

$$\text{Term 2} \quad = -\frac{\partial^2 \overline{v'w'}}{\partial r^2}$$

$$\text{Term 3} \quad = -\frac{1}{r}\frac{\partial \overline{v'w'}}{\partial r}$$

$$\text{Term 4} = \frac{\overline{v'w'}}{r^2}$$

Where v' and w' are the turbulent fluctuation of the transverse respectively the vertical velocity.

Comparing the HOM-terms of the measurements in the different cross-sections, we see the inhomogeneity of the turbulent stresses increasing in the bend. Especially along the walls and the surface are the turbulent stresses inhomogeneous (see Figure C-174 and Figure C-180). This can be explained by the presence of the impermeable wall respectively the surface, which reduces the velocities normal to the boundaries.

The Q89_LES shows only along the bottom strong negative values of the HOM-term (for all three cross-sections, Figure C-175, Figure C-178 and Figure C-181). The distribution for the m25 cross-section is approximately the same but the strength is an order of magnitude smaller. In the 060 and 150 cross-sections the distribution differs much from the one according to the measurements. A region of relatively high values appears in the lower part of the flume, directly above the negative bar along the bottom. The random fluctuations are nearly absent.

Simulation Q89_1_D3D shows also an increase of the HOM-term in the bend but the inhomogeneity is less randomly distributed over the cross-section as was visible for the measurements and the strength is much lower. In the lower part of the inner bend a positive valued hump is visible (Figure C-179) in the bend but the strength of this hump decreases in the 150 cross-section (Figure C-182). The distribution is more or less the same as for the Q89_LES.

Comparing the different sub terms of the HOM-term, it can be concluded that the first sub term is the most important term. The second term has some influence along the walls and the third and fourth sub terms are more than one order of magnitude smaller (see Figure C-183 to Figure C-218).

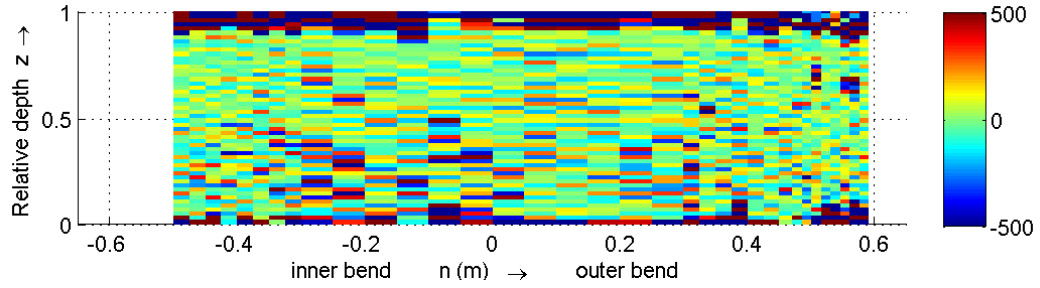

Figure C-174 HOM for cross-section m25, according to the measurements, shortened colour bar

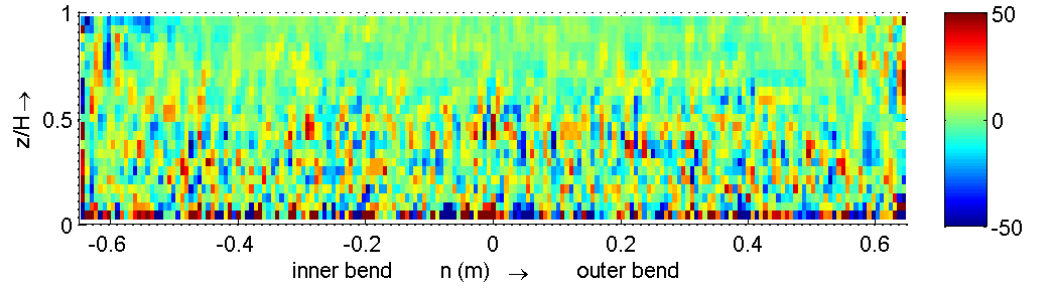

Figure C-175 HOM for cross-section m25, according to the Q89_LES, shortened colour bar

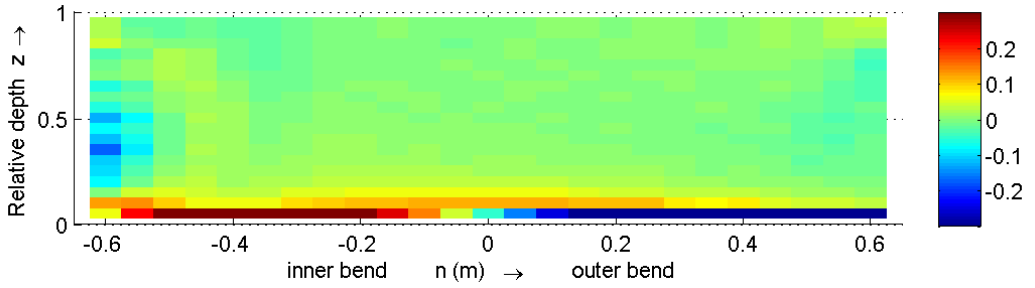

Figure C-176 HOM for cross-section m25, according to simulation Q89_1_D3D, shortened colour bar

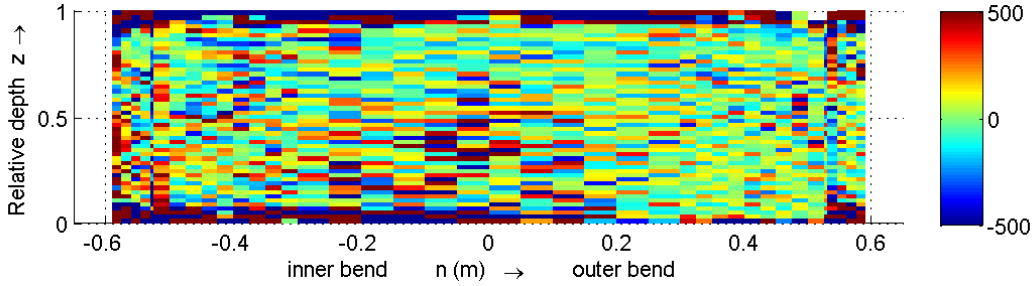

Figure C-177 HOM for cross-section 060, according to the measurements, shortened colour bar

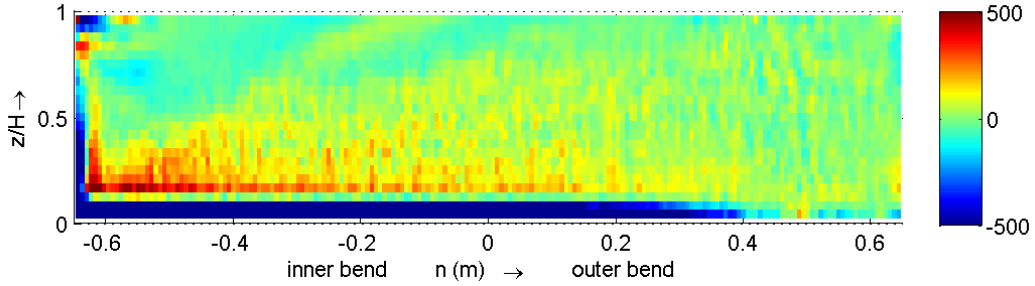

Figure C-178 HOM for cross-section 060, according to the Q89_LES, shortened colour bar

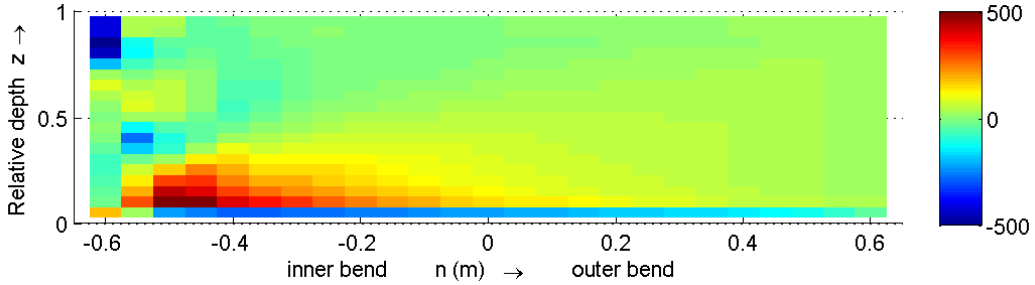

Figure C-179 HOM for cross-section 060, according to simulation Q89_1_D3D

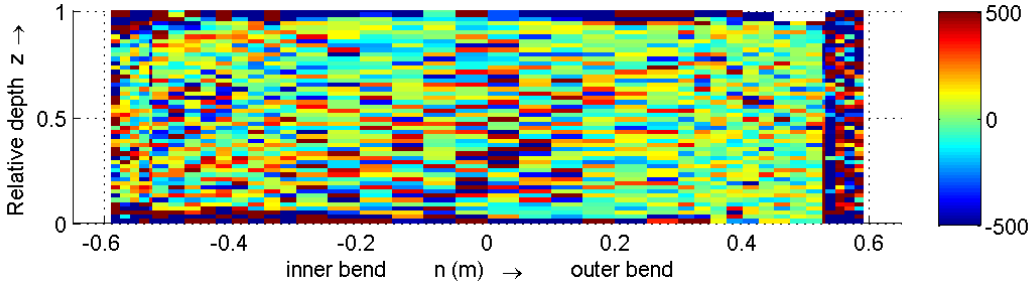

Figure C-180 HOM for cross-section 150, according to the measurements, shortened colour bar

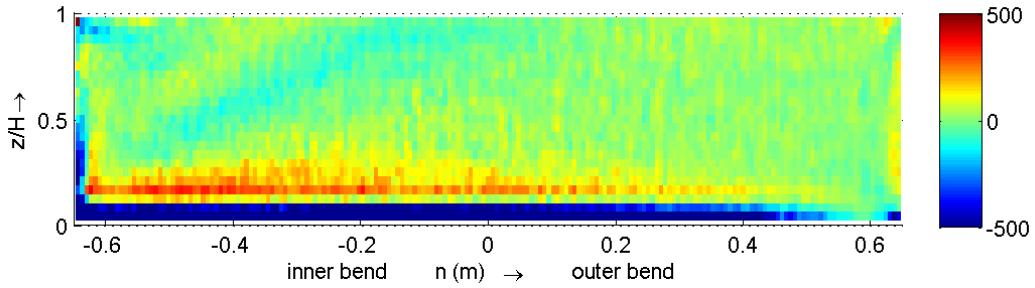

Figure C-181 HOM for cross-section 150, according to the Q89_LES, shortened colour bar

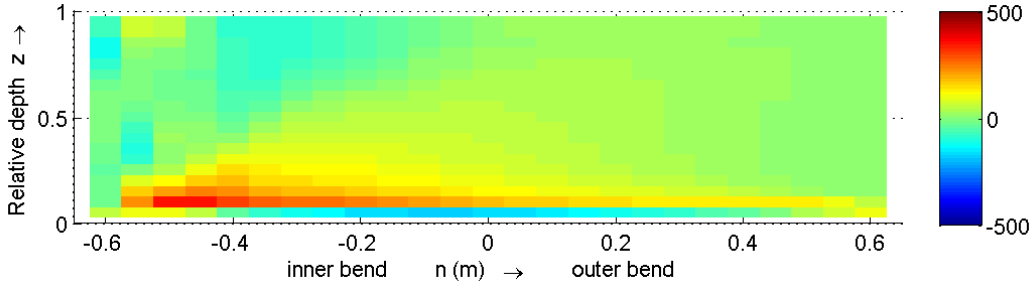

Figure C-182 HOM for cross-section 150, according to simulation Q89_1_D3D

C.9.1 Sub terms of the homogeneity term

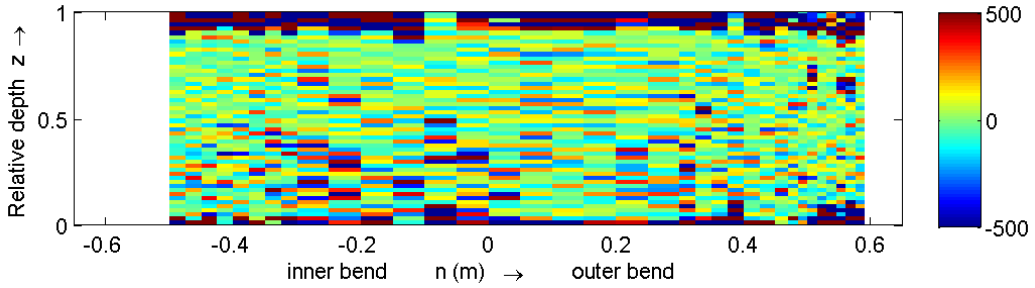

Figure C-183 Term 1, according to measurements, cross-section m25, shortened colour bar

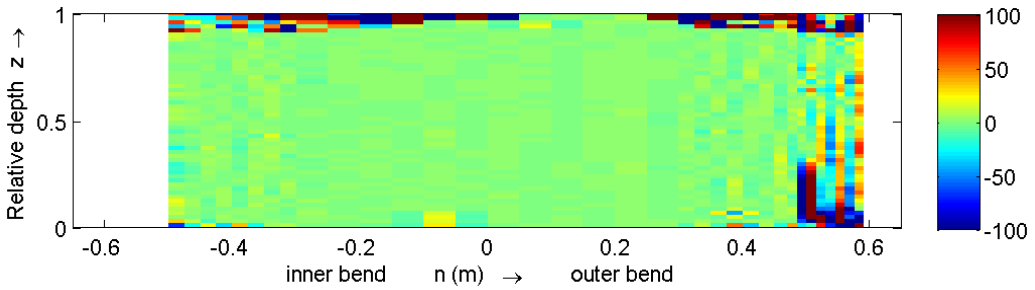

Figure C-184 Term 2, according to measurements, cross-section m25, shortened colour bar

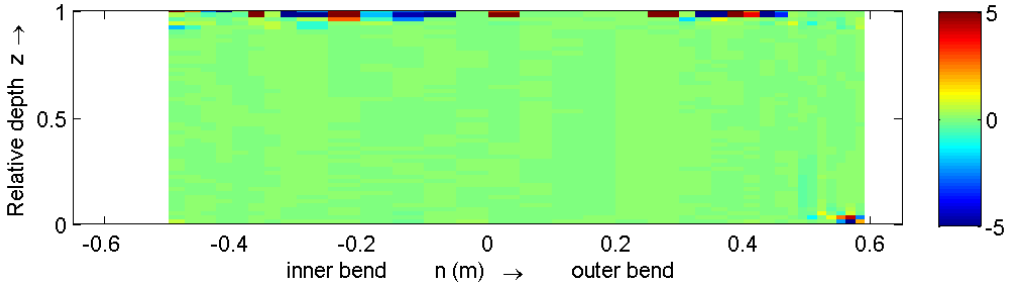

Figure C-185 Term 3, according to measurements, cross-section m25, shortened colour bar

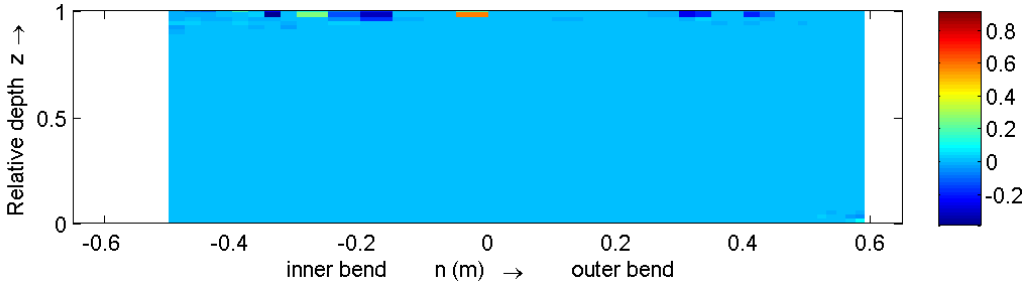

Figure C-186 Term 4, according to measurements, cross-section m25, shortened colour bar

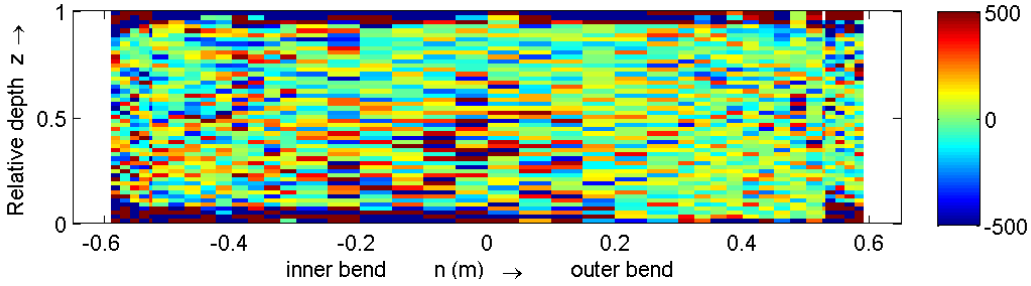

Figure C-187 Term 1, according to measurements, cross-section 060, shortened colour bar

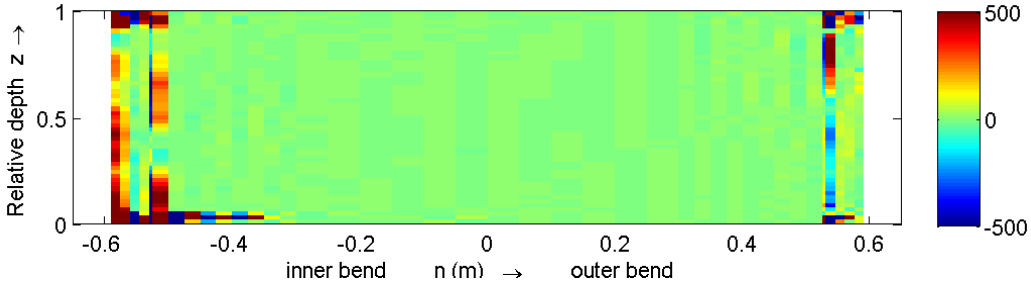

Figure C-188 Term 2, according to measurements, cross-section 060, shortened colour bar

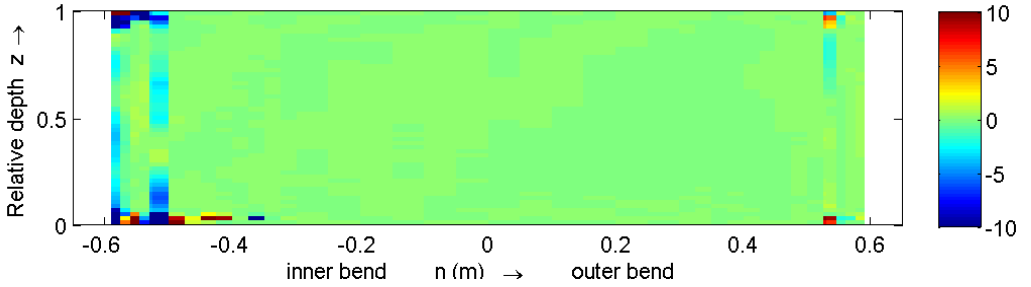

Figure C-189 Term 3, according to measurements, cross-section 060, shortened colour bar

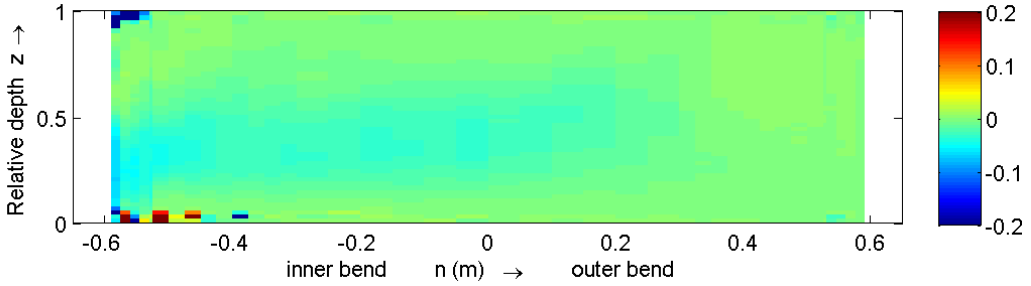

Figure C-190 Term 4, according to measurements, cross-section 060, shortened colour bar

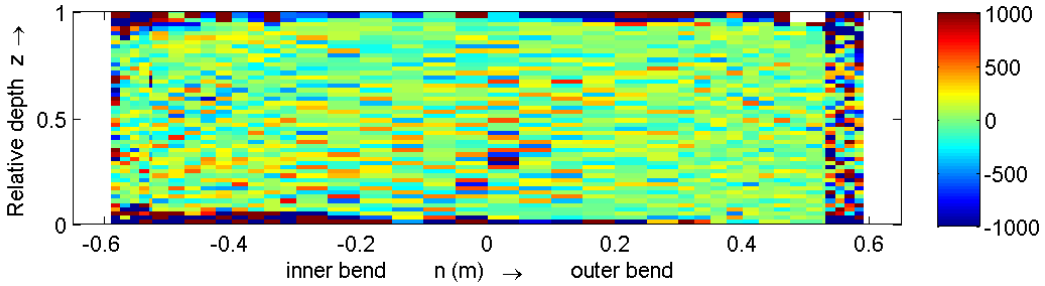

Figure C-191 Term 1, according to measurements, cross-section 150, shortened colour bar

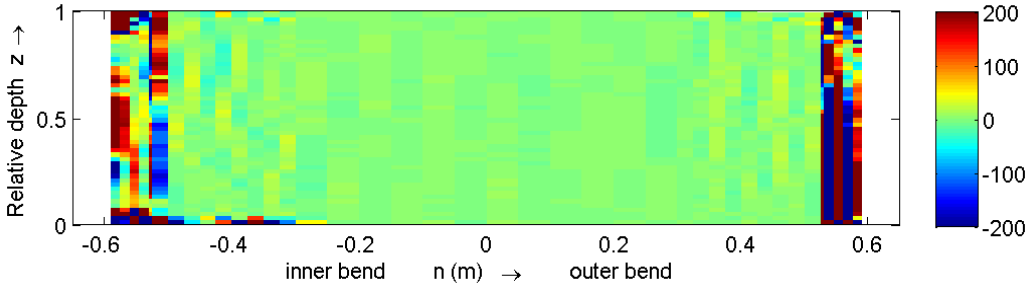

Figure C-192 Term 2, according to measurements, cross-section 150, shortened colour bar

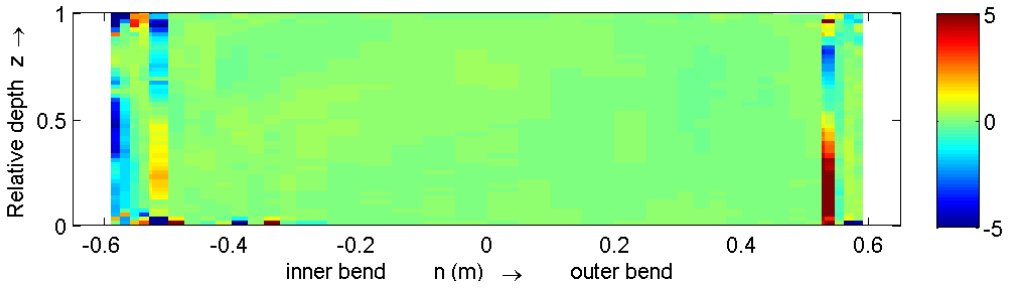

Figure C-193 Term 3, according to measurements, cross-section 150, shortened colour bar

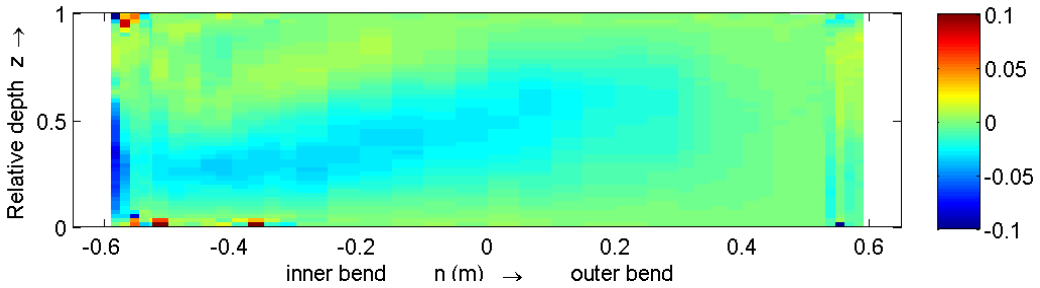

Figure C-194 Term 4, according to measurements, cross-section 150, shortened colour bar

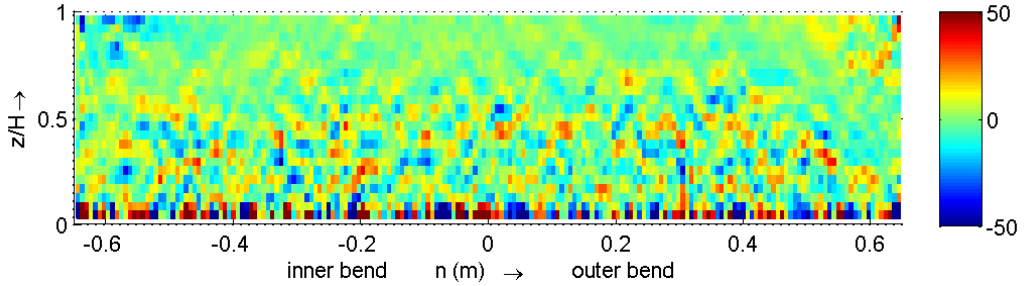

Figure C-195 Term 1, according to the Q89_LES, cross-section m25, shortened colour bar

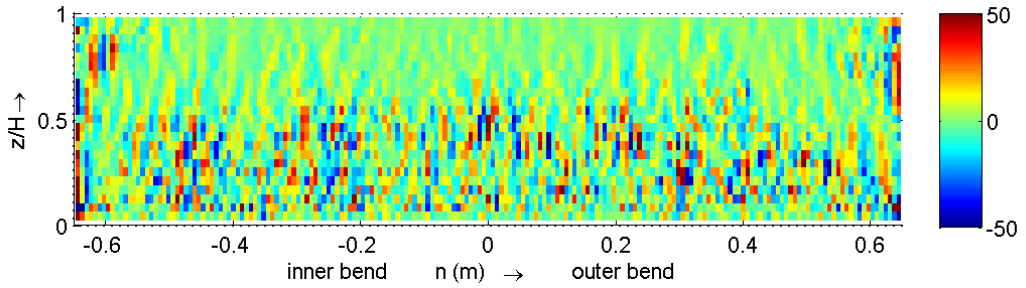

Figure C-196 Term 2, according to the Q89_LES, cross-section m25

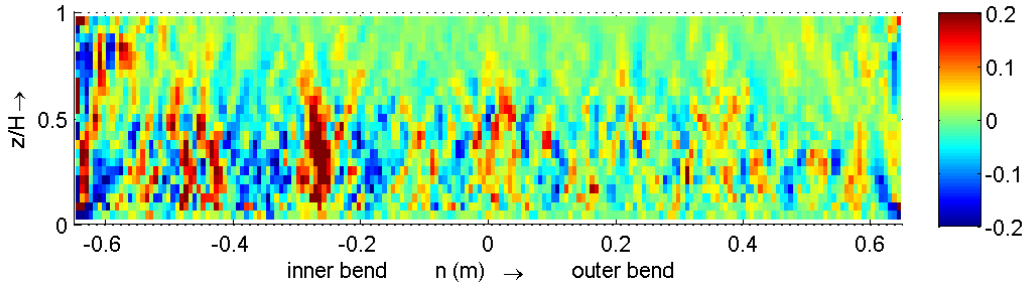

Figure C-197 Term 3, according to the Q89_LES, cross-section m25

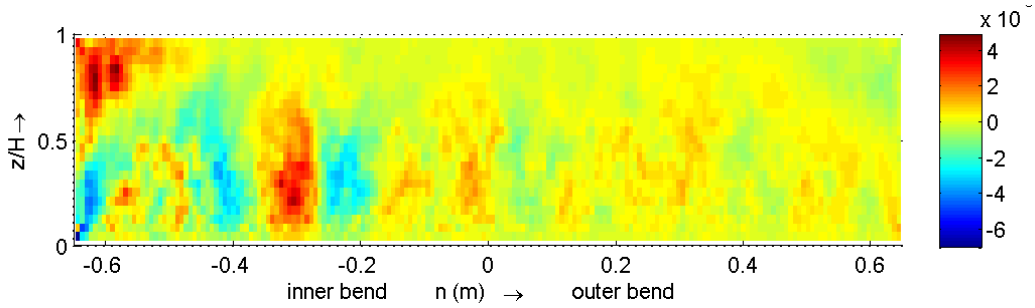

Figure C-198 Term 4, according to the Q89_LES, cross-section m25

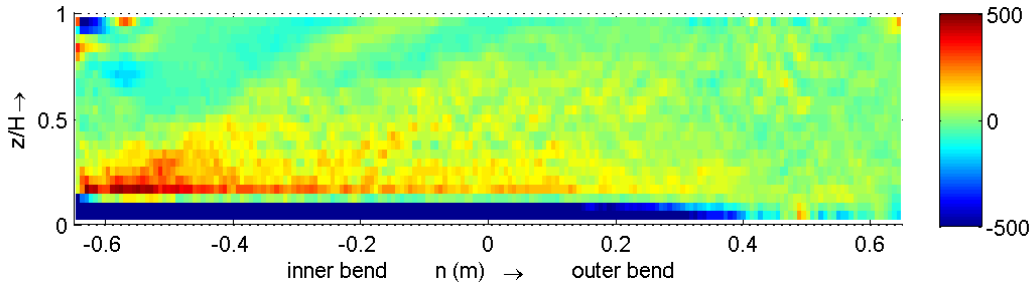

Figure C-199 Term 1, according to the Q89_LES, cross-section 060, shortened colour bar

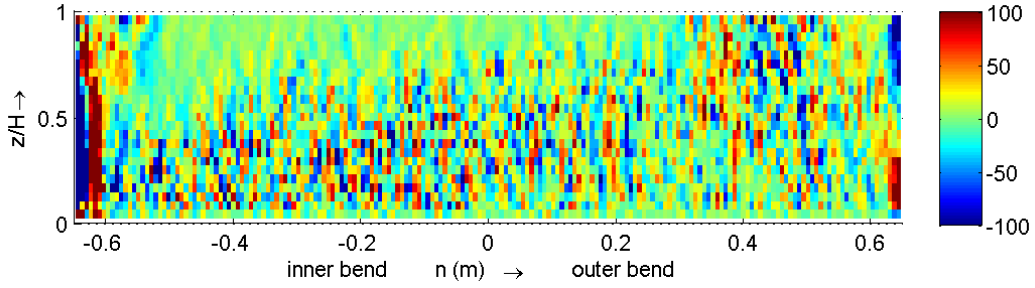

Figure C-200 Term 2, according to the Q89_LES, cross-section 060, shortened colour bar

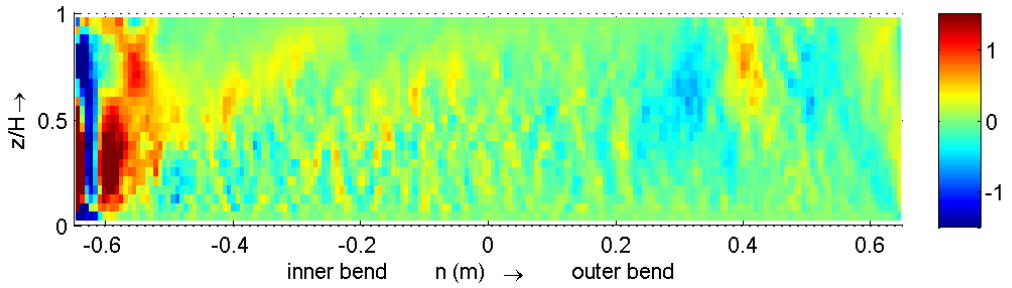

Figure C-201 Term 3, according to the Q89_LES, cross-section 060, shortened colour bar

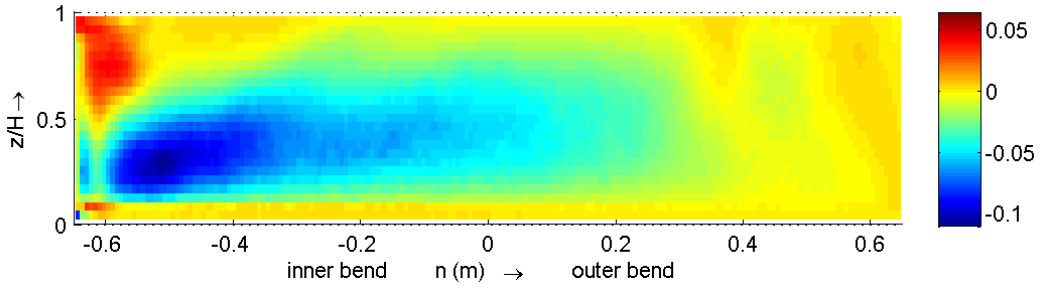

Figure C-202 Term 4, according to the Q89_LES, cross-section 060

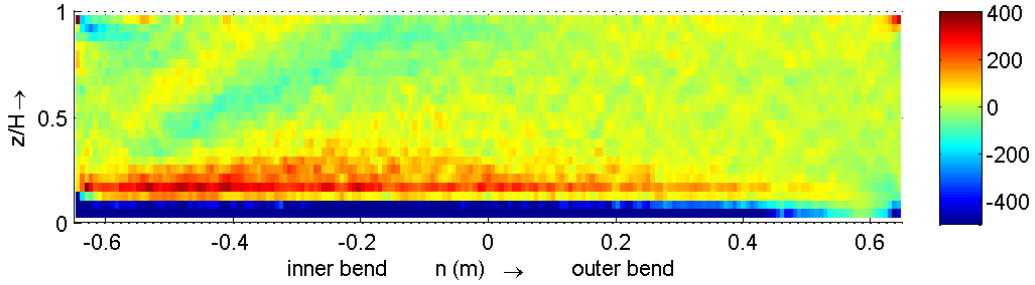

Figure C-203 Term 1, according to the Q89_LES, cross-section 150, shortened colour bar

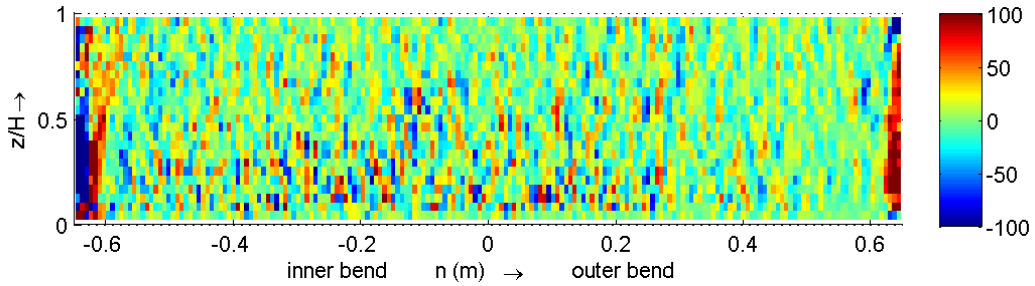

Figure C-204 Term 2, according to the Q89_LES, cross-section 150, shortened colour bar

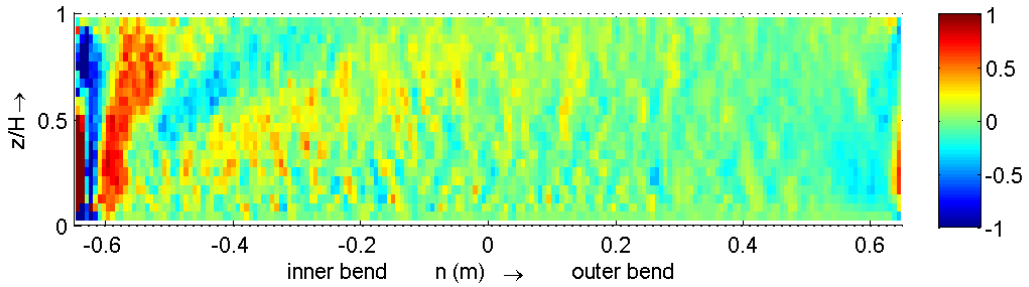

Figure C-205 Term 3, according to the Q89_LES, cross-section 150, shortened colour bar

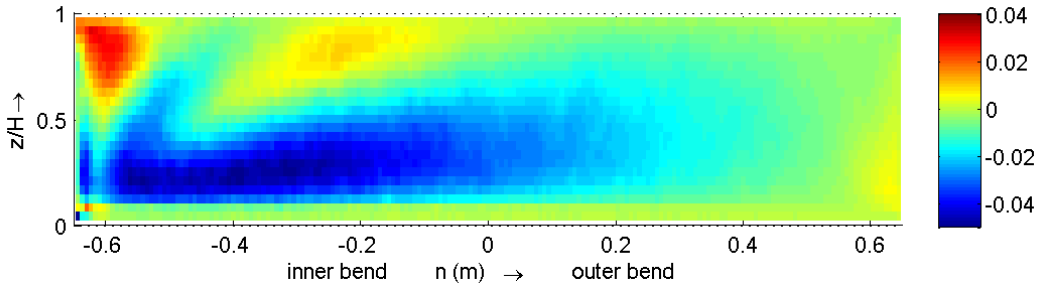

Figure C-206 Term 4, according to the Q89_LES, cross-section 150

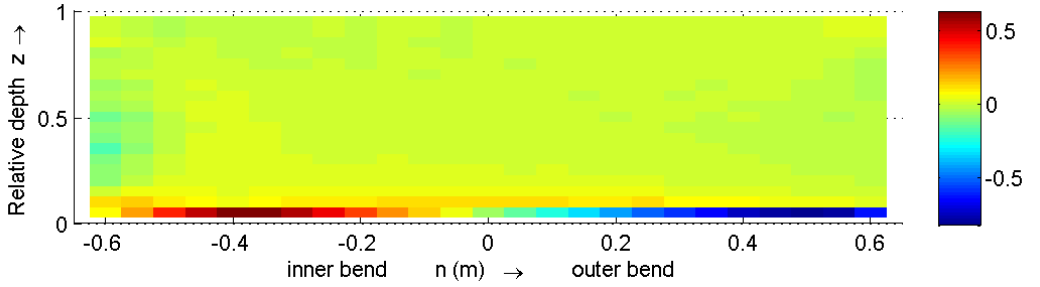

Figure C-207 Term 1, according to simulation Q89_1_D3D, m25 cross-section

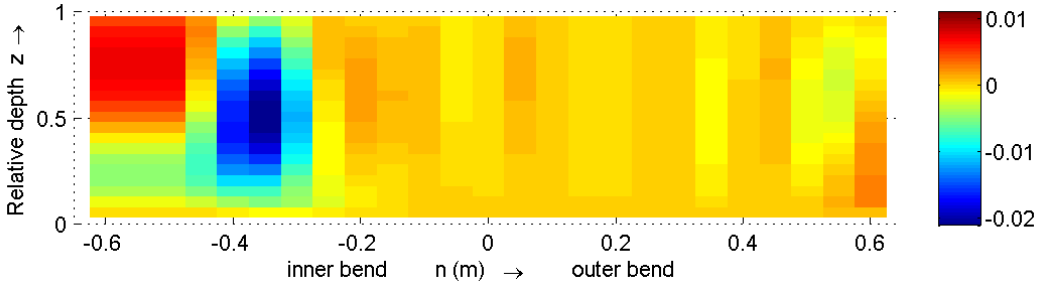

Figure C-208 Term 2, according to simulation Q89_1_D3D, m25 cross-section

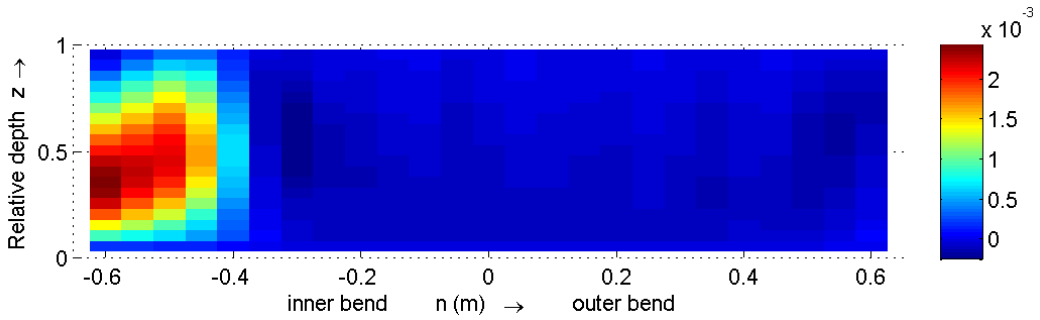

Figure C-209 Term 3, according to simulation Q89_1_D3D, m25 cross-section

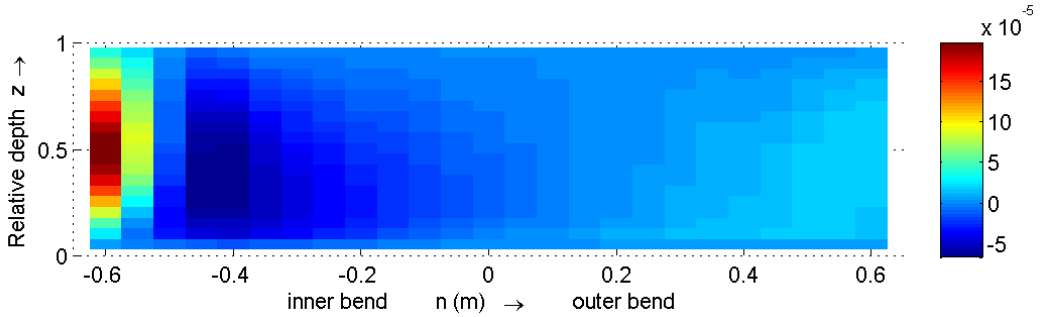

Figure C-210 Term 4, according to simulation Q89_1_D3D, m25 cross-section

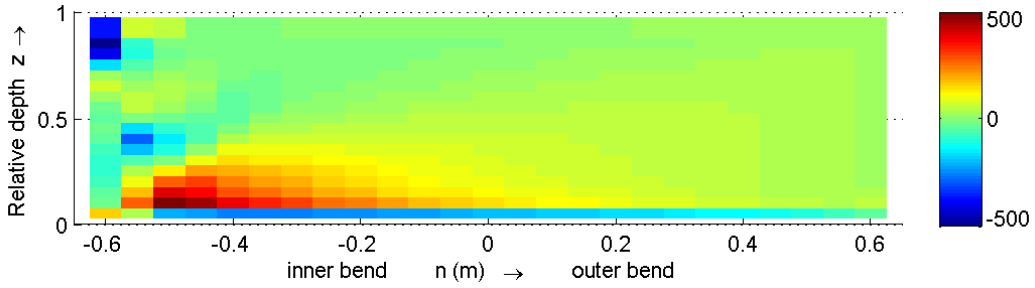

Figure C-211 Term 1, according to simulation Q89_1_D3D, 060 cross-section

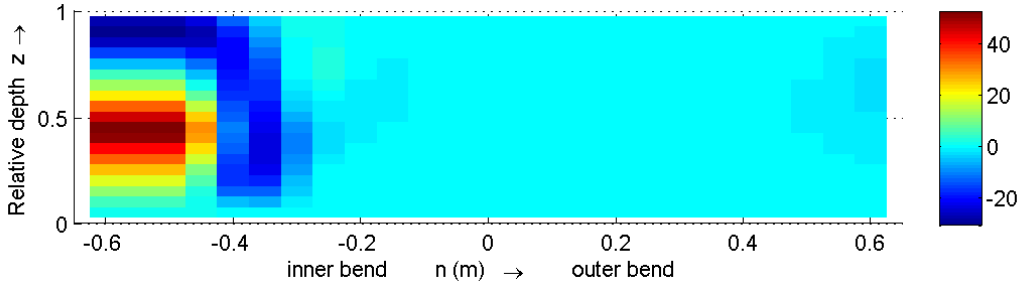

Figure C-212 Term 2, according to simulation Q89_1_D3D, 060 cross-section

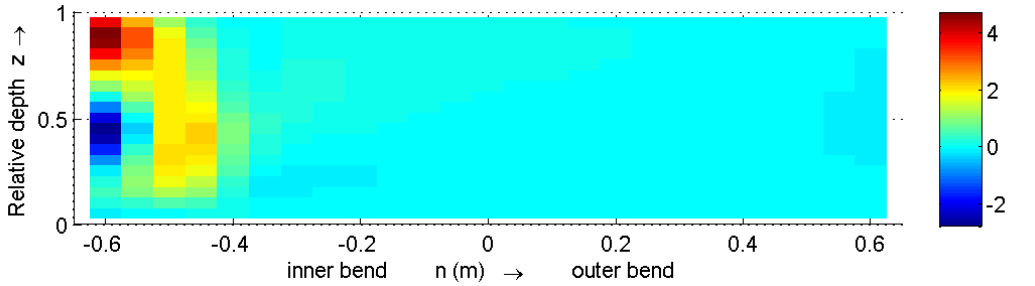

Figure C-213 Term 3, according to simulation Q89_1_D3D, 060

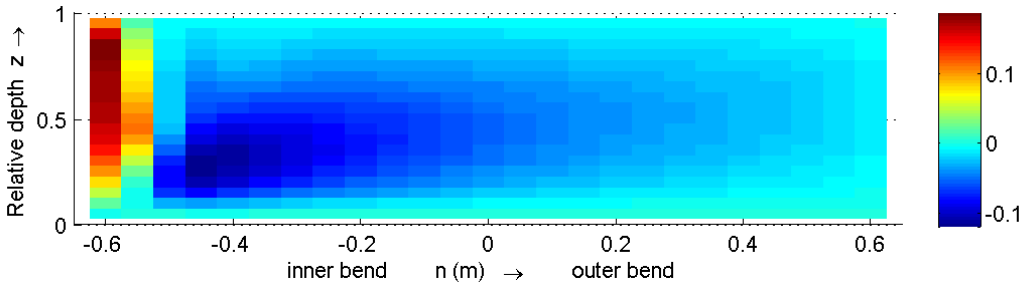

Figure C-214 Term 4, according to simulation Q89_1_D3D, 060

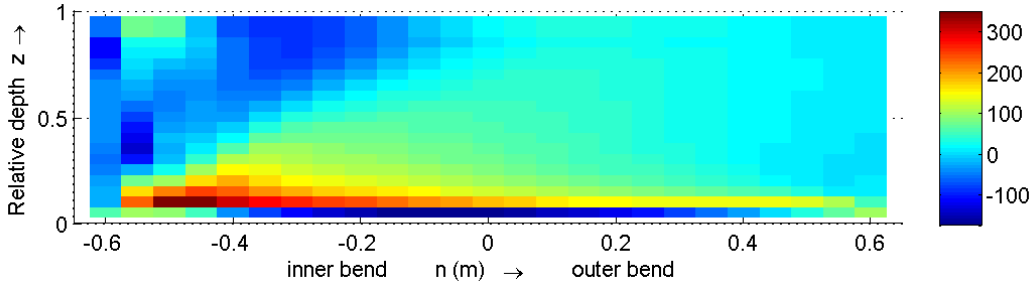

Figure C-215 Term 1, according to simulation Q89_1_D3D, 150

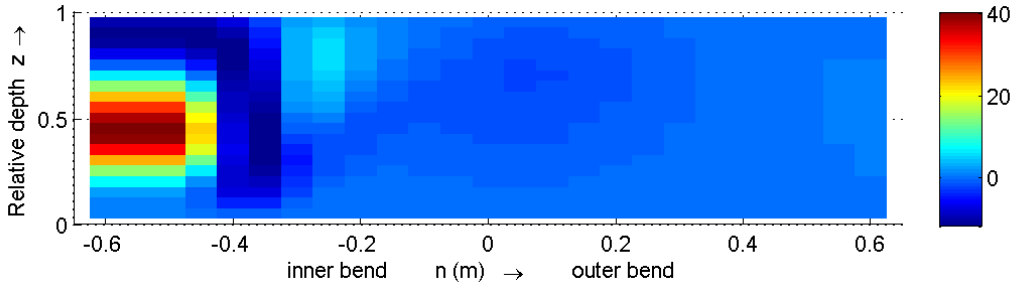

Figure C-216 Term 2, according to simulation Q89_1_D3D, 150

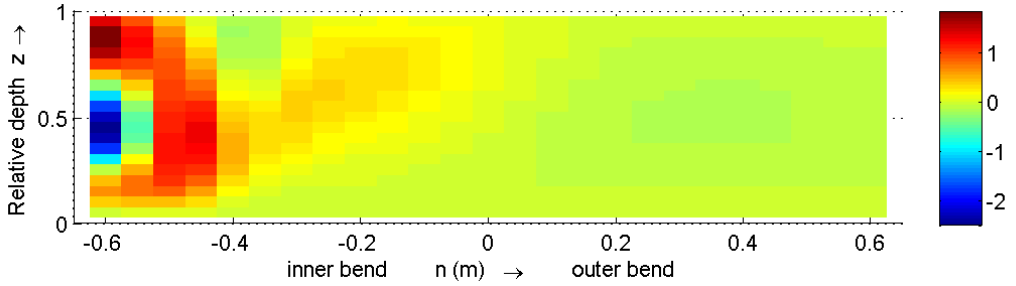

Figure C-217 Term 3, according to simulation Q89_1_D3D, 150

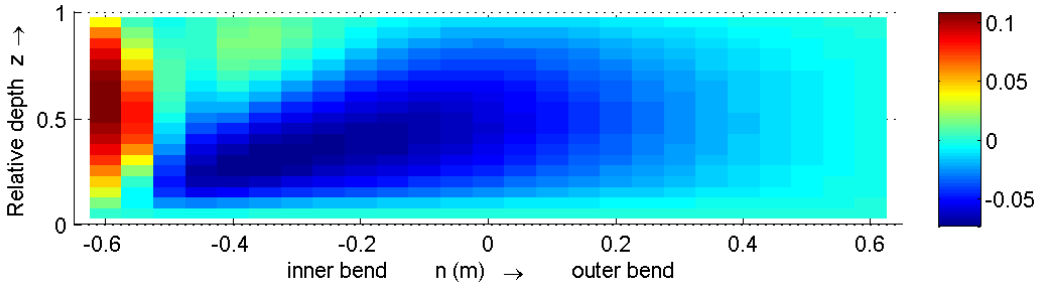

Figure C-218 Term 4, according to simulation Q89_1_D3D, 150

C.10 Skewness term

In this paragraph some plots of the skewness term (SKW) of the downstream vorticity balance equation will be shown. The SKW-term represents the redistribution of the downstream vorticity (ω_s) by skewness of the velocity field (excluding terms that can be associated with centrifugal effects) (van Balen *et al.*, 2009b). All figures are normalized by 1000 * H^2/U^2.

The skewness term is defined as (van Balen *et al.*, 2009b):

$$\text{SKW} = \frac{v}{r}\frac{\partial w}{\partial r} - \frac{v}{r}\frac{\partial v}{\partial z} + \frac{1}{r}\frac{\partial v}{\partial \theta}\frac{\partial u}{\partial z} + \frac{u}{r^2}\frac{\partial w}{\partial \theta} - \frac{1}{r}\frac{\partial w}{\partial \theta}\frac{\partial u}{\partial r}$$

This term is divided in five sub terms.

$$\text{Term 1} = \frac{v}{r}\frac{\partial w}{\partial r}$$

$$\text{Term 2} = -\frac{v}{r}\frac{\partial v}{\partial z}$$

$$\text{Term 3} = \frac{1}{r}\frac{\partial v}{\partial \theta}\frac{\partial u}{\partial z}$$

$$\text{Term 4} = \frac{u}{r^2}\frac{\partial w}{\partial \theta}$$

$$\text{Term 5} = -\frac{1}{r}\frac{\partial w}{\partial \theta}\frac{\partial u}{\partial r}$$

In the m25 cross-section the SKW-term is quite homogeneous (Figure C-227 to Figure C-229). There is some decrease of the skewness visible. For the measurements the decrease is situated along the outer wall and the bottom. The Q89_LES and simulation Q89_1_D3D show only some fluctuations along the bottom. The decrease is determined by the third sub term. This can clarify the region along the outer wall for the measurements. The third term is partly determined by a downstream derivative and as mentioned in section C.6, the downstream derivatives of the measured data are derived from two consecutive cross-sections. Because the distance between two consecutive cross-sections for the measurements is big, the accuracy of the derivative is low.

Along the flume (060 and 150 cross-sections, see Figure C-230 to Figure C-235), the SKW-term is mainly determined by sub term two and three. The other sub terms have only a minor contribution along the inner bend. Simulation Q89_1_D3D under predicts the SKW-term; the maximum is only half of the maximum according to the Q89_LES and measurements. For the Q89_LES and the measurements, the effect of the outer bank cell is vague visible but for simulation Q89_1_D3D this is absent which is due to the shortcomings of the turbulence model.

Figure C-219 shows |vLES| - |vSIM|, normalized by U and Figure C-220 shows |SKW_LES|-|SKW_SIM|, normalized by 1000 * H^2/U^2. The patterns in Figure C-219 and Figure C-220 look quite similar to each other. When analyzing the figures, we see in the blue circle for both figures an area with relative high values which means an under prediction of both quantities by simulation Q89_1_D3D. The area above the blue circle has the same shape in both figures, with high values along the water surface, decreasing toward the centre of the flume. In the green circle, for both figures are the values lower. In the outer bend an area with varying values is visible. The red square indicates the middle area with higher values. The upper and lower areas have lower values.

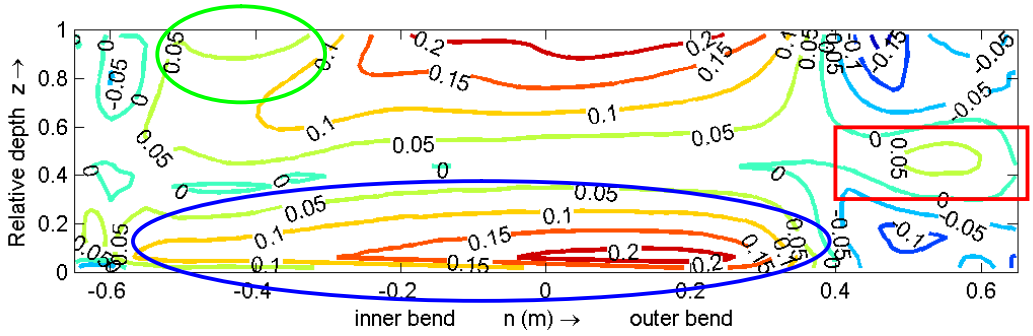

Figure C-219 |vLES|-|vSIM|, normalized (by U) for cross-section 060

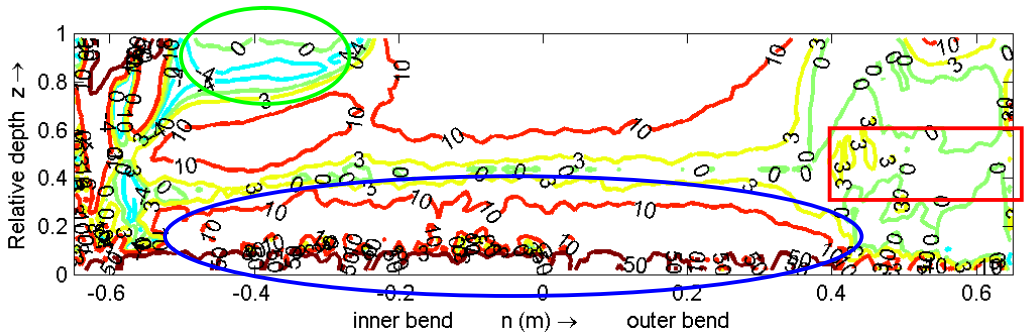

Figure C-220 |SKW_LES|-|SKW_SIM|, normalized (by 1000 * H^2/U^2) for cross-section 060

It seems that the SKW-term is strongly related to transverse velocity in the centre region of the flow. In the outer bend, other terms (especially the CFG-term) are more important but the SKW-term has some influence too. What happens along the outer wall is mainly caused by the anisotropy of the turbulent stresses (as stated by van Balen *et al.* (2009b) and Demuren and Rodi (1984)). This causes a distortion of the velocity profile which in its turn initiates the centrifugal effects which is the driving mechanism of the outer bank cell.

It seems that due to the existence of the outer bank cell, the skewness in the cross-section is induced and this skewness is important for the transverse velocities in the centre of the flume.

The following hypothesis is tested:

1) The anisotropic turbulent stresses induce a distortion of the downstream velocity profile in the outer bend. This distortion causes the centrifugal effects to become important and become the driving force of the outer bank cell. This is also concluded by van Balen *et al.* (2009b).

2) The outer bank cell causes skewness in the cross-section. Because the SKW-term is relative important in the centre region of the cross-section, it becomes a relative important driving mechanism for the transverse velocity in the centre region. Because simulation Q89_1_D3D does not predict the outer bank cell, the skewness is underestimated severely. This underestimation of the SKW-term causes also the underestimation of the transverse velocity. The (50%) underestimation of both the SKW-term and the transverse velocity in the 060 cross-section along the bottom of the flume, underpins this hypothesis.

If this hypothesis is true, it should also be visible in the SKW-term and the transverse velocities according to the measurements in the 060 and 150 cross-sections. Besides that, it should be absent in the 150 cross-section of the Q89_LES because the outer bank cell disappeared already for the Q89_LES in cross-section 150.

Starting with the comparison of the transverse velocity and the SKW-term in the 150 cross-section we will take a look at Figure C-221 (|vLES| - |vSIM|, normalized by U) and Figure C-222 (|SKW_LES|-|SKW_SIM|, normalized by 1000 * H^2/U^2), there is still some relation visible. Both the transverse velocity and the SKW-term are underestimated in the lower part (the blue circle) but the shape in the upper part (green circle) changes quite a bit. The transverse velocities are overestimated by simulation Q89_1_D3D. It was expected, based on our hypothesis, that the transverse velocities of the Q89_LES and simulation Q89_1_D3D showed less difference. The difference in the upper part (green circle) can be explained by the outward shift of the core of the downstream velocity.

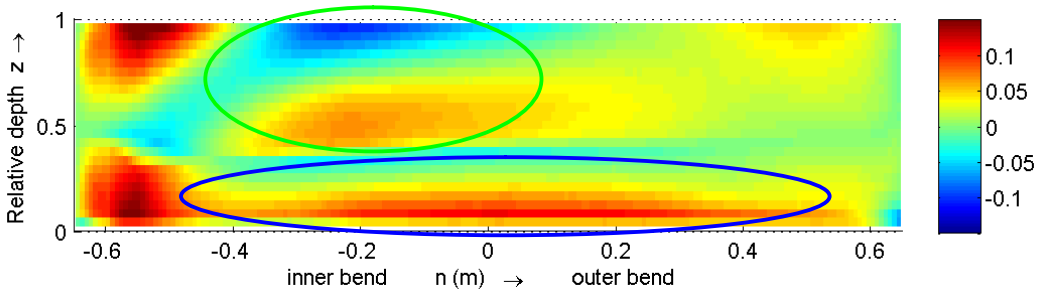

Figure C-221 |vLES|-|vSIM|, normalized (by U) for cross-section 150

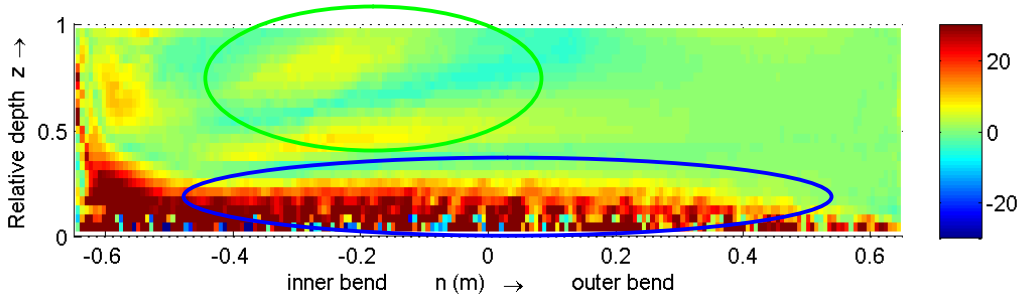

Figure C-222 |SKW-LES|-|SKW-SIM|, normalized (by 1000 * H^2/U^2) for cross-section 150

Comparing the differences in the SKW-term and transverse velocities of the measurements and simulation Q89_1_D3D, the relation between both quantities is less clear (see Figure C-223 and Figure C-224). Along the bottom the comparison is quite good (see the blue circle in Figure C-223 and Figure C-224). The transverse velocities are about 50% under predicted by simulation Q89_1_D3D, the SKW-term shows an under prediction of about 60%. In the upper part of the flume, there is no clear relation visible in the 060 cross-section. In the 150 cross-section it is difficult to say something useful about the relation between the SKW-term and the transverse velocities. Figure C-233 and Figure C-235 show the SKW-term of the measurements respectively simulation Q89_1_D3D for cross-section 150. The skewness in the lower part of the flume contains large negative values according to the measurements, while they are positive according to simulation Q89_1_D3D. Looking at the sub terms (Figure C-266 to Figure C-270) we see that the large negative values are caused by the third term, which contains a downstream derivative which is an inaccurate quantity. The third sub term according to the Q89_LES (Figure C-273) is positive. This gives reason to doubt about the accuracy of that specific term. Looking at Figure C-225 (which represent |SKW_MEAS|-|SKW_SIM| for the 150 cross-section) there is an unnatural transition in the lower part of the flume. The upper part seems to show a kind of relation but the reason for this is not yet clear.

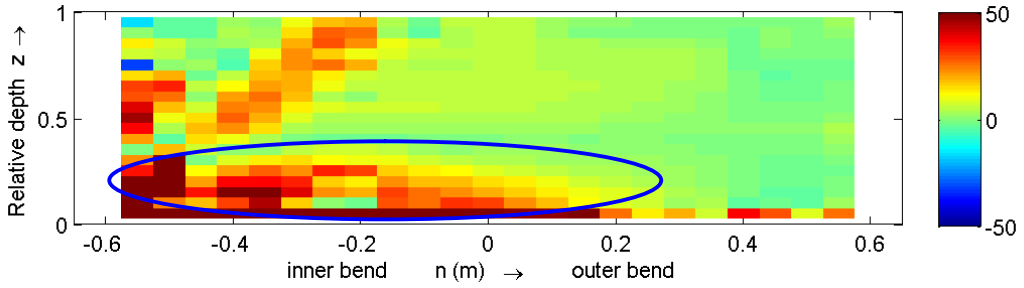

Figure C-223 |SKW_MEAS|-|SKW_SIM|, normalized (by 1000 * H^2/U^2) for cross-section 060

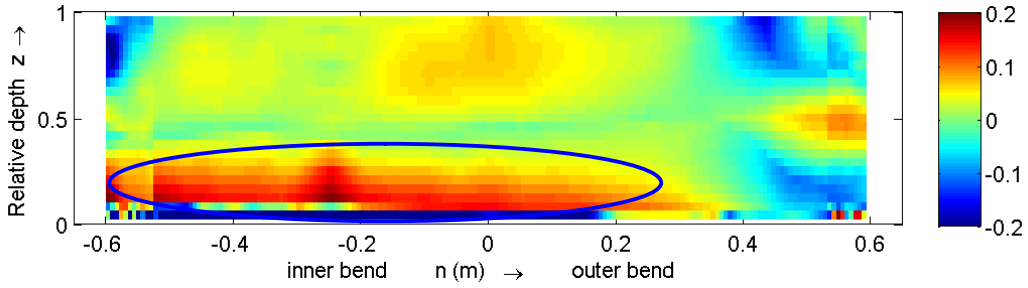

Figure C-224 |v_MEAS|-|v_SIM|, normalized (by /U) for cross-section 060

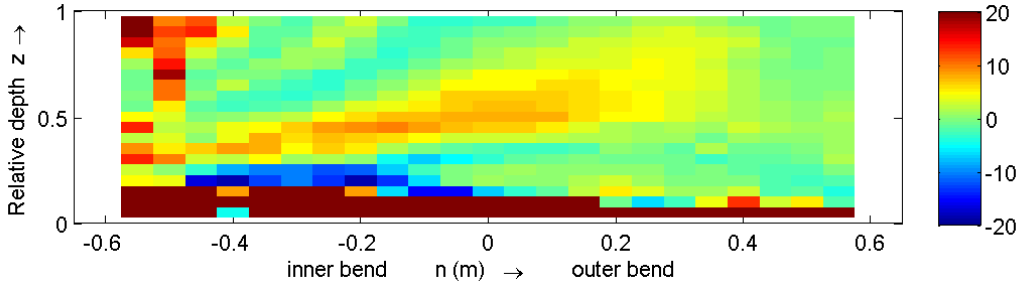

Figure C-225 |SKW_MEAS|-|SKW_SIM|, normalized (by 1000 * H^2/U^2) for cross-section 150

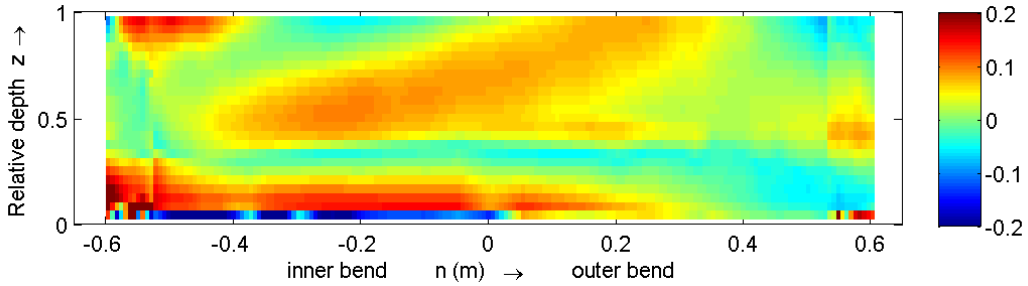

Figure C-226 |v_MEAS|-|v_SIM|, normalized (by /U) for cross-section 150

It can be concluded that the SKW-term is more important in the centre region of the flume than along the wall boundaries. The hypothesis can be rejected. The skewness is not induced by the outer bank cell because the effects are still visible in cross-sections where the outer bank cell already disappeared (150 cross-section, Q89_LES and simulation Q89_1_D3D compared). There is a relation between the skewness and the transverse velocities. The skewness affects the transverse velocity, especially along the bottom of the flume.

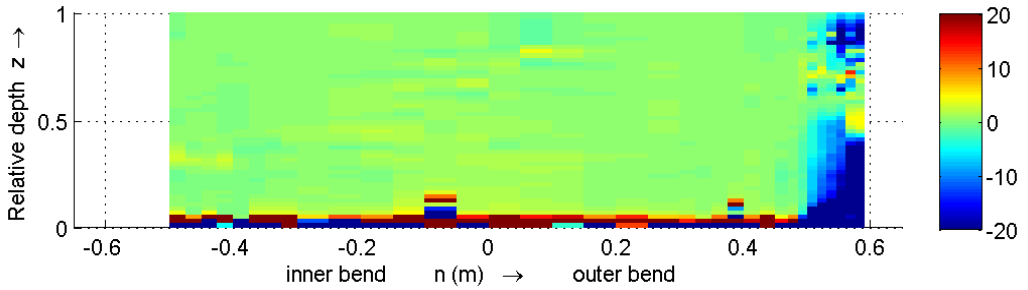

Figure C-227 SKW for cross-section m25, according to the measurements. Shortened colour bar

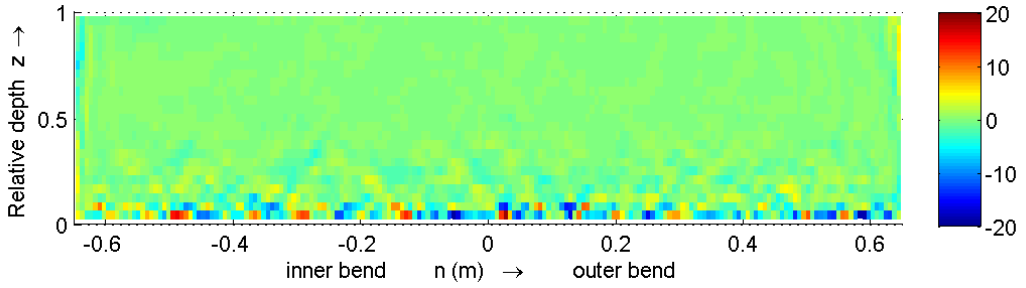

Figure C-228 SKW for cross-section m25, according to the Q89_LES

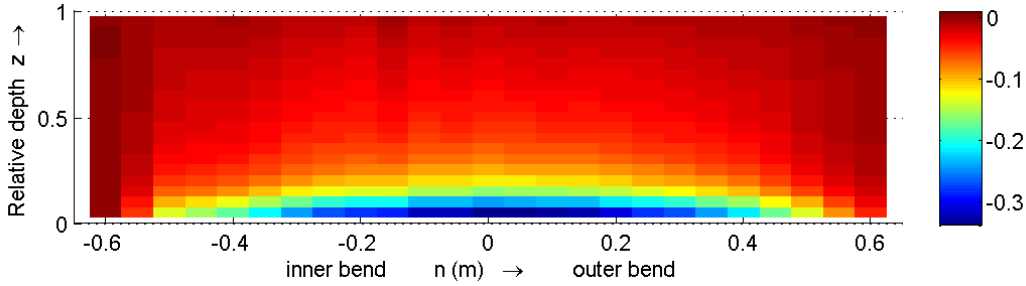

Figure C-229 SKW for cross-section m25, according to simulation Q89_1_D3D

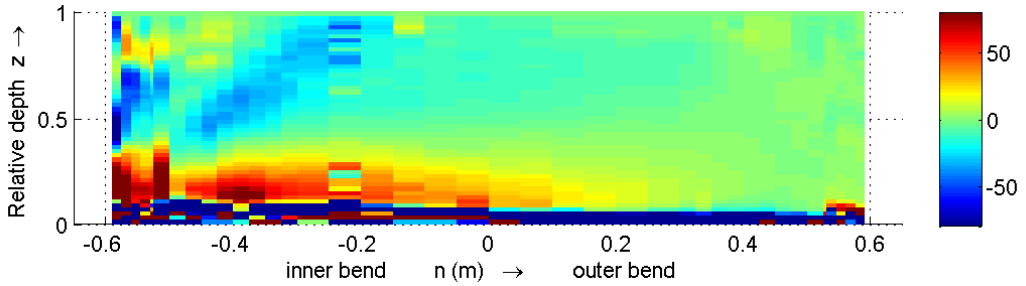

Figure C-230 SKW for cross-section 060, according to the measurements. Shortened colour bar

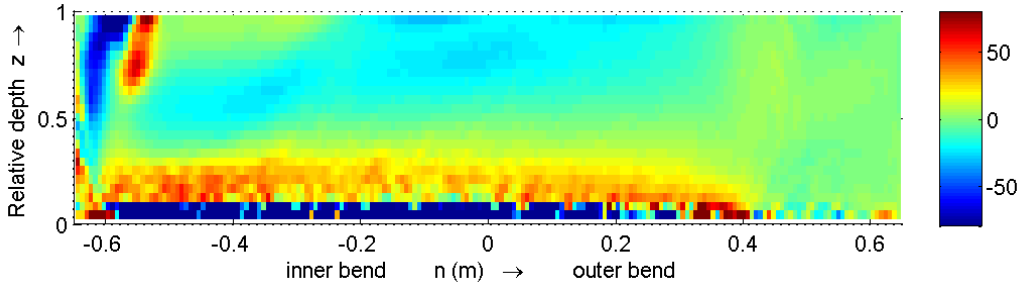

Figure C-231 SKW for cross-section 060, according to the Q89_LES. Shortened colour bar

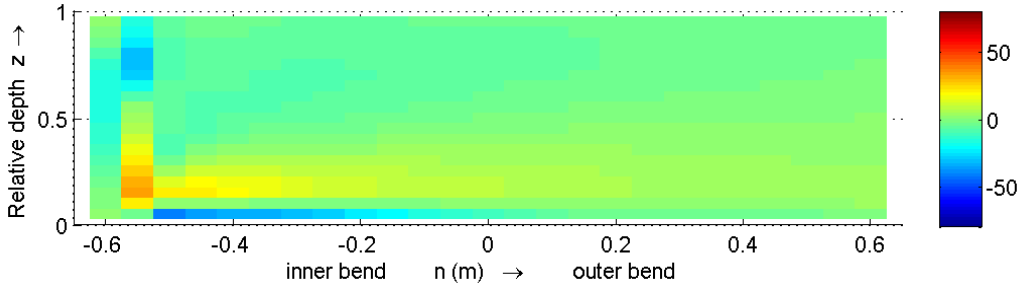

Figure C-232 SKW for cross-section 060, according to simulation Q89_1_D3D

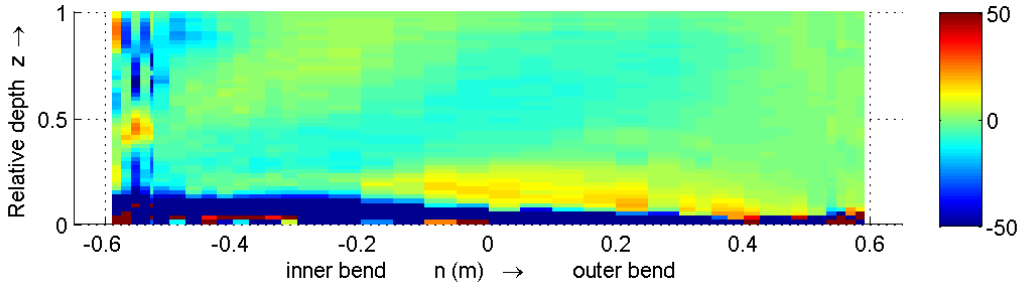

Figure C-233 SKW for cross-section 150, according to the measurements. Shortened colour bar

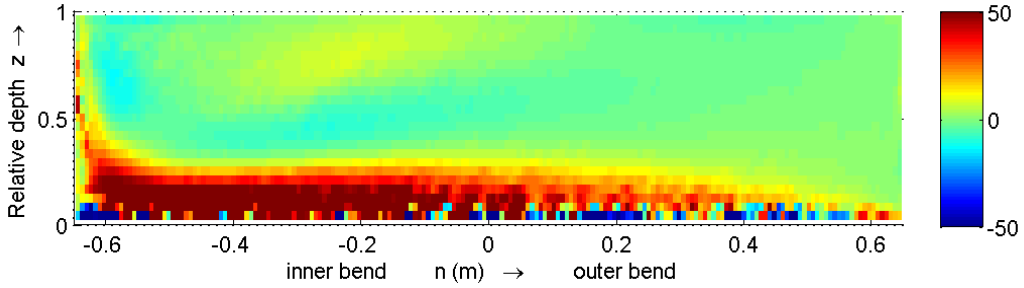

Figure C-234 SKW for cross-section 150, according to the Q89_LES. Shortened colour bar

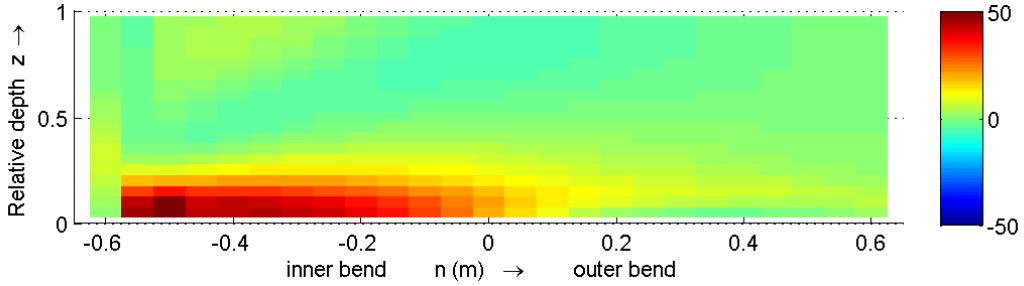

Figure C-235 SKW for cross-section 150, according to simulation Q89_1_D3D

C.10.1 Sub terms of the skewness term

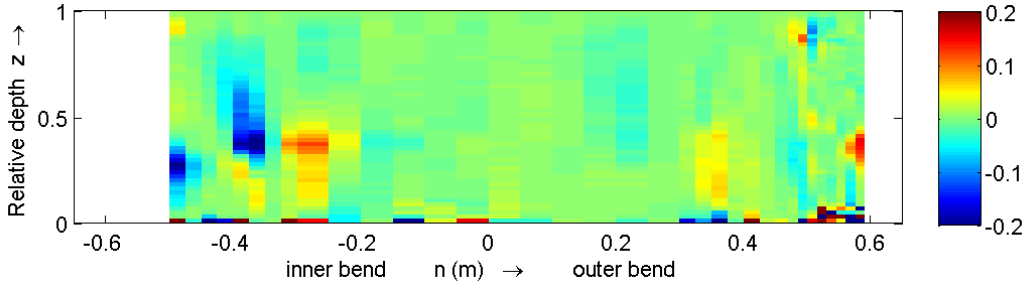

Figure C-236 Term 1 for cross-section m25, according to the measurements. Shortened colour bar

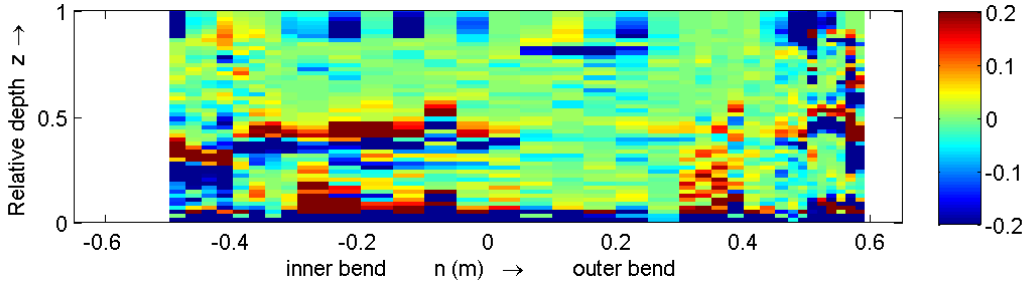

Figure C-237 Term 2 for cross-section m25, according to the measurements. Shortened colour bar

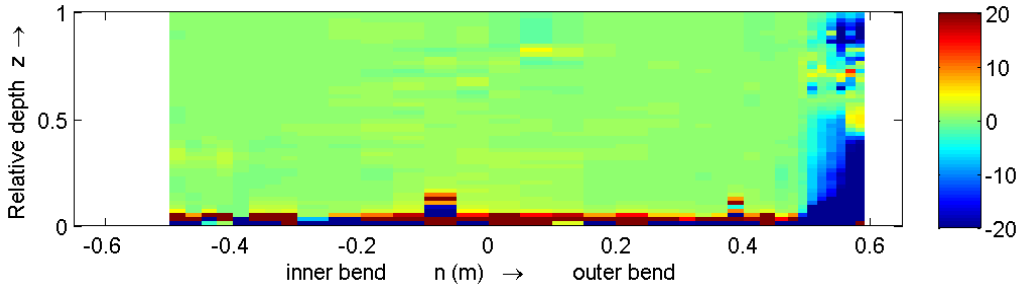

Figure C-238 Term 3 for cross-section m25, according to the measurements. Shortened colour bar

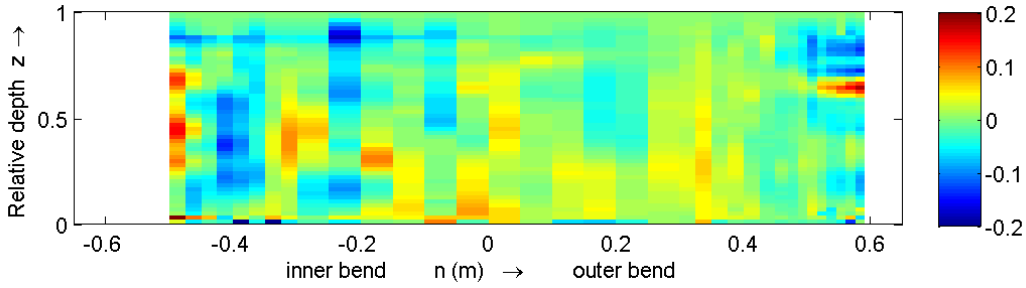

Figure C-239 Term 4 for cross-section m25, according to the measurements

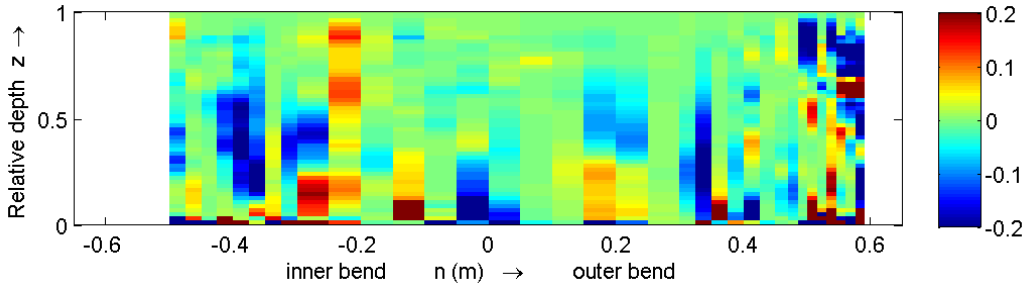

Figure C-240 Term 5 for cross-section m25, according to the measurements. Shortened colour bar

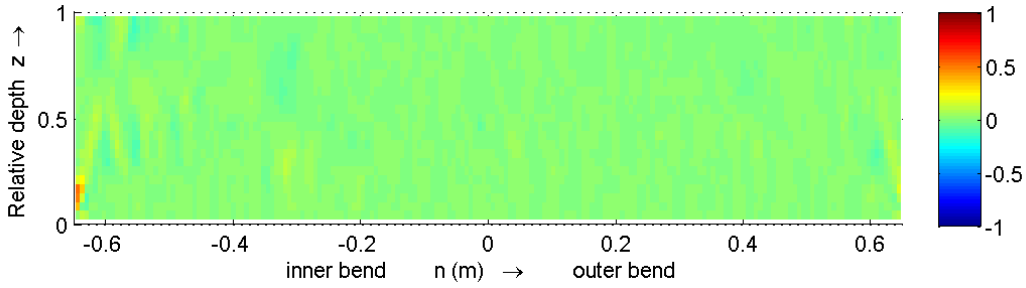

Figure C-241 Term 1 for cross-section m25, according to the Q89_LES

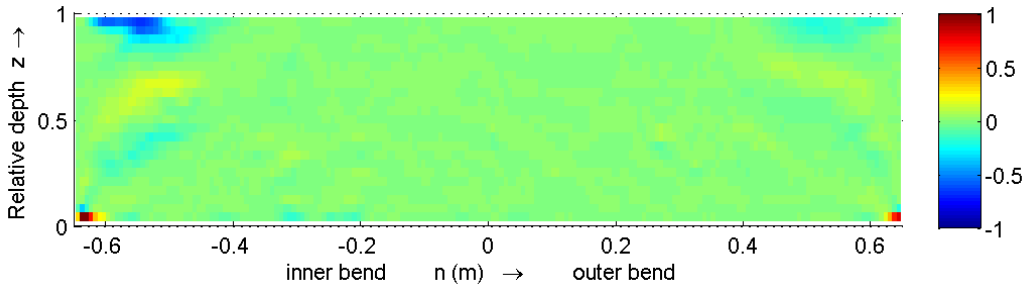

Figure C-242 Term 2 for cross-section m25, according to the Q89_LES

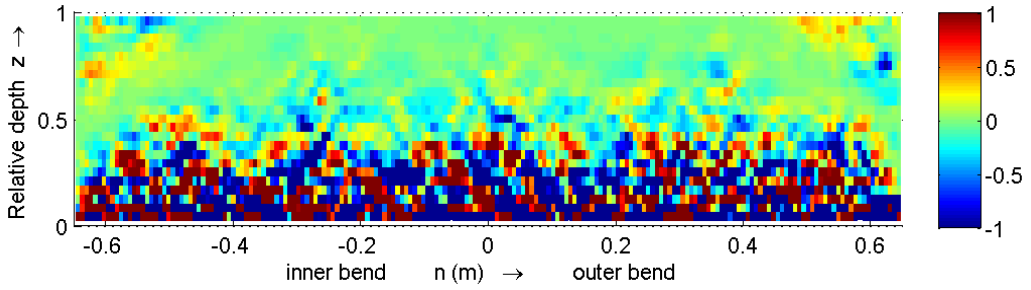

Figure C-243 Term 3 for cross-section m25, according to the Q89_LES. Shortened colour bar

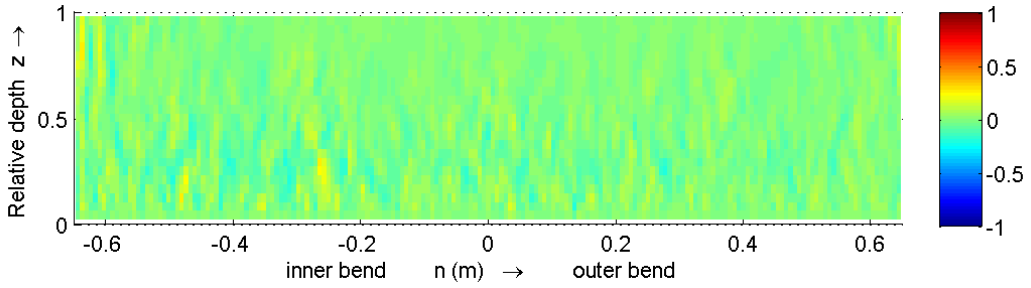

Figure C-244 Term 4 for cross-section m25, according to the Q89_LES

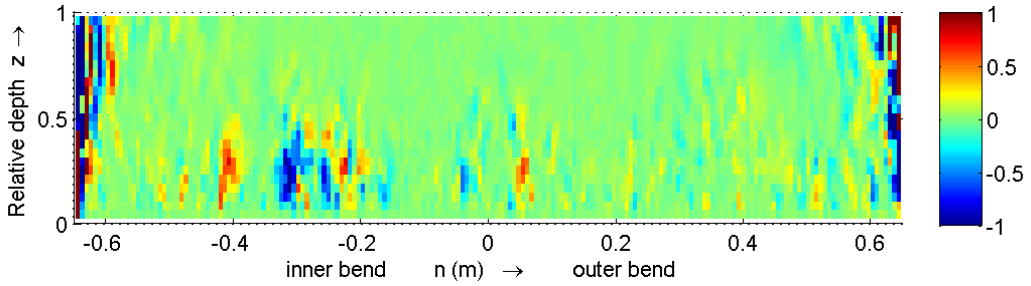

Figure C-245 Term 5 for cross-section m25, according to the Q89_LES. Shortened colour bar

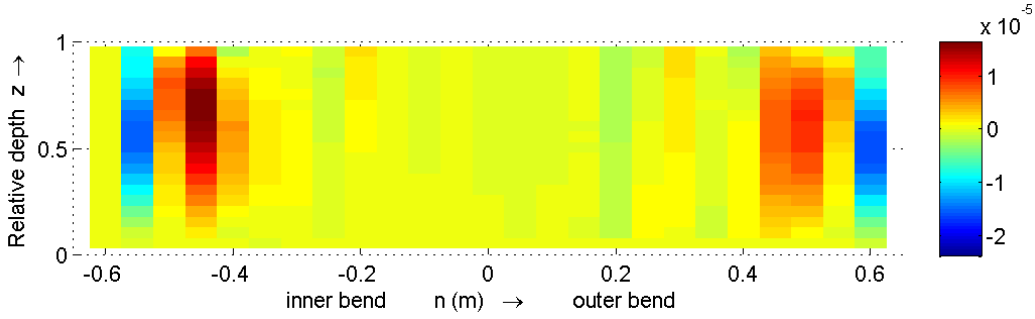

Figure C-246 Term 1 for cross-section m25, according to simulation Q89_1_D3D

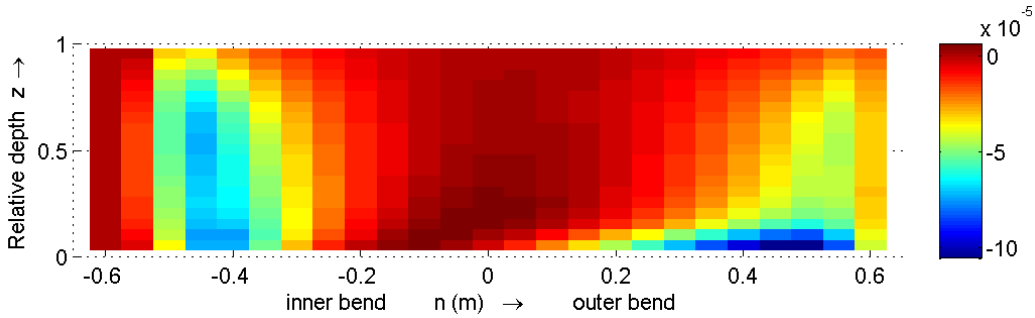

Figure C-247 Term 2 for cross-section m25, according to simulation Q89_1_D3D

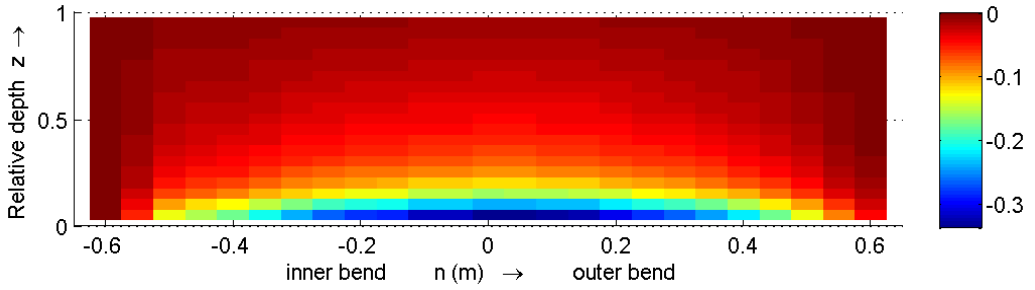

Figure C-248 Term 3 for cross-section m25, according to simulation Q89_1_D3D

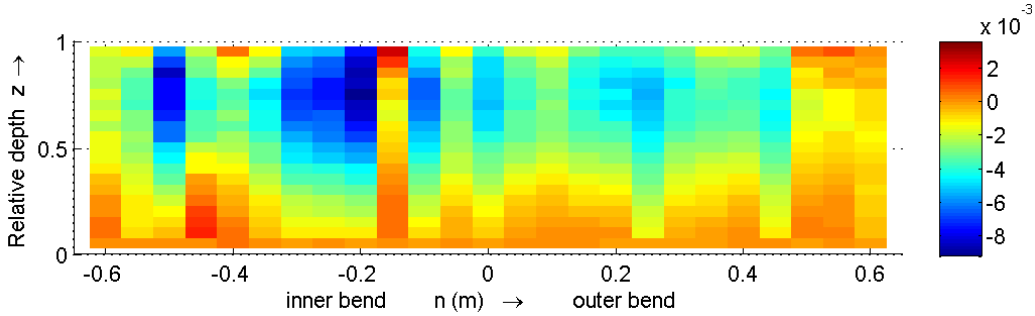

Figure C-249 Term 4 for cross-section m25, according to simulation Q89_1_D3D

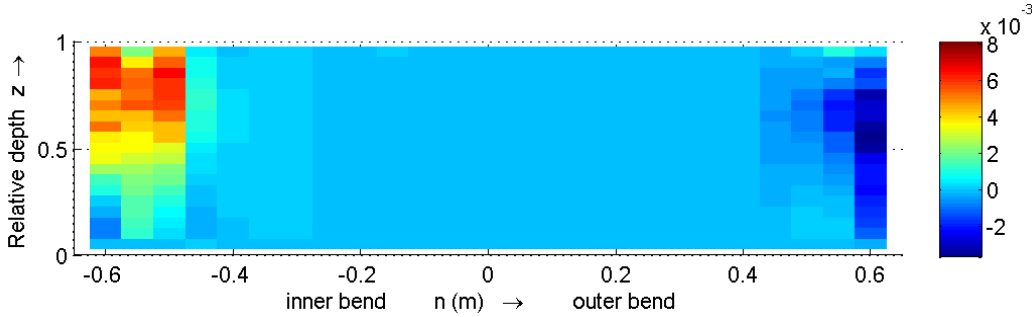

Figure C-250 Term 5 for cross-section m25, according to simulation Q89_1_D3D

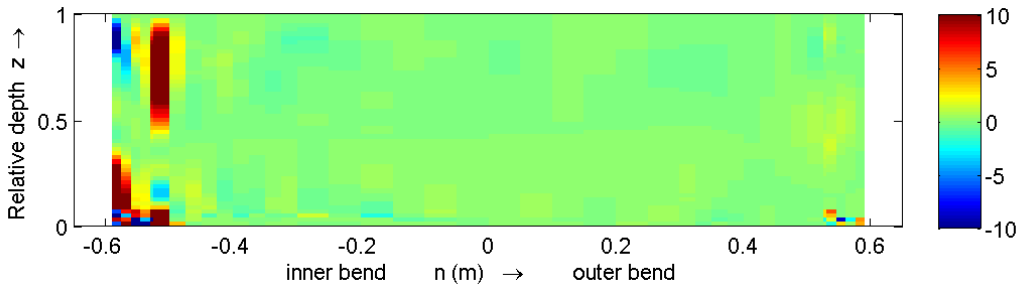

Figure C-251 Term 1 for cross-section 060, according to the measurements. Shortened colour bar

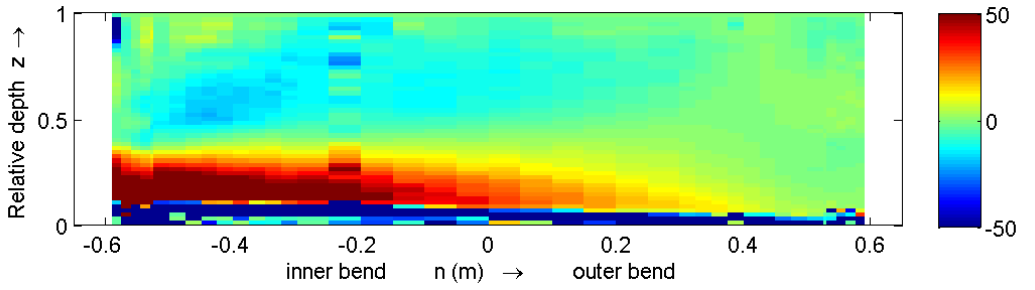

Figure C-252 Term 2 for cross-section 060, according to the measurements. Shortened colour bar

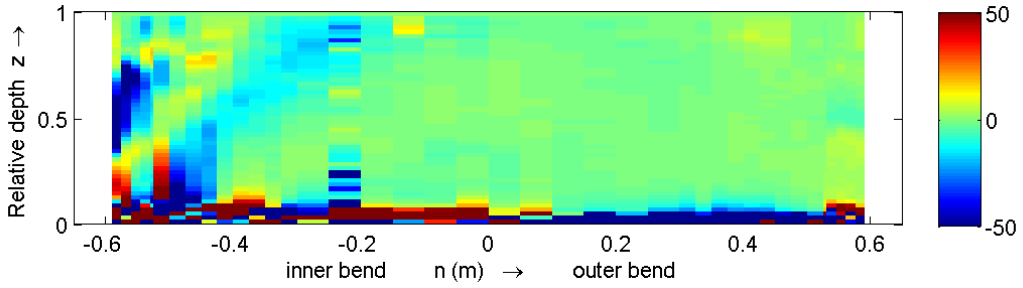

Figure C-253 Term 3 for cross-section 060, according to the measurements. Shortened colour bar

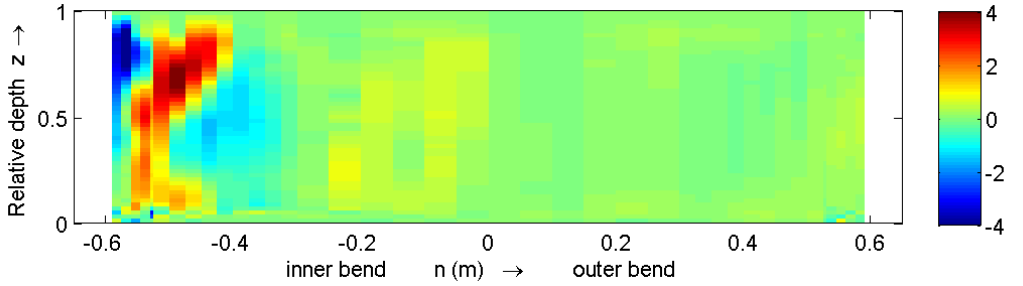

Figure C-254 Term 4 for cross-section 060, according to the measurements

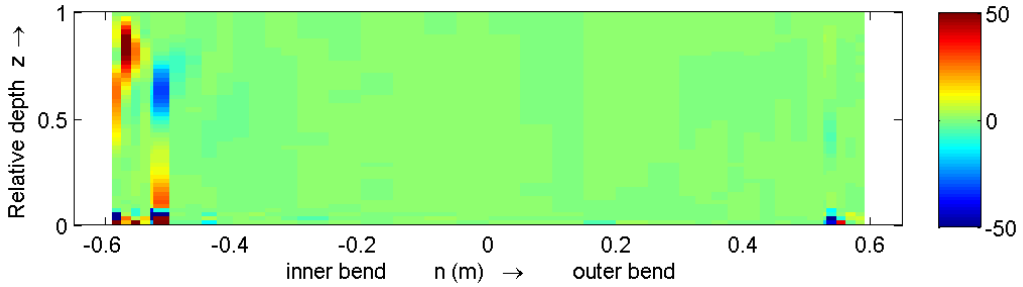

Figure C-255 Term 5 for cross-section 060, according to the measurements. Shortened colour bar

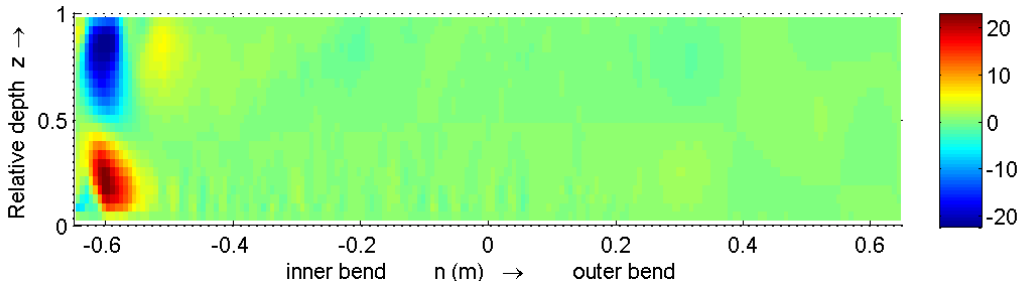

Figure C-256 Term 1 for cross-section 060, according to the Q89_LES

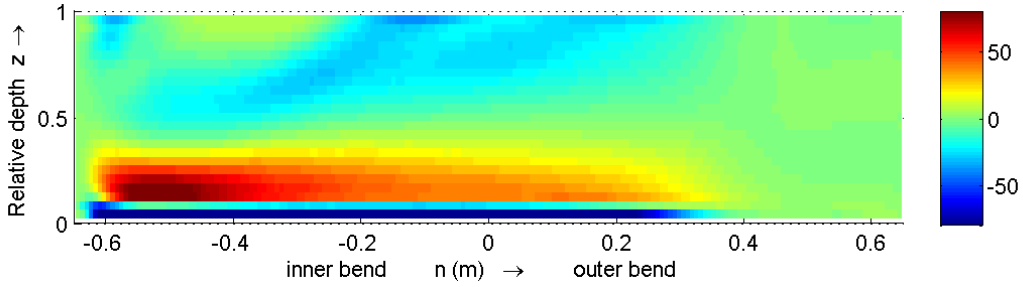

Figure C-257 Term 2 for cross-section 060, according to the Q89_LES. Shortened colour bar

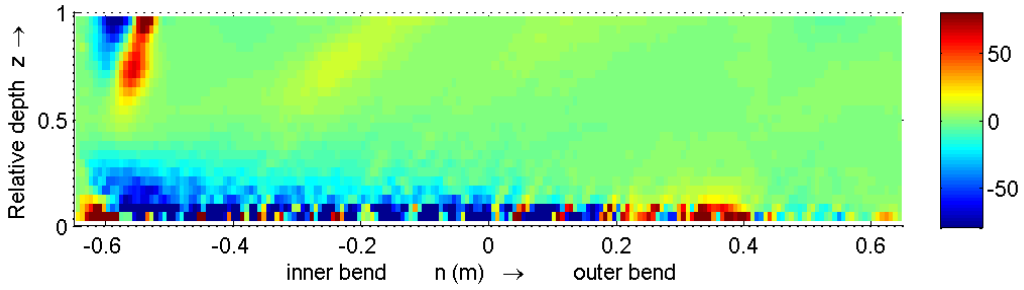

Figure C-258 Term 3 for cross-section 060, according to the Q89_LES. Shortened colour bar

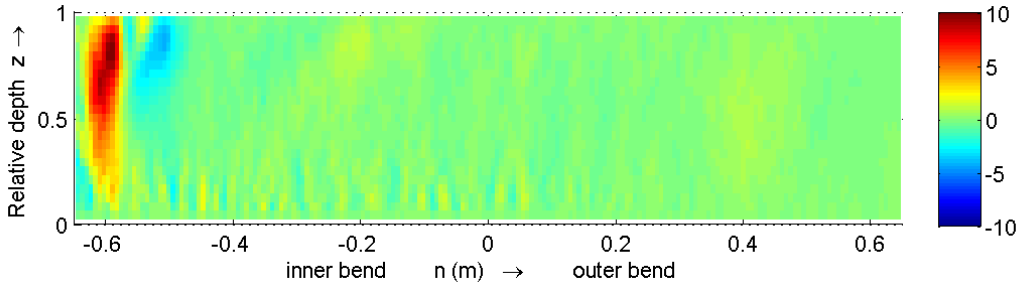

Figure C-259 Term 4 for cross-section 060, according to the Q89_LES

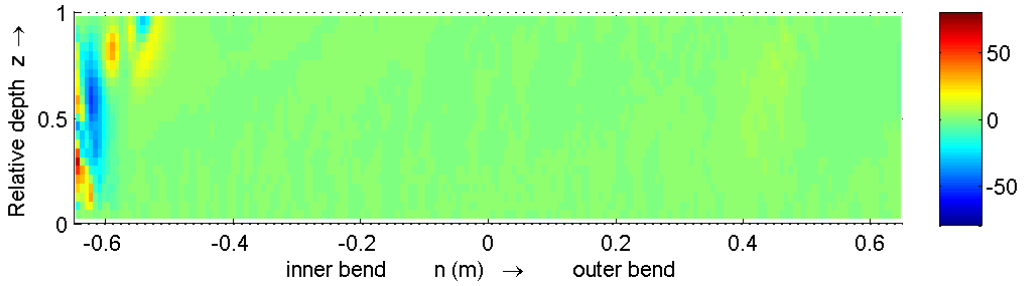

Figure C-260 Term 5 for cross-section 060, according to the Q89_LES

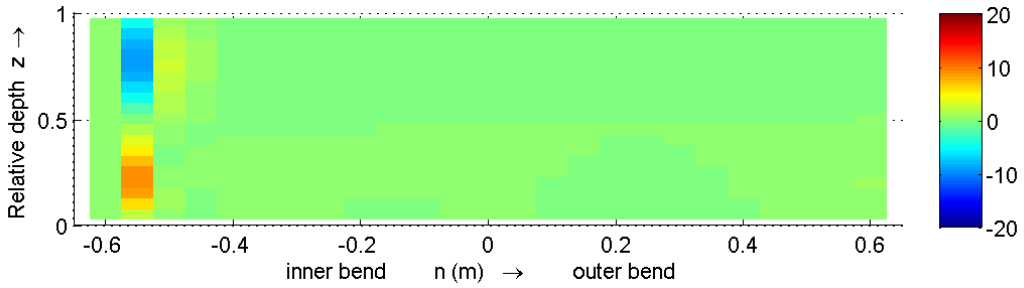

Figure C-261 Term 1 for cross-section 060, according to simulation Q89_1_D3D

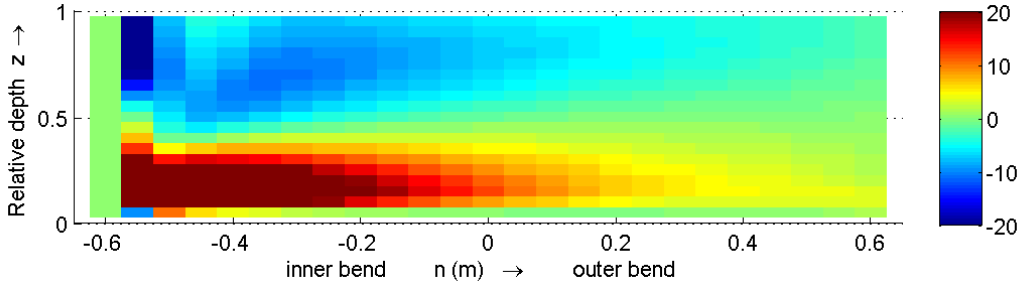

Figure C-262 Term 2 for cross-section 060, according to simulation Q89_1_D3D. Shortened colour bar

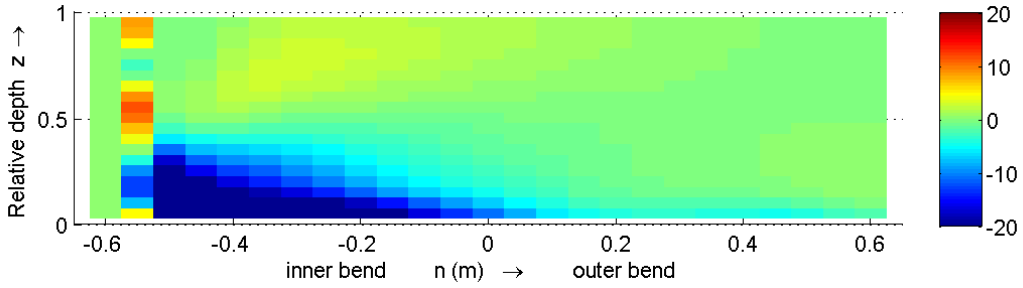

Figure C-263 Term 3 for cross-section 060, according to simulation Q89_1_D3D. Shortened colour bar

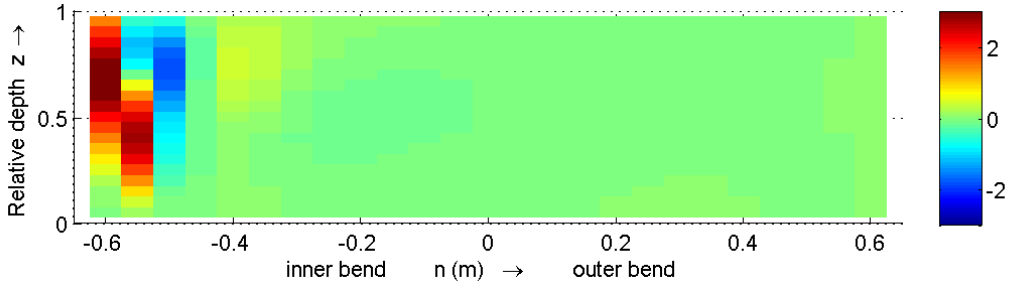

Figure C-264 Term 4 for cross-section 060, according to simulation Q89_1_D3D. Shortened colour bar

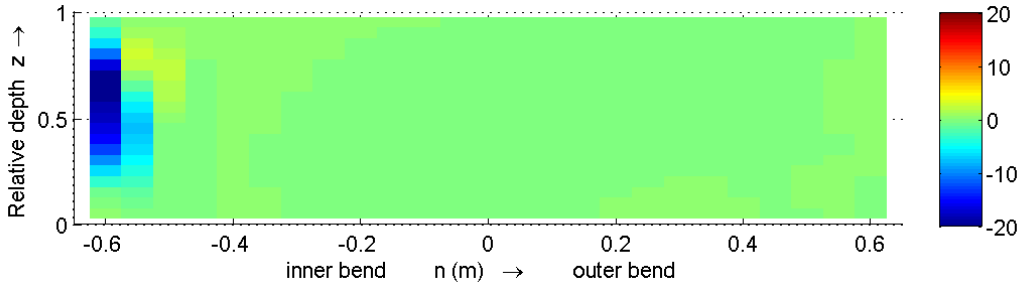

Figure C-265 Term 5 for cross-section 060, according to simulation Q89_1_D3D

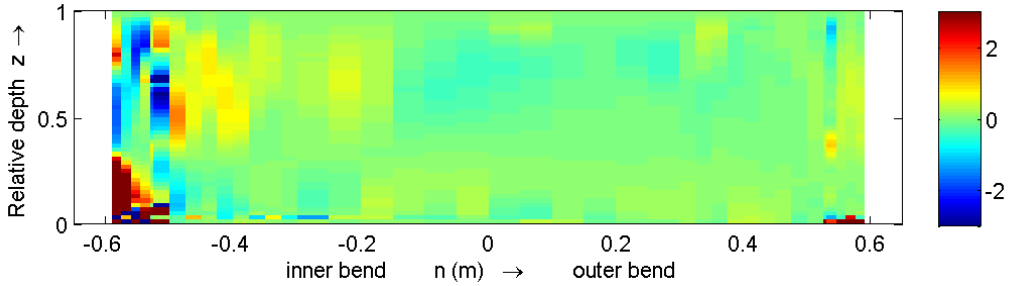

Figure C-266 Term 1 for cross-section 150, according to the measurements. Shortened colour bar

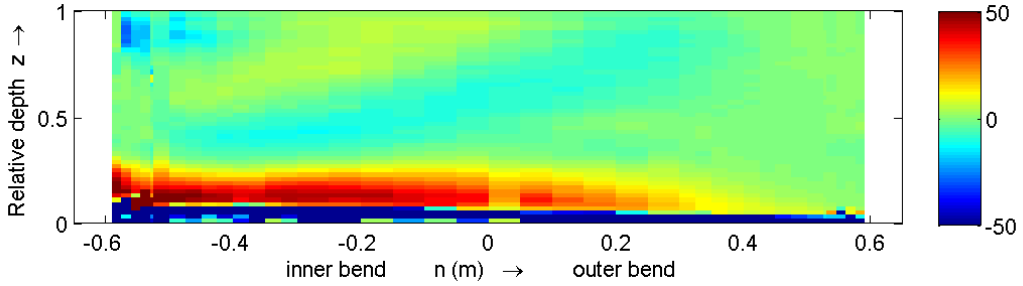

Figure C-267 Term 2 for cross-section 150, according to the measurements. Shortened colour bar

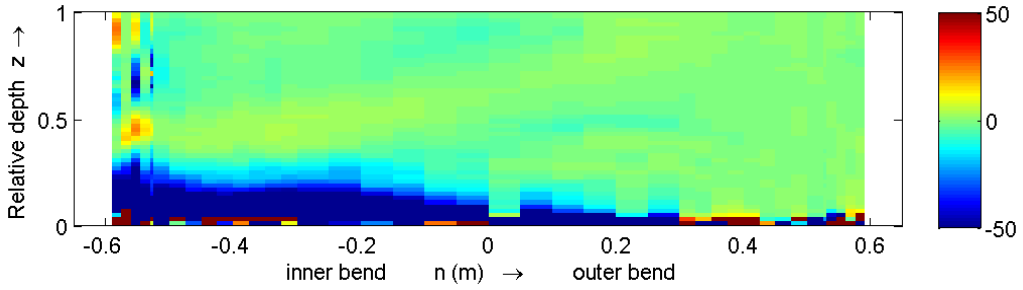

Figure C-268 Term 3 for cross-section 150, according to the measurements. Shortened colour bar

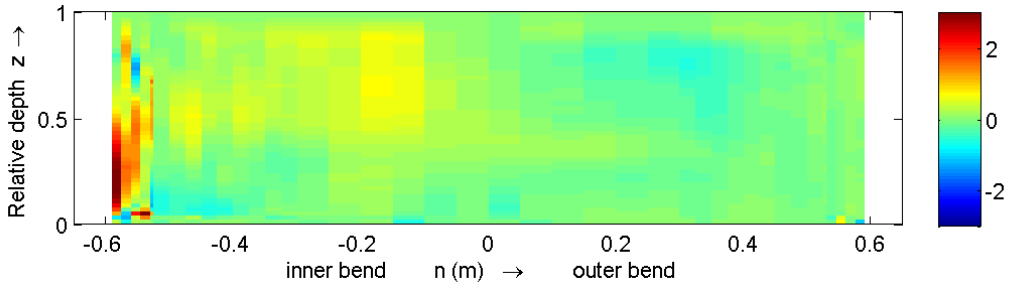

Figure C-269 Term 4 for cross-section 150, according to the measurements. Shortened colour bar

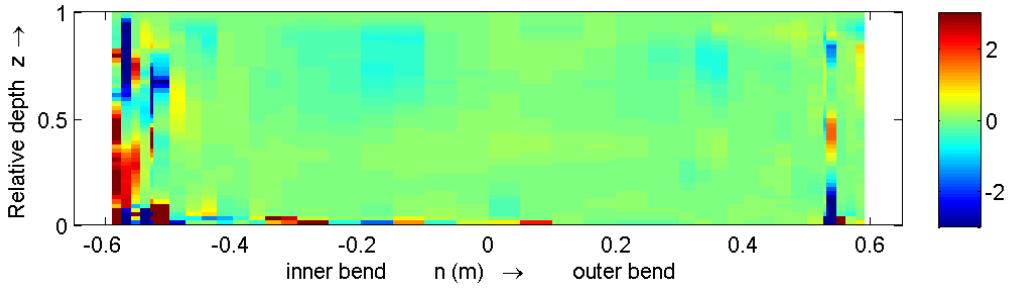

Figure C-270 Term 5 for cross-section 150, according to the measurements. Shortened colour bar

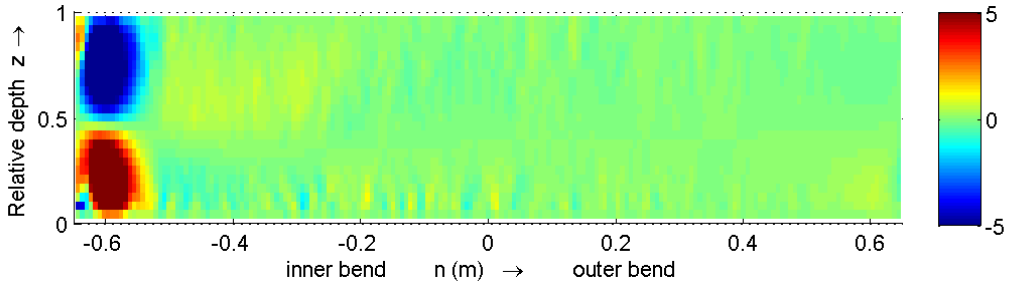

Figure C-271 Term 1 for cross-section 150, according to the Q89_LES. Shortened colour bar

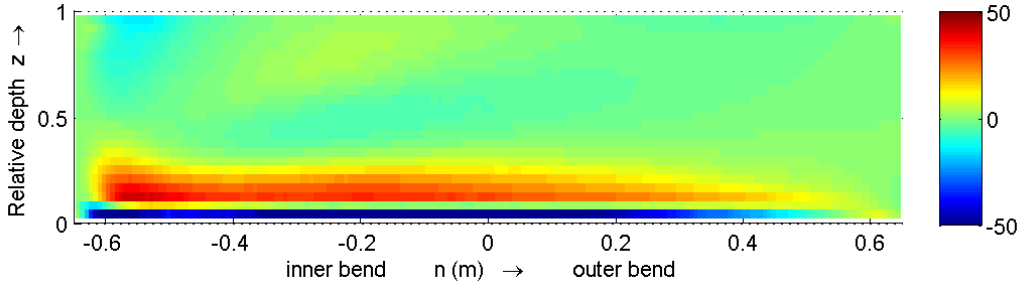

Figure C-272 Term 2 for cross-section 150, according to the Q89_LES. Shortened colour bar

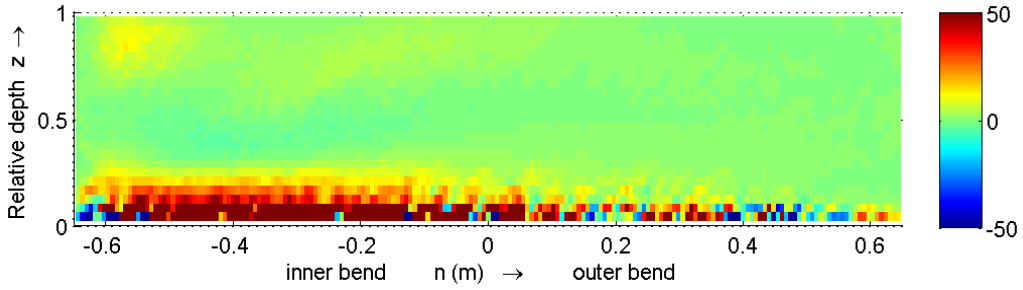

Figure C-273 Term 3 for cross-section 150, according to the Q89_LES. Shortened colour bar

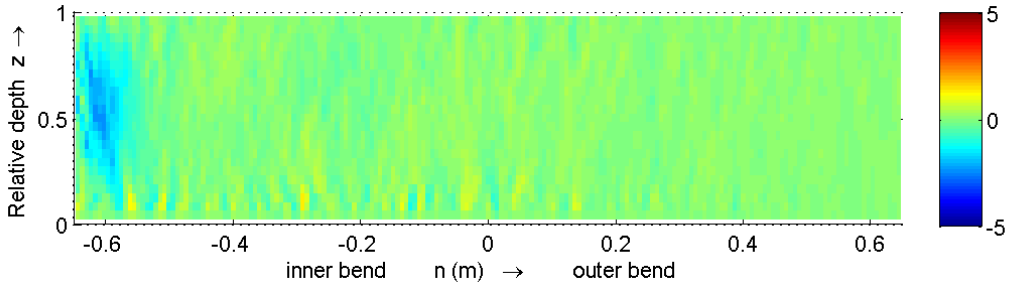

Figure C-274 Term 4 for cross-section 150, according to the Q89_LES

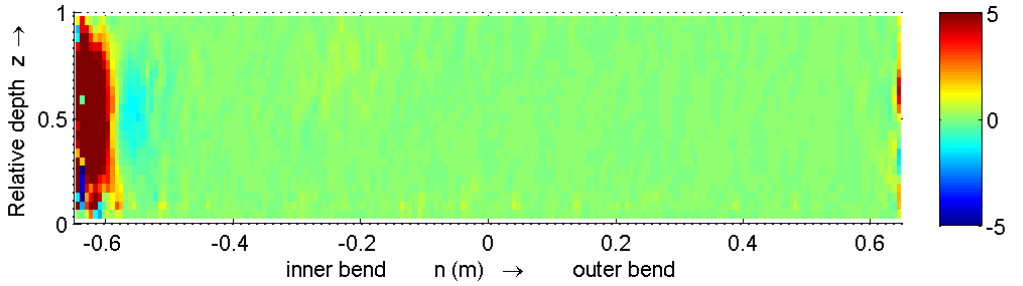

Figure C-275 Term 5 for cross-section 150, according to the Q89_LES. Shortened colour bar

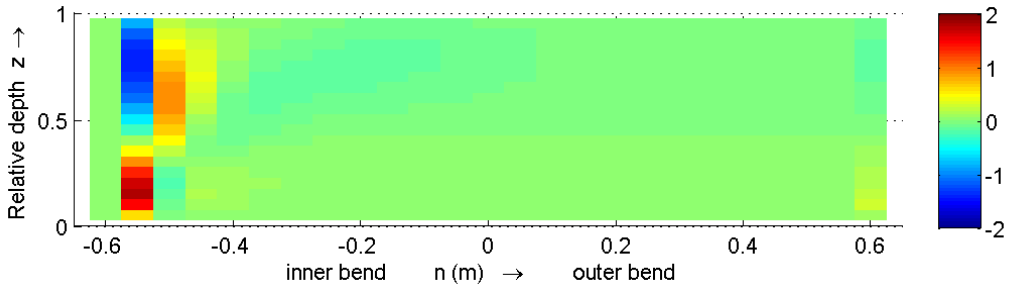

Figure C-276 Term 1 for cross-section 150, according to simulation Q89_1_D3D

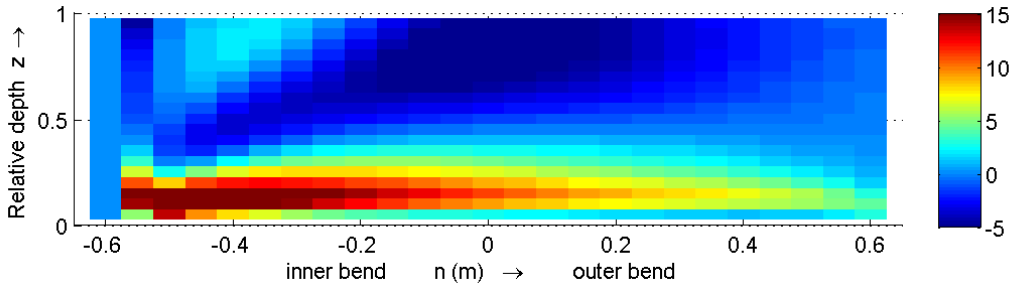

Figure C-277 Term 2 for cross-section 150, according to simulation Q89_1_D3D. Shortened colour bar

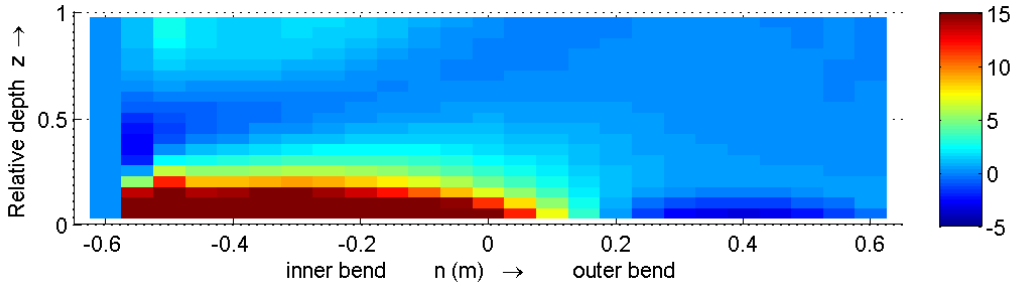

Figure C-278 Term 3 for cross-section 150, according to simulation Q89_1_D3D. Shortened colour bar

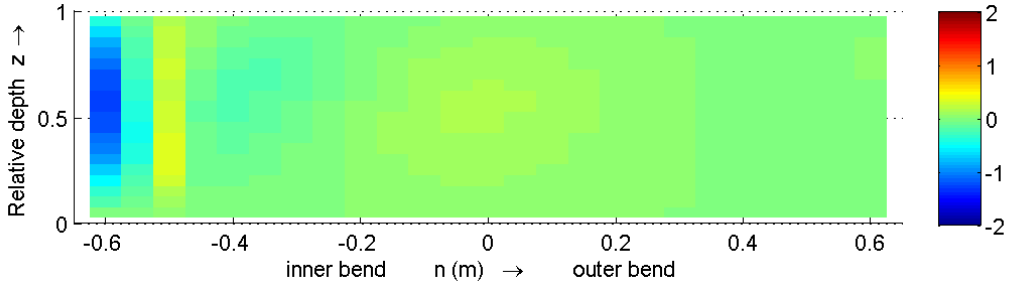

Figure C-279 Term 4 for cross-section 150, according to simulation Q89_1_D3D

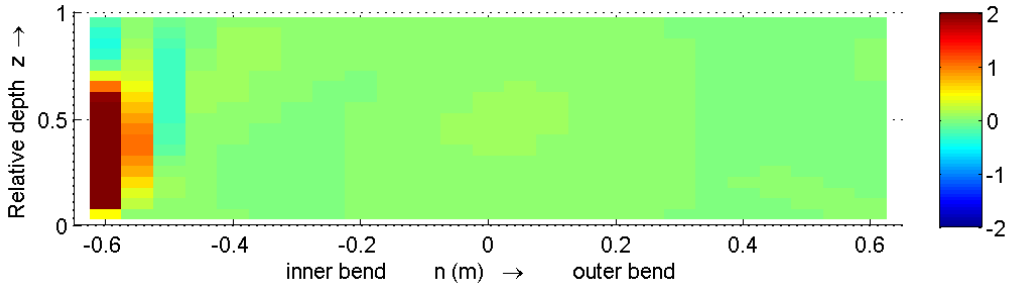

Figure C-280 Term 5 for cross-section 150, according to simulation Q89_1_D3D. Shortened colour bar

C.11 Downstream non-uniformity (DNU)

In this paragraph some plots of the downstream non-uniformity term (DNU) of the downstream vorticity balance equation will be shown. The DNU-term represents the downstream non-uniformity of the turbulence stresses, including vortex stretching (which is represented by the last term of the DNU-term, van Balen *et al.*, 2009b). All figures are normalized by 1000 * H^2/U^2.
The downstream non-uniformity term is defined as (van Balen *et al.*, 2009b):

$$\frac{\partial}{\partial z}\left(\frac{1}{r}\frac{\partial \overline{u'v'}}{\partial \theta}\right)-\frac{\partial}{\partial r}\left(\frac{1}{r}\frac{\partial \overline{u'w'}}{\partial \theta}\right)+\omega_\theta \frac{1}{r}\frac{\partial u}{\partial \theta}$$

This term is divided in sub terms. With

$$\text{Term 1} \quad = \frac{\partial}{\partial z}\left(\frac{1}{r}\frac{\partial \overline{u'v'}}{\partial \theta}\right)$$

$$\text{Term 2} \quad = -\frac{\partial}{\partial r}\left(\frac{1}{r}\frac{\partial \overline{u'w'}}{\partial \theta}\right)$$

$$\text{Term 3} \quad = \omega_\theta \frac{1}{r}\frac{\partial U}{\partial \theta}$$

Where u', v' and w' are the turbulent fluctuation of the velocity in the downstream respectively transverse and vertical direction

In the m25 cross-section the DNU-term is of minor importance in the centre of the flume. The Q89_LES and measurements show fluctuations in the centre region (see Figure C-281 and Figure C-282). The fluctuations along the outer bend wall according to the measurements are due to sub term one. The fluctuations along the bottom and the surface can be explained because the accuracy of the measurements is poor and the borders introduce a discontinuity. The reason of the fluctuations along the side walls is unclear. Simulation Q89_1_D3D gives some fluctuations along the side walls too (especially the inner wall) but these fluctuations are two orders of magnitude smaller than the fluctuations according to the measurements.

In the 060 cross-section (Figure C-284 to Figure C-286) the DNU-term gains importance and is mainly determined by the third sub term (the vortex stretching). This can be explained by the phenomena of the shift of the core. As we saw in section 3.2, the core of the downstream velocity shifts outward, towards the outer bend. This will result in relative high downstream gradients (in the downstream velocity) and a high DNU-term. In the centre of the flume is the strength of the DNU-term increased, also due to the downstream vortex stretching. The Q89_LES gives in the inner bend the same pattern as the measurements while in the centre, it seems that the upper and lower part of the flume are changed. The Q89_LES shows positive values in the lower part and negative values in the upper part while for the measurements the positive and negative values are changed. Simulation Q89_1_D3D gives lower values for the DNU-term with exception of the upper part of the inner bend. In that place, the simulation and measurements have opposite signs and the absolute value of the DNU-term is overestimated.

In the 150 cross-section the DNU-term is again determined by vortex stretching (compare Figure C-287 to Figure C-289 with Figure C-298, Figure C-307 and Figure C-316 respectively). The strength decreases (just like the vorticity which decreases too in the 150 cross-section) and the shape changes too. The Q89_LES behaves different than the measurements says. The positive valued region in the inner bend according to the measurements is absent. The negative valued region in the outer bend seems to be extended over the whole width of the flume. Simulation Q89_1_D3D still under predicts the DNU-term.

Generally it can be said that simulation Q89_1_D3D under predicts the DNU-term and the Q89_LES has a wrong prediction of the distribution of the DNU-term. Besides that, the DNU-term is relatively unimportant (with respect to the CFG- and ADV-terms).

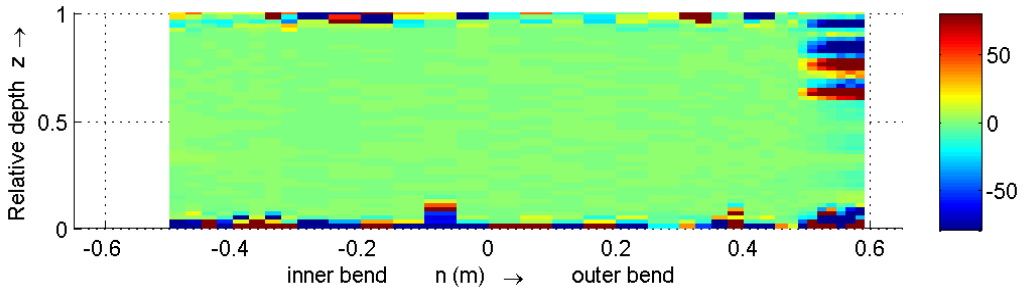

Figure C-281 DNU for cross-section m25, according to the measurements. Shortened colour bar

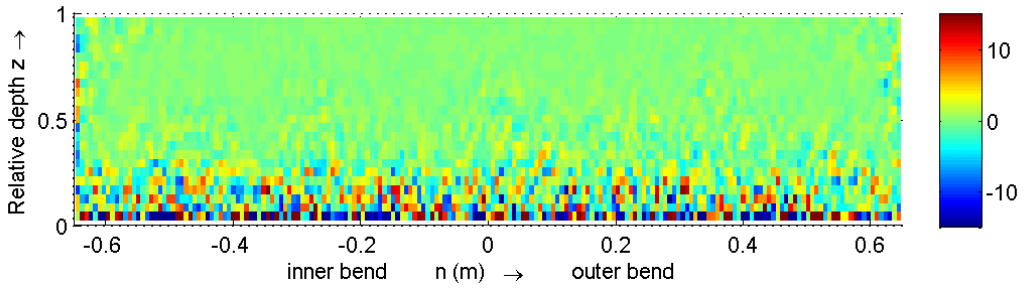

Figure C-282 DNU for cross-section m25, according to the Q89_LES. Shortened colour bar

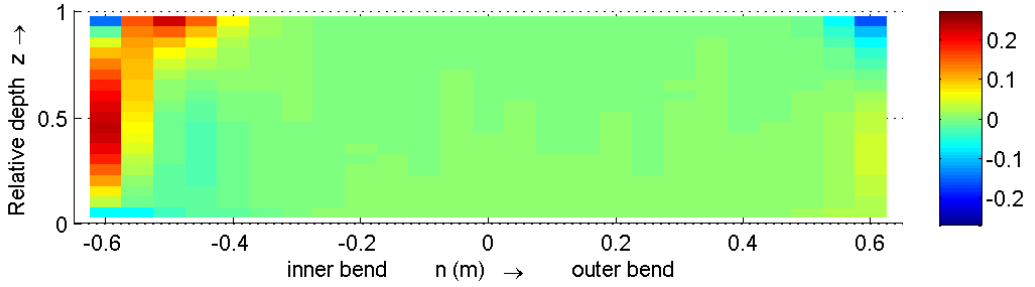

Figure C-283 DNU for cross-section m25, according to simulation Q89_1_D3D

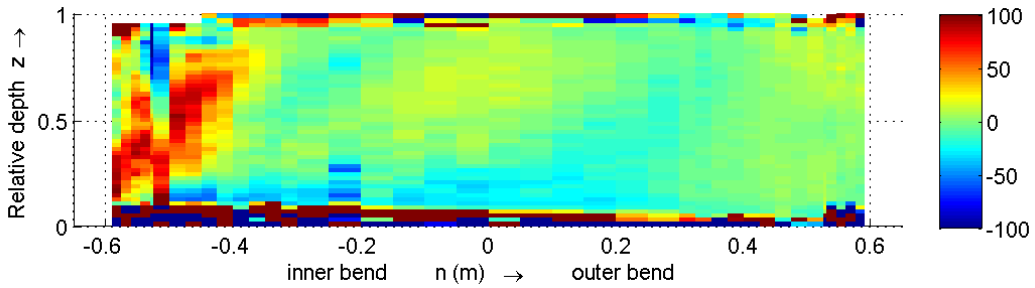

Figure C-284 DNU for cross-section 060, according to the measurements. Shortened colour bar

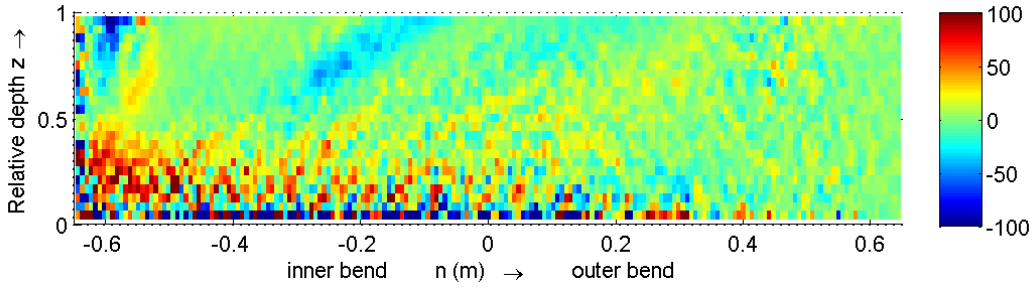

Figure C-285 DNU for cross-section 060, according to the Q89_LES. Shortened colour bar

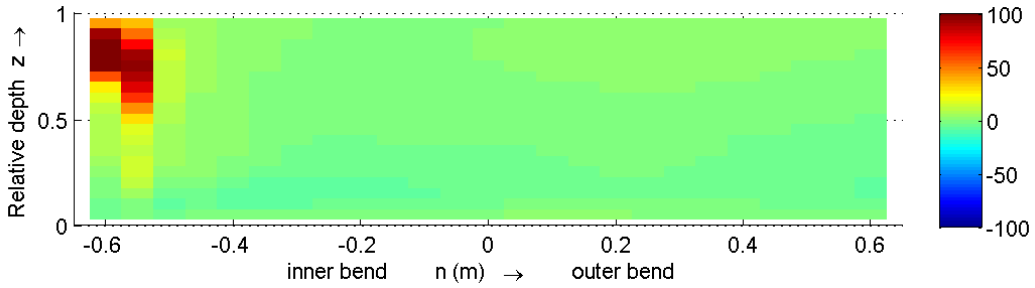

Figure C-286 DNU for cross-section 060, according to simulation Q89_1_D3D

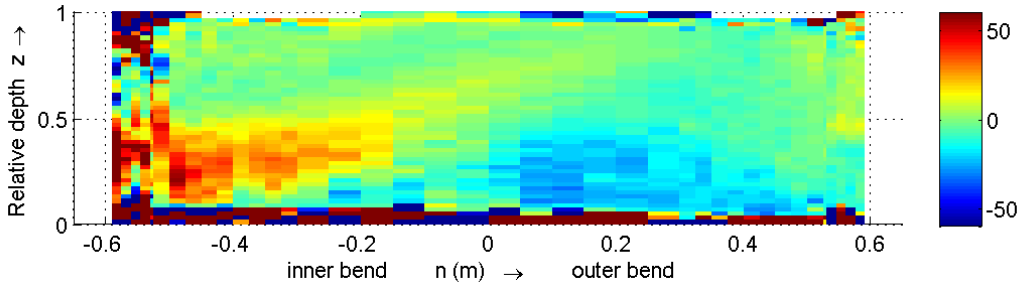

Figure C-287 DNU for cross-section 150, according to the measurements. Shortened colour bar

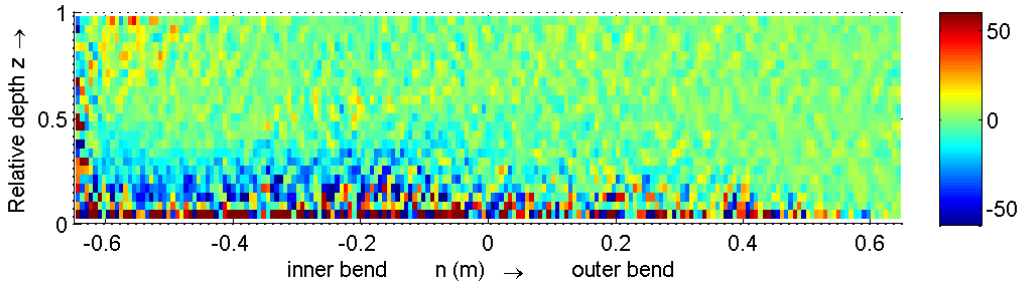

Figure C-288 DNU for cross-section 150, according to the Q89_LES. Shortened colour bar

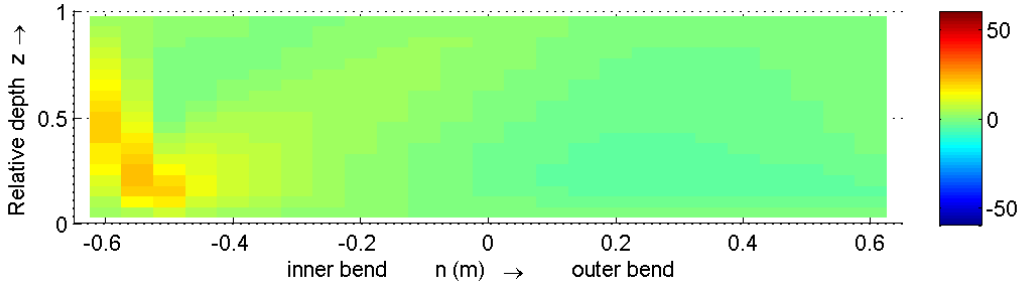

Figure C-289 DNU for cross-section 150, according to simulation Q89_1_D3D

C.11.1 Sub terms of the DNU term

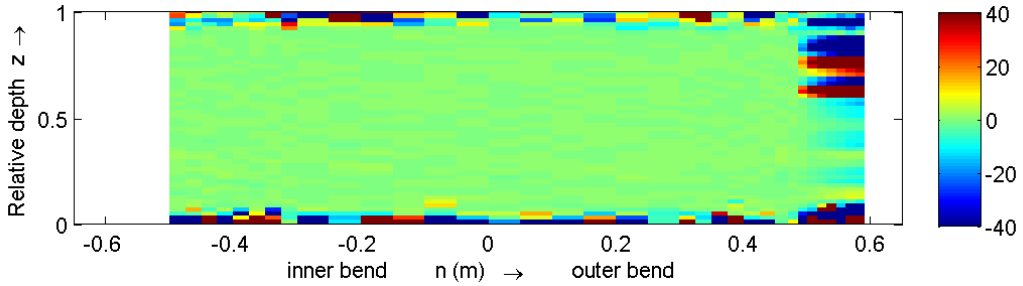

Figure C-290 Term 1 for cross-section m25, according to the measurements. Shortened colour bar

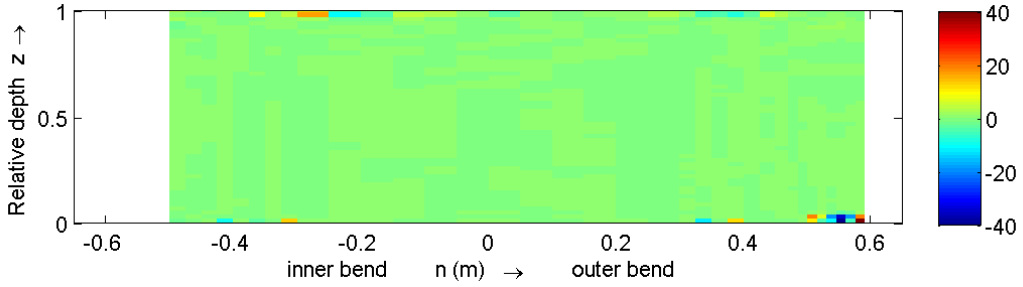

Figure C-291 Term 2 for cross-section m25, according to the measurements. Shortened colour bar

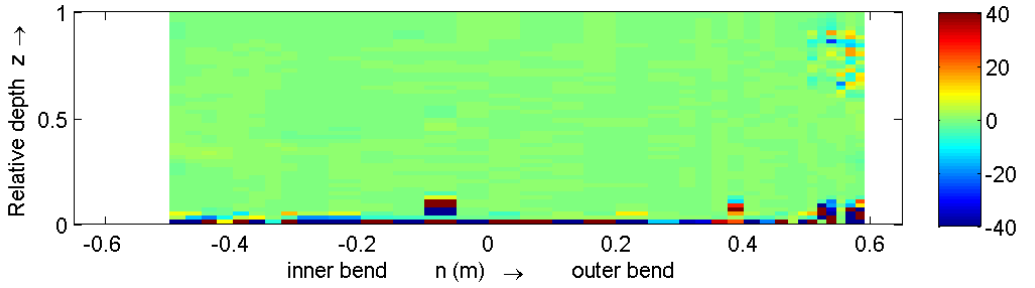

Figure C-292 Term 3 for cross-section m25, according to the measurements. Shortened colour bar

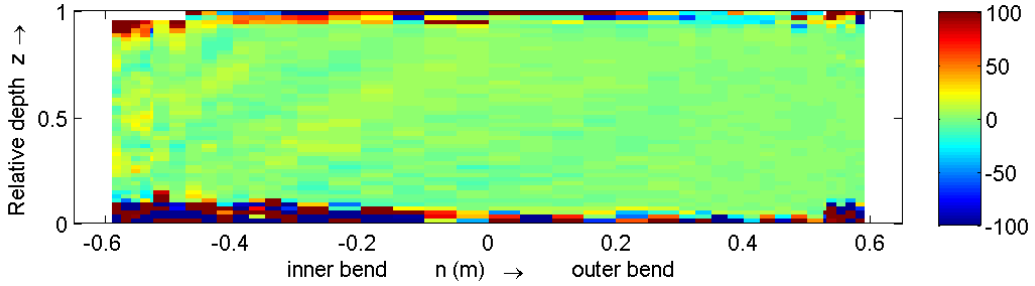

Figure C-293 Term 1 for cross-section 060, according to the measurements. Shortened colour bar

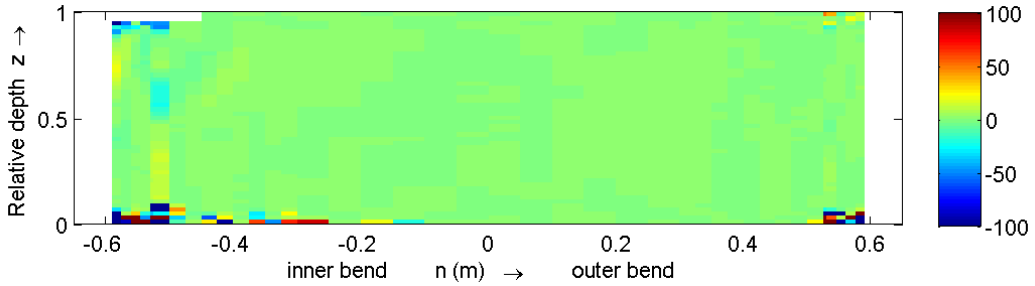

Figure C-294 Term 2 for cross-section 060, according to the measurements. Shortened colour bar

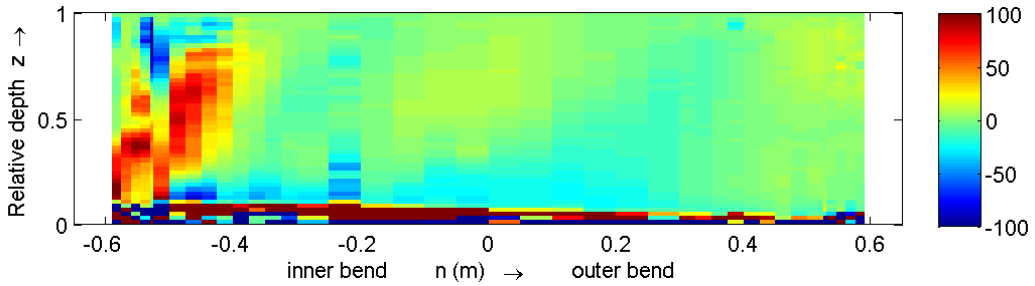

Figure C-295 Term 3 for cross-section 060, according to the measurements. Shortened colour bar

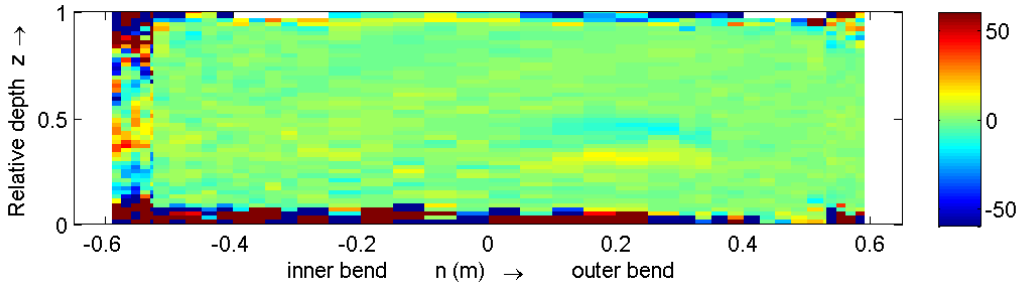

Figure C-296 Term 1 for cross-section 150, according to the measurements. Shortened colour bar

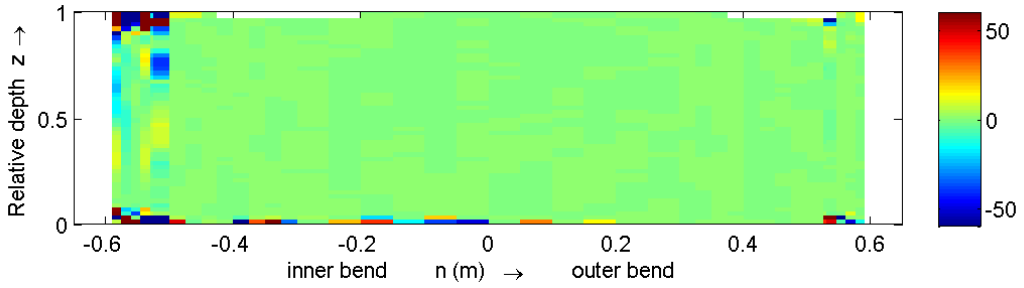

Figure C-297 Term 2 for cross-section 150, according to the measurements. Shortened colour bar

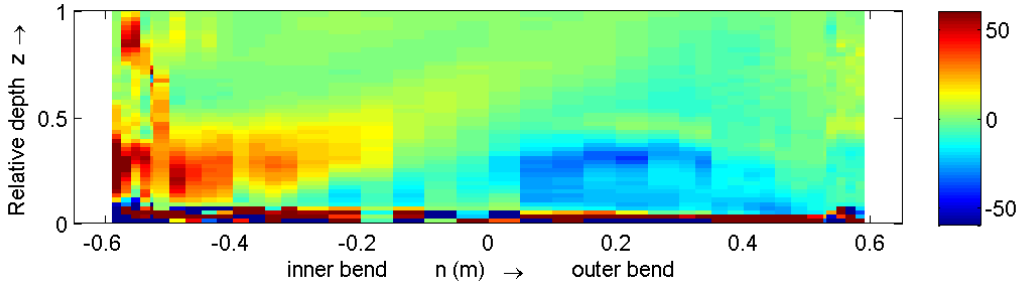

Figure C-298 Term 3 for cross-section 150, according to the measurements. Shortened colour bar

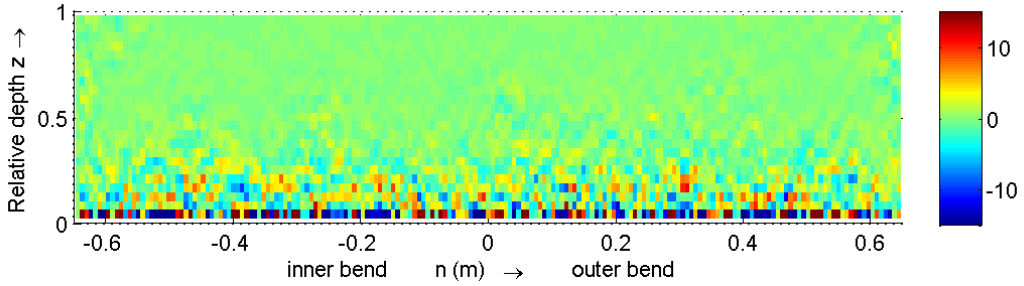

Figure C-299 Term 1 for cross-section m25, according to the Q89_LES. Shortened colour bar

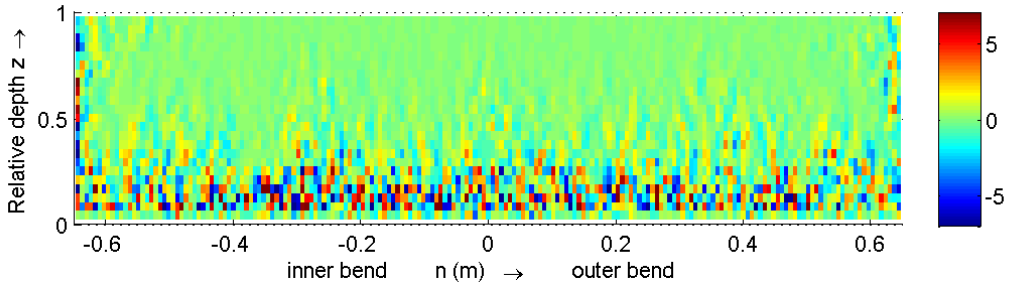

Figure C-300 Term 2 for cross-section m25, according to the Q89_LES. Shortened colour bar

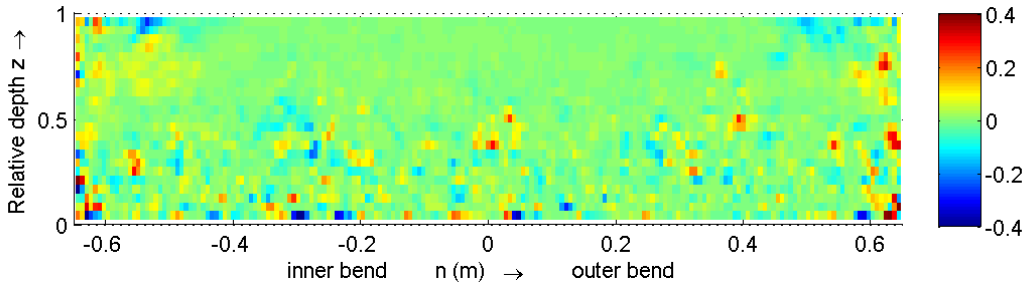

Figure C-301 Term 3 for cross-section m25, according to the Q89_LES. Shortened colour bar

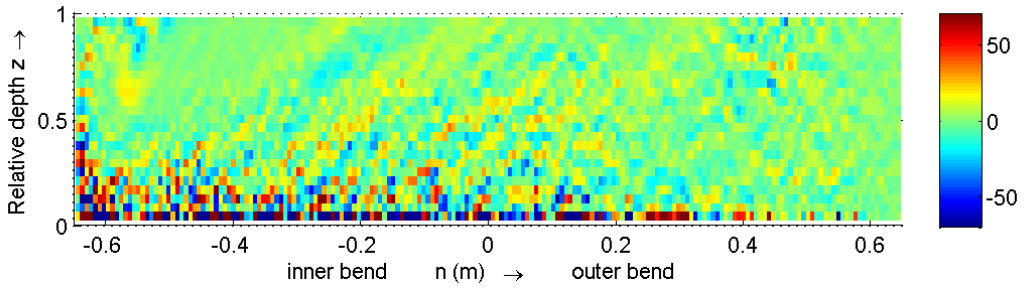

Figure C-302 Term 1 for cross-section 060, according to the Q89_LES. Shortened colour bar

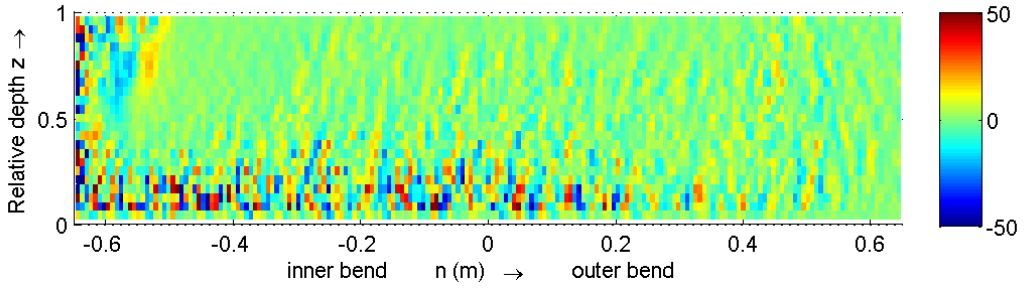

Figure C-303 Term 2 for cross-section 060, according to the Q89_LES. Shortened colour bar

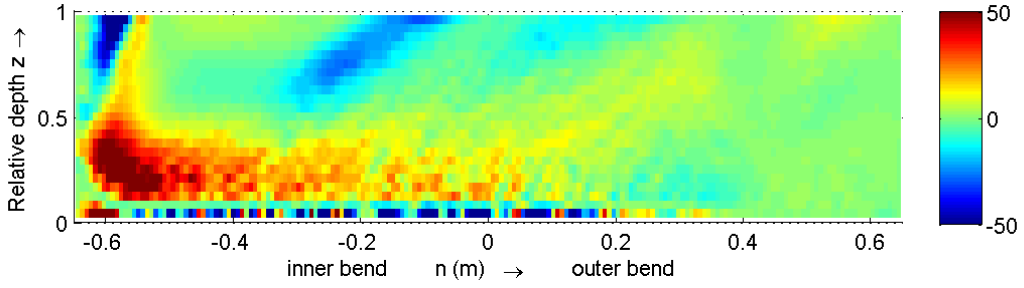

Figure C-304 Term 3 for cross-section 060, according to the Q89_LES. Shortened colour bar

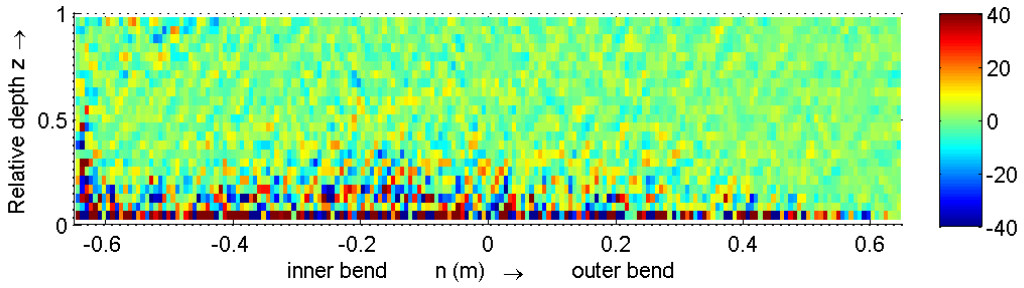

Figure C-305 Term 1 for cross-section 150, according to the Q89_LES. Shortened colour bar

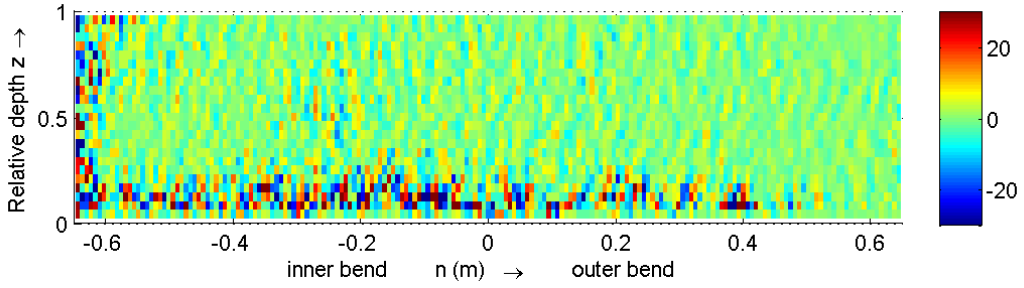

Figure C-306 Term 2 for cross-section 150, according to the Q89_LES. Shortened colour bar

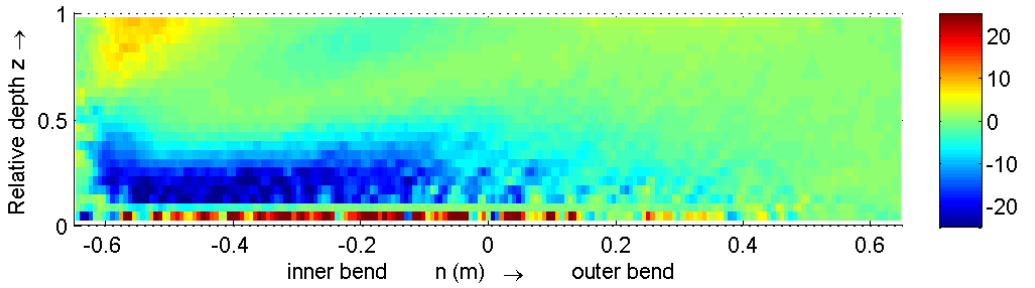

Figure C-307 Term 3 for cross-section 150, according to the Q89_LES. Shortened colour bar

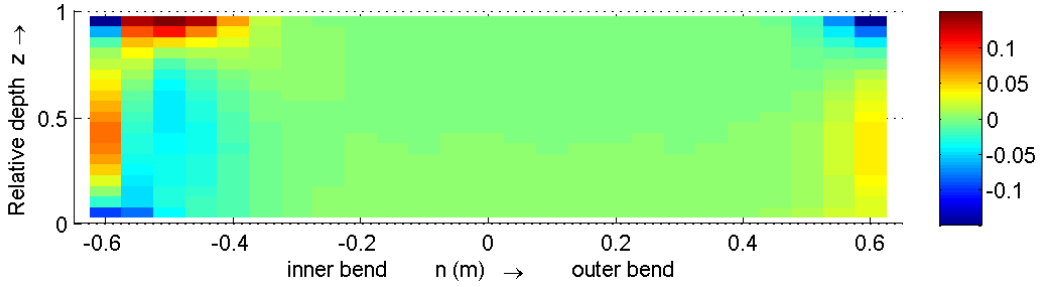

Figure C-308 Term 1 for cross-section m25, according to simulation Q89_1_D3D

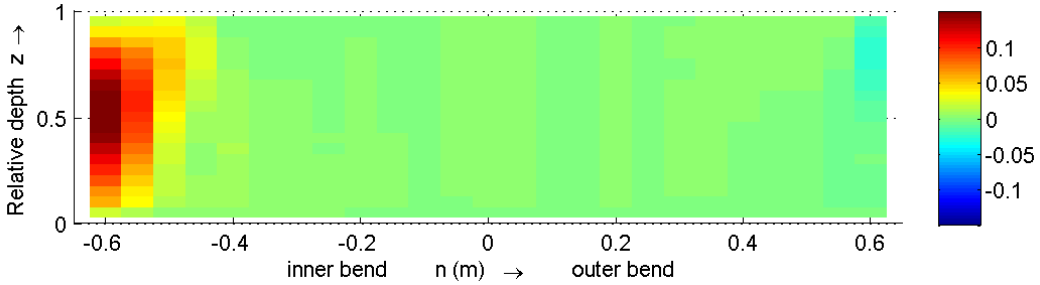

Figure C-309 Term 2 for cross-section m25, according to simulation Q89_1_D3D

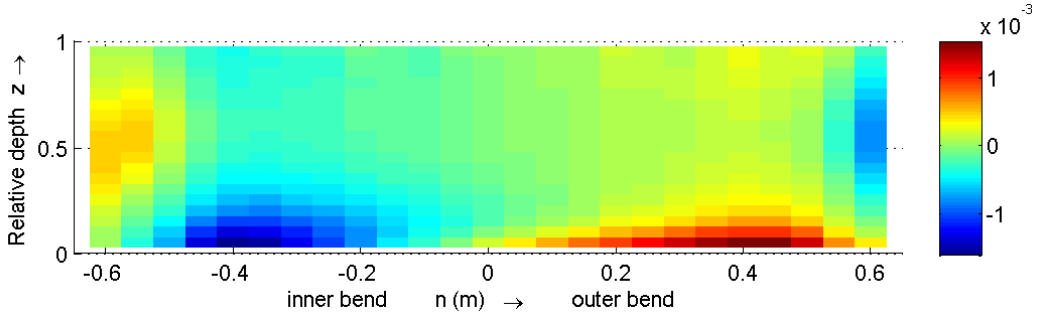

Figure C-310 Term 3 for cross-section m25, according to simulation Q89_1_D3D

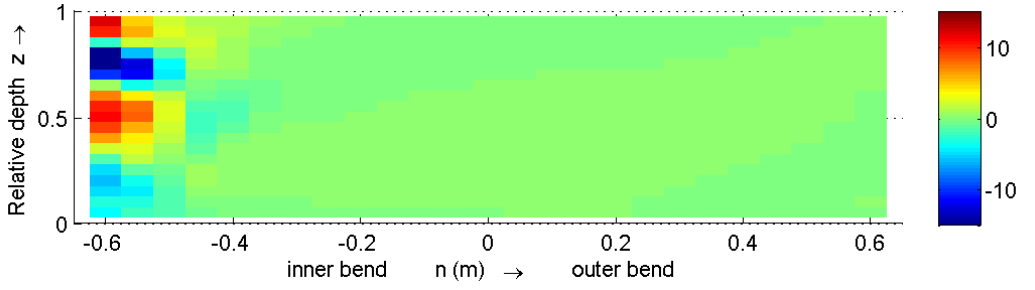

Figure C-311 Term 1 for cross-section 060, according to simulation Q89_1_D3D. Shortened colour bar

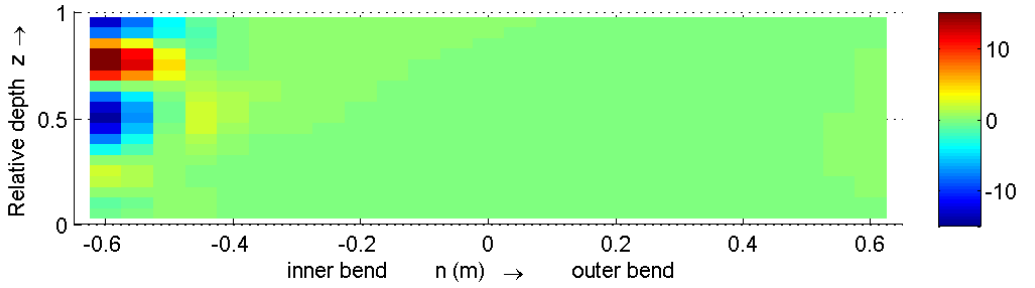

Figure C-312 Term 2 for cross-section 060, according to simulation Q89_1_D3D. Shortened colour bar

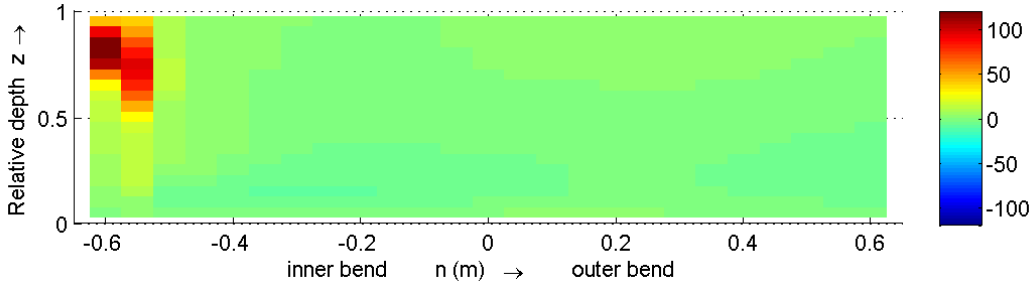

Figure C-313 Term 3 for cross-section 060, according to simulation Q89_1_D3D. Shortened colour bar

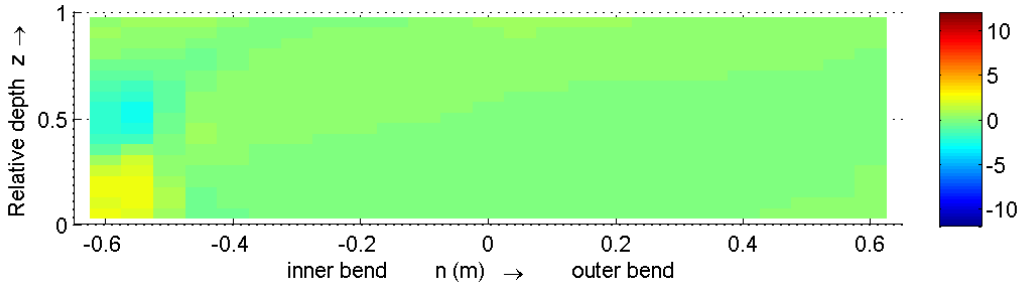

Figure C-314 Term 1 for cross-section 150, according to simulation Q89_1_D3D

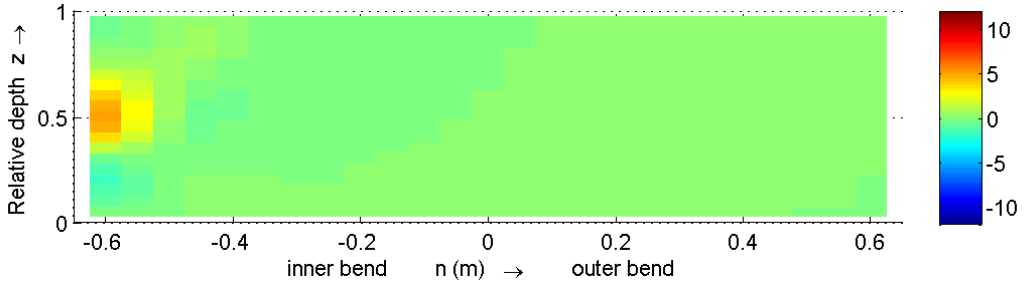

Figure C-315 Term 2 for cross-section 150, according to simulation Q89_1_D3D

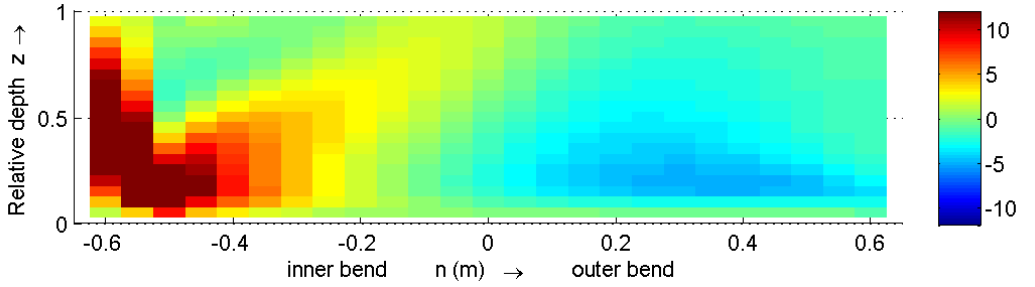

Figure C-316 Term 3 for cross-section 150, according to simulation Q89_1_D3D. Shortened colour bar

C.12 Turbulent stresses

The turbulent stresses are averaged in time. Only the $\overline{u'v'}$, $\overline{u'w'}$ and $\overline{v'w'}$ stresses for cross-section 060 are shown because these are the most interesting quantities. The normal stresses can be related to the pressure and compared to the pressure are these stresses small. The turbulent shear stresses are large compared to the viscous shear forces. The figures are all normalized by U_{bulk}^2.

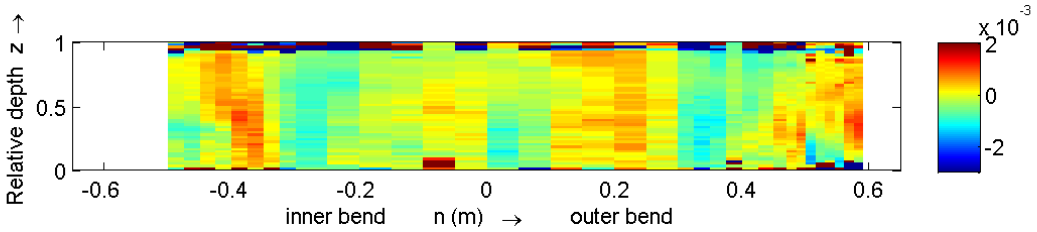

Figure C-317 Normalized $\overline{u'v'}$ according to the measurements, cross-section m25

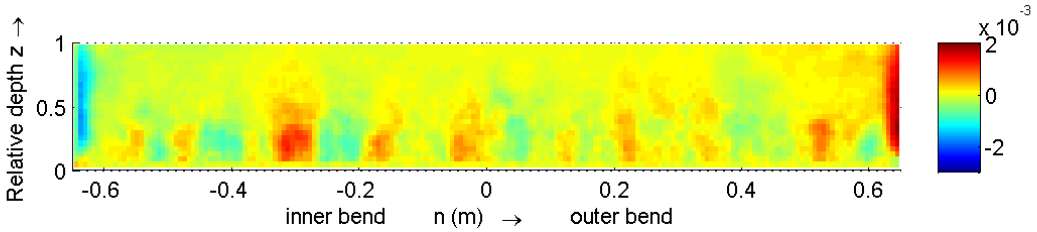

Figure C-318 Normalized $\overline{u'v'}$ according to the Q89_LES, cross-section m25

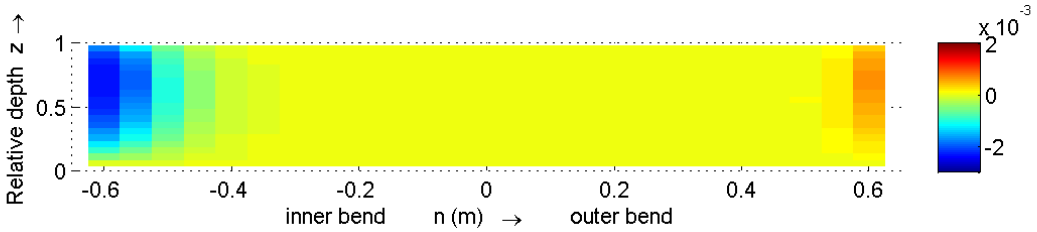

Figure C-319 Normalized $\overline{u'v'}$ according to simulation Q89_1_D3D, cross-section m25

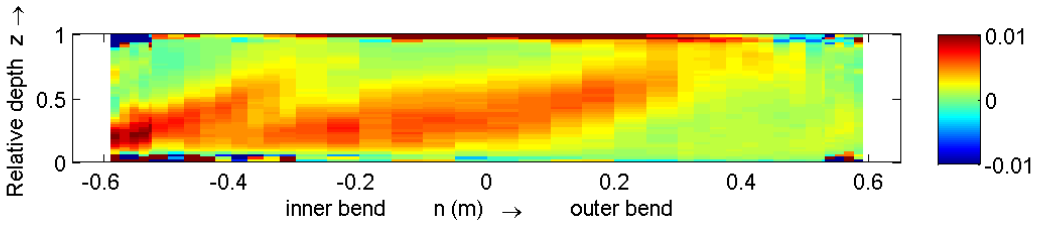

Figure C-320 Normalized $\overline{u'v'}$ according to the measurements, cross-section 060

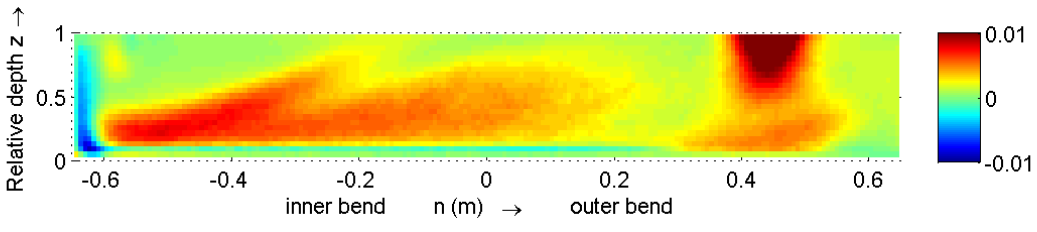

Figure C-321 Normalized $\overline{u'v'}$ according to the Q89_LES, cross-section 060

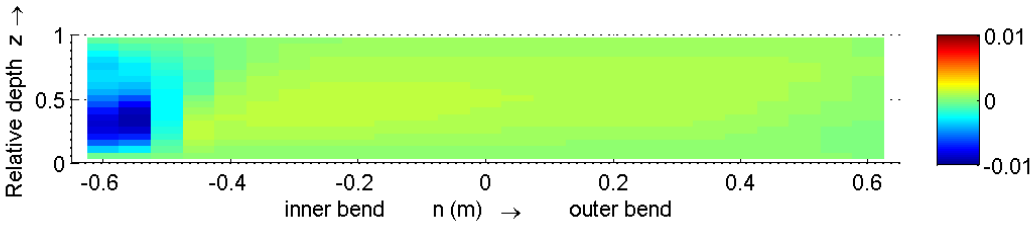

Figure C-322 Normalized $\overline{u'v'}$ according to simulation Q89_1_D3D, cross-section 060

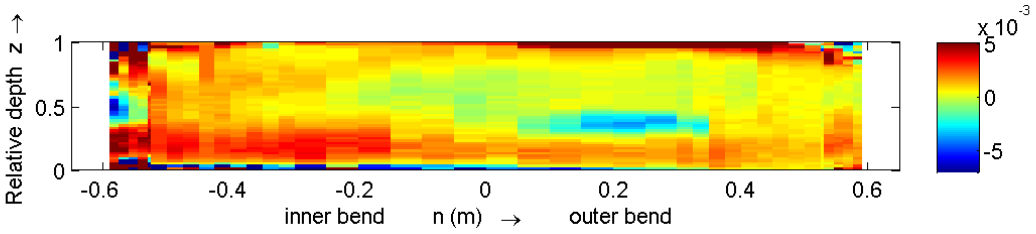

Figure C-323 Normalized $\overline{u'v'}$ according to the measurements, cross-section 150

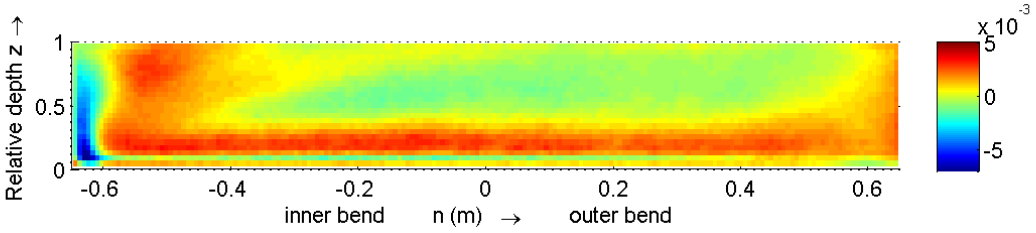

Figure C-324 Normalized $\overline{u'v'}$ according to the Q89_LES, cross-section 150

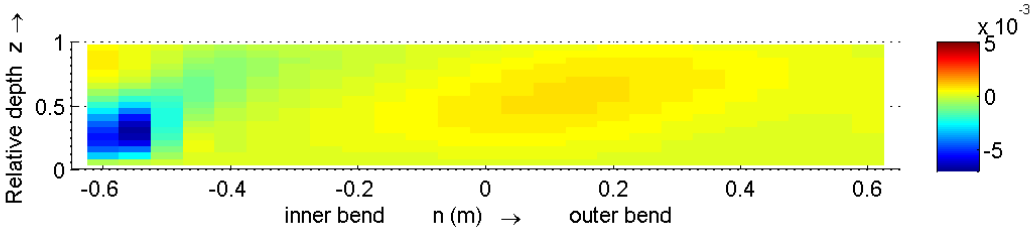

Figure C-325 Normalized $\overline{u'v'}$ according to simulation Q89_1_D3D, cross-section 150

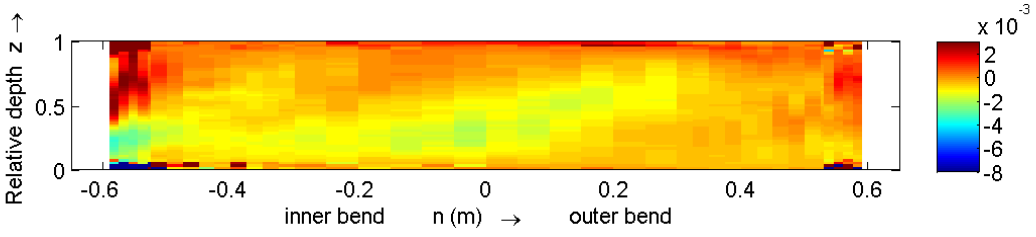

Figure C-326 Normalized $\overline{u'w'}$ according to the measurements, cross-section 060

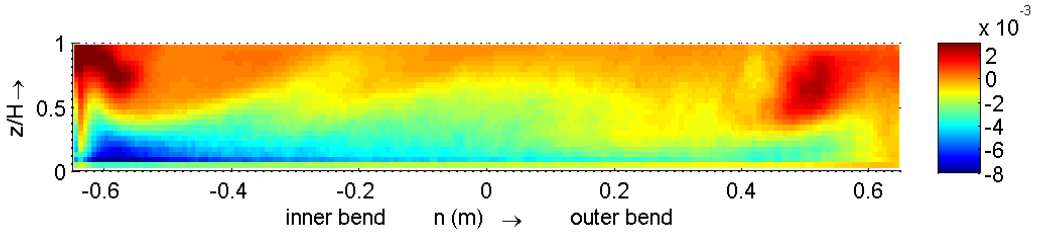

Figure C-327 Normalized $\overline{u'w'}$ according to the Q89_LES, cross-section 060

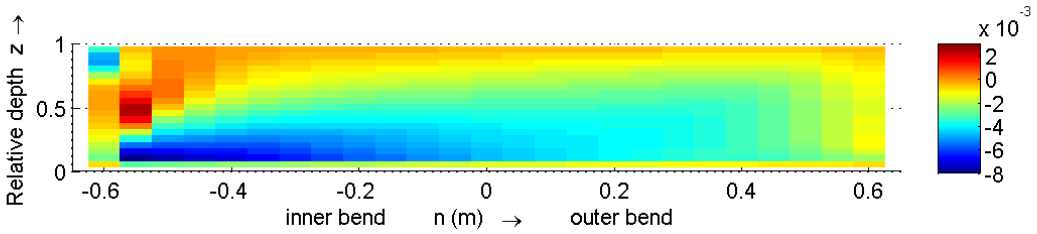

Figure C-328 Normalized $\overline{u'w'}$ according to simulation Q89_1_D3D, cross-section 060

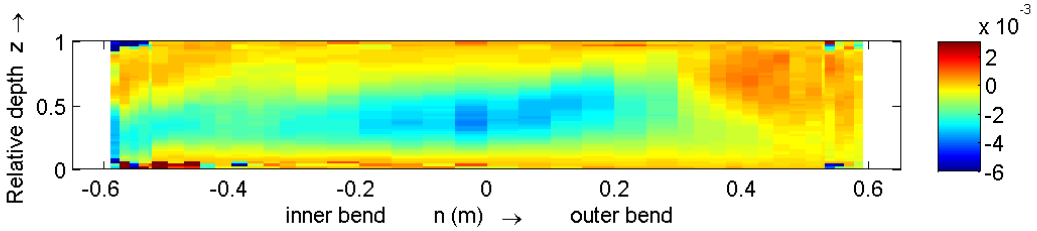

Figure C-329 Normalized $\overline{v'w'}$ according to the measurements, cross-section 060

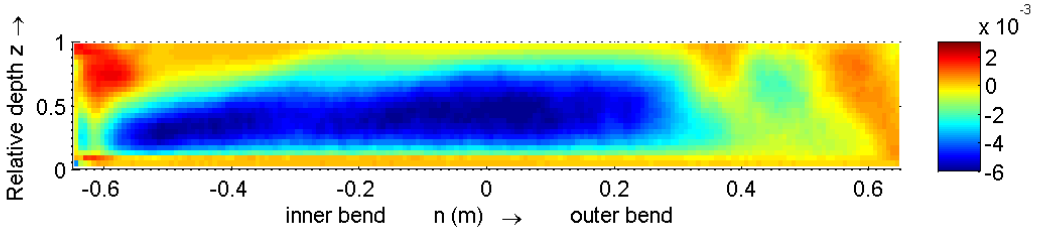

Figure C-330 Normalized $\overline{v'w'}$ according to the Q89_LES, cross-section 060

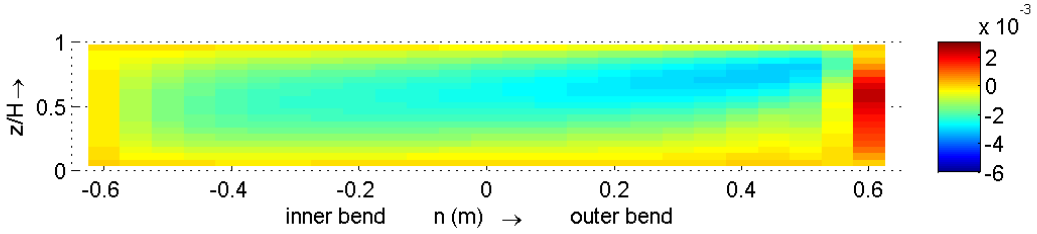

Figure C-331 Normalized $\overline{v'w'}$ according to simulation Q89_1_D3D, cross-section 060

C.13 Turbulent kinetic energy

In this paragraph some plots of the turbulent kinetic energy (TKE)is shown for simulation Q89_1_D3D). The turbulent kinetic energy (TKE) tells us at which places turbulent energy is

available. The TKE is given as: $\left(v_s'^2 + v_n'^2 + v_z'^2\right)/2$. The depth averaged TKE is normalized by 0.5 * u_*^2, whereas u_* is given as $\sqrt{(g)}\, U_{bulk}/C$.

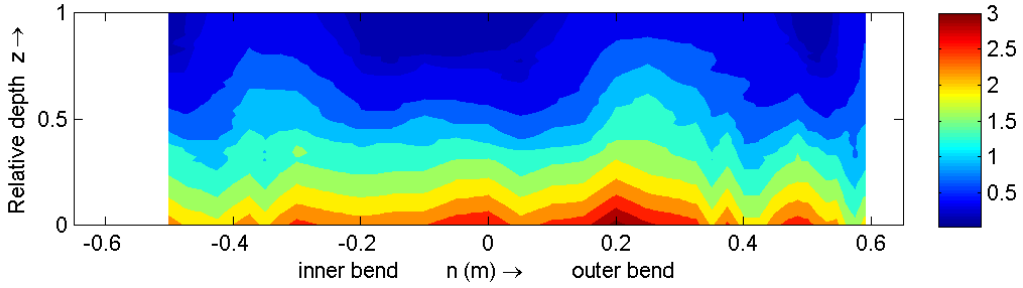

Figure C-332 Turbulent kinetic energy (measured, m25), normalized by (0.5 *u_*^2)

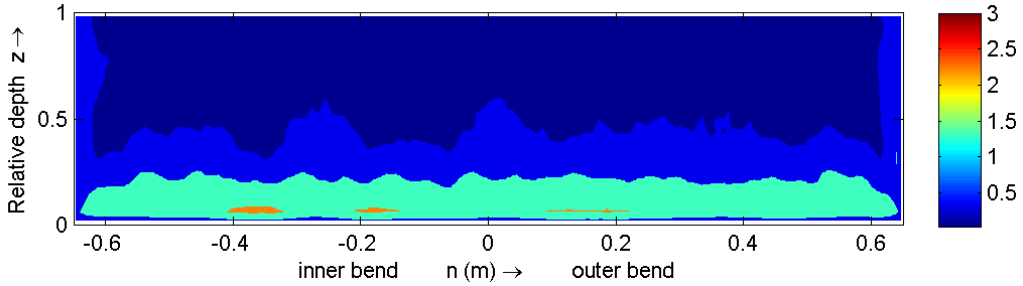

Figure C-333 Turbulent kinetic energy (Q89_LES, m25), normalized by (0.5 *u_*^2)

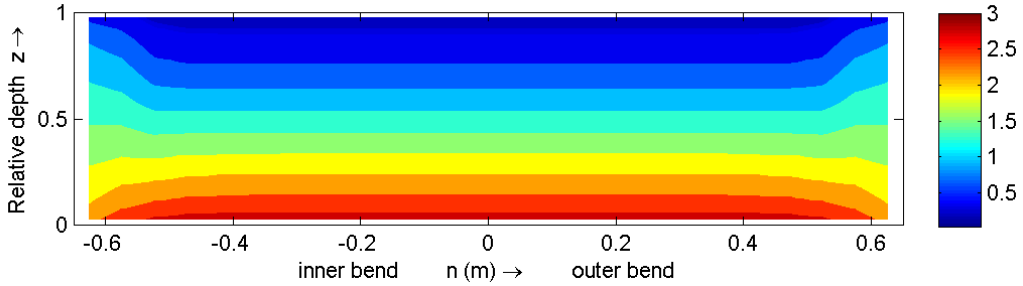

Figure C-334 Turbulent kinetic energy (simulation Q89_1_D3D, m25), normalized by (0.5 *u_*^2)

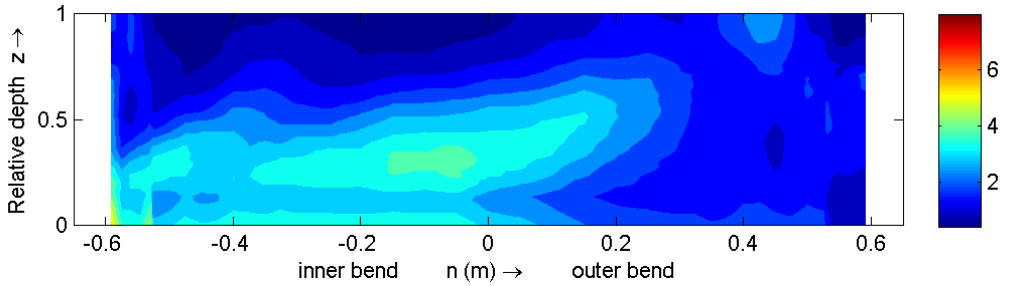

Figure C-335 Turbulent kinetic energy (measured, 060), normalized by (0.5 *u_*^2)

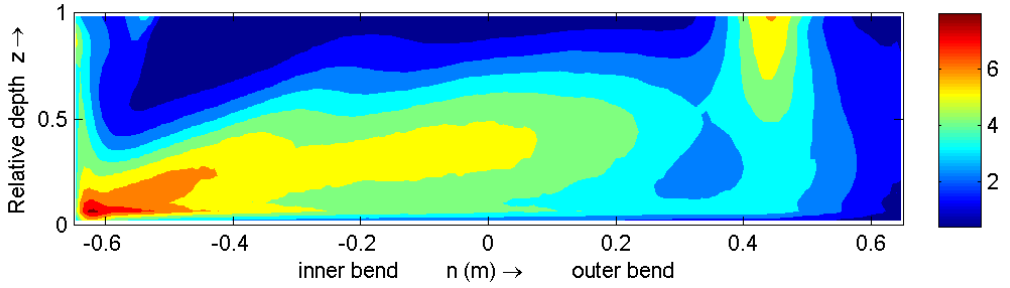

Figure C-336 Turbulent kinetic energy (Q89_LES, 060), normalized by (0.5 *u_*^2)

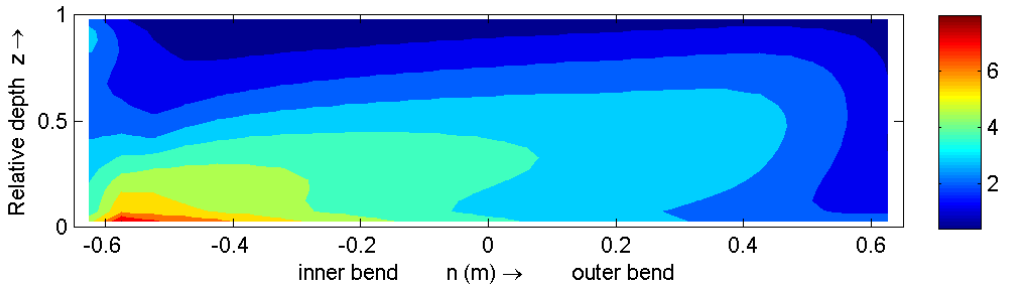

Figure C-337 Turbulent kinetic energy (simulation Q89_1_D3D, 060), normalized by (0.5 *u_*^2)

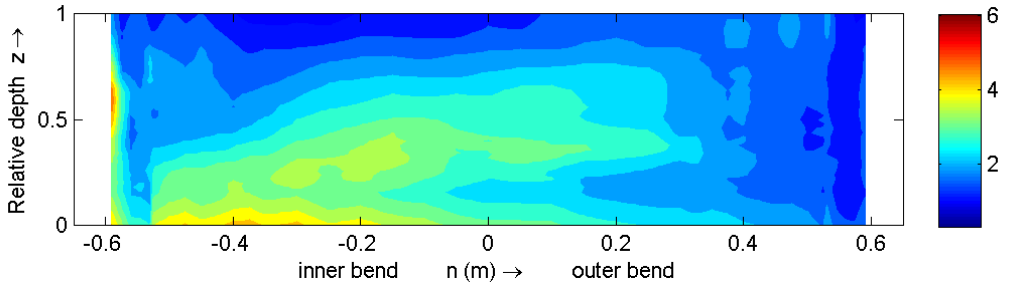

Figure C-338 Turbulent kinetic energy (measured, 150), normalized by (0.5 *u_*^2)

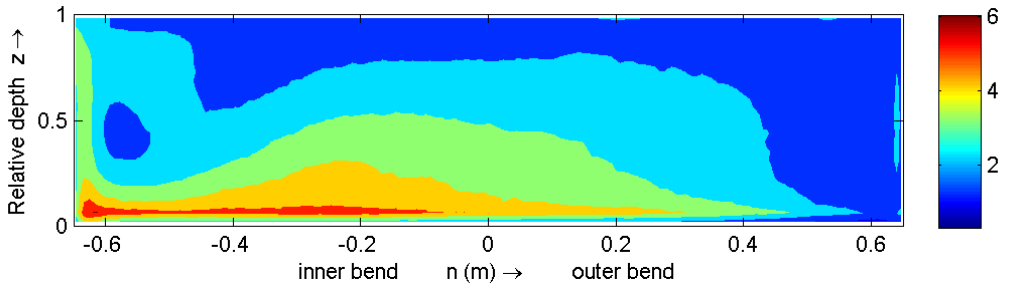

Figure C-339 Turbulent kinetic energy (Q89_LES, 150), normalized by (0.5 *u_*^2)

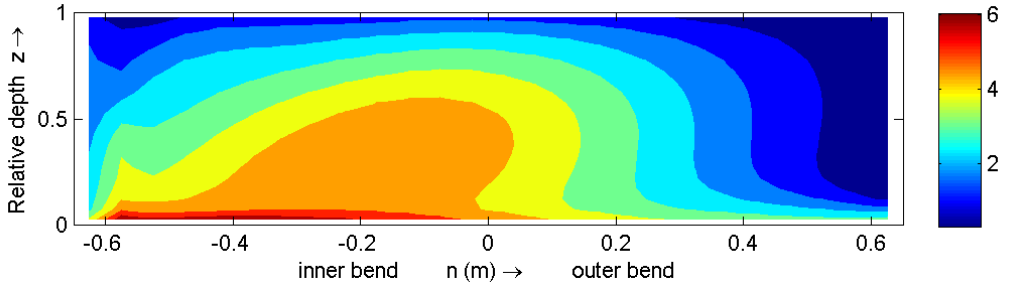

Figure C-340 Turbulent kinetic energy (simulation Q89_1_D3D, 150), normalized by (0.5 *u_*^2)

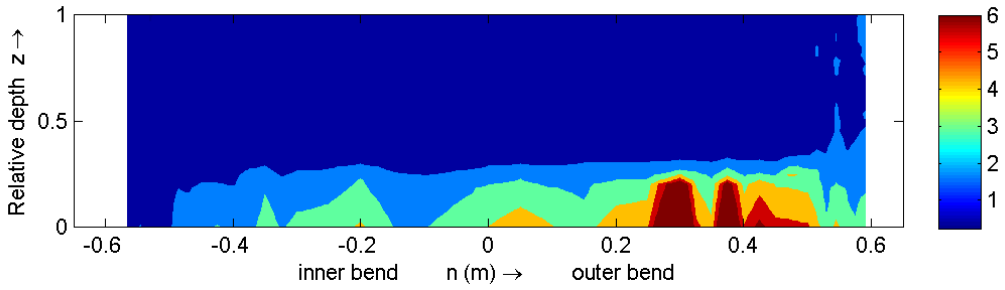

Figure C-341 Turbulent kinetic energy (measured, p25), normalized by (0.5 *u_*^2)

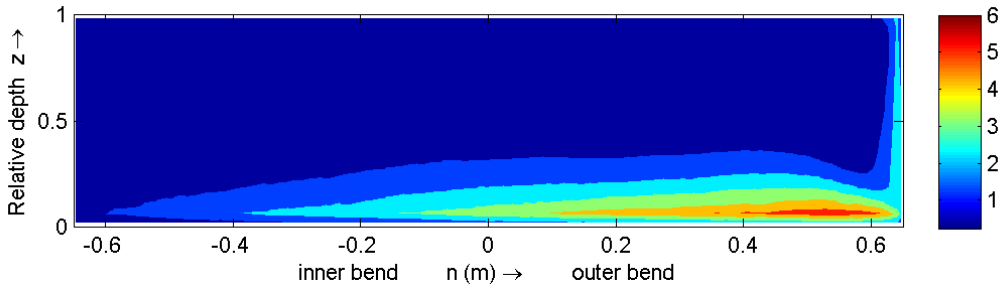

Figure C-342 Turbulent kinetic energy (Q89_LES, p25), normalized by (0.5 *u_*^2)

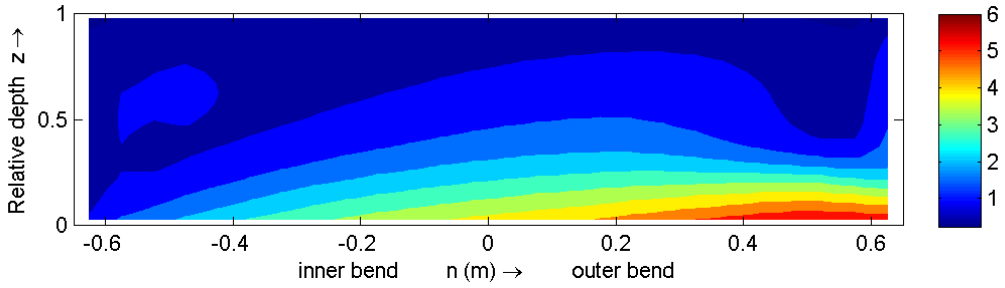

Figure C-343 Turbulent kinetic energy (simulation Q89_1_D3D, p25), normalized by (0.5 *u_*^2)

Appendix D Figures of D3D simulation with increased viscosity

D.1 Downstream velocities

This paragraph contains cross-sectional plots of the downstream velocity according to the Delft3D-FLOW simulations. For the cross-sections m25, 060 and 150 a plot is made for simulation Q89_1_D3D and a plot for simulation Q89_2_D3D. All figures are normalized by the bulk velocity (0.43 m/s).

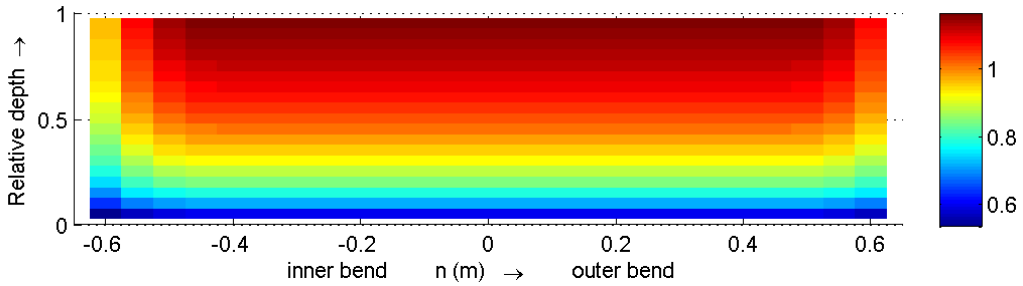

Figure D-1 Downstream velocity in cross-section m25 according to simulation Q89_1_D3D, normalized by U_{bulk}

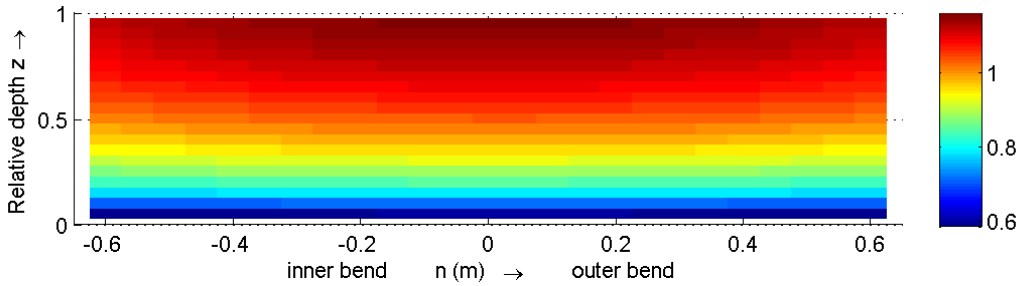

Figure D-2 Downstream velocity in cross-section m25 according to simulation Q89_2_D3D, normalized by U_{bulk}

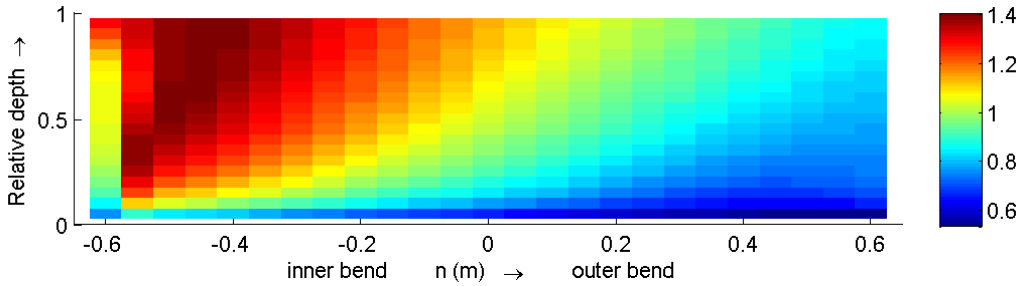

Figure D-3 Downstream velocity in cross-section 060 according to simulation Q89_1_D3D, normalized by U_{bulk}

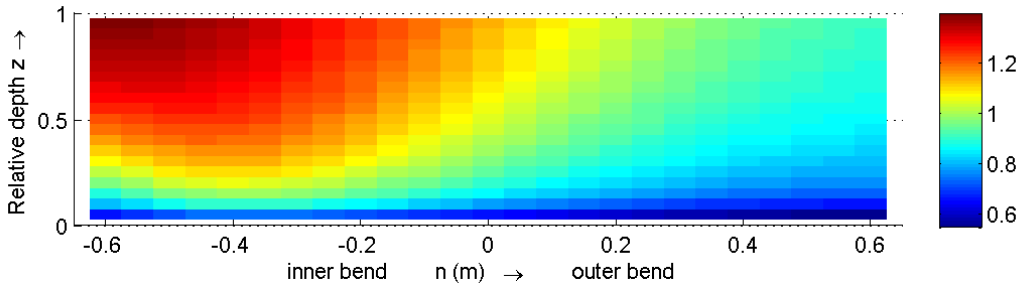

Figure D-4 Downstream velocity in cross-section 060 according to simulation Q89_2_D3D, normalized by U_{bulk}

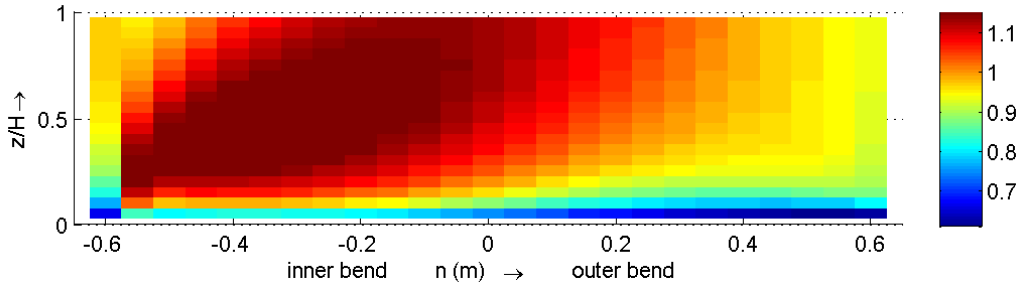

Figure D-5 Downstream velocity in cross-section 150 according to simulation Q89_1_D3D, normalized by U_{bulk}

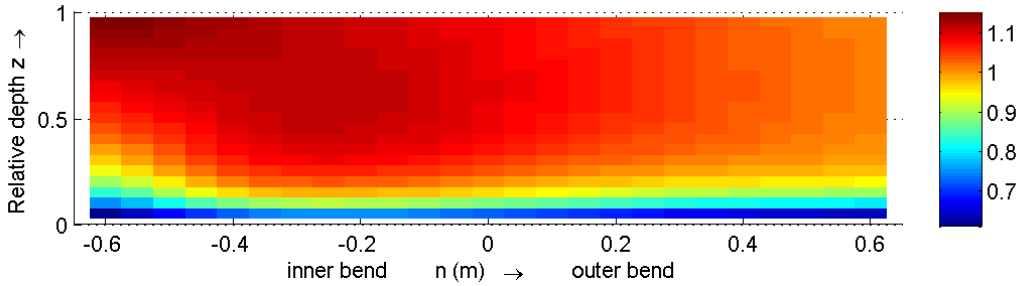

Figure D-6 Downstream velocity in cross-section 150 according to simulation Q89_2_D3D, normalized by U_{bulk}

D.2 Transversal velocities

This paragraph contains the cross-sectional plots of the normalized transverse velocities according to simulation Q89_2_D3D. The velocities are normalized by the bulk velocity.

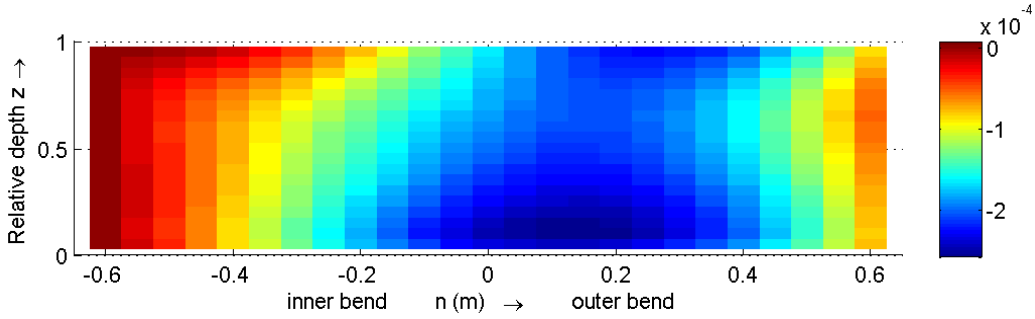

Figure D-7 Transversal velocity in cross-section m25 according to simulation Q89_2_D3D, normalized by U_{bulk}

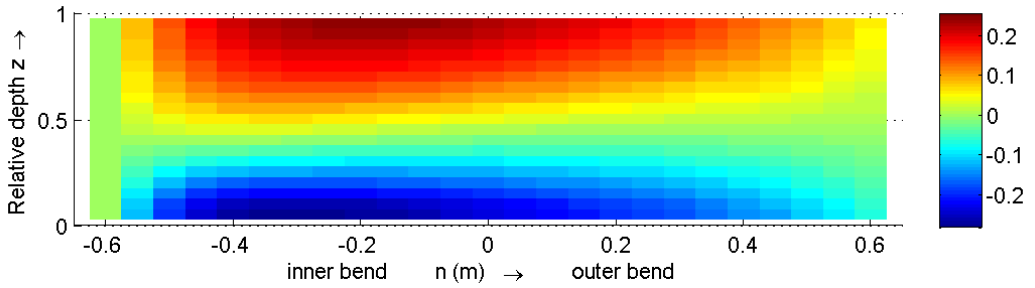

Figure D-8 Transversal velocity in cross-section 060 according to simulation Q89_2_D3D, normalized by U_{bulk}

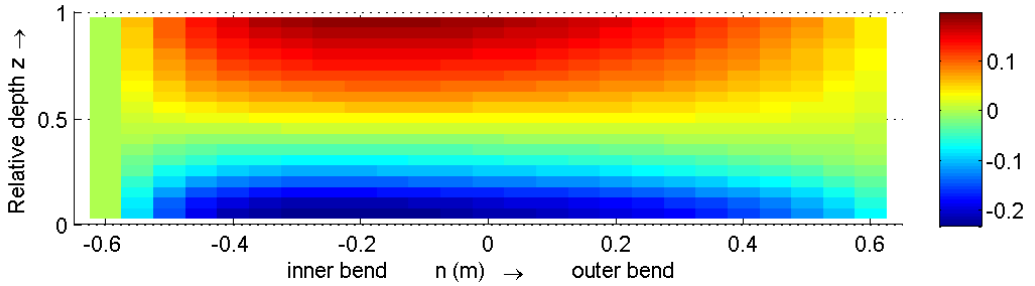

Figure D-9 Transversal velocity in cross-section 150 according to simulation Q89_2_D3D, normalized by U_{bulk}

D.3 Turbulent velocities

The turbulent stresses are averaged in time. Only the time averaged $\overline{u'v'}$, $\overline{u'w'}$ and $\overline{v'w'}$ stresses for cross-section 060 are shown because these are the most interesting quantities. The normal stresses can be related to the pressure and compared to the pressure are these stresses small. The turbulent shear stresses are large compared to the viscous shear forces. The figures are all normalized by U_{bulk}^2.

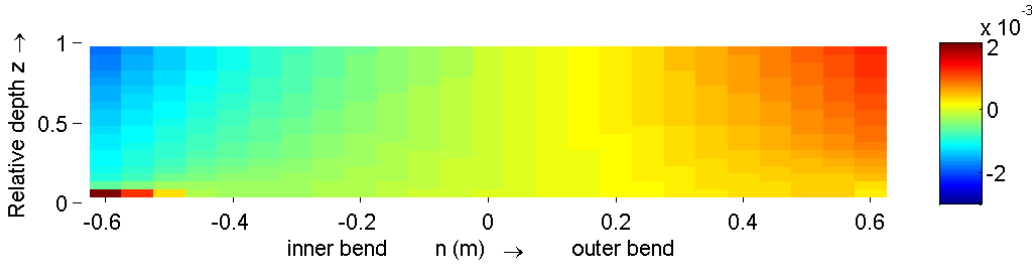

Figure D-10 Normalized $\overline{u'v'}$ according to simulation Q89_2_D3D, cross-section m25, normalized by U_{bulk}^2

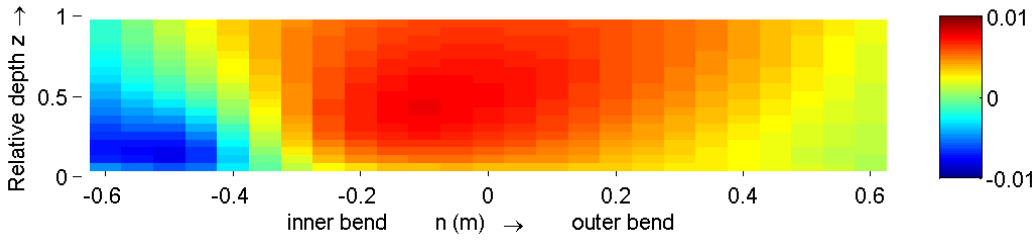

Figure D-11 Normalized $\overline{u'v'}$ according to simulation Q89_2_D3D, cross-section 060, normalized by U_{bulk}^2

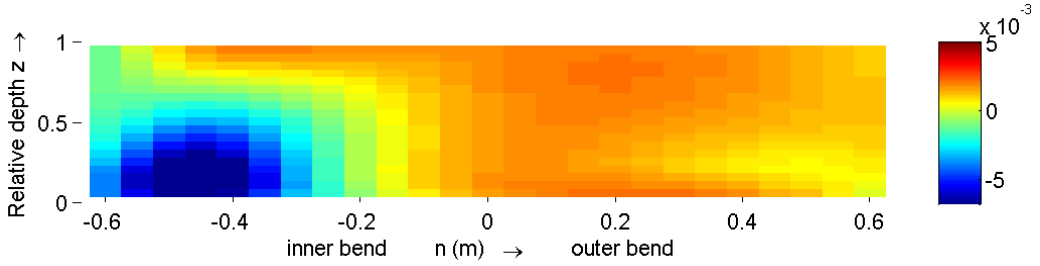

Figure D-12 Normalized $\overline{u'v'}$ according to simulation Q89_2_D3D, cross-section 150, normalized by U_{bulk}^2

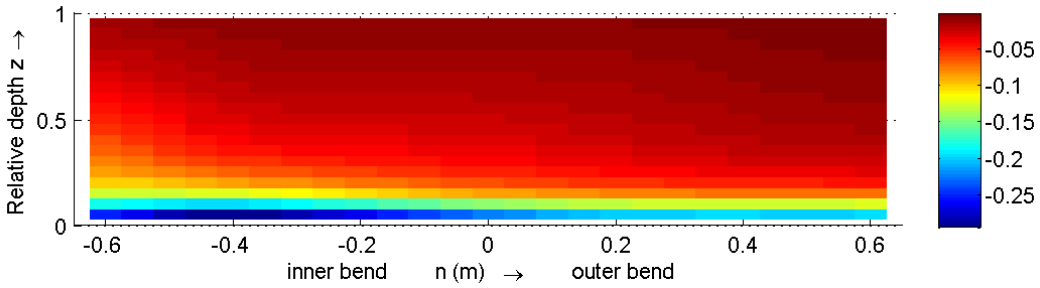

Figure D-13 Normalized $\overline{u'w'}$ according to simulation Q89_2_D3D, cross-section 060, normalized by U_{bulk}^2

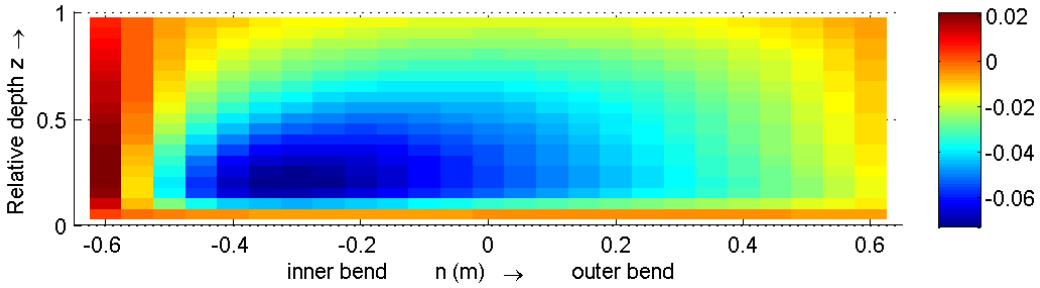

Figure D-14 Normalized $\overline{v'w'}$ according to simulation Q89_2_D3D, cross-section 060, normalized by U_{bulk}^2

D.4 Turbulent kinetic energy

In this paragraph some plots of the turbulent kinetic energy (TKE)is shown for simulation Q89_2_D3D). The TKE is given as: $\left(v_s'^2 + v_n'^2 + v_z'^2\right)/2$. The depth averaged TKE is normalized by 0.5 * u_*^2, whereas u_* is given as $\sqrt{(g)}\ U_{bulk}/C$.

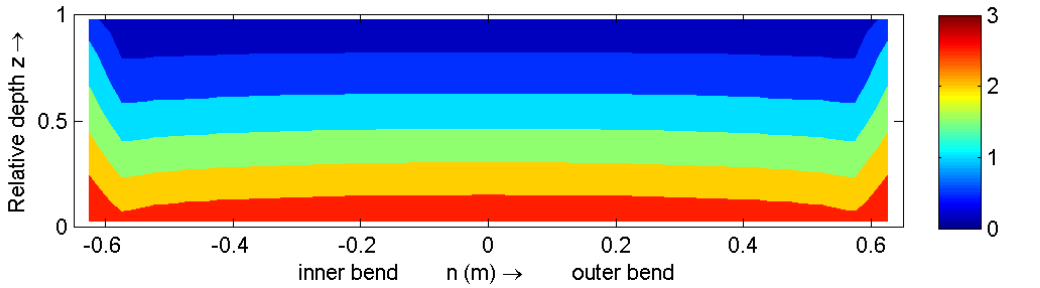

Figure D-15 Turbulent kinetic energy (simulation Q89_2_D3D, m25), normalized by (0.5 *u_*^2)

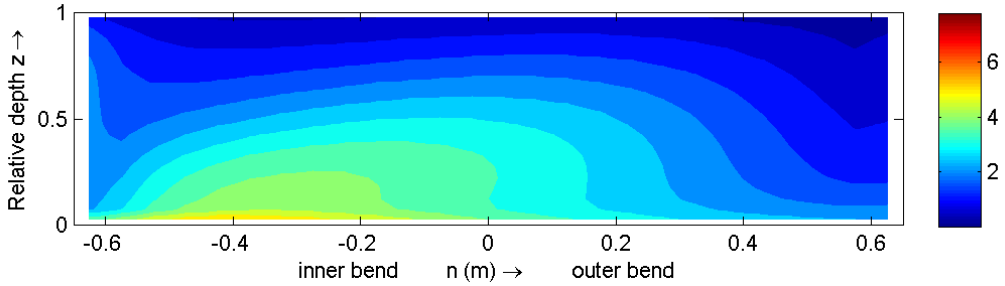

Figure D-16 Turbulent kinetic energy (simulation Q89_2_D3D, 060), normalized by (0.5 *u_*^2)

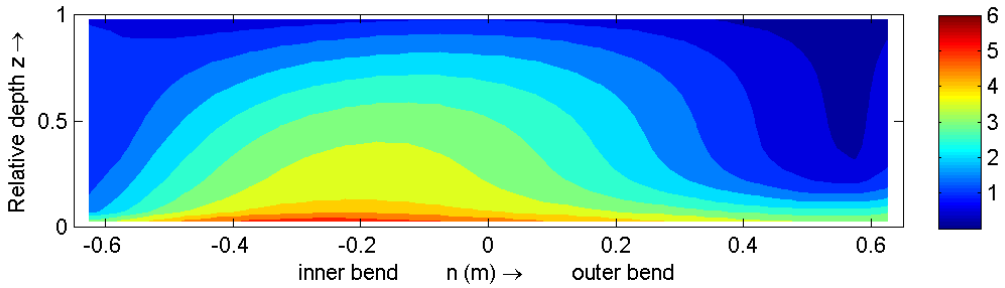

Figure D-17 Turbulent kinetic energy (simulation Q89_2_D3D, 150), normalized by (0.5 *u_*^2)

Appendix E Figures M89 results

E.1 Cross-sectional plots of downstream velocity(M89)

This paragraph contains several cross-sectional plots of the downstream velocities. The cross-sections shown here are the m22, 060 and 150 cross-section. The plots are made for the following data sets: the measurements, the M89_LES and the Delft3D-FLOW simulation M89_1_D3D. Besides that, three plots are added with the Froude number. In these plots (Figure E-10 to Figure E-12) it becomes clear that the simulations show super critical flow over the bar in the innerbend around the 060 cross-section.

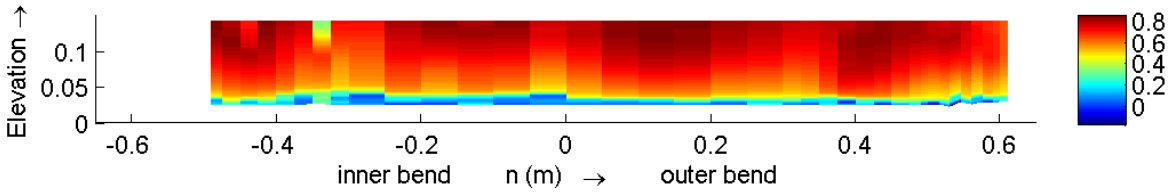

Figure E-1 Downstream velocity according to the measurements, cross-section m22

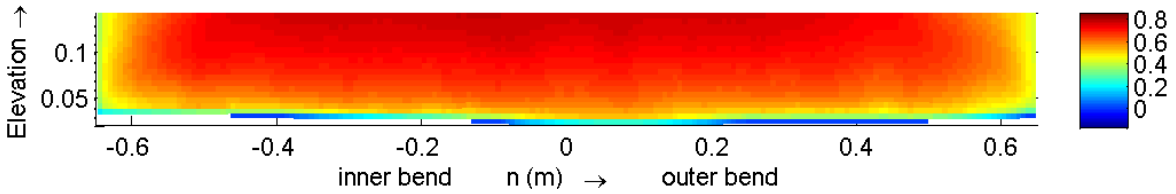

Figure E-2 Downstream velocity according to the M89_LES, cross-section m22

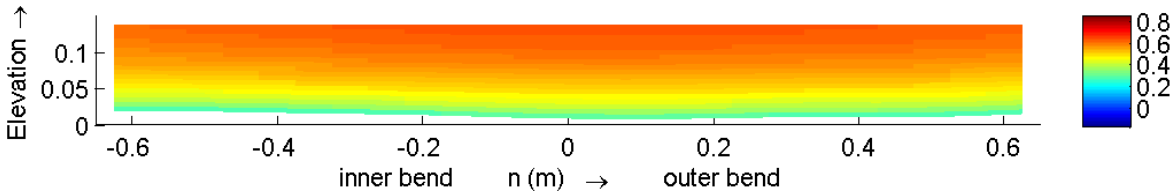

Figure E-3 Downstream velocity according to simulation M89_1_D3D, cross-section m22

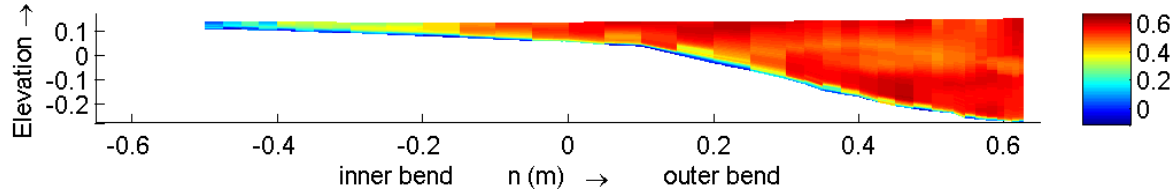

Figure E-4 Downstream velocity according to the measurements, cross-section 060

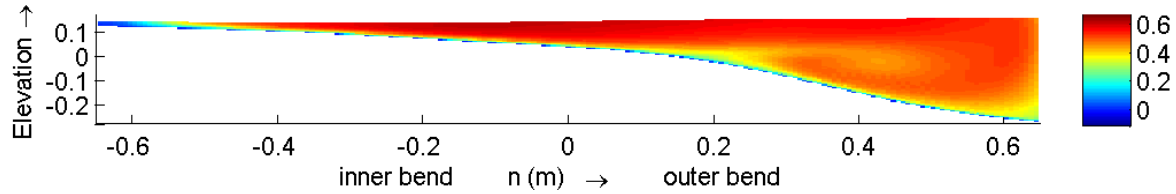

Figure E-5 Downstream velocity according to the M89_LES cross-section 060

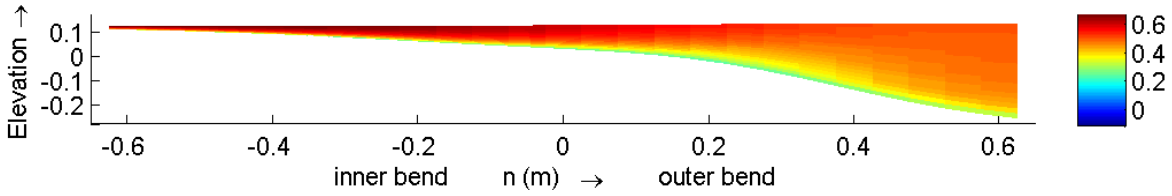

Figure E-6 Downstream velocity according to simulation M89_1_D3D, cross-section 060

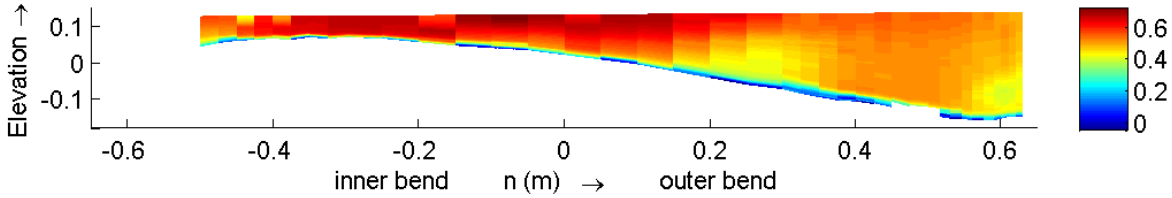

Figure E-7 Downstream velocity according to the measurements, cross-section 150

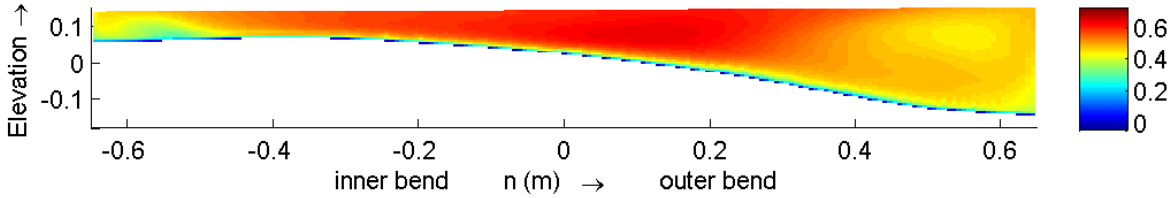

Figure E-8 Downstream velocity according to the M89_LES, cross-section 150

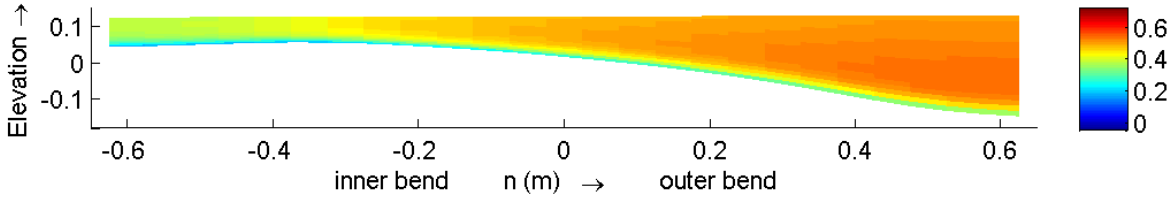

Figure E-9 Downstream velocity according to simulation M89_1_D3D, cross-section 150

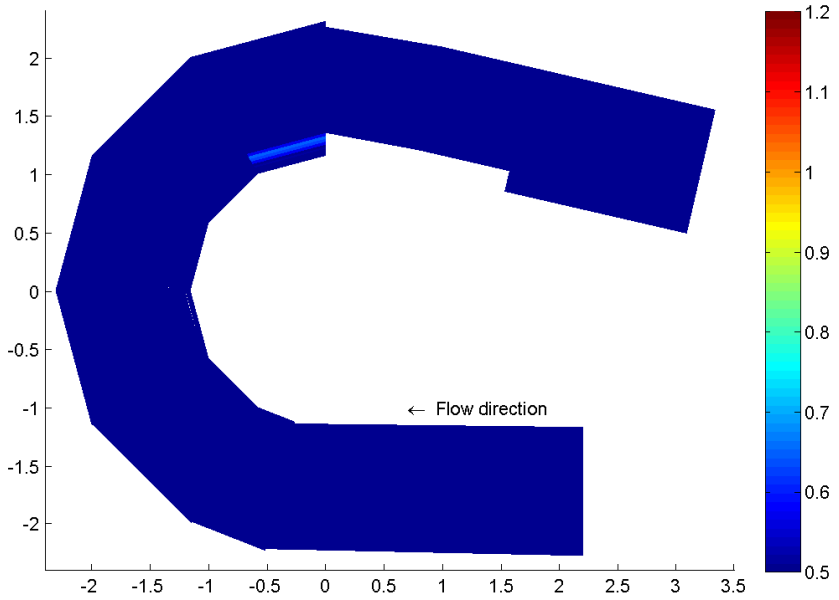

Figure E-10 Froude number ($U^2/(gd)$) according to the measurements

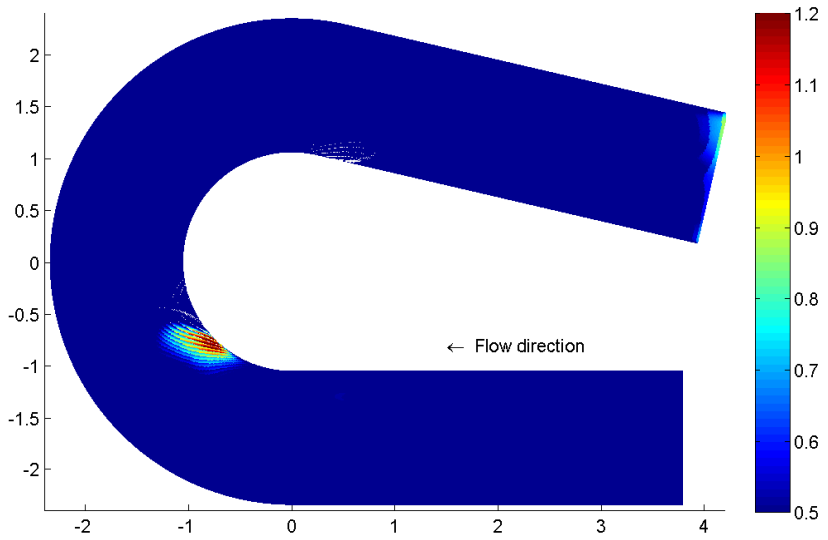

Figure E-11 Froude number ($U^2/(gd)$) according M89_LES

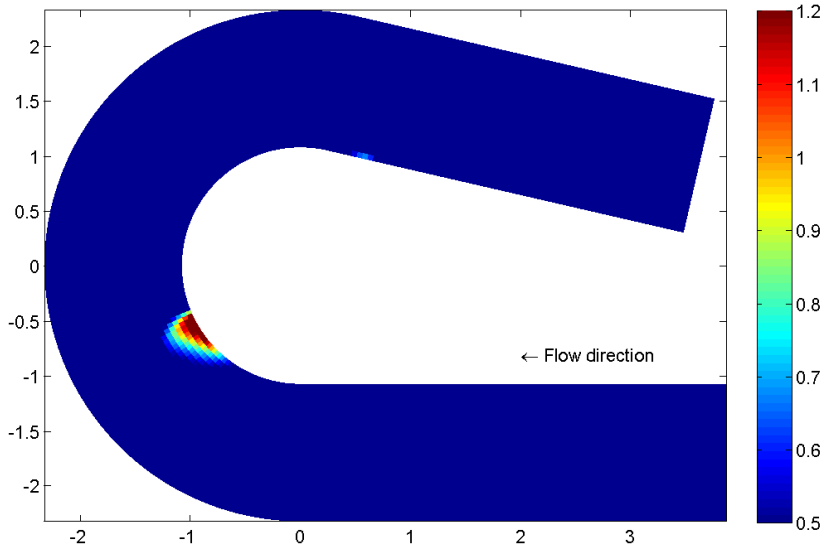

Figure E-12 Froude number ($U^2/(gd)$) according to simulation M89_1_D3D

E.2 Cross-sectional plots of transverse velocities (M89)

This paragraph contains several cross-sectional plots of the transverse velocities. The cross-sections shown here are the m22, 060 and 150 cross-section. The plots are made for the following data sets: the measurements, the M89_LES and the Delft3D-FLOW simulation M89_1_D3D.

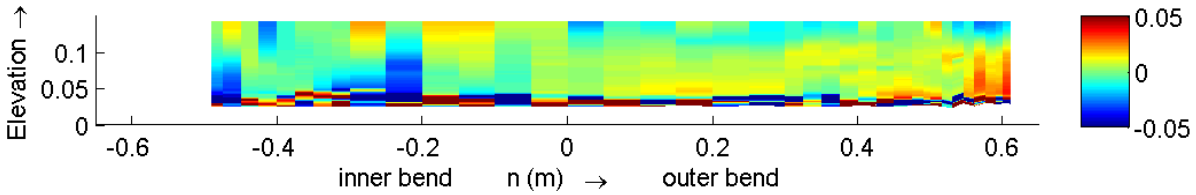

Figure E-13 Transverse velocity according to the measurements, cross-section m22

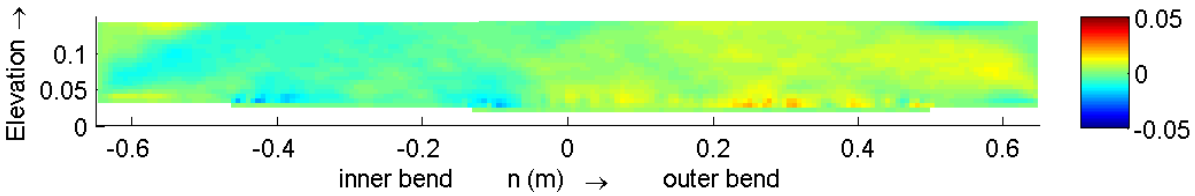

Figure E-14 Transverse velocity according to the M89_LES, cross-section m22

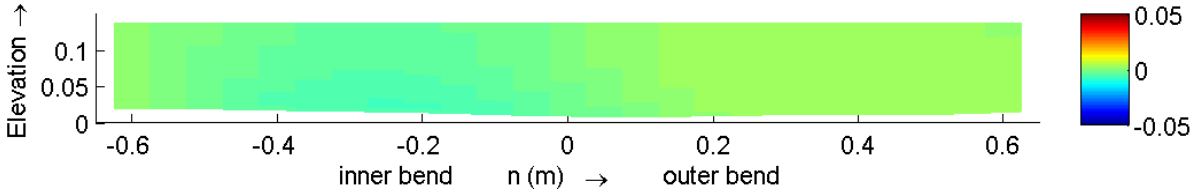

Figure E-15 Transverse velocity according to simulation M89_1_D3D, cross-section m22

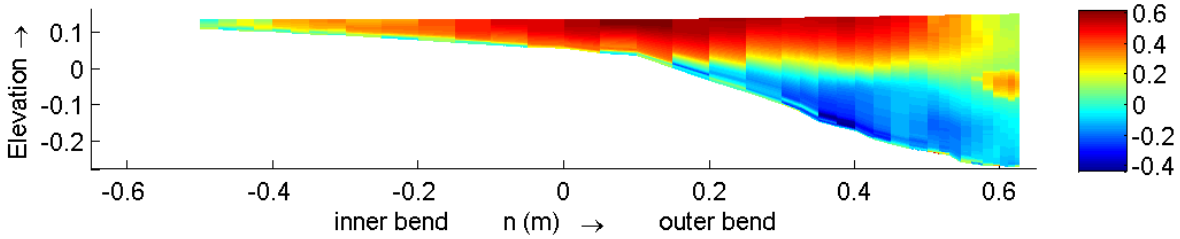

Figure E-16 Transverse velocity according to the measurements, cross-section 060

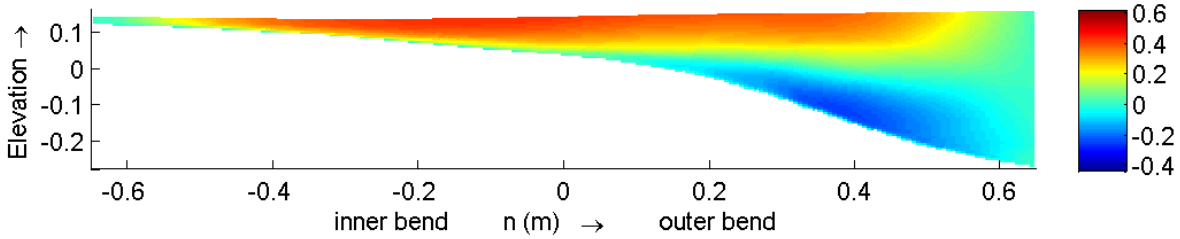

Figure E-17 Transverse velocity according to the M89_LES, cross-section 060

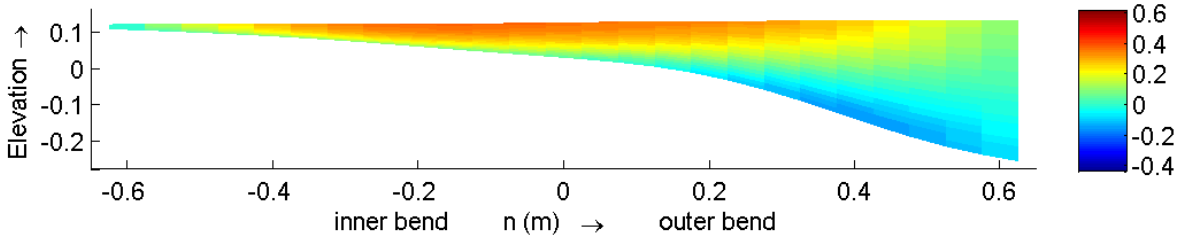

Figure E-18 Transverse velocity according to simulation M89_1_D3D, cross-section 060

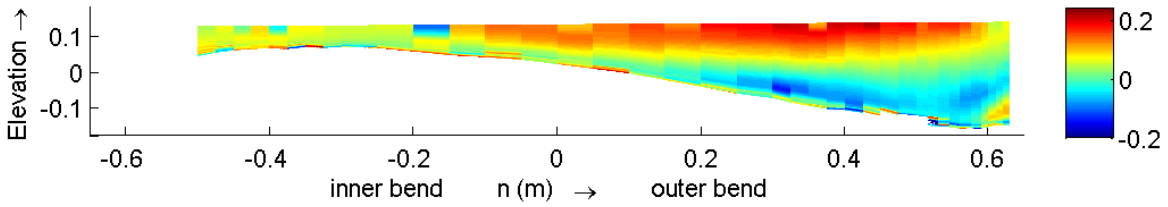

Figure E-19 Transverse velocity according to the measurements, cross-section 150

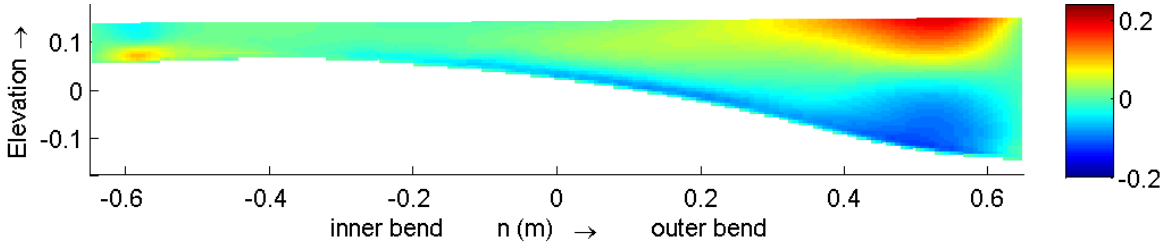

Figure E-20 Transverse velocity according to the M89_LES, cross-section 150

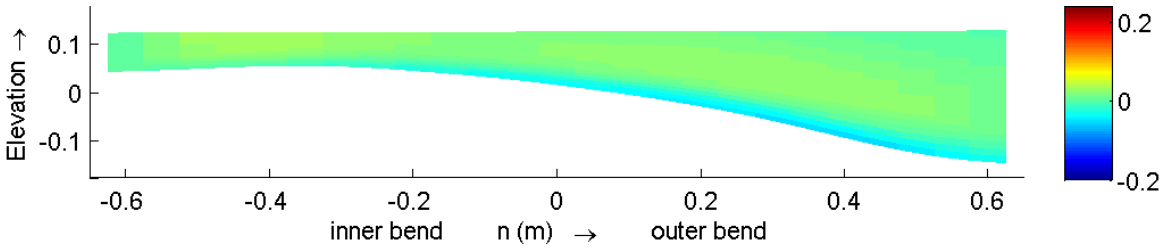

Figure E-21 Transverse velocity according to simulation M89_1_D3D, cross-section 150

E.3 Turbulent velocities

The turbulent stresses are averaged in time. Only the $\overline{u'v'}$, $\overline{u'w'}$ and $\overline{v'w'}$ stresses for cross-section 060 are shown because these are the most interesting quantities. The normal stresses can be related to the pressure and compared to the pressure these stresses are small. The turbulent shear stresses are large compared to the viscous shear forces.

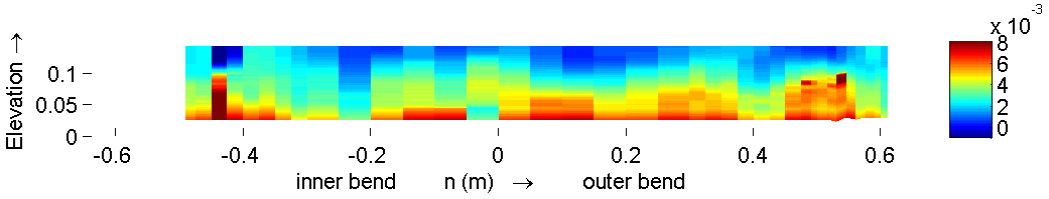

Figure E-22 Turbulent velocity $\overline{u'v'}$ according to the measurements, cross-section m22

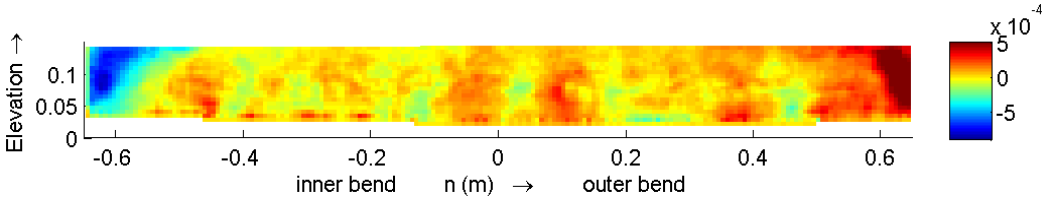

Figure E-23 Turbulent velocity $\overline{u'v'}$ according to the M89_LES, cross-section m22

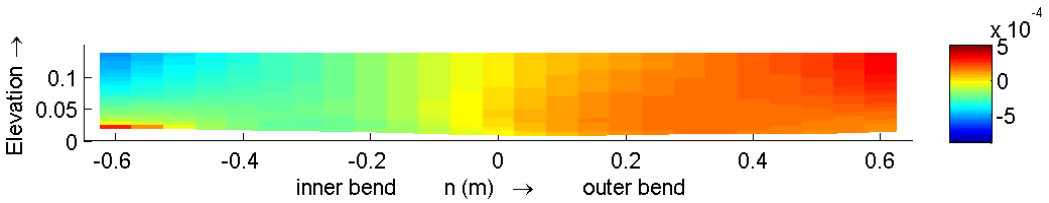

Figure E-24 Turbulent velocity $\overline{u'v'}$ according to simulation M89_1_D3D, cross-section m22

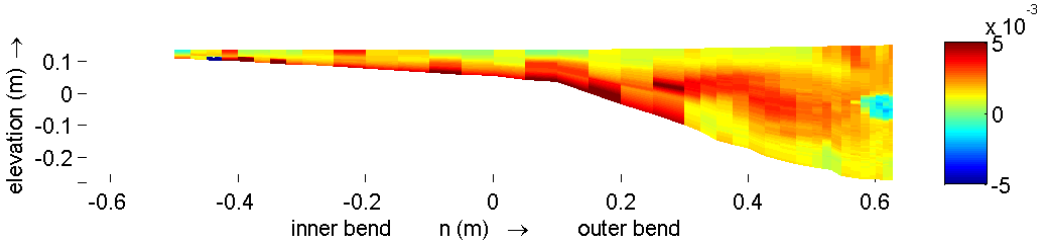

Figure E-25 Turbulent velocity $\overline{u'v'}$ according to the measurements, cross-section 060

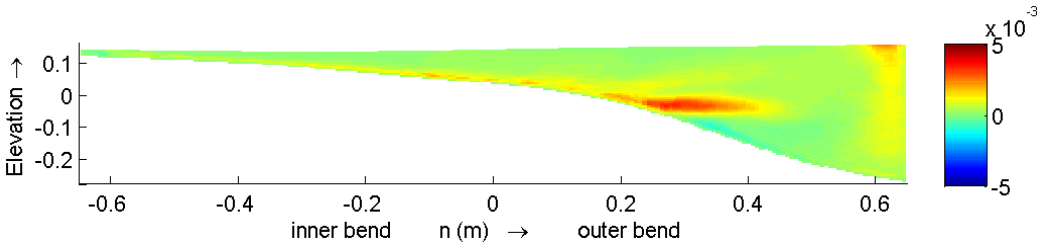

Figure E-26 Turbulent velocity $\overline{u'v'}$ according to the M89_LES, cross-section 060

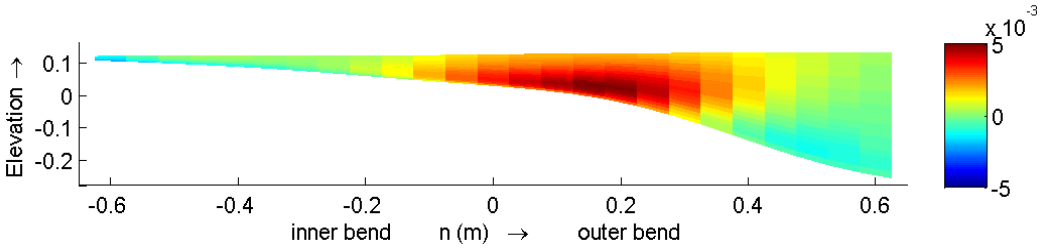

Figure E-27 Turbulent velocity $\overline{u'v'}$ according to simulation M89_1_D3D, cross-section 060

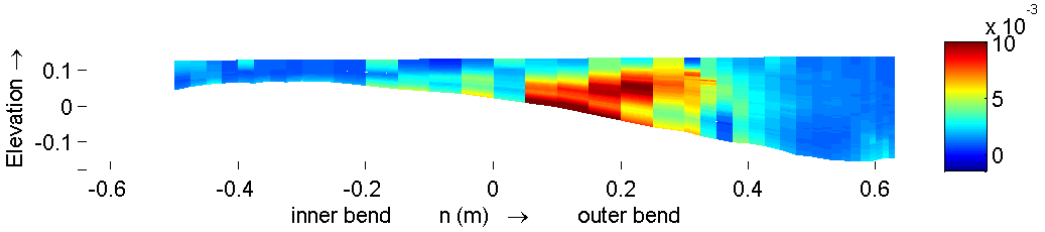

Figure E-28 Turbulent velocity $\overline{u'v'}$ according to the measurements, cross-section 150

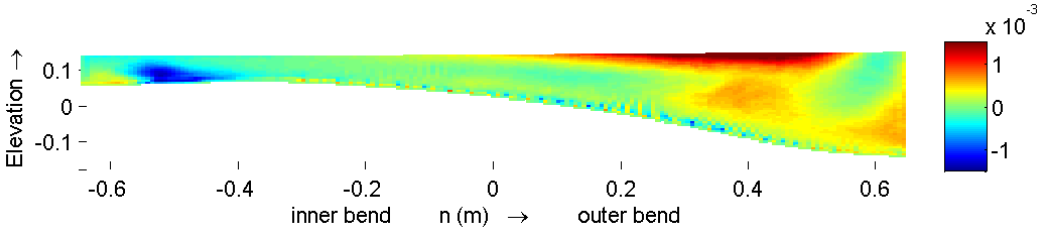

Figure E-29 Turbulent velocity $\overline{u'v'}$ according to the M89_LES, cross-section 150

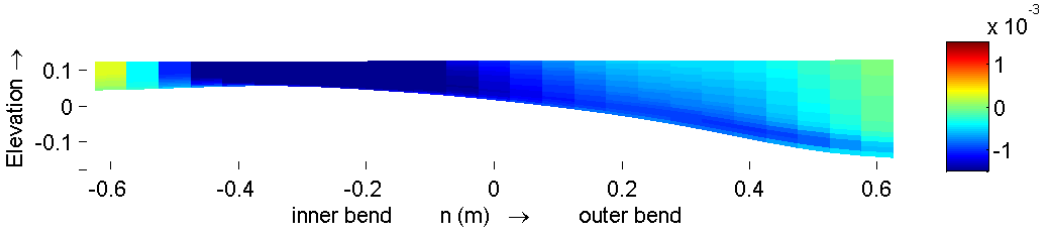

Figure E-30 Turbulent velocity $\overline{u'v'}$ according to simulation M89_1_D3D, cross-section 150

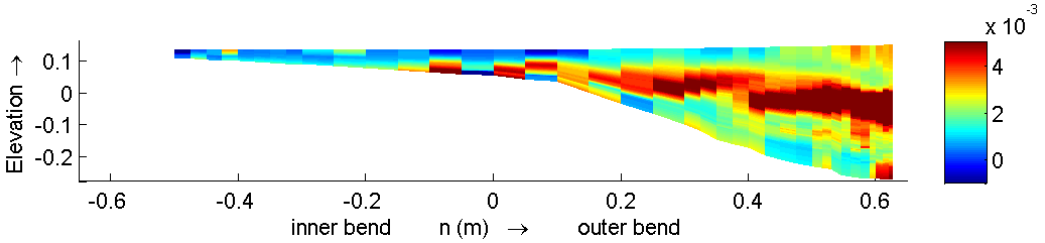

Figure E-31 Turbulent velocity $\overline{u'w'}$ according to the measurements, cross-section 060

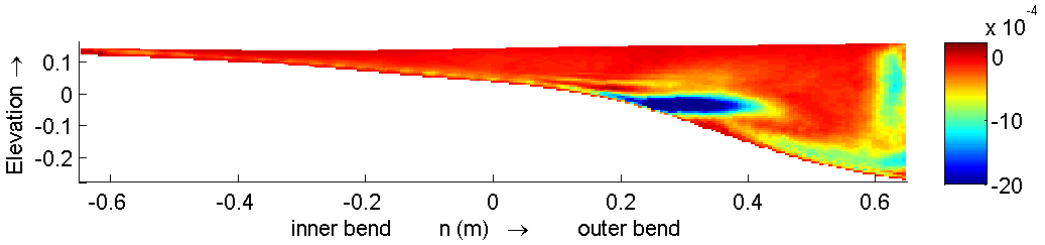

Figure E-32 Turbulent velocity $\overline{u'w'}$ according to the M89_LES, cross-section 060

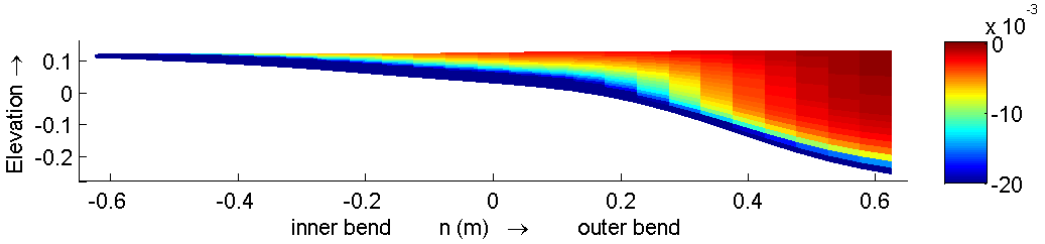

Figure E-33 Turbulent velocity $\overline{u'w'}$ according to simulation M89_1_D3D, cross-section 060

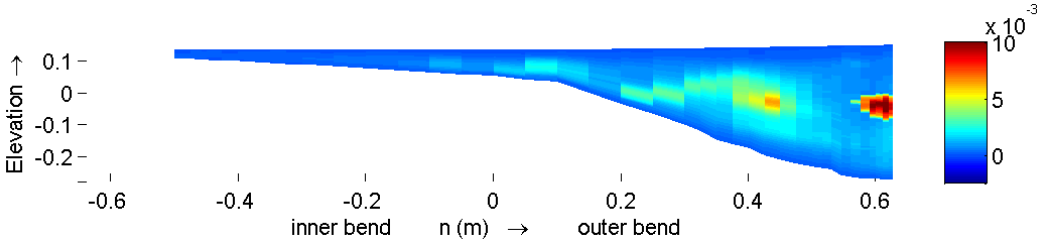

Figure E-34 Turbulent velocity $\overline{v'w'}$ according to the measurements, cross-section 060

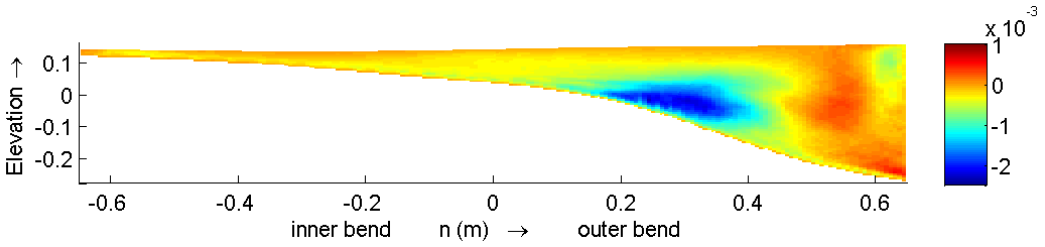

Figure E-35 Turbulent velocity $\overline{v'w'}$ according to the M89_LES, cross-section 060

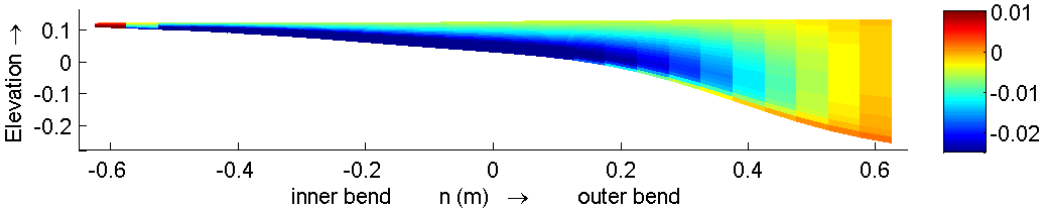

Figure E-36 Turbulent velocity $\overline{v'w'}$ according to simulation M89_1_D3D, cross-section 060